1976

Effects of Reynolds number and corner radius on two-dimensional flow around octagonal, dodecagonal and hexdecagonal cylinders

William David James
Iowa State University

INFORMATION TO USERS

This material was produced from a microfilm copy of the original document. While the most advanced technological means to photograph and reproduce this document have been used, the quality is heavily dependent upon the quality of the original submitted.

The following explanation of techniques is provided to help you understand markings or patterns which may appear on this reproduction.

1. The sign or "target" for pages apparently lacking from the document photographed is "Missing Page(s)". If it was possible to obtain the missing page(s) or section, they are spliced into the film along with adjacent pages. This may have necessitated cutting thru an image and duplicating adjacent pages to insure you complete continuity.

2. When an image on the film is obliterated with a large round black mark, it is an indication that the photographer suspected that the copy may have moved during exposure and thus cause a blurred image. You will find a good image of the page in the adjacent frame.

3. When a map, drawing or chart, etc., was part of the material being photographed the photographer followed a definite method in "sectioning" the material. It is customary to begin photoing at the upper left hand corner of a large sheet and to continue photoing from left to right in equal sections with a small overlap. If necessary, sectioning is continued again – beginning below the first row and continuing on until complete.

4. The majority of users indicate that the textual content is of greatest value, however, a somewhat higher quality reproduction could be made from "photographs" if essential to the understanding of the dissertation. Silver prints of "photographs" may be ordered at additional charge by writing the Order Department, giving the catalog number, title, author and specific pages you wish reproduced.

5. PLEASE NOTE: Some pages may have indistinct print. Filmed as received.

University Microfilms International
300 North Zeeb Road
Ann Arbor, Michigan 48106 USA
St. John's Road, Tyler's Green
High Wycombe, Bucks, England HP10 8HR

Effects of Reynolds number and corner radius on two-dimensional flow around octagonal, dodecagonal and hexdecagonal cylinders

by

William David James

A Dissertation Submitted to the
Graduate Faculty in Partial Fulfillment of
The Requirements for the Degree of
DOCTOR OF PHILOSOPHY

Majors: Aerospace Engineering
Electrical Engineering

Approved:

Signature was redacted for privacy.

In Charge of Major Work

Signature was redacted for privacy.

For the Major Departments

Signature was redacted for privacy.

For the Graduate College

Iowa State University
Ames, Iowa
1976

TABLE OF CONTENTS

LIST OF FIGURES

ABSTRACT

The effects of Reynolds number and corner radius on two-dimensional flow around octagonal, dodecagonal and hexdecagonal cylinders were investigated. All models were studied at at least three model-relative wind orientations to determine the effect of angular alignment. In general it was found that the greatest drag coefficient was experienced with one of the corners pointing directly into the relative wind. The corner radii studied for each family of cylinders were 0.0, 9.1, 17.5, 24.5, 40.5, 57.7 and 74.2 percent of the radius of the inscribed circular cylinder. Data from these radii were compared with base line data obtained from a circular cylinder. It was found that at corner radii greater than 26 percent the hexdecagonal cylinder experiences a smaller drag than that of the circular cylinder. At corner radii smaller than 26 percent the drag of the hexdecagonal cylinder increases approximately linearly from a drag equal to that of a circular cylinder, to a value approximately 1.5 times that of a circular cylinder for the 0.0 percent corner radius. The dodecagonal cylinders experience the same trend, decreasing linearly from a drag coefficient approximately 1.5 times that of a circular cylinder at a corner radius of 9.1 percent to a value of drag coefficient 3 percent greater than that of a circular cylinder at a corner radius of 34 percent. At corner radii greater than 0.34 the drag remains constant at

this value. Drag coefficients for the octagonal cylinder are significantly greater than those of the circular cylinder except at corner radii approaching 100 percent.

The effect of corner radius on the coefficient of lift was negligible except at the larger corner radii where for increasing radius the lift coefficient approached zero. Model orientation and number of sides had the major effects on lift coefficient. As the number of sides increased the maximum values of lift decreased from 0.4 for 8-sided cylinders to approximately 0 for the 16-sided bodies. The direction of the force is determined by the angular orientation between the model and the relative wind. At orientations close to that having a flat side perpendicular to the relative wind the lift acts toward the side rotated in the downwind direction, while at orientations close to that having a corner pointing directly into the relative wind the lift force acts toward the side rotated up stream. At orientations where the upper and lower surfaces are symmetrical with respect to the relative wind the lift is approximately zero, but for rotations where this symmetry is missing the lift can be as large as 50 percent of the drag.

Empirical equations are proposed for the prediction of the variation of the total aerodynamic force coefficient with change in model corner radius for a Reynolds number of 1,000,000.

NOMENCLATURE

a	Speed of sound
C	Cross-sectional area of test section
C_d	Coefficient of drag
C_f	Total aerodynamic force coefficient
C_L	Coefficient of lift
C_p	Pressure coefficient
d	Diameter or breadth of body
D	Drag
Fr	Froude number $\sqrt{\frac{V^2}{g\ell}}$
g	Acceleration due to gravity
h	Height of test section
k	Base pressure parameter in Equation 8
ℓ	Characteristic length of model
M	Mach number V/a
P_b	Static base pressure
P_T	Total pressure
q	Free-stream dynamic pressure
r	Ratio of corner radius to radius of the inscribed circular cylinder
Rn	Reynolds number $\frac{\rho V \ell}{\mu}$
S	Cross-sectional area of model
t	Thickness of the base portion of the body in the wake

V	Relative velocity between the body and the fluid in which it is immersed
η	Glauert's empirical factor in Equation 4
μ	Coefficient of viscosity of the fluid
ρ	Density of free-stream fluid

Subscripts:

c	Indicates corrected value

INTRODUCTION

Background

The need for cross-flow lift and drag coefficients for polygonal cylinders is becoming increasingly important. Most of this new-found interest in the polygonal cross-sections stems from the belief of many manufacturers that it is easier to manufacture a tapered polygonal cylinder than it is to manufacture a circular cylinder of the same diameter and taper. One of the major uses for polygonal cylinders is as luminaire towers for the lighting of athletic events, and more recently, highway interchanges. Polygonal cylinders used as supports for lights at athletic events have a light structure at the top of the tower which provides a drag load at least an order of magnitude greater than that of the tower itself. Therefore, the drag coefficient used for the tower was relatively unimportant. Because of this, the overall structure was designed using a coefficient of drag for the polygonal tower that seemed reasonable to the designer, very often one selected as being just slightly above that of a circular cylinder since many-sided round-cornered cylinders approximate the shape of a circular cylinder. It wasn't until the polygonal towers were used as luminaire towers on the Interstate Highway System interchanges that any concern was really given to the drag coefficients of the actual

cross-sectional shapes being used. Most luminaire towers are constructed of 8-, 12- or 16-sided polygonal cylinders which, due to the small size and numbers of lighting fixtures mounted on each tower, provides the majority of the drag load experienced by the luminaire tower.

At the time the first tall luminaire towers were installed on the Interstate System, there were no known reports documenting experimental tests on the polygonal cross-sections being used. However, sometime around 1970 a report published in 1959 by C. F. Cowdrey and J. A. Lawes of the Aerodynamics Division of the National Physical Laboratory of England (3) was discovered by the Federal Bureau of Roads. This report contained both the variations of the coefficients of lift and drag of a sharp-cornered dodecagonal cylinder as functions of Reynolds number and the orientation of the model to the relative wind. The report showed that regardless of the Reynolds number, the maximum value of the coefficient of drag never decreased much below 1.1. Based on this AASHO, the American Association of State Highway Officials, set this value as the suggested design value for 12-sided towers. The Meyer Manufacturing Company of Red Wing, Minnesota felt that this value was too large and would effectively price them, as builders of polygonal towers, out of the market since they were forced to compete with builders of circular towers who were designing to more realistic standards. They

therefore had a test conducted on a 12-sided cylinder, having a corner radius to distance between flat sides of 0.128, at Iowa State University in 1970 and 1971 by this author (9). Results from these tests indicated that for the round-cornered shapes actually being produced for use as luminaire towers, a maximum coefficient of drag of 0.8 was a realistic value at Reynolds numbers less than 1.5×10^6. Based on these results the design value for 12-sided cylinders was reduced to the maximum values determined in the ISU tests by AASHO in 1975 (21). At the present time the NPL report (3) and the ISU report (9) are the only ones known to contain data on dodecagonal cylinders.

Data on 8-sided cylinders are even more scarce with only one known source. In a report published in 1967 by the Geoffrey DeHavilland Aeronautical Laboratories (8), test results on an apparently round-cornered 8-sided cylinder are reported. Unfortunately information on the corner radii is not given which greatly reduces the value of the data supplied in view of the large effect of corner radius noted for other polygonal cylinders (4,9,16). For the 16-sided cylinders there are no known test results available.

This lack of test results for the polygonal cylinder is especially unfortunate since bluff bodies behave so differently than streamlined bodies when immersed in low-speed fluid flows. For streamlined shapes the variation of

the coefficients of lift and drag with change in Reynolds number is fairly independent of changes in body shape except for major modifications. On the other hand for bluff bodies the variation of the coefficients of lift and drag with changes in Reynolds number is very strongly dependent on body shape. This is the result of the tendency of subsonic flows to separate at all corners, and especially at those which are sharp. This is especially true in the case of the cross-sectional shapes considered in this report, those of the 8-, 12- and 16-sided polygonal cylinders. For these shapes the variation of the coefficients of lift and drag with variation in Reynolds number is strongly dependent on the radius of the corners of the polygonal cylinder. Dramatic variations in the coefficient of drag for a fixed Reynolds number occur as the radius of the corners changes from zero (sharp-cornered) to the radius of the inscribed circular cylinder. This behavior is strongly pointed out by the data presented in references 4, 9 and 16. In reference 9 test data are presented for both sharp-cornered and round-cornered (corner radius/distance between parallel faces = 0.128) dodecagonal sectional cylinders. The test results presented give a maximum coefficient of drag of 1.33 for the sharp-cornered dodecagonal sectional cylinder and a value of 0.80, a decrease of approximately 40 percent from the maximum sharp-cornered value, for the round-cornered case. The same

trend is pointed out for triangular and rectangular sectional cylinders in references 4 and 16; except that for these cross-sections the decrease in the coefficient of drag is even larger than in the dodecagonal case as the corners are rounded.

Objectives

The work reported herein is a continuation of the work started at Iowa State in 1970. At the completion of the tests for Meyer Industries it was realized that two large gaps still existed in the force measurements on the polygonal cylinders most frequently used for highway interchange luminaire towers. For 12-sided cylinders there were data for two corner radii, only one of which could practically be manufactured, plus the circular cylinder. The values of the coefficient of drag for other corner radii were not known. The second gap lay with the complete lack of data for round-cornered cylinders of either 8 or 16 sides. The research project described in this report was undertaken to fill the two gaps.

The research program described herein had two objectives. The first was to obtain data on the variation of the coefficients of lift and drag with change in Reynolds number for several families of polygonal cylinders, with each family

of cylinders having several corner radii. The families that were studied were the octagonal, the dodecagonal and the hexdecagonal. The corner radii studied for each cross-sectional shape were 0.0, 9.1, 17.5, 24.5, 40.5, 57.7 and 74.2 percent of the radius of the inscribed circular cylinder. The models studied were all approximately 12.25 inches between parallel flat sides. Figure 1 shows the terminology used in describing the polygonal cylinders. In addition to the 12.25 inch diameter polygonal cylinders, an 11.97 inch diameter circular cylinder having the same surface finish as the polygonal cylinders was also studied as a source of base line data. Figures 2 and 3 show the models studied.

The second objective of the research project was to attempt to find a relationship between the variation in the coefficient of drag and the variation of corner radius at a fixed Reynolds number. Such an empirical relationship would simplify the writing of specifications for general round-cornered polygonal cylinders.

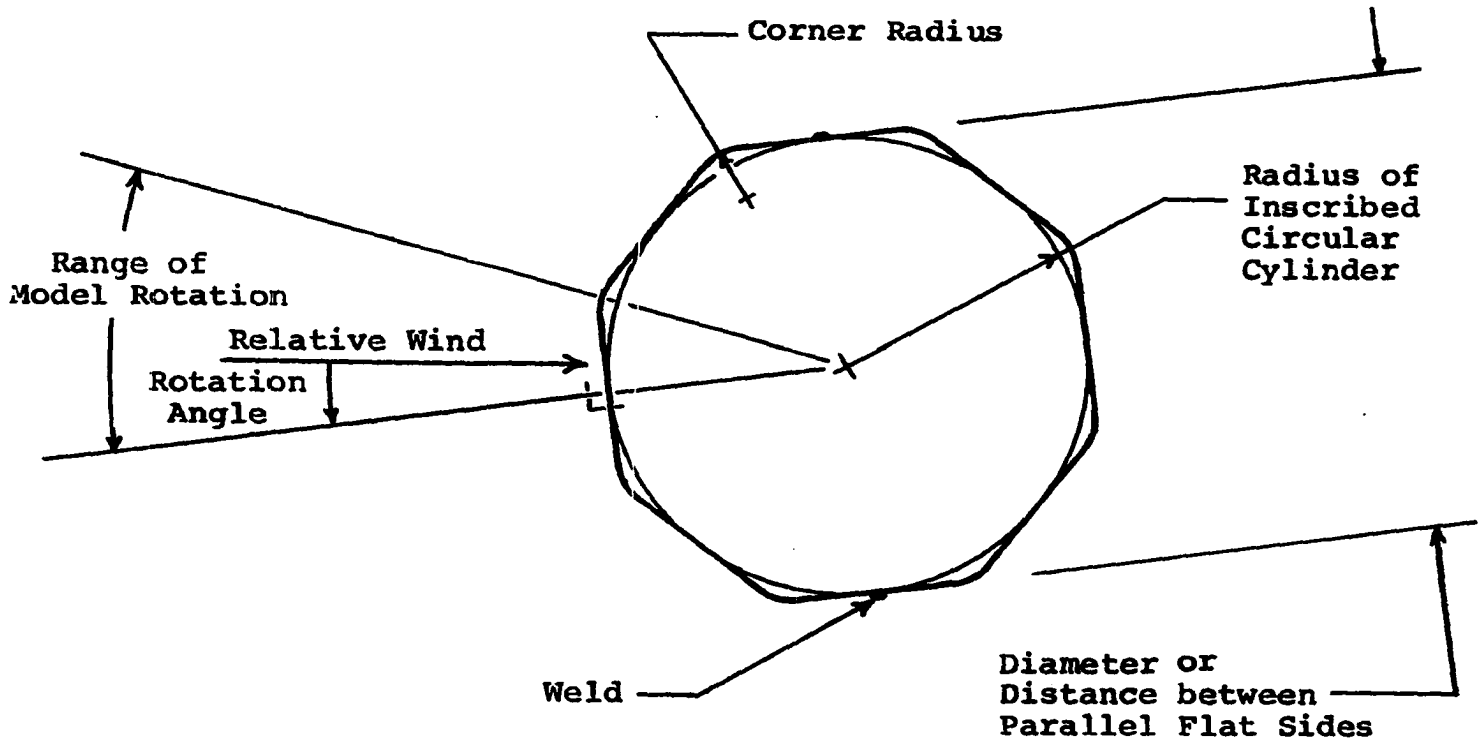

Figure 1. Terminology, model rotation and model orientation for polygonal cylinders. Shown for octagonal cylinder.

Figure 2. 6 and 12 inch diameter wind tunnel models.

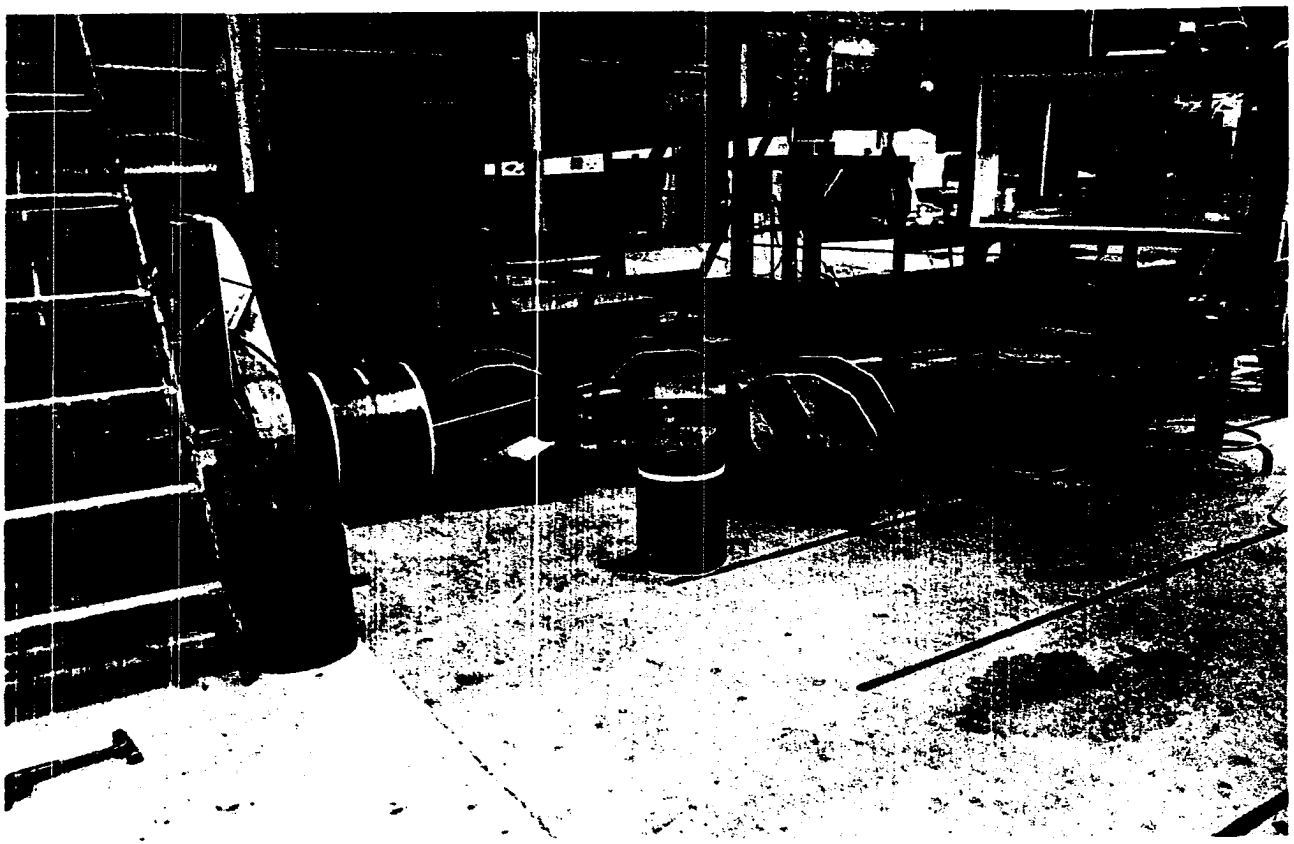

Figure 3. 24 inch diameter wind tunnel models.

FLOW SIMULATION

The purpose of the wind tunnel tests that have been conducted on the polygonal cylinders was to determine the variation of the aerodynamic forces acting on the wind tunnel models with variation of Reynolds number. This was done so that the aerodynamic forces which act on structures of similar shapes existing in nature can be predicted. The accuracy of these predictions depends on the exactness with which the flow around the model reproduces the flow around the structure in nature; i.e., the similarity of the two flows. Wind tunnel testing is thus based on studying physically similar phenomena. We say that two phenomena are similar when all the physical characteristics at corresponding points in the two phenomena have the same relationship. Experience, aided by dimensional analysis, has shown that certain nondimensional relationships among these physical characteristics hold the key to physical similarity.

In the field of ordinary fluid dynamics the most important nondimensional relationships are the ratios of the forces produced as the model moves through a fluid. They have been named for the men who first drew attention to their importance and are the

$$\text{Reynolds number} = Rn = \frac{\text{Inertial Force}}{\text{Viscous Force}} = \frac{\rho V \ell}{\mu} \qquad (1)$$

where ρ is the fluid density, V is the relative velocity between the body and the fluid, ℓ is a characteristic length of the body and μ is the coefficient of viscosity of the fluid,

$$\text{Mach number} = M = \frac{\text{Inertial Force}}{\text{Elastic Force}} = \frac{V}{a} \qquad (2)$$

Where a is the speed of sound in the fluid and

$$\text{Froude number} = Fr = \frac{\text{Inertial Force}}{\text{Gravitational Force}} = \sqrt{\frac{V^2}{\ell g}} \qquad (3)$$

where g is the acceleration due to gravity.

For special flow problems, such as those involving thermal conductivity, rarefied gases or rotational motion, there are other nondimensional parameters of importance that must also be considered.

Exact similarity between two systems requires that all of the nondimensional parameters are equal in both systems. It also requires geometrically similar bodies that are similarly oriented to the flow. To obtain equality of all parameters is extremely difficult if not impossible, and for that reason it is possible to obtain only partial similarity. In doing this, those parameters on which the phenomena of

interest most strongly depend must first be determined and then equated in both systems. In the research project carried out on the polygonal cylinders, the phenomena of interest were the static forces and pressures acting on the bodies. Since the models were held rigidly in the tunnel, the Froude number, which is of importance in spin and dynamic tests or in tests involving a free surface, loses importance and has only a negligibly small effect upon the flow patterns and flow forces being measured. In addition, the top relative velocities were in the range of 200 ft./sec. which yielded a Mach number of around 0.20. At Mach numbers in this range the flow can still be assumed to be incompressible, density remains constant, and the Mach number becomes less important. This leaves only the need for geometric, orientation and Reynolds number equality to ensure that systems are similar which means that the forces, pressures and flow patterns between the structure in nature and the wind tunnel model can be directly scaled.

Although the cross-sectional shapes of the models were similar to those of the actual towers, geometric similarity was not obtained in the program in the sense that a luminaire tower has a finite length and is therefore three-dimensional while the tests were conducted on two-dimensional bodies. In addition luminaire towers are usually tapered while the wind tunnel models had a constant diameter. Both the taper

and the free end have an effect on the flow around the tower. The effect of taper is to change the characteristic length of the tower between two cross-sections and therefore the Reynolds number and shedding frequency of the wake. Although the exact phenomena is not understood the total tower behaves as though it had a constant diameter equal to the actual diameter of the tower located approximately 75 percent of the length of the tower above its base. However, the effect of an increasing characteristic length of the tower as the base is approached is offset by the variation of the free-stream velocity of the air as the surface of the earth is approached. This is due to boundary layer formed over the surface by the wind. The shape and height of this boundary layer is affected by the terrain of the earth and any vegetation or structures on the surface. Because of this the net effect of taper and boundary layer varies from location to location and day to day and is therefore very difficult to model.

The effect of the top is to permit flow to pass over the end and modify the pressure distributions around the surface. As the ratio of tower diameter to tower length becomes smaller the end affects a smaller percentage of the tower. Since for luminaire towers this ratio is in the neighborhood of 0.007, end effects can usually be neglected in the calculating of forces without causing an appreciable error.

Because of this, wind loads on towers are calculated assuming a constant diameter tower in a two-dimensional flow. The effects of taper and the top are then accounted for by the use of empirical factors (21). Therefore the need was for two-dimensional results, called sectional characteristics, which were obtained.

Thus for the research project reported herein the aerodynamic forces acting on the cylinders depend only on the Reynolds number and the orientation of the body to the flow. As will be pointed out in the next section the requirement for body orientation was fulfilled by taking data at several body-relative wind orientations. The dependence of the forces on this parameter can be seen in any of the figures where a force coefficient is plotted versus Reynolds number for constant body shape. The same curves show the force dependence on Reynolds number. As pointed out in Equation 1, Reynolds number can be varied by changing either the density or coefficient of viscosity of the testing medium, the size of the model or the relative velocity between the model and the fluid. For the wind tunnel utilized in this project the testing medium was air and therefore the density and coefficient of viscosity were fixed and essentially constant. This left variation of speed and size as the only methods of changing Reynolds number; both were used. Data were taken on models ranging from 6 inches to 24 inches in

diameter and at tunnel speeds of from zero to 210 feet per second. These variations produced a range of corrected Reynolds numbers from 0 to approximately 1.2×10^6 for the 12 inch models and 2.1×10^6 for the 24 inch models. The Reynolds number of a 24 inch diameter luminaire tower experiencing an 80 mph wind on a standard day at an altitude of 1000 feet is 1,454,000. Thus in addition to geometric similarity and model orientation similarity mentioned above there was also Reynolds number similarity. Because of this the forces, pressures and flow patterns found in the wind tunnel tests on the models in this project should be the same as those actually experienced by towers in nature.

EXPERIMENTAL SETUP

The research program reported herein was conducted in a low turbulence, 0.1 percent, open circuit, flow visualization wind tunnel at Iowa State University. The tunnel has an area contraction ratio of 22.5:1 between the inlet and test section and is powered by a two speed 100 horsepower, variable pitch, axial flow fan capable of providing continuous variation in airspeed from 0 to 215 feet per second. The two-dimensional test section designed specifically for this study is approximately 72 inches high and 15.25 inches deep with a cross-sectional area of 1092 square inches, see Figure 4. The front, top and bottom are plexiglas and the back is constructed of wood and painted black to aid flow visualization. The front and back walls are parallel but the top and bottom diverge at an included angle of 1° to provide a nearly constant static pressure throughout the test section.

The models were mounted on a hollow round metal shaft that was cantilevered through the rear wall and mounted in bearings outside the back of the tunnel as shown in Figure 5. This permitted the model to be rotated to any desired angular position with respect to the free-stream flow permitting fulfillment of one of the requirements for similarity. This rotation was necessary since, unlike a

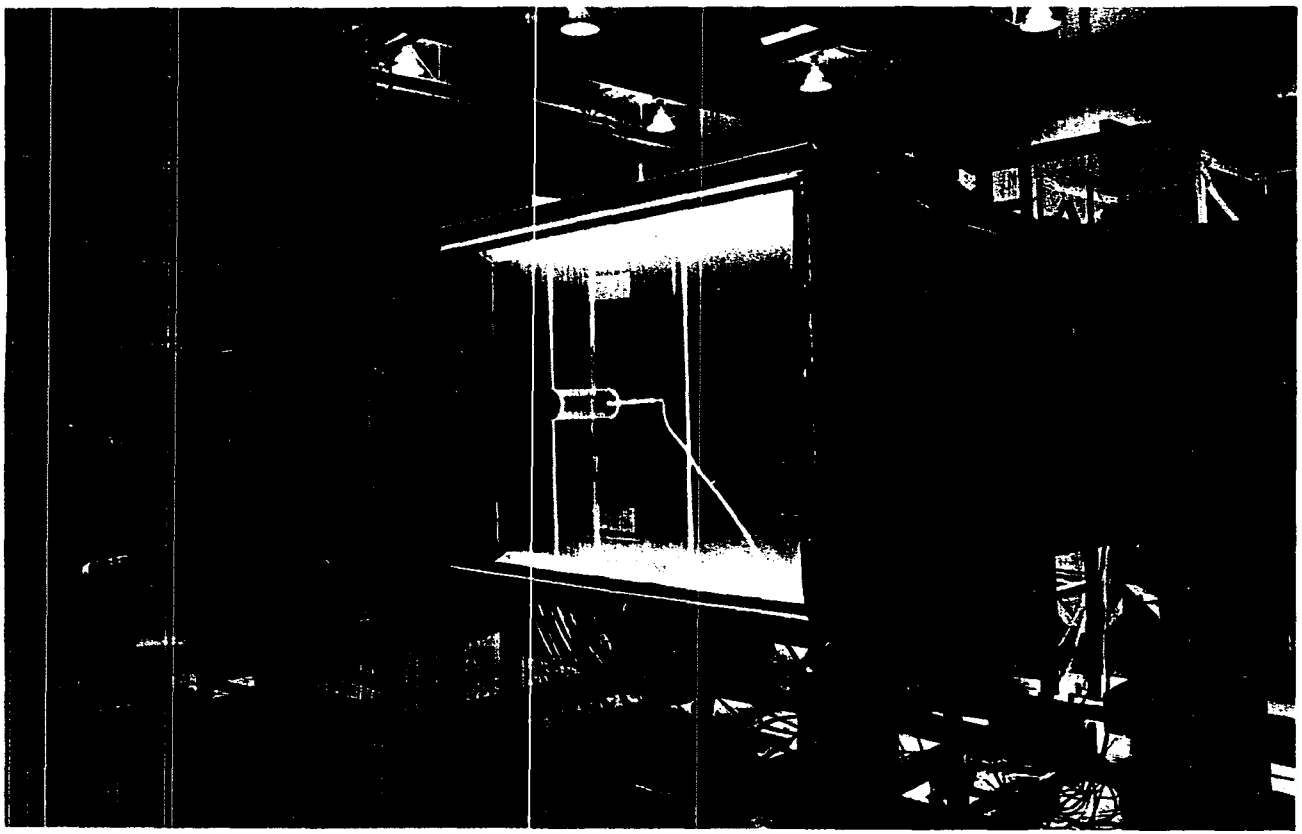

Figure 4. Front view of test section looking toward inlet of wind tunnel. Probe for injection of liquid nitrogen is visible downstream (to right) of model.

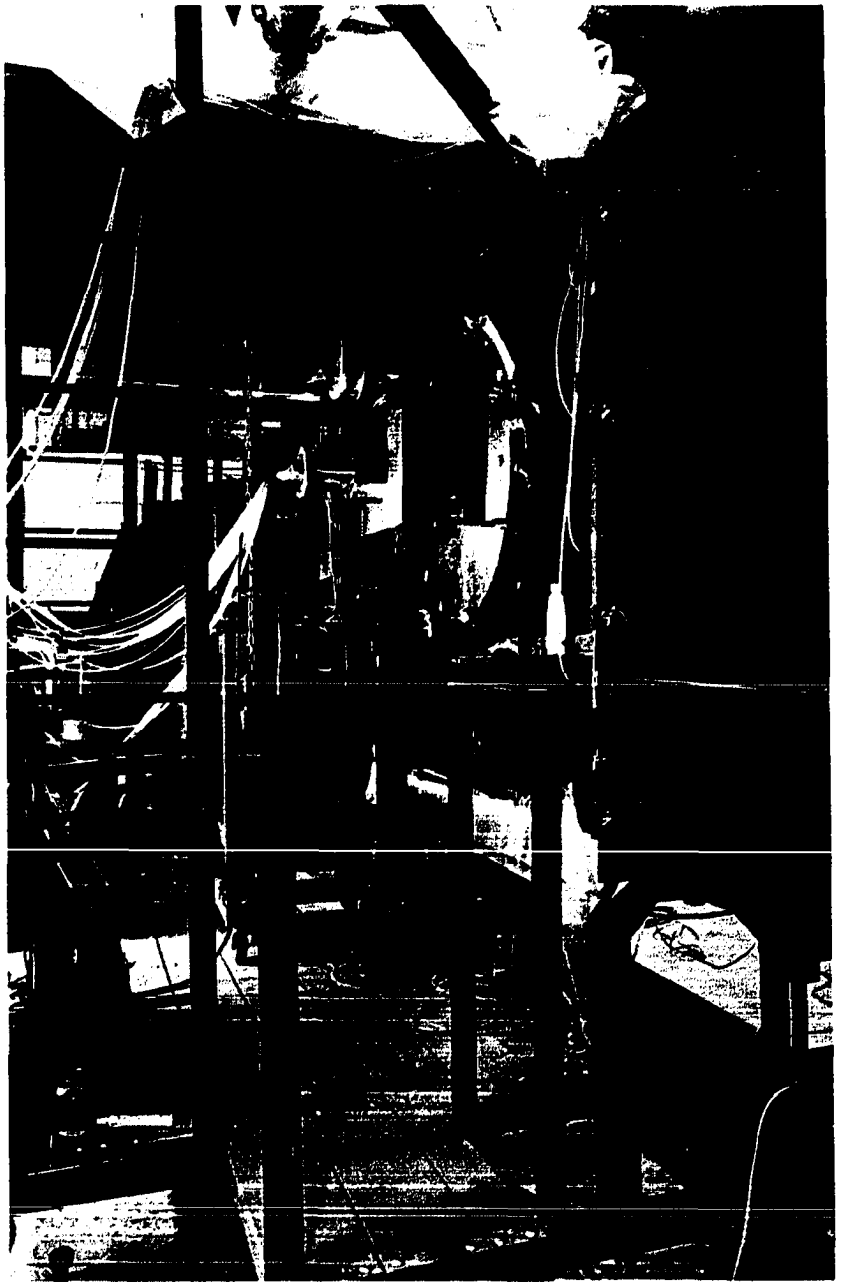

Figure 5. Model support showing exit of pressure tubes.

circular cylinder, the shape of a polygonal cylinder possesses only a periodic symmetry. Because of this the forces acting on the polygonal models studied will repeat periodically as the model-relative wind orientation is changed. The number of periods in a complete model-relative wind rotation of 360° is equal to the number of sides of the cylinder. The variation of forces during a period is such that by measuring the forces over one-half of the period the variation of forces over the complete period is known. The model rotation to yield the complete variation of forces was chosen the same for all models and is shown in Figure 1 using the octagonal cylinder as an example. For each of the families, the 0° angle of rotation was selected as the orientation where the relative wind was perpendicular to a flat side. The flat side selected to face into the wind was chosen so that the welds would be on the two sides parallel to the free-stream relative wind. This angular position was the start of the one-half period. The end of the one-half period was the model orientation having one corner pointing directly into the relative wind. This was a rotation of 22.5°, 15° and 11.25° for the octagonal, dodecagonal and hexdecagonal cylinders respectively. A positive rotation was taken as the case where the upper surface moved toward the relative wind as shown in Figure 1. Due to the symmetry of the body the same results would have been obtained had the body been rotated in the opposite

direction. To determine how the forces varied as the model-relative wind orientation changed, measurements were made with the models orientated at both ends of the one-half period plus one or two orientations in between. For the 8- and 12-sided cylinders, measurements were made at two equally spaced intermediate angles of 7.5° and 15° for the 8-sided and 5° and 10° for the 12-sided cylinders. For the 16-sided cylinders only one intermediate measurement was taken, and that at an angle of 5.625°.

Lift and drag forces were obtained for each model by an integration of the static pressures acting upon the surface of the models. Ninety-six static pressure ports were evenly spaced around each polygonal model and 90 ports around each circular model in a spanwise plane located 8 inches from the rear wall of the test section. The static pressure lines ran through the center of the metal shaft supporting the model, out the backside of the tunnel to two 48 inch tall manometer boards containing 52 tubes each as shown in Figure 6. A third manometer board was used to measure wall pressures at various locations in the test section. All manometers used water as their liquid. Thirty-five mm slides were taken of each manometer board to permit reading of the data at a later date and also to preserve a record of the pressures.

A gap of approximately 0.03 inches existed between the ends of the model and the front and rear walls of the test

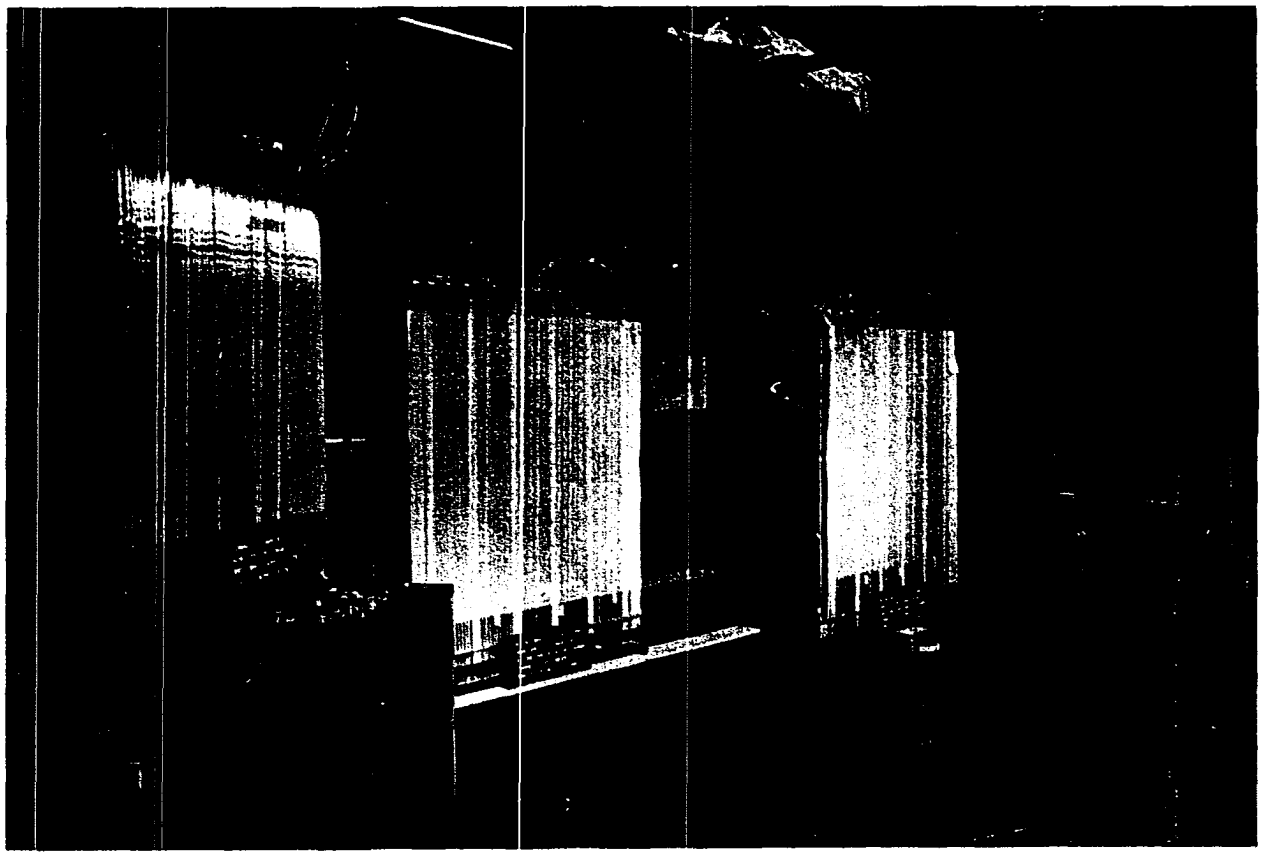

Figure 6. Manometer boards used for display of static pressures. The two boards to the right were used to display the model surface pressures.

section. These gaps were sealed by wrapping a layer of masking tape around each end of the model, as can be seen in Figure 4, so that it sealed against both the front and back sides of the test section. In order to determine how close the flow over the center section of the models came to actually being two-dimensional, the 11.97 inch diameter circular cylinder was instrumented with 6 rows of pressure ports running in the spanwise direction along the model. Each row consisted of 14 static ports which were located 1 inch apart and started approximately 1 inch from the rear wall. By rotating the model once it was possible to determine the spanwise pressure distributions along the model at approximately every 16° as shown in Figures 7 and 8. These spanwise distributions are for 14° or 18° increments starting at the stagnation point, 0°, and continuing to 162° which is within the separated wake region. They show that within the region of decreasing pressure, see Figure 9, the deviation between the largest and smallest surface pressures over the middle 7 inches of the model span is less than 4.0 percent. The maximum deviation occurred near the point of minimum pressure and was 9.7 percent. Beyond the point of minimum pressure, through the laminar separation bubble and the subsequent turbulent reattachment (10), 88° to approximately 100° depending on Reynolds number, and then well into the separated wake region the variation in surface pressure along the middle

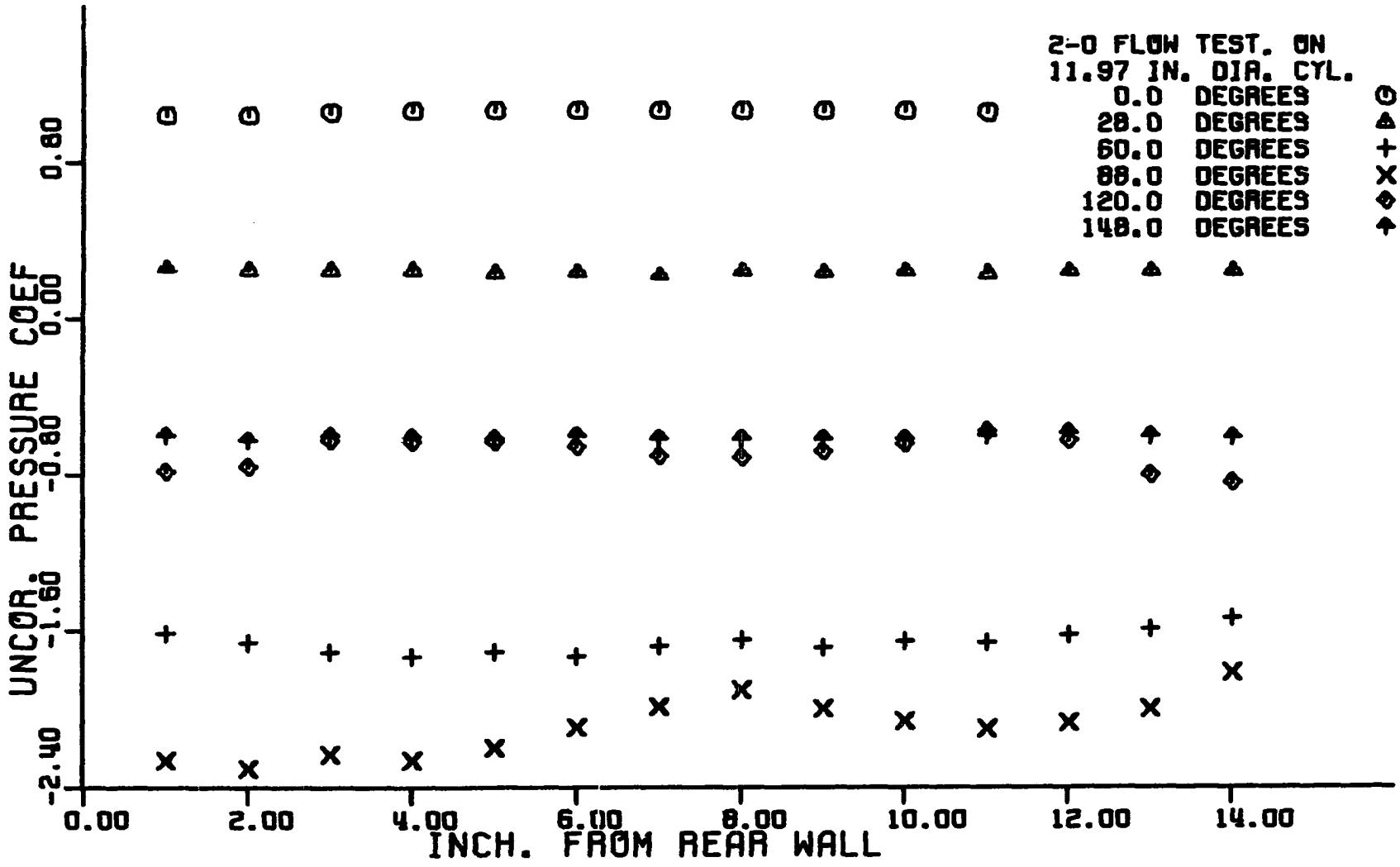

Figure 7. Variation of uncorrected surface pressure coefficient on 11.97 inch diameter circular cylinder with distance from rear wall.

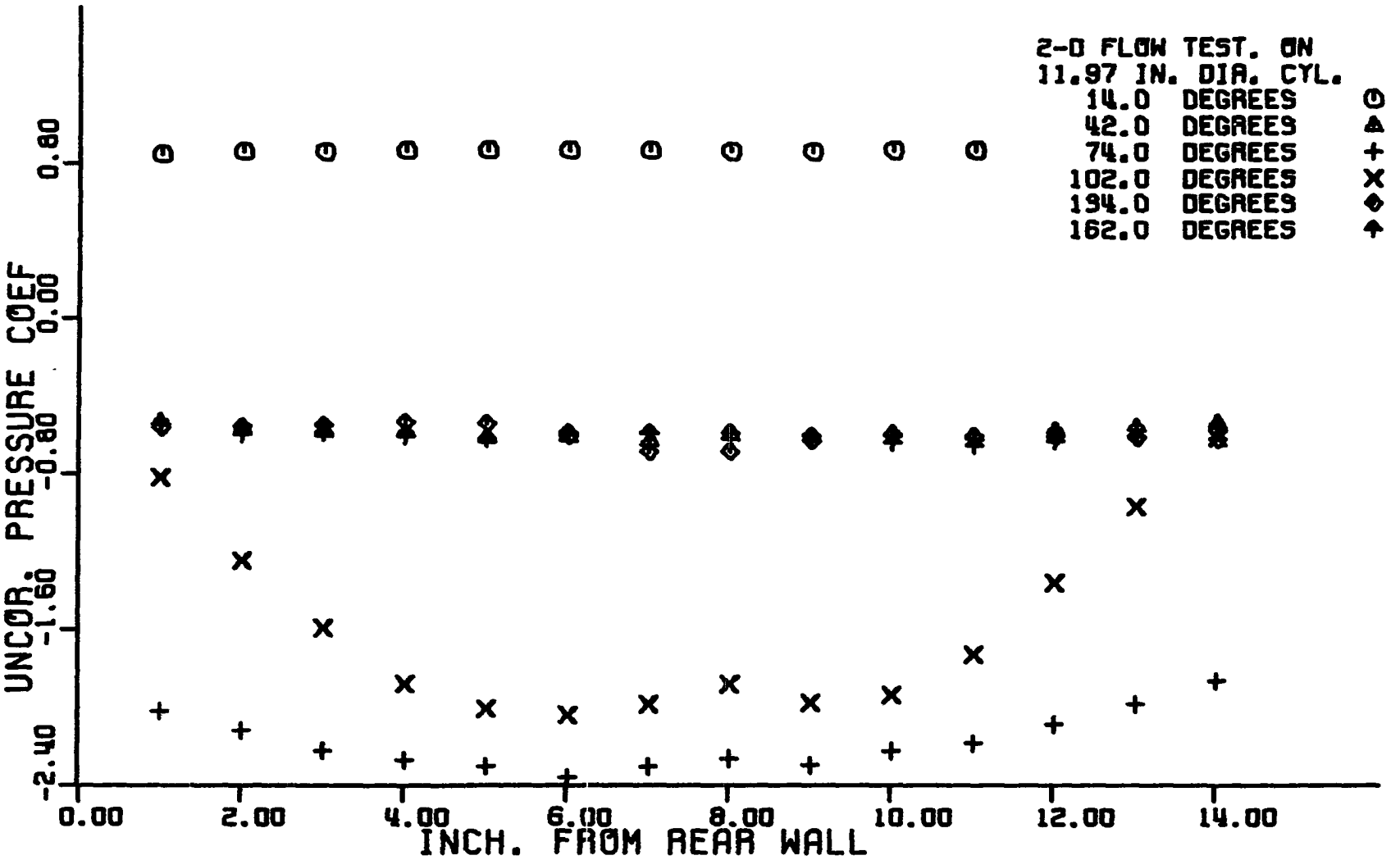

Figure 8. Variation of uncorrected surface pressure coefficient on 11.97 inch diameter circular cylinder with distance from rear wall.

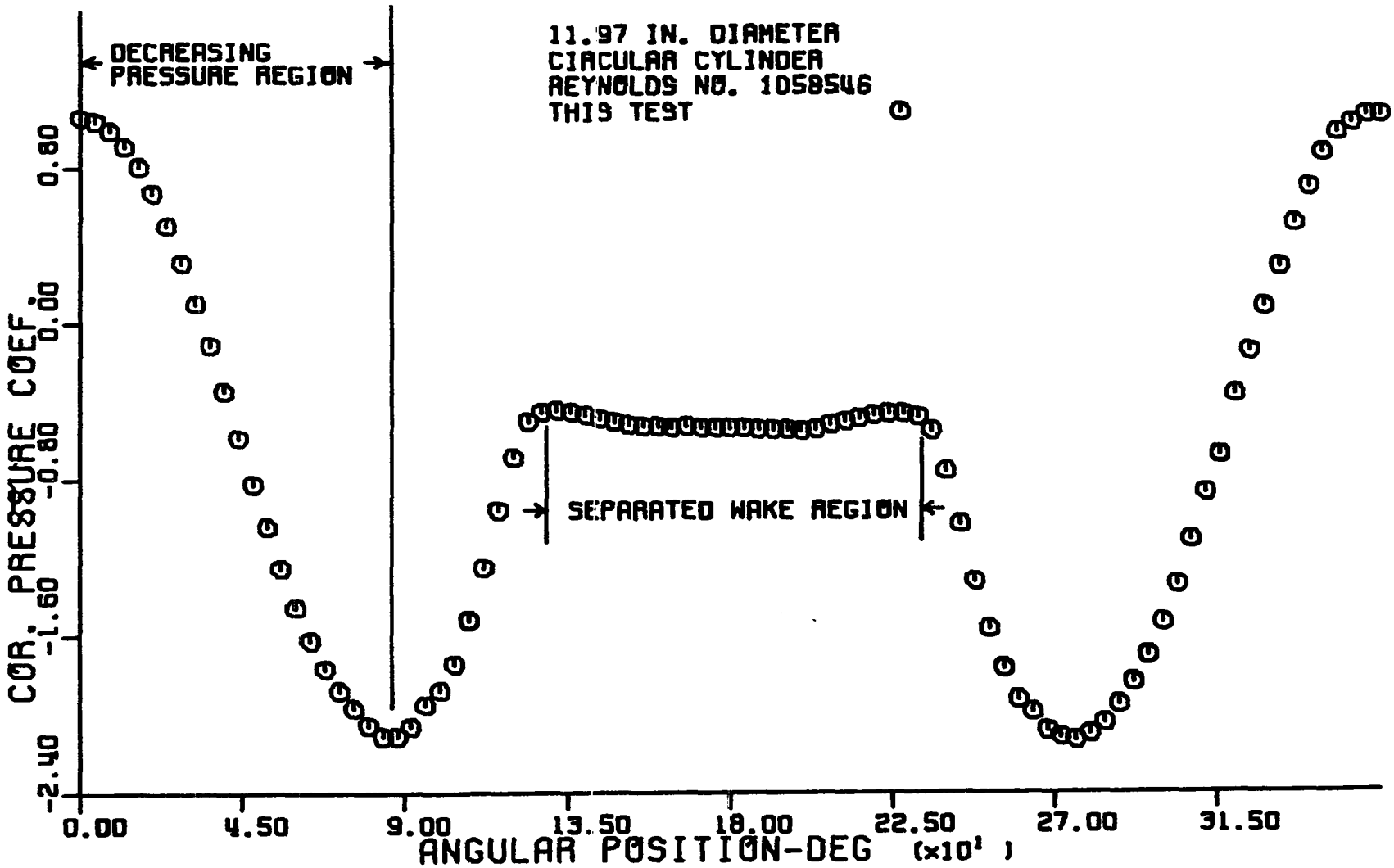

Figure 9. Corrected pressure distribution around the 11.97 inch diameter circular cylinder at a corrected Reynolds number of 1,060,000.

7 inches of the model span was no more than 5.3 percent. Since in a turbulent region it is impossible to maintain two-dimensional flow, the greater deviation in pressures within the turbulent and separation regions was expected. On the basis of the pressure coefficients shown in Figures 7 and 8, the flow over the models was assumed to be two-dimensional in the region that borders the plane in which the static pressures were being measured.

Flow visualization was obtained by introducing a mixture of liquid nitrogen and steam into the wake directly behind the body as shown in Figures 4, 10 and 11. Readings of the static pressure ports near the outlet of the liquid nitrogen and steam line both with and without the nitrogen and steam being injected into the wake showed no variation. Based on these findings the flow visualization pictures were taken at the same time the pressure measurements were being made in an effort to minimize tunnel run time. No corrections were applied to the model pressures inside the wake. The cloud formed by the boiling nitrogen mixing with the steam filled the separated region behind the models permitting the size and location of the wake to be determined as well as the location of the separation point on both the upper and lower surfaces of the model. Both 35mm and 16mm still and motion pictures respectively were taken simultaneously to document the flow about each model. A picture showing the wake region

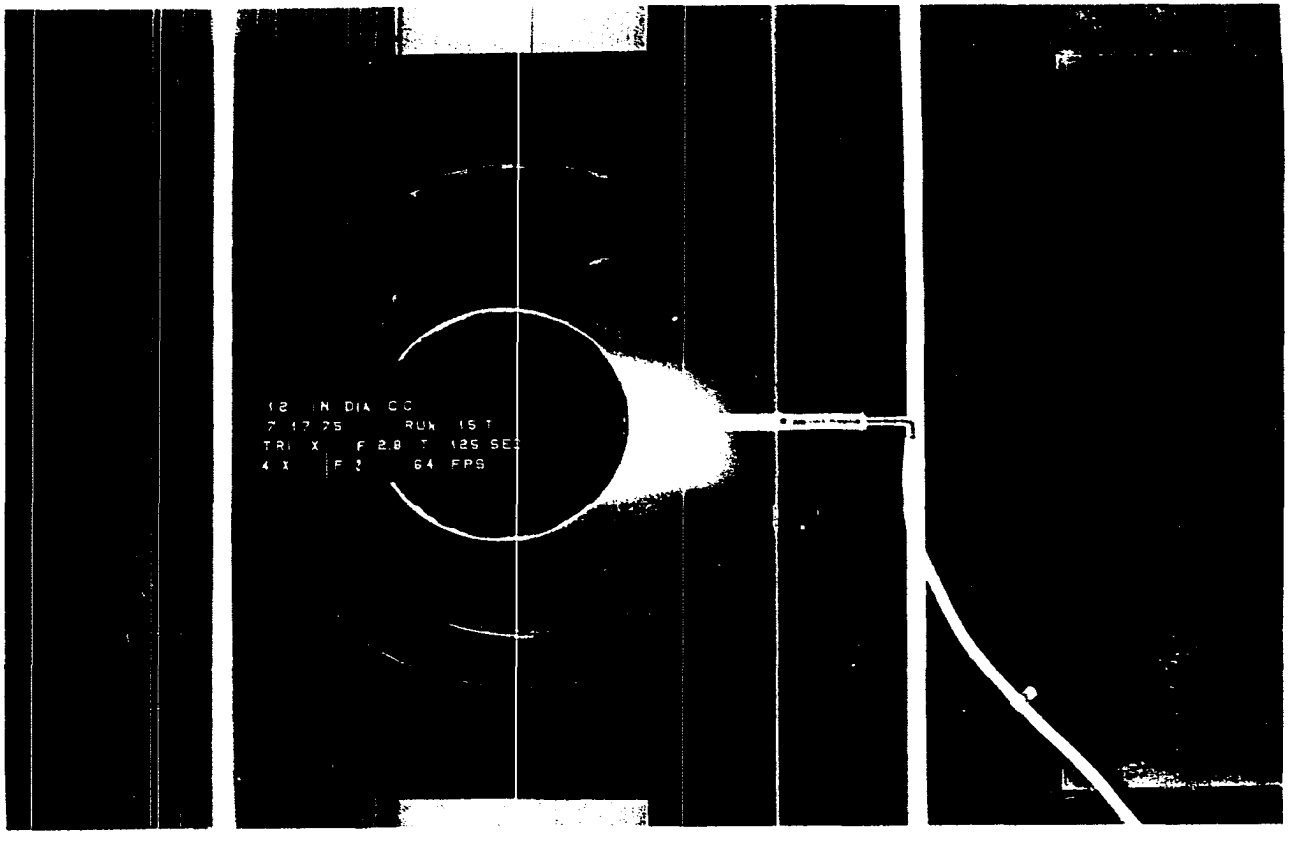

Figure 10. Wake region behind the 11.97 inch diameter circular cylinder at a super critical Reynolds number of 1,060,000 showing turbulent separation.

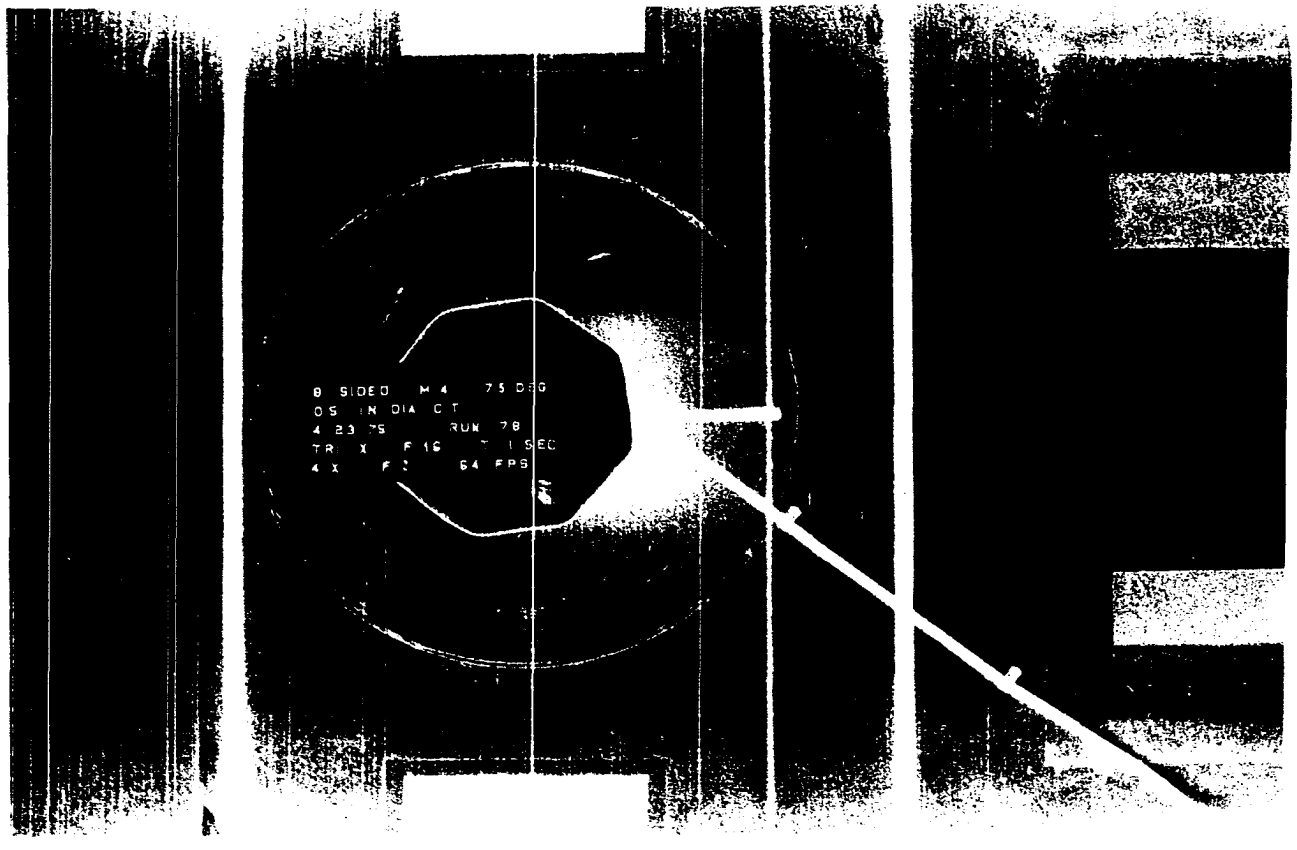

Figure 11. Wake region behind the 12.25 inch diameter octagonal cylinder with 24.5 percent corner radii. Model orientated at 7.5° with respect to the relative wind at a super critical Reynolds number of 1,047,000.

behind the 11.97 inch diameter circular cylinder model is shown in Figure 10 while the wake region behind an octagonal cylinder at 7.5° is shown in Figure 11. The Reynolds number of both flows is in the neighborhood of 10^6. The wake region was outlined since in the flow around bluff bodies it is the location of the wake region that determines the magnitude of both the lift and drag coefficients acting on the body.

DATA PREPARATION

Blockage Corrections

The conditions under which the polygonal models were tested in the wind tunnel differed in only one important aspect from the conditions that exist when the structure is standing in nature. In the wind tunnel the flow past the models is constrained by the top and bottom walls of the test section. These rigid walls prevent the free lateral displacement of the airflow as it passes the body giving rise to what is known as blockage constraint. This constraint modifies the flow patterns around a body and effectively increases the velocity of the flow immersing the body. This increased velocity which is not necessarily uniform throughout the flow field, gives rise to an increase in the forces acting on the body and a correction must be applied if the test results are to provide a firm basis for predicting the behavior of the structure in nature.

Blockage corrections for streamlined bodies are handled by calculating a correction to the free stream velocity based in part on the size of the model and in part on the size of the wake. Methods for determining the corrections can easily be found (17). However, since most testing in the past was done on streamlined bodies, only recently has any attention been paid to the problem of blockage corrections for bluff

bodies where both the lateral displacement of the streamlines and wake size are much greater than for streamlined shapes. Chronologically the history of bluff body corrections began with Glauert (6) who proposed in 1933 that corrections to measured drag D be made according to the equation

$$D_c = D(1-\frac{\eta t}{h})^2 \tag{4}$$

where D_c is the corrected drag, t is the thickness of the base portion of the body included in the wake, h is the height of the tunnel and η is a factor to be determined empirically. As in all such cases where the answer must be known before the correction can be determined, Glauert's method was not widely used (14).

Glauert's work was followed by Thom (23) and then Allen and Vincenti (2) who in 1944 proposed corrections to measured velocity V and drag coefficient C_d for cylinders based on

$$\frac{V_c}{V} = 1 + 0.25C_d \frac{d}{h} + 0.82 \left(\frac{d}{h}\right)^2 \tag{5}$$

$$\frac{C_{d_c}}{C_d} = 1 - 0.50\, C_d \frac{d}{h} - 2.5 \left(\frac{d}{h}\right)^2 \tag{6}$$

where d is the diameter or breadth of the body and the subscript c indicates corrected quantities. In their approach Allen and Vincenti followed the lead of those working in the

streamlined field and assumed the net effect of the blockage was an effective increase in the dynamic pressure of the flow resulting from the increased velocity. In Equations 5 and 6 the second and third terms represent the interference between the wall and the wake and the wall and the body, respectively. Although their analysis neglected any possible effect of the wall on the structure of the wake or on the separation mechanism, it is fairly accurate in regions where the drag coefficient is not changing rapidly with Reynolds number (5,19).

The state of the art remained essentially at this level until the early 1960's. Then due to an increased interest in high lift wings operating near stall and near the ground, researchers began to question the applicability of blockage corrections to bluff bodies that were essentially derived from theories valid only for streamlined flow. This need brought forth several new attempts at solutions to this difficult problem (13,14,15). Perhaps the most widely accepted has been the one put forth by E. C. Maskell in 1965 (14). In his work Maskell still assumed the net effect of blockage to be an effective increase in the free-stream dynamic pressure of the flow, but he obtained his blockage correction by using a simple free-stream representation of the flow around the body and wake and considering the momentum balance within this flow. He also made two assumptions.

First he neglected all effects assumed to be $O[(d/h)^2]$ or higher, and second he assumed that

$$\frac{C_d}{k^2} = \text{const} \tag{7}$$

independent of constraint where k is defined by Equation 8

$$P_T = P_b + k^2 q \tag{8}$$

where P_T and q are the total and dynamic pressures of the undisturbed flow respectively and P_b the average static base pressure on the part of the model within the wake. Upon applying these assumptions to his momentum balance Maskell obtained the relations

$$\frac{k^2}{k_c^2} = \frac{C_d}{C_{d_c}} = \frac{q_c}{q} = \frac{1-C_p}{1-C_{p_c}} \tag{9}$$

where C_p is the pressure coefficient and k_c^2 is obtained from the equation

$$2k_c^2 = 1 + k^2 - \frac{C_d S}{C} + \left(\left(1+k^2 - \frac{C_d S}{C}\right)^2 - 4k^2\right)^{1/2} \tag{10}$$

where C and S are the cross-sectional areas of the test section and model respectively.

An inspection of Equation 9 shows how corrections are applied, based upon the assumption that the net effect of

blockage is an effective increase in the free-stream dynamic pressure of the flow. The basic assumption of this technique is that measured forces or static pressures are correct, but that they were produced by an effective free-stream dynamic pressure larger than that measured. The problem then is to determine this effective dynamic pressure from the measured quantities. In Maskell's approach this involves using C_d and k^2 in Equation 10 to find k_c, and then inserting k_c, along with q and k in Equation 11 to find q_c.

$$q_c = q \frac{k^2}{k_c^2} \tag{11}$$

Since the measured force is assumed correct, the relationship between the values of drag coefficient assuming measured dynamic pressure q and that assuming the effective dynamic pressure q_c is given by Equation 12.

$$D = qC_dS = q_cC_{d_c}S \tag{12}$$

Rearranging this equation can yield either Equation 9 or an expression for the corrected coefficient of drag

$$C_{d_c} = C_d \frac{q}{q_c} \tag{13}$$

Likewise the expressions for corrected coefficient of lift and Reynolds number are given by Equations 14 and 15.

$$C_{L_c} = C_L \frac{q}{q_c} \tag{14}$$

$$Rn_c = Rn \frac{\sqrt{q_c}}{\sqrt{q}} \tag{15}$$

In general, test results have validated Maskell's claim that this correction works for blockage ratios of less than 10 percent; however, for bluff bodies in which the base pressure distribution is essentially constant, as in the case of the bodies tested in this project, it has been shown to be valid to blockage ratios considerably higher than this (5). It should be pointed out that for blockage ratios greater than 10 percent both this author and others (5) have found that the radical in Equation 10 becomes negative and Maskell's correction fails. Results from this work indicate body shape as well as blockage ratio influences the breakdown of Maskell's correction with, for a fixed blockage ratio, the correction working better for the sharp cornered models than for those more circular in cross-section.

In recent years the concept of the net effect of blockage being to increase the dynamic pressure of the free-stream flow has been challenged and a new approach, the free-stream method, has been put forth. The free-stream method is a numerical technique which utilizes point sources and vortices, plus empirically determined separation points, to model the

potential flow around the body and the wake behind it. The premise behind the new technique is that the effects of the walls on the flow will vary around the body and therefore the net effect of blockage cannot be handled by a simple increase in free-stream dynamic pressure. At the present time this method has just been extended to cover general body shapes (5) and is still too complicated for use except for simple shapes.

The methods briefly outlined above represent the state of the art in bluff body blockage corrections at the present time. Although some methods do work better than others, they all have their shortcomings and because of this, it is still widely agreed that the application of blockage corrections to bluff bodies is still in its infancy and must be approached with extreme caution on a case by case basis. With this in mind it was decided to attempt to use Maskell's corrections for two reasons. First they apparently work as well on cylindrical type bodies as any of the methods found (5), and secondly they are much easier to apply. It was found, as will be documented shortly, that these corrections worked as well as could be expected on models with diameters up to 12 inches. For the 24 inch models the radical in Equation 10 became negative and the method failed. For these models the method of Allen and Vincenti was used with acceptable success, limiting its use to Reynolds numbers

greater than the critical Reynolds number for reasons discussed above.

A series of models was included in the research program for the purpose of attempting to document the success of blockage corrections. These models included the 11.97 inch diameter circular cylinder that has been previously mentioned, both a 6.06 inch and a 24.06 inch diameter circular cylinder and several polygonal cylinders that will be discussed later. The circular cylinders were included solely for base line data and for validating the boundary corrections. The results of using Maskell's corrections on the 6 and 12 inch cylinders and those due to Allen and Vincenti on the 24 inch diameter cylinder are shown in Figure 12. Figure 12 demonstrates one of the main problems that arises when data from several diameter cylinders is compared, namely the problem of surface roughness. Shown in the figure are curves for cylinders having ratios of RMS surface roughness to model diameter of 1.11×10^{-5}, 110×10^{-5}, and 450×10^{-5} taken from references 12 and 1 respectively. As is pointed out in references 1 and 22 and is obvious from the figure, increasing surface roughness to model size shifts the drag coefficient vs. Reynolds number curve up and to the left. This means that any attempts to match data from circular cylinders must also take into account surface condition.

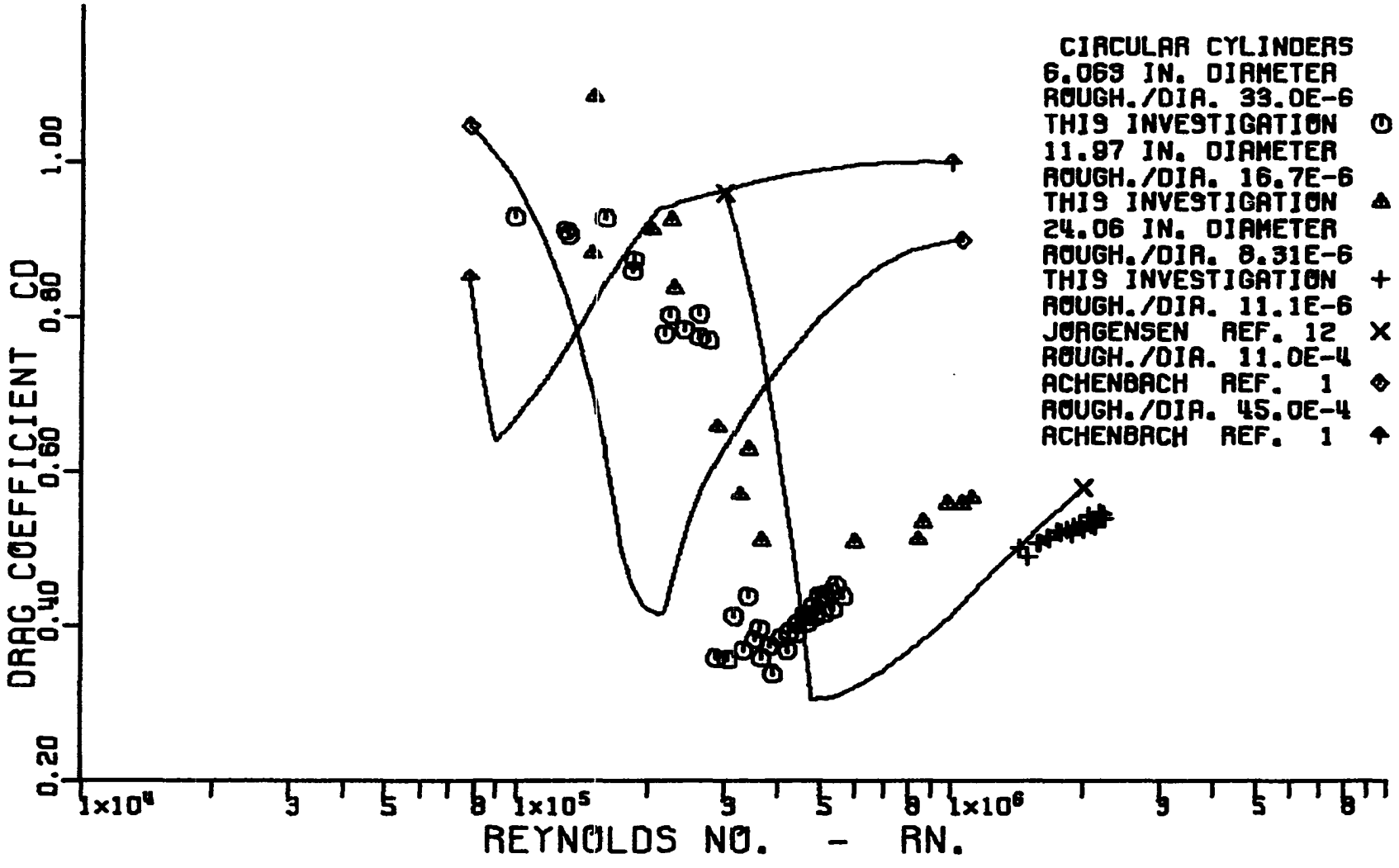

Figure 12. Variation of corrected cross-flow drag coefficient with corrected cross-flow Reynolds number for circular cylinders at cross-flow Mach numbers less than 0.2.

All models tested in the project had surface roughness RMS values of approximately 200 microinches. This yielded surface roughness to model diameter ratios of 3.3×10^{-5}, 1.66×10^{-5} and 0.83×10^{-5} for the 6.06, 11.97 and 24.06 inch diameter cylinders respectively. Comparing the corrected data for these cylinders with that from references 1 and 12, it is seen that within experimental uncertainty, all of the data falls in the proper place. Based on this, the same corrections were then applied to the 8-, 12- and 16-sided polygonal cylinders. As mentioned above, several polygonal cylinders were included in the tests, in addition to the circular cylinders, for the purpose of checking blockage corrections. These models included octagonal cylinders measuring 6.22 and 24.30 inches between parallel flat sides, dodecagonal cylinders measuring 6.23 and 24.24 inches between parallel flat sides and hexdecagonal cylinders measuring 6.23 and 24.21 inches between parallel flat sides. These polygonal cylinders were all constructed with corner radii approximately equal to 24.5 percent of the radius of the inscribed circular cylinder in an attempt to make them similar to one of the 12 inch diameter models being tested for data. The corrected test data for these 6, 12 and 24 inch models are shown in Figures 14-17 for the octagonal cylinders, Figures 18-21 for the dodecagonal cylinders and Figures 22-24 for the hexdecagonal cylinders. Data was taken

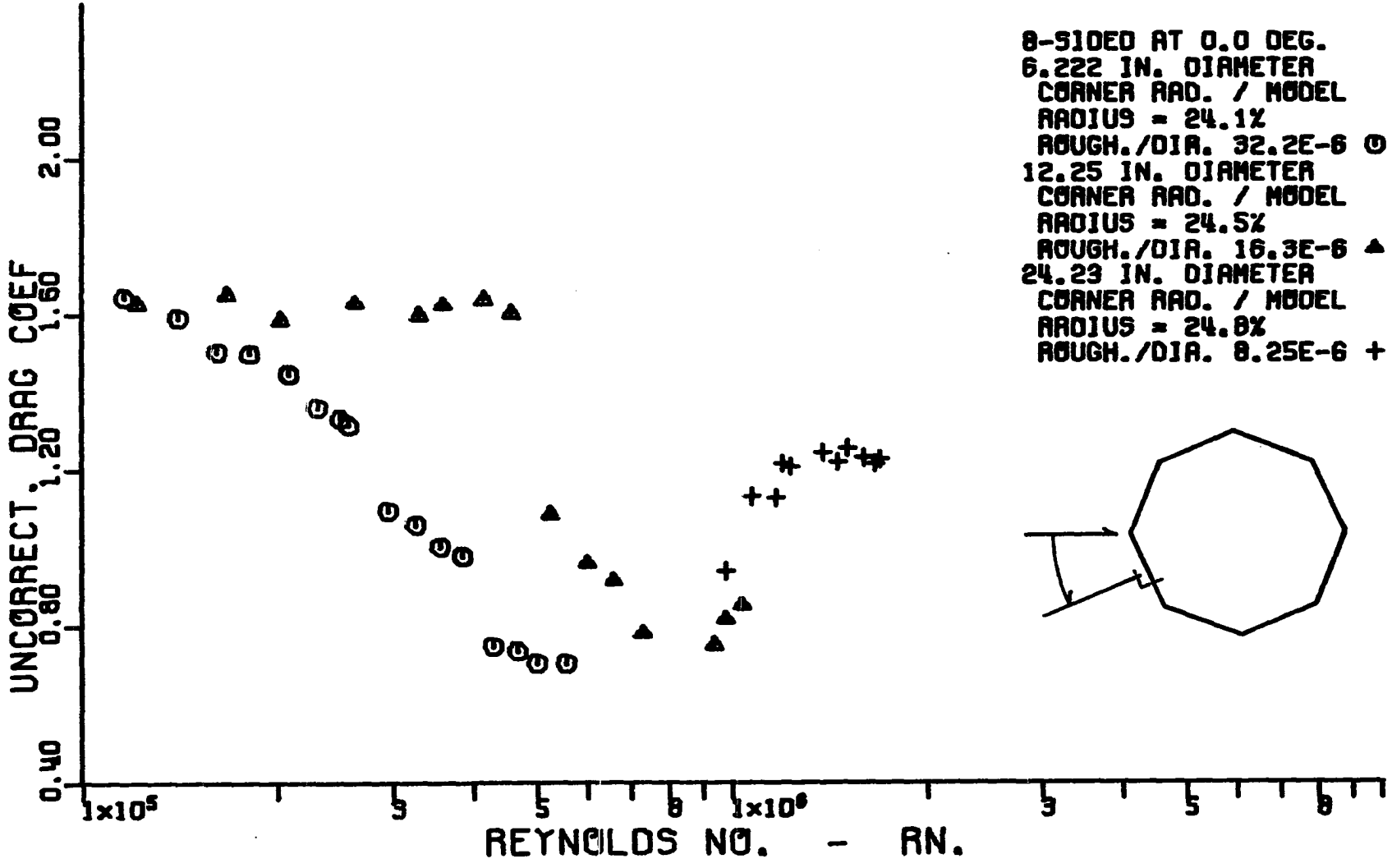

Figure 13. Variation of uncorrected cross-flow drag coefficient with uncorrected cross-flow Reynolds number for similar octagonal cylinders. Models orientated at 0.0° with respect to the relative wind.

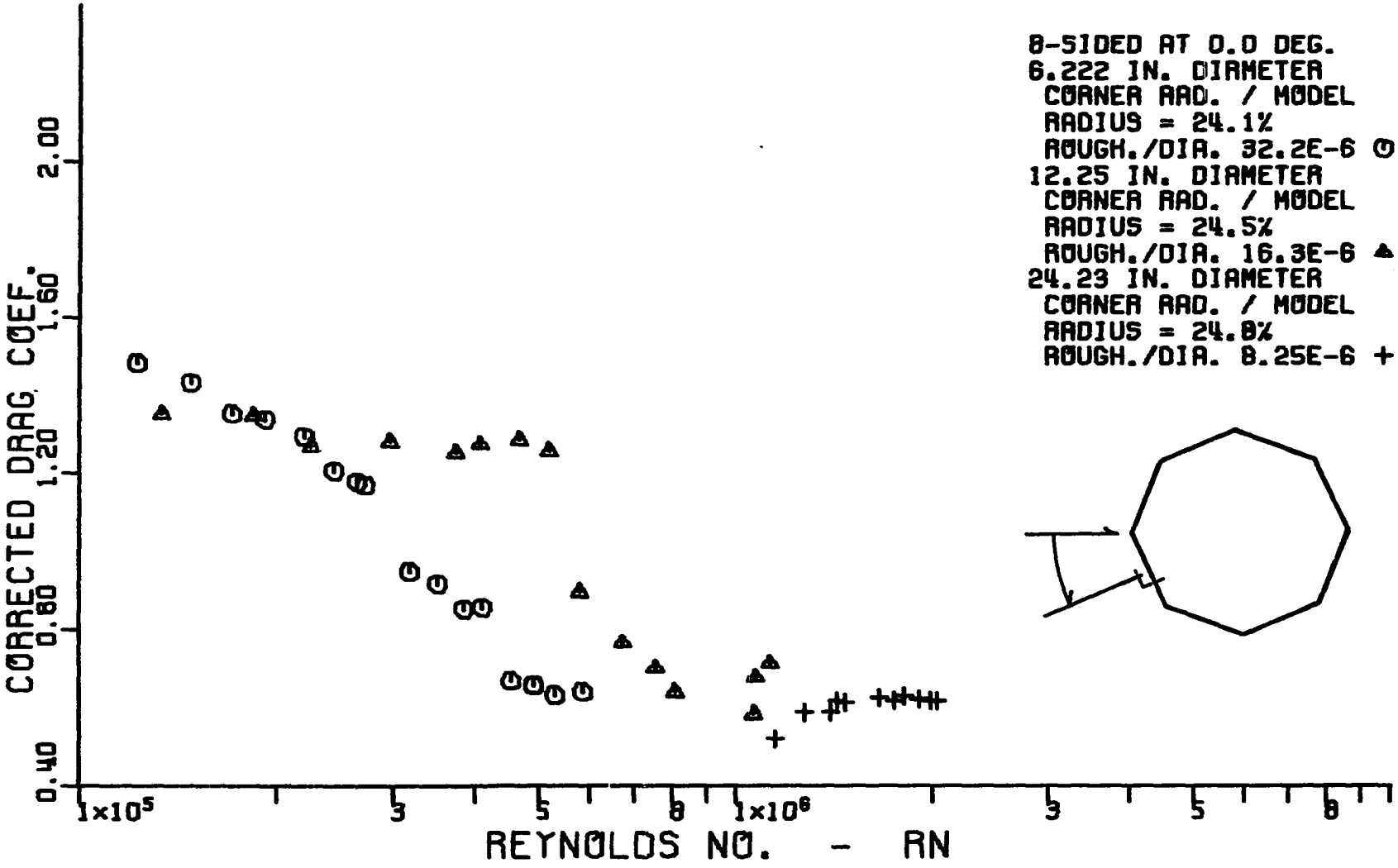

Figure 14. Variation of corrected cross-flow drag coefficient with corrected cross-flow Reynolds number for similar octagonal cylinders. Models orientated at 0.0° with respect to the relative wind.

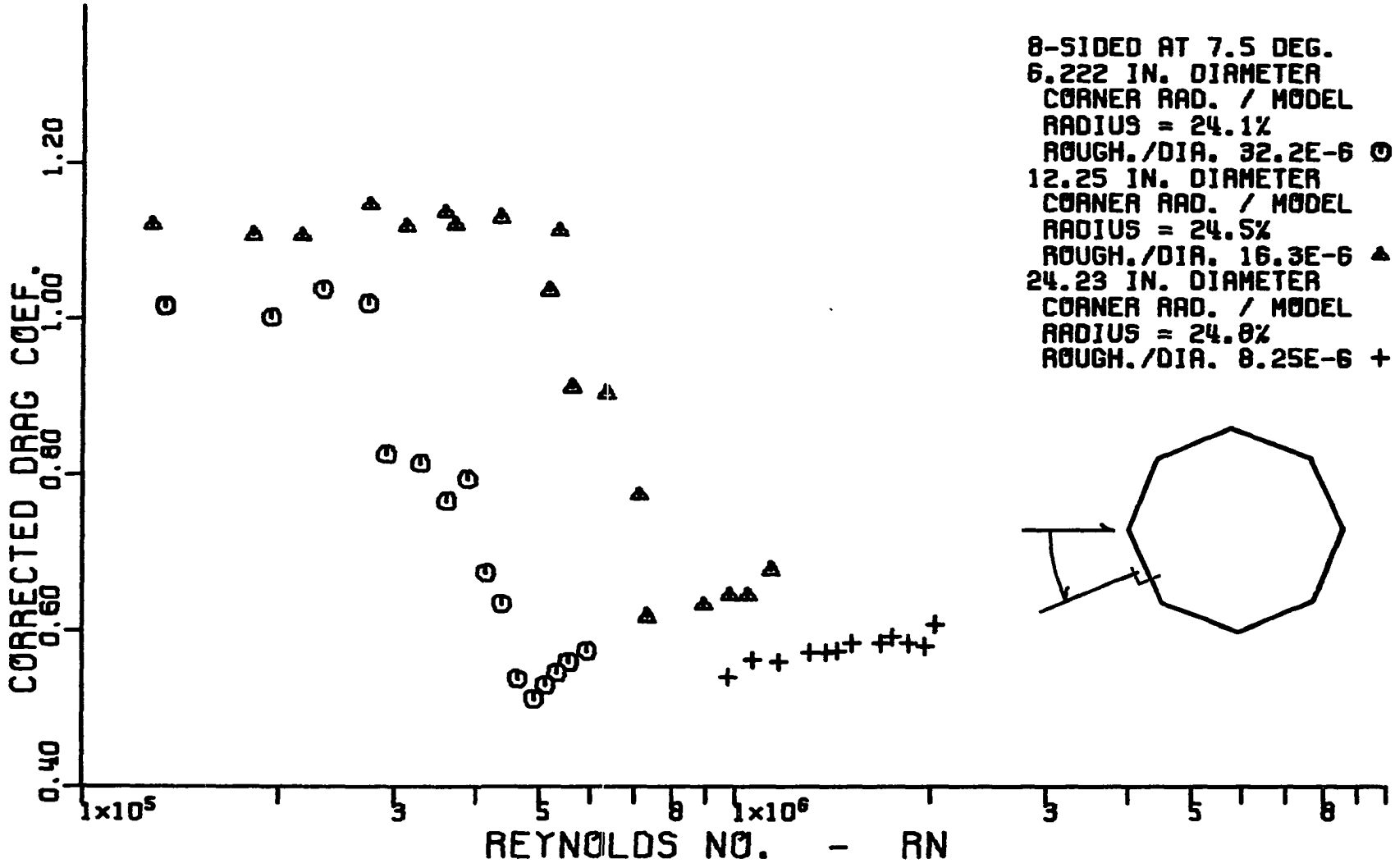

Figure 15. Variation of corrected cross-flow drag coefficient with corrected cross-flow Reynolds number for similar octagonal cylinders. Models orientated at 7.5° with respect to the relative wind.

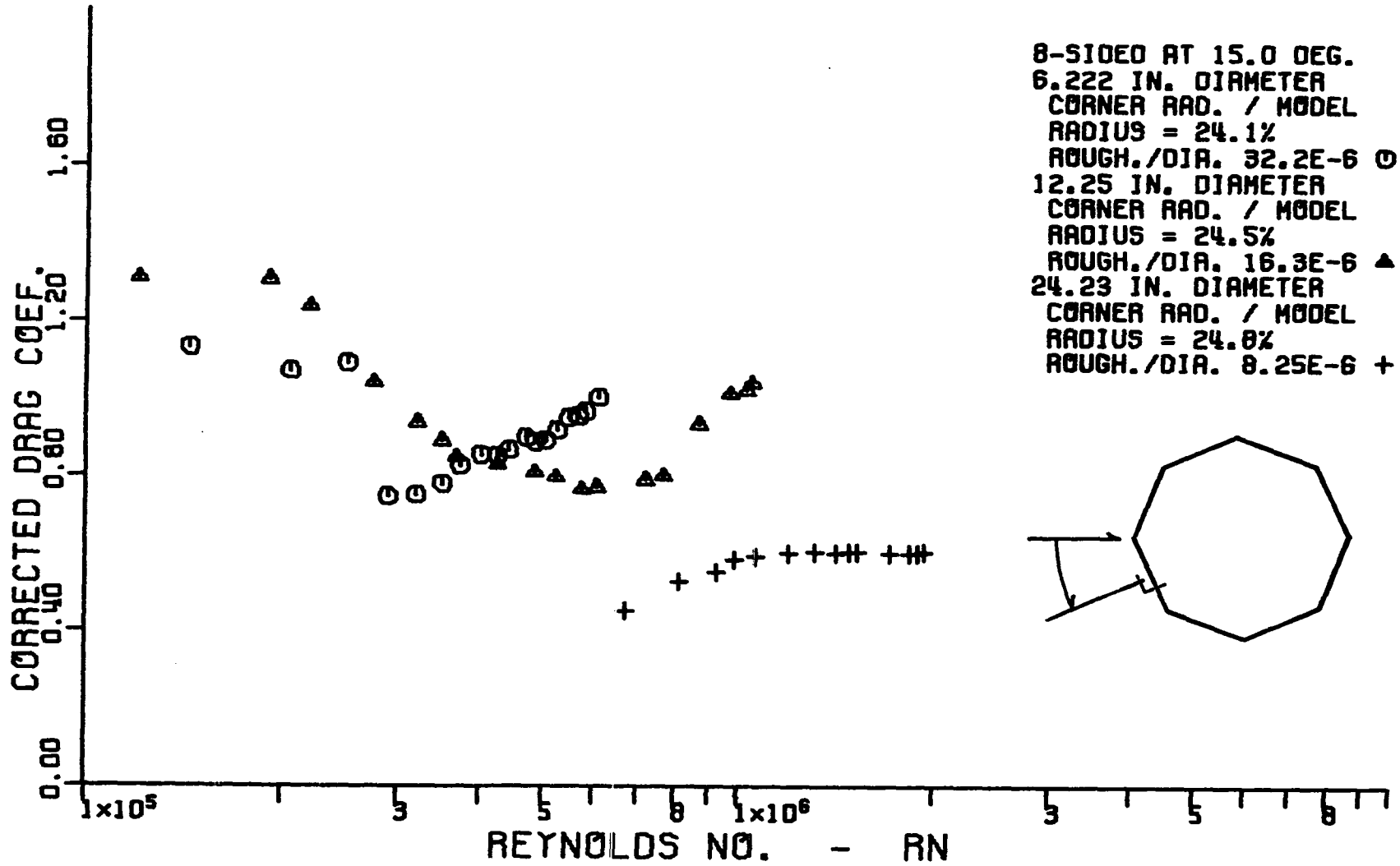

Figure 16. Variation of corrected cross-flow drag coefficient with corrected cross-flow Reynolds number for similar octagonal cylinders. Models orientated at 15.0° with respect to the relative wind.

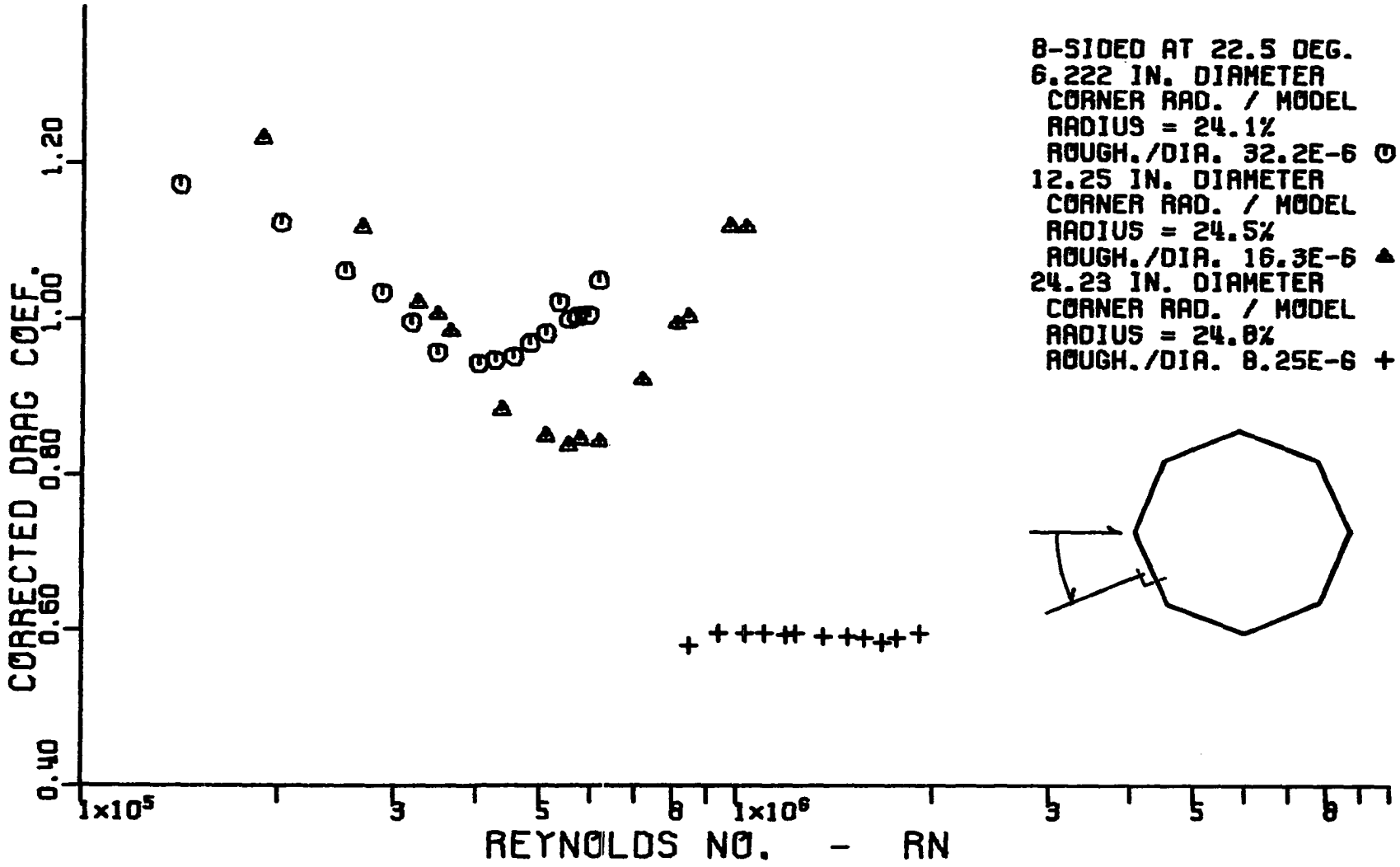

Figure 17. Variation of corrected cross-flow drag coefficient with corrected cross-flow Reynolds number for similar octagonal cylinders. Models orientated at 22.5° with respect to the relative wind.

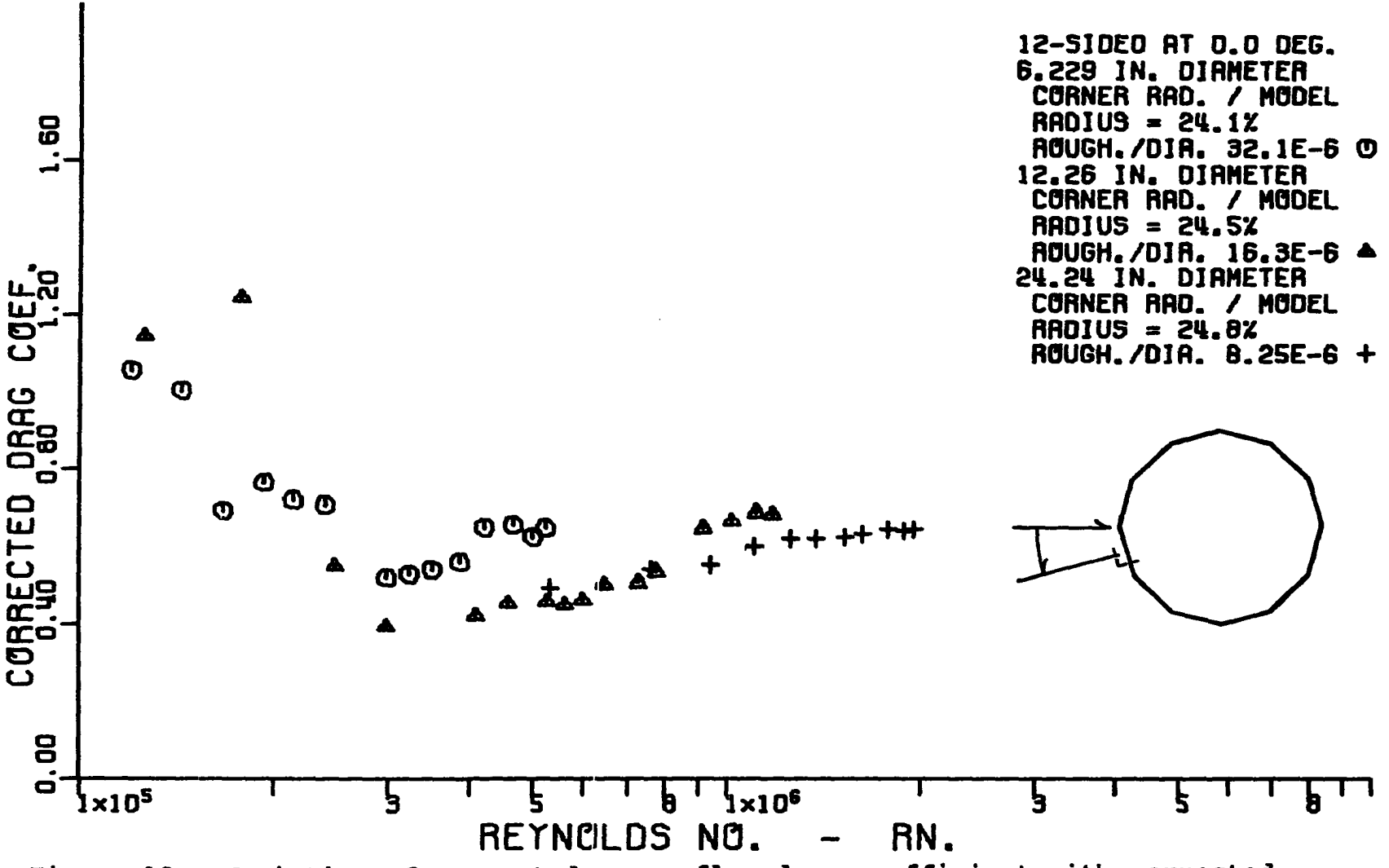

Figure 18. Variation of corrected cross-flow drag coefficient with corrected cross-flow Reynolds number for similar dodecagonal cylinders. Models orientated at 0.0° with respect to the relative wind.

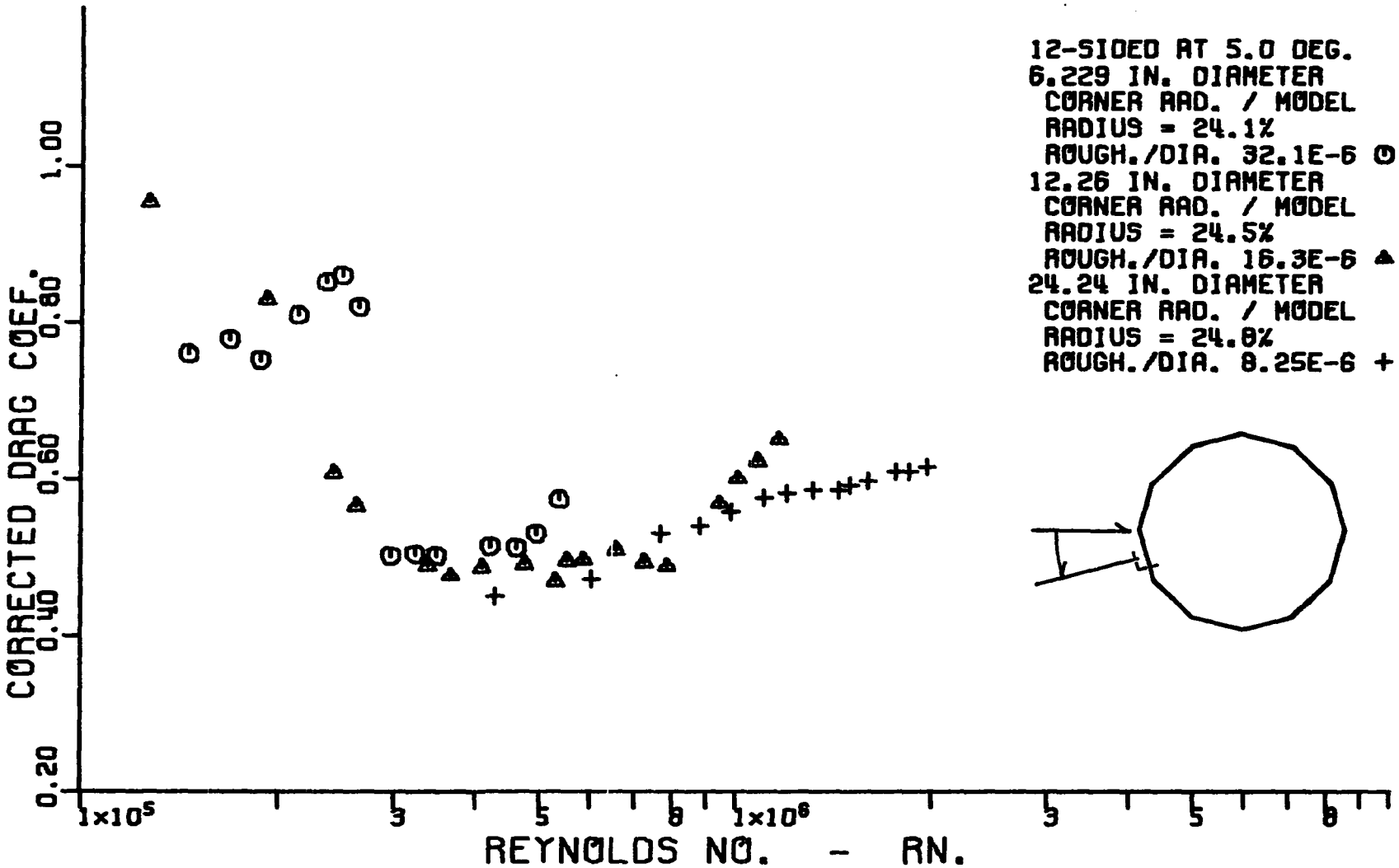

Figure 19. Variation of corrected cross-flow drag coefficient with corrected cross-flow Reynolds number for similar dodecagonal cylinders. Models orientated at 5.0° with respect to the relative wind.

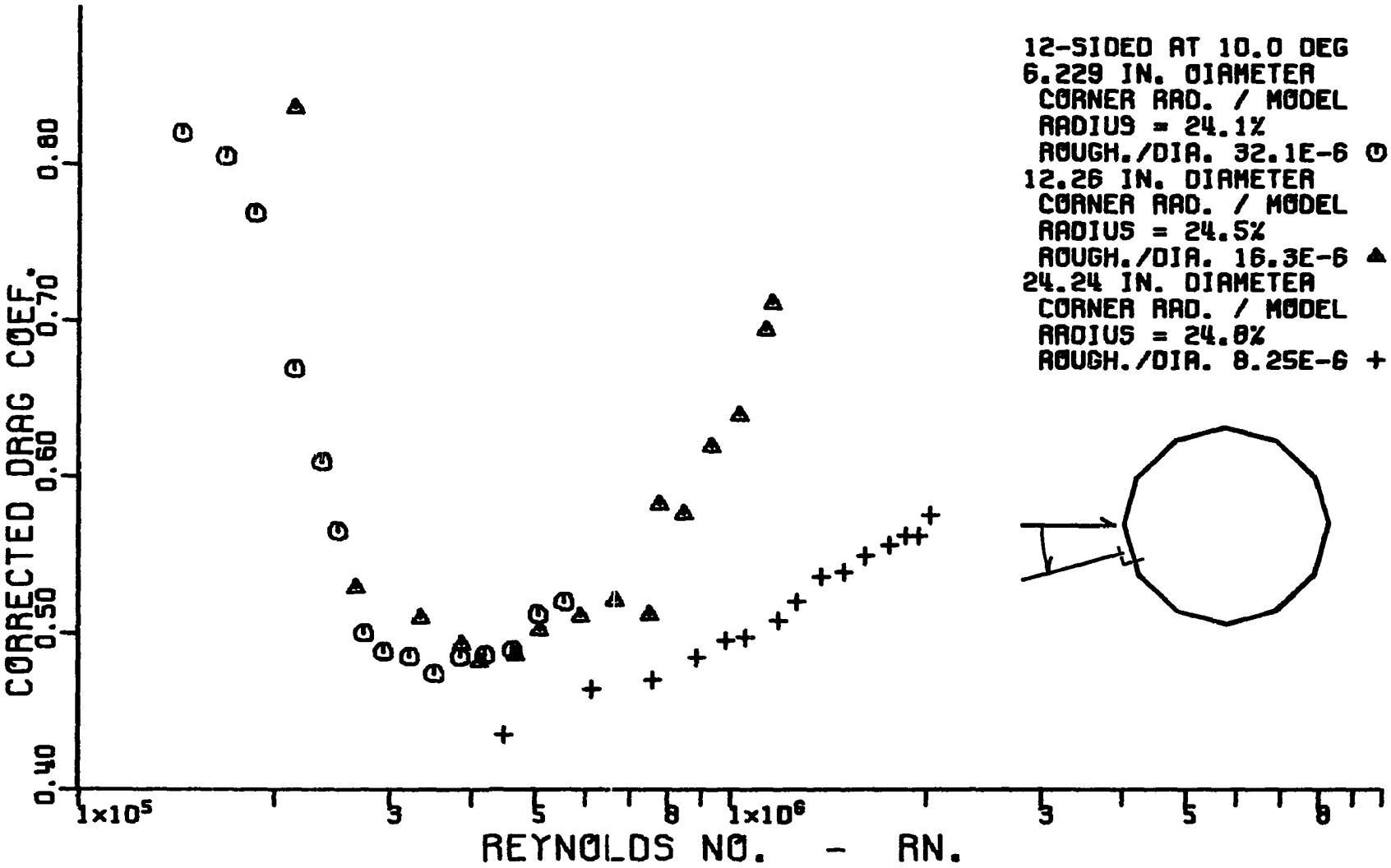

Figure 20. Variation of corrected cross-flow drag coefficient with corrected cross-flow Reynolds number for similar dodecagonal cylinders. Models orientated at 10.0° with respect to the relative wind.

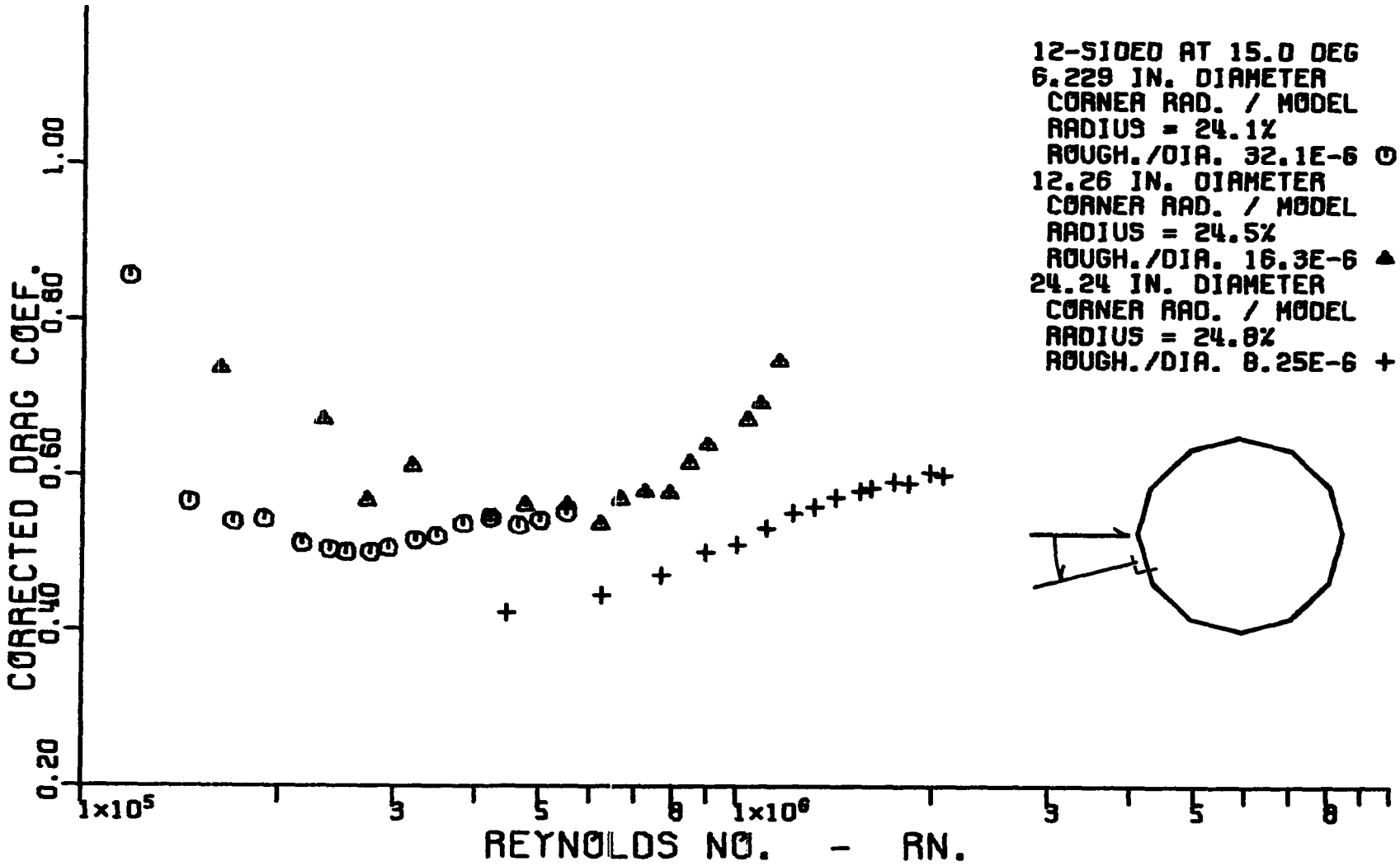

Figure 21. Variation of corrected cross-flow drag coefficient with corrected cross-flow Reynolds number for similar dodecagonal cylinders. Models orientated at 15.0° with respect to the relative wind.

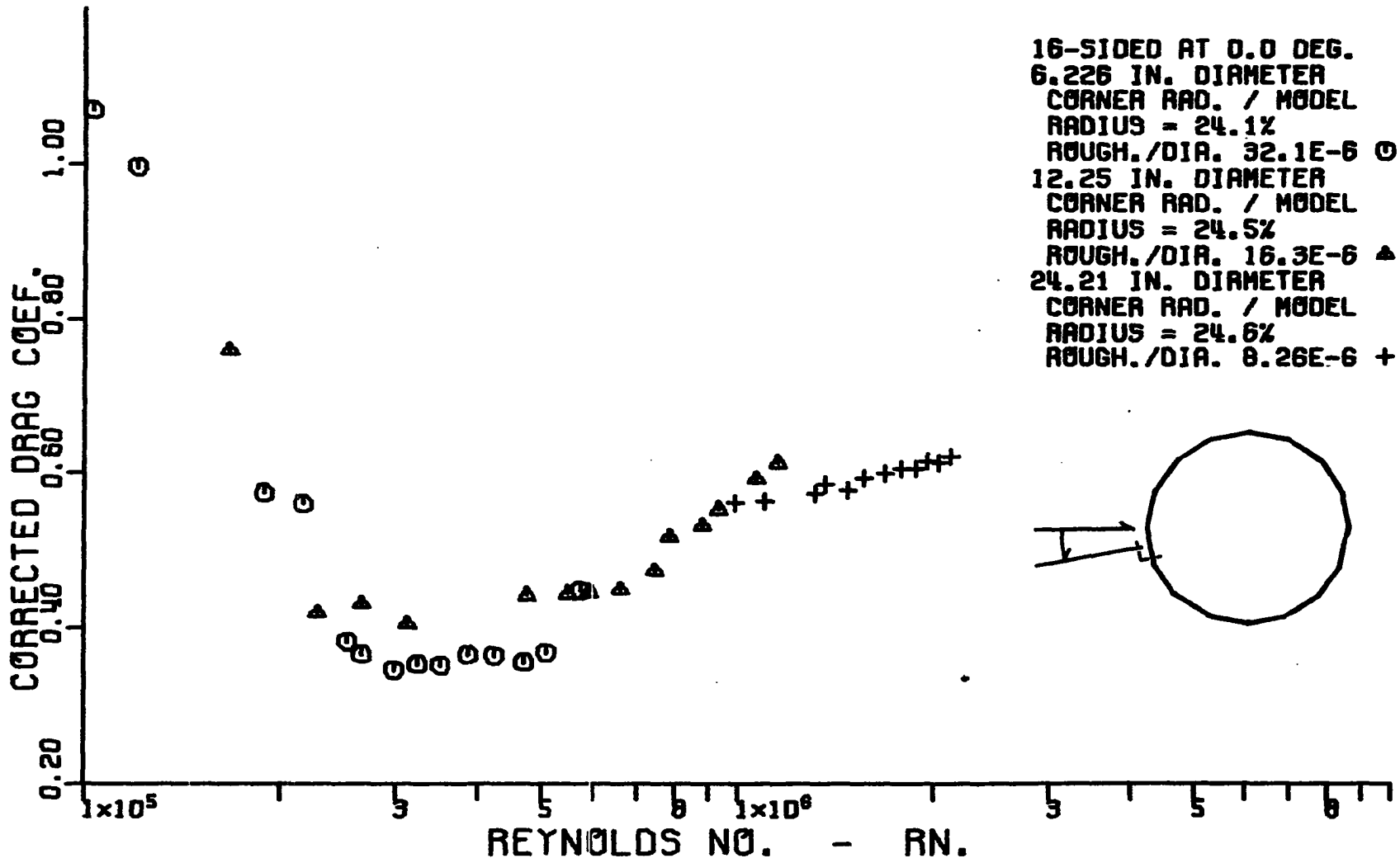

Figure 22. Variation of corrected cross-flow drag coefficient with corrected cross-flow Reynolds number for similar hexdecagonal cylinders. Models orientated at 0.0° with respect to the relative wind.

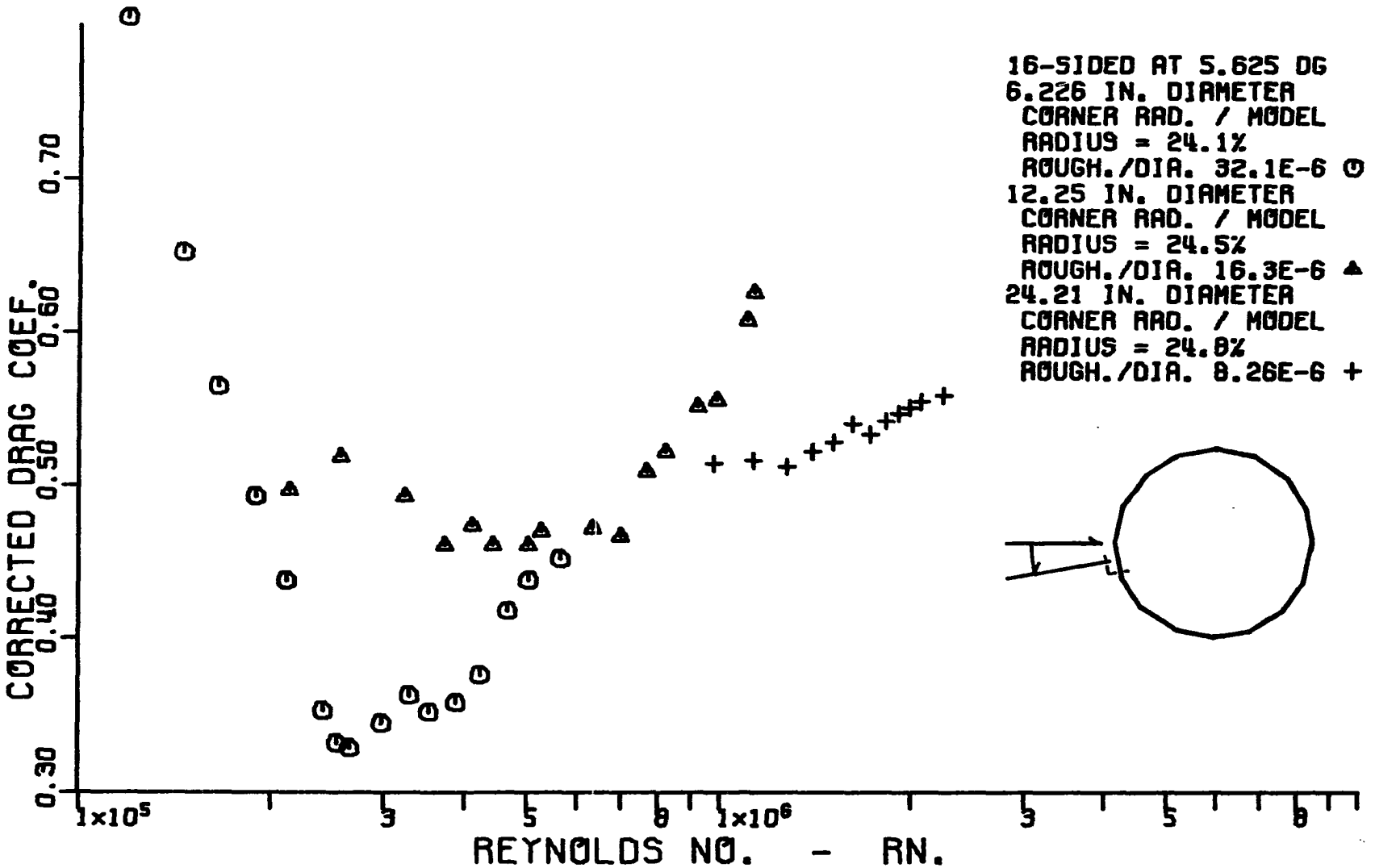

Figure 23. Variation of corrected cross-flow drag coefficient with corrected cross-flow Reynolds number for similar hexdecagonal cylinders. Models orientated at 5.625° with respect to the relative wind.

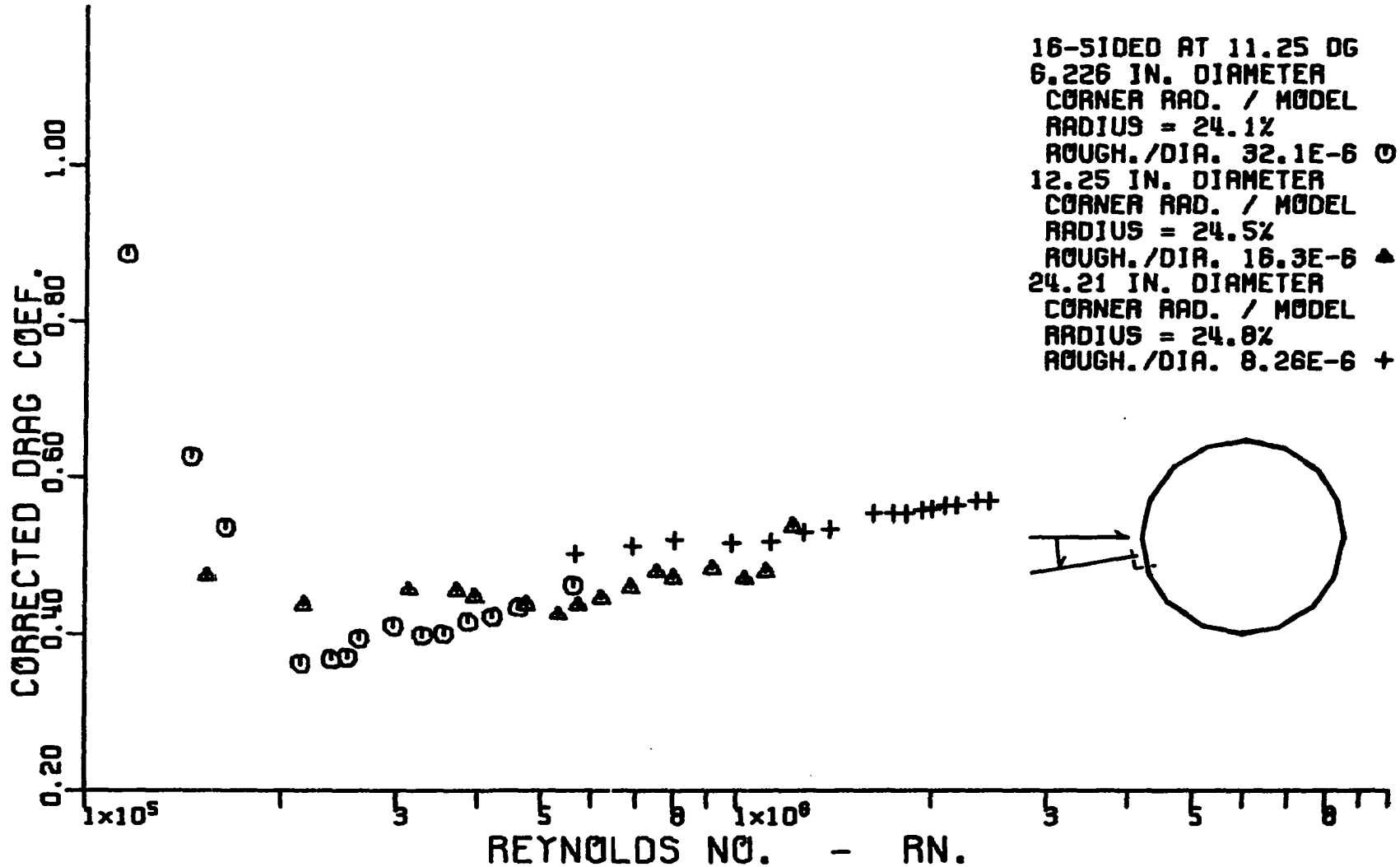

Figure 24. Variation of corrected cross-flow drag coefficient with corrected cross-flow Reynolds number for similar hexdecagonal cylinders. Models orientated at 11.25° with respect to the relative wind.

for all models at two rotations, with a flat surface perpendicular to the relative wind and the second with a corner pointing directly into the relative wind. For the 16-sided cylinders data was also taken at a third orientation, one-half way between the other two, while for the 8- and 12-sided cylinders data were taken at two orientations equally spaced between the extremes. The effects and magnitudes of the blockage corrections on the drag coefficient and Reynolds number can be seen by comparing the results shown in Figures 13 and 14. Data for the octagonal cylinders at 0.0° rotation are shown in these figures, the uncorrected data in Figure 13 and the corresponding corrected data in Figure 14. It will be noticed that the corrections get larger as the model size and hence blockage ratio increase. Drag corrections run from around a 7 percent decrease in drag coefficient for the 6 inch models to 15 percent for the 12 inch and about 50 percent for the 24 inch models. These percentages remain fairly constant, independent of body cross section and model rotation. The blockage corrections decrease the measured drag coefficient and increase the measured Reynolds number. In general the behavior of the corrected data follows the trends described above for the circular cylinders; however there are exceptions such as Figure 24 where the curves shift up and to the right for decreasing relative roughness. The only explanation that can be offered is the dissimilarities

of the models.

The models were constructed using essentially the production line techniques used in the construction of the actual luminaire towers. They were formed in two halves using a break press and then welded together and because of this are not perfect; i.e., each corner and face is not exactly like every other corner or face on the model. Thus the models are not symmetrical nor perfectly similar to the other models of the same family having different diameters. Therefore, deviations from the predicted behavior are not only possible but should be expected. Because of this, although not all figures show the expected trend, it is felt they sufficiently demonstrate the validity of the boundary corrections applied to justify the assumption that the blockage effects have been removed from the results. If there is any error, it would appear to be that the corrections to the 12 inch models are slightly too small since it could be argued that the 12 inch results often appear to be a little large when compared to the 6 inch results. Due to the numerous factors affecting the results, such as relative roughness, surface irregularities, and nonsimilarities, it is impossible to verify this. Such an error, if it exists, makes the final values conservative and therefore safe if used as a standard.

Data Reduction

As stated earlier the model surface pressures were displayed on 52-tube manometer boards which were photographed to both provide a permanent record and to permit analysis at a later date. At the time the slides were analyzed they were projected on a screen at approximately one and one-half times full size and the heights of the water in the tubes recorded. Heights were determined using the tube background, 10 x 10 to the inch graph paper, as the measuring scale. Tests in which the same slides were read by two or more people indicated that the tube heights could be read to an accuracy of ±0.01 inch. At low Reynolds numbers, in the range of 250,000, this accuracy resulted in possible reading errors as large as ±3 percent, a value which increased considerably at the lower Reynolds numbers. However for increasing Reynolds numbers, the range of real interest for simulation, the possible reading error was below ±1 percent for most manometer tubes at a Reynolds number of 350,000 and continued to decrease as Reynolds number increased. An example of the 35mm slide of the manometer boards is shown in Figure 25.

The data read from the 35mm slides was punched on cards and reduced by digital computer to corrected lift and drag coefficients and Reynolds number, with the coefficients of lift and drag being obtained using a numerical integration

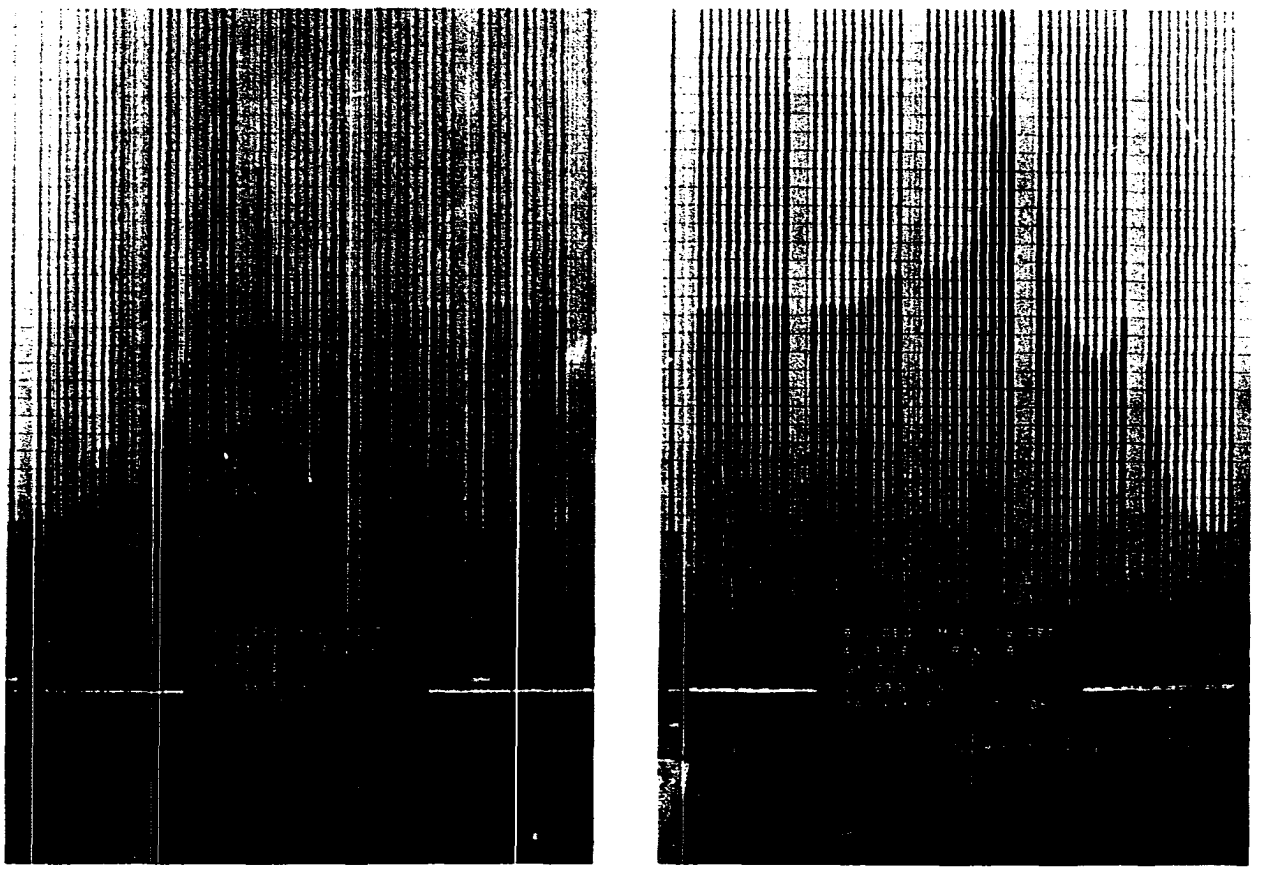

Figure 25. Photographs of the manometer boards showing the surface static pressure variation around the 12.25 inch diameter octagonal cylinder with 24.5 percent corner radii. Model orientated at 7.5° with respect to the relative wind at a super critical Reynolds number of 1,047,000.

based on Simson's Rule. Since this required knowledge of the coordinates of every pressure port, each shape was defined by a mathematical model. This model assumed symmetry, with the dimensions, port locations and corner radii the same for every side. The dimensions and distances between ports used for the mathematical model were the average of the measured values obtained from the actual wind tunnel models. The measurements of the wind tunnel models indicated that the symmetry of the actual models was off no more than 0.25 inch in 12.25 inches or by approximately 2 percent. Because of this it was felt that the use of the theoretical mathematical model was acceptable. In this reduction a correction was applied to the measured values of manometer tube heights to account for the parallax due to the camera.

The determination of the coefficient of drag from the integration of the surface static pressures as is done in this report assumes that the drag force due to skin friction is negligibly small compared to the drag due to the pressure or form drag. Experimental measurements have verified this assumption (1) and found that for circular cylinders the skin friction forces are approximately 1 percent of the total drag force in the subcritical range of Reynolds numbers and 3 percent in the supercritical flow range. This increase in the importance of skin friction is due to the significant decrease in drag that occurs at the critical Reynolds number

which will be discussed in more detail in the next chapter. For the polygonal cylinders studied in this project the relative magnitude of skin friction to total drag forces should be of the same order of magnitude as those just mentioned. These percentages will decrease for cylinders which have a drag greater than that of the circular cylinder and increase slightly for those cylinders having less drag.

The final corrected results are affected by the errors in similarity, symmetry, blockage corrections and measurements discussed above. Of these, the error in the final results due to the error in the blockage corrections used is the hardest to judge since there exists no fixed standard against which these errors can be measured. However, as stated above it is felt that the blockage effects were successfully removed by Maskell's method. Because of this and because the errors in similarity, symmetry and measurements have been shown to be small, it is believed that the final corrected results are accurate to within ± 5 percent of the actual values.

RESULTS

Variation of Force Coefficients with Corner Radius

As was mentioned in the Introduction, the objectives of the research project reported in this paper were first, to find the variation of the coefficients of lift and drag with change in Reynolds number for several families of polygonal cylinders, with each family of cylinders having several corner radii, and second to try to find an empirical relationship between the variation in drag coefficient with variation of corner radii at a fixed Reynolds number. The families of polygonal cylinders studied were those having 8, 12 and 16 sides while the corner radii studied were 0.0, 9.1, 17.5, 24.5, 40.5, 57.7 and 74.2 percent of the radius of the inscribed circular cylinder. In order to determine the variation of forces with model rotation the octagonal cylinders were tested at 0°, 7.5°, 15° and 22.5°, the dodecagonal cylinders at 0°, 5°, 10° and 15° and the hexdecagonal cylinders at 0°, 5.6° and 11.25°.

Coefficient of drag

Partial results are shown in Figures 26 to 36 where the variation in corrected drag coefficient is plotted versus variation in corrected Reynolds number for constant model-relative wind orientations. In these figures data are plotted

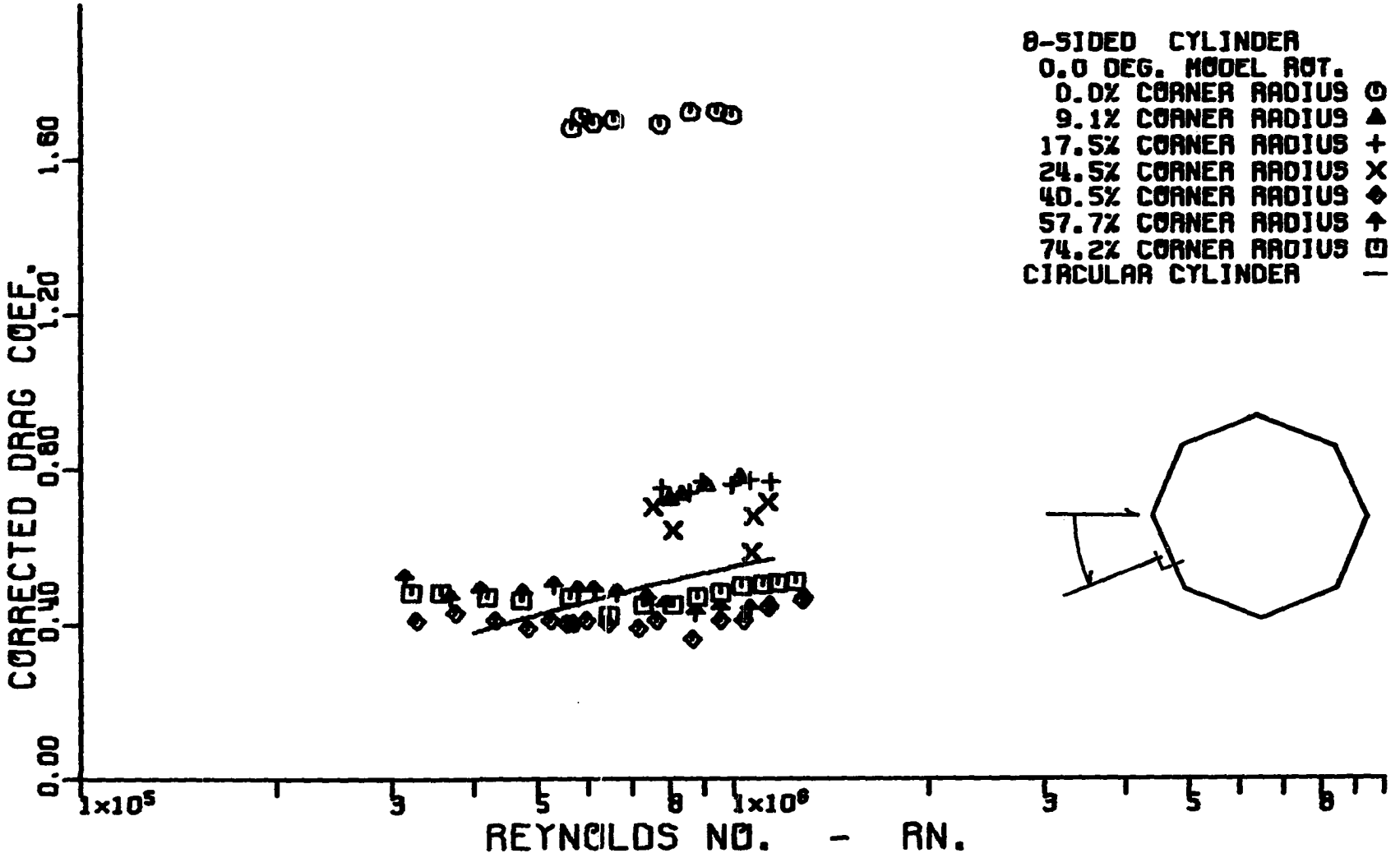

Figure 26. Variation of corrected cross-flow drag coefficient with corrected cross-flow Reynolds number for octagonal cylinders. Models orientated at 0.0° with respect to the relative wind.

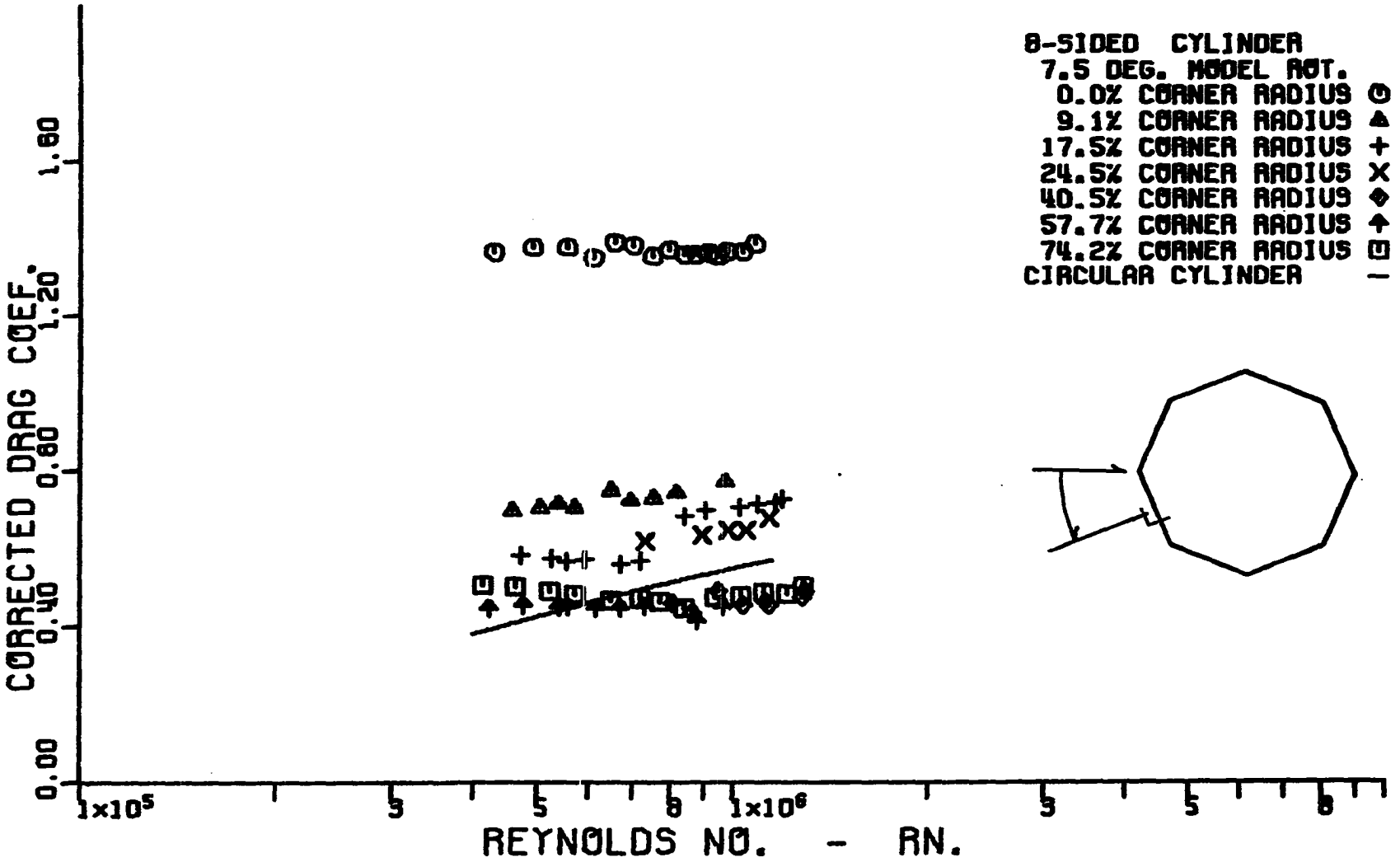

Figure 27. Variation of corrected cross-flow drag coefficient with corrected cross-flow Reynolds number for octagonal cylinders. Models orientated at 7.5° with respect to the relative wind.

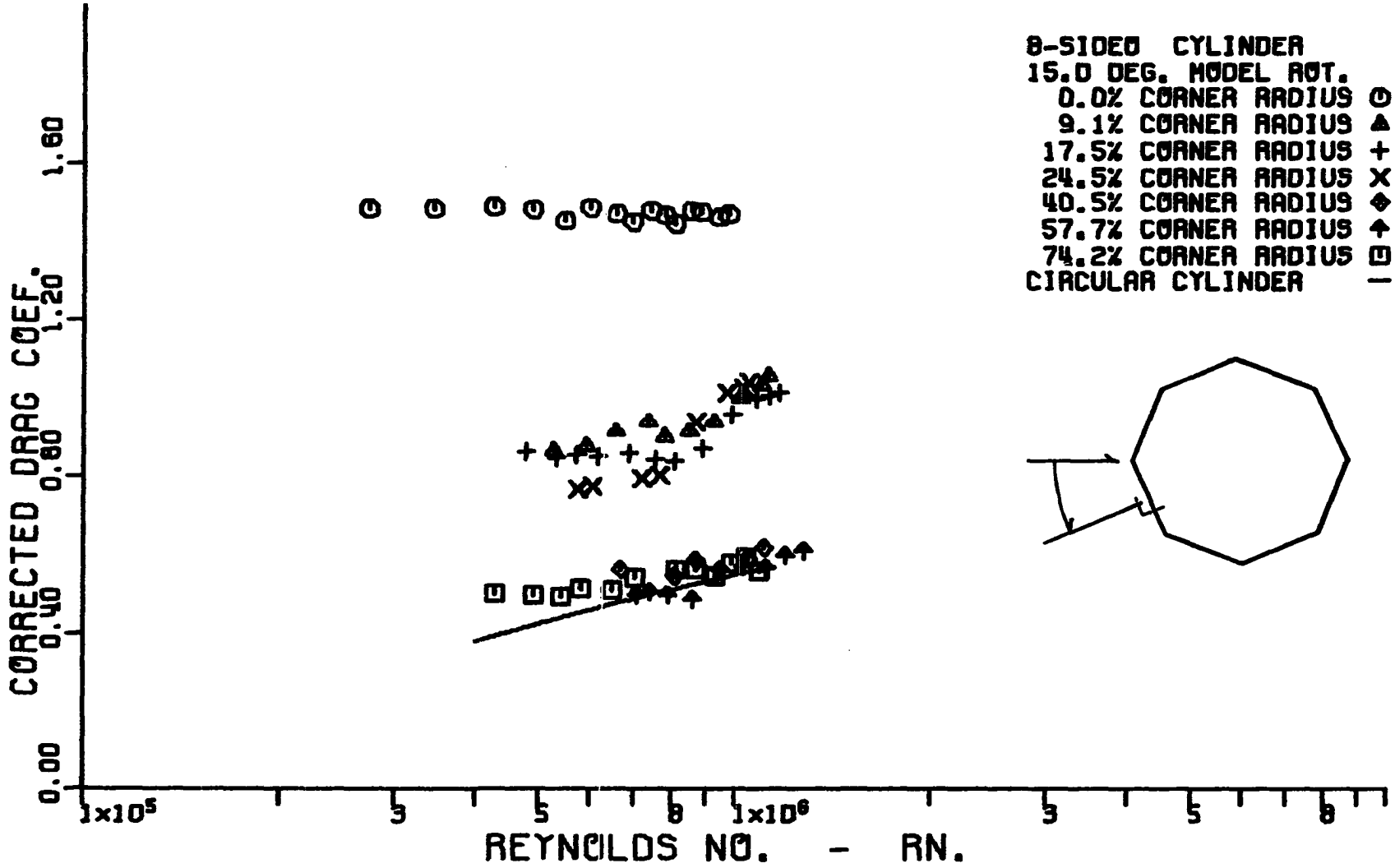

Figure 28. Variation of corrected cross-flow drag coefficient with corrected cross-flow Reynolds number for octagonal cylinders. Models orientated at 15.0° with respect to the relative wind.

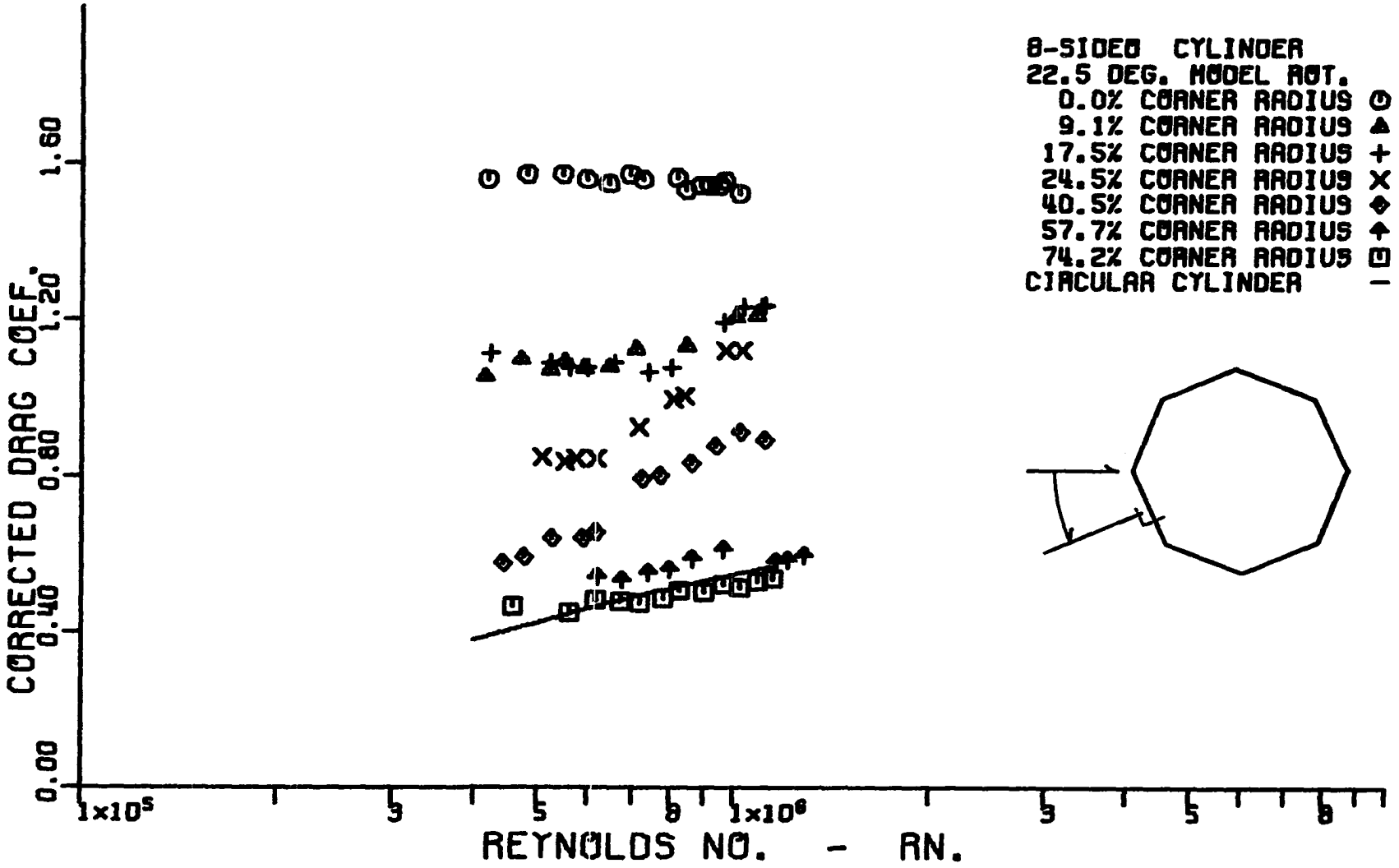

Figure 29. Variation of corrected cross-flow drag coefficient with corrected cross-flow Reynolds number for octagonal cylinders. Models orientated at 22.5° with respect to the relative wind.

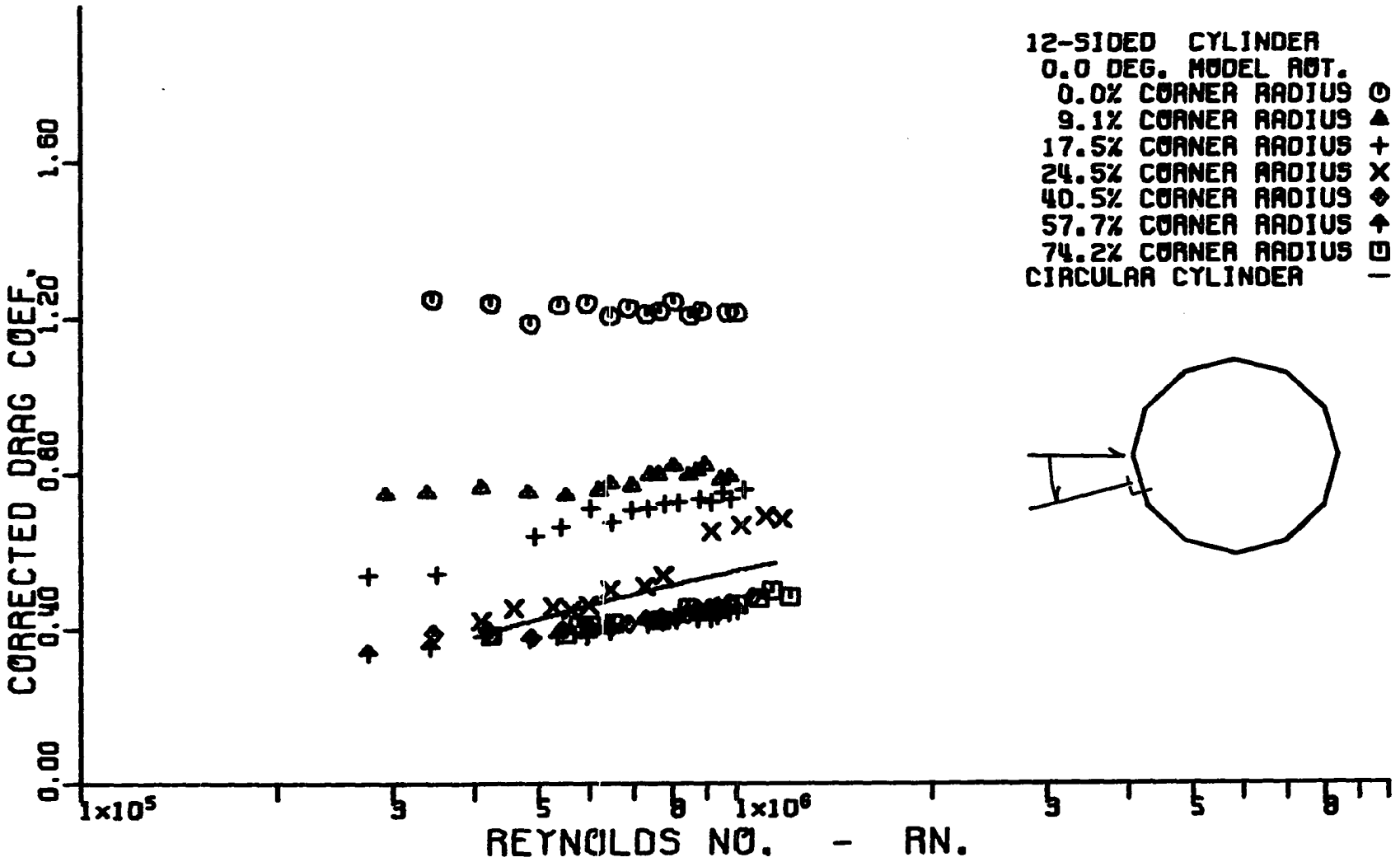

Figure 30. Variation of corrected cross-flow drag coefficient with corrected cross-flow Reynolds number for dodecagonal cylinders. Models orientated at 0.0° with respect to the relative wind.

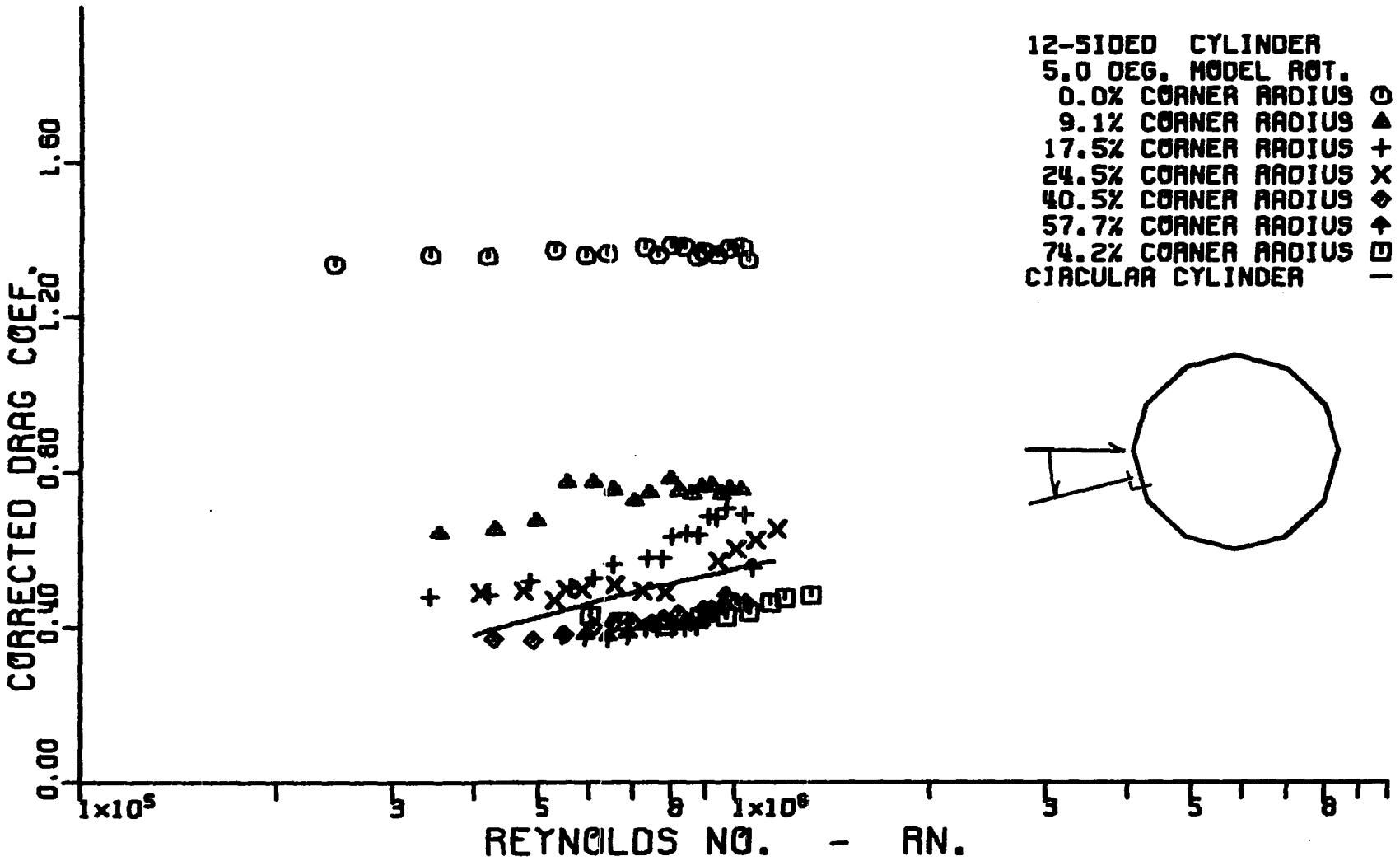

Figure 31. Variation of corrected cross-flow drag coefficient with corrected cross-flow Reynolds number for dodecagonal cylinders. Models orientated at 5.0° with respect to the relative wind.

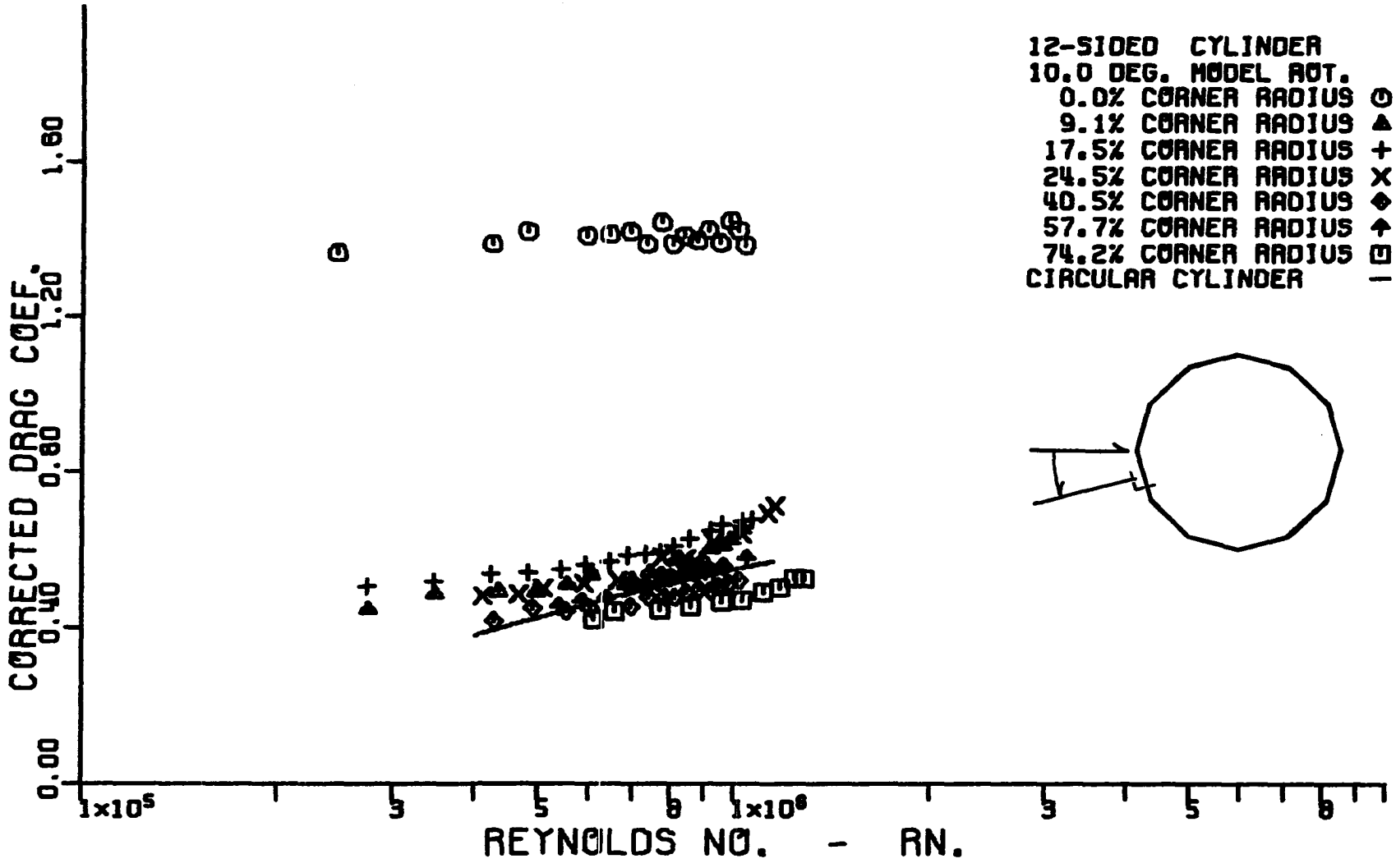

Figure 32. Variation of corrected cross-flow drag coefficient with corrected cross-flow Reynolds number for dodecagonal cylinders. Models orientated at 10.0° with respect to the relative wind.

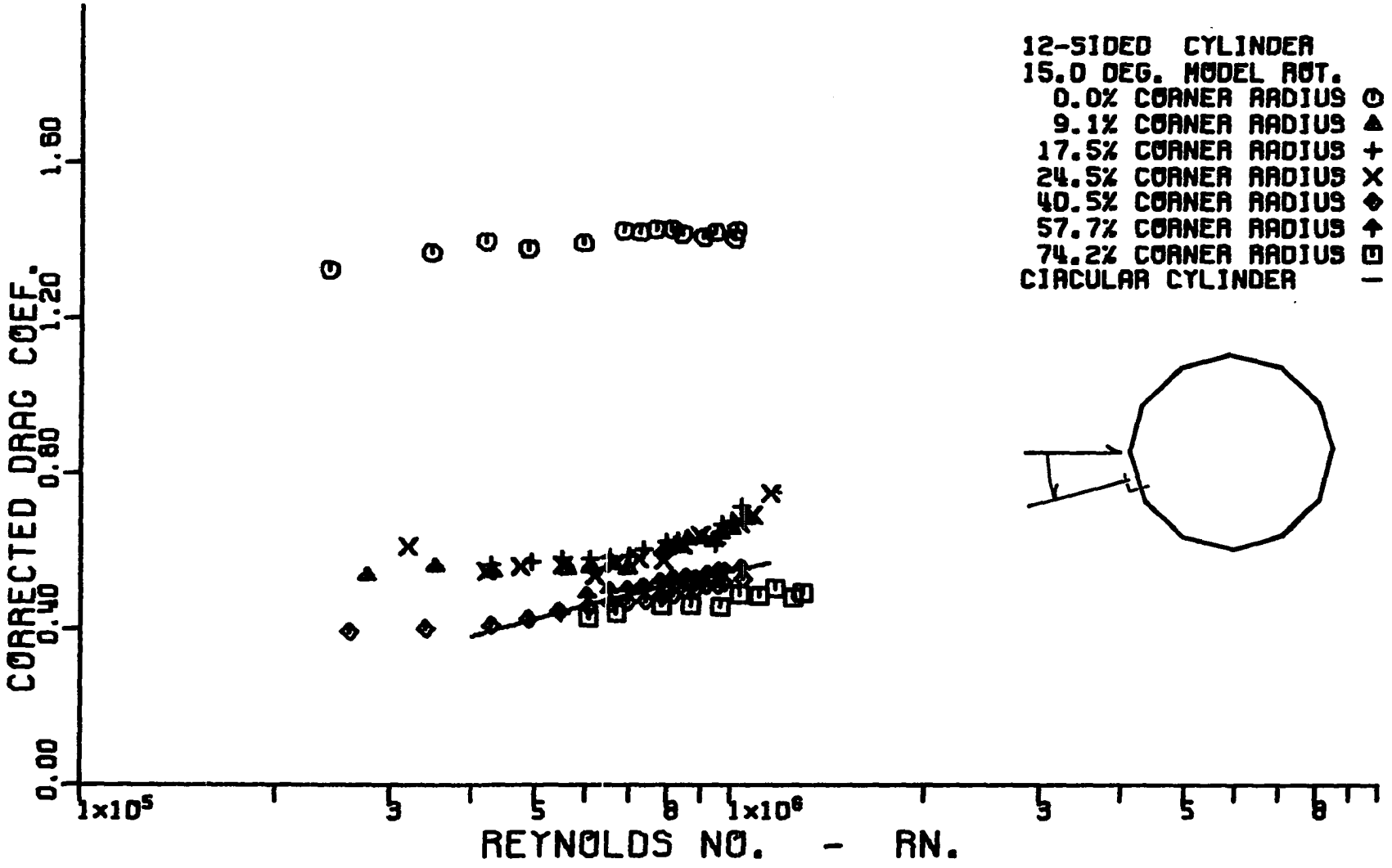

Figure 33. Variation of corrected cross-flow drag coefficient with corrected cross-flow Reynolds number for dodecagonal cylinders. Models orientated at 15.0° with respect to the relative wind.

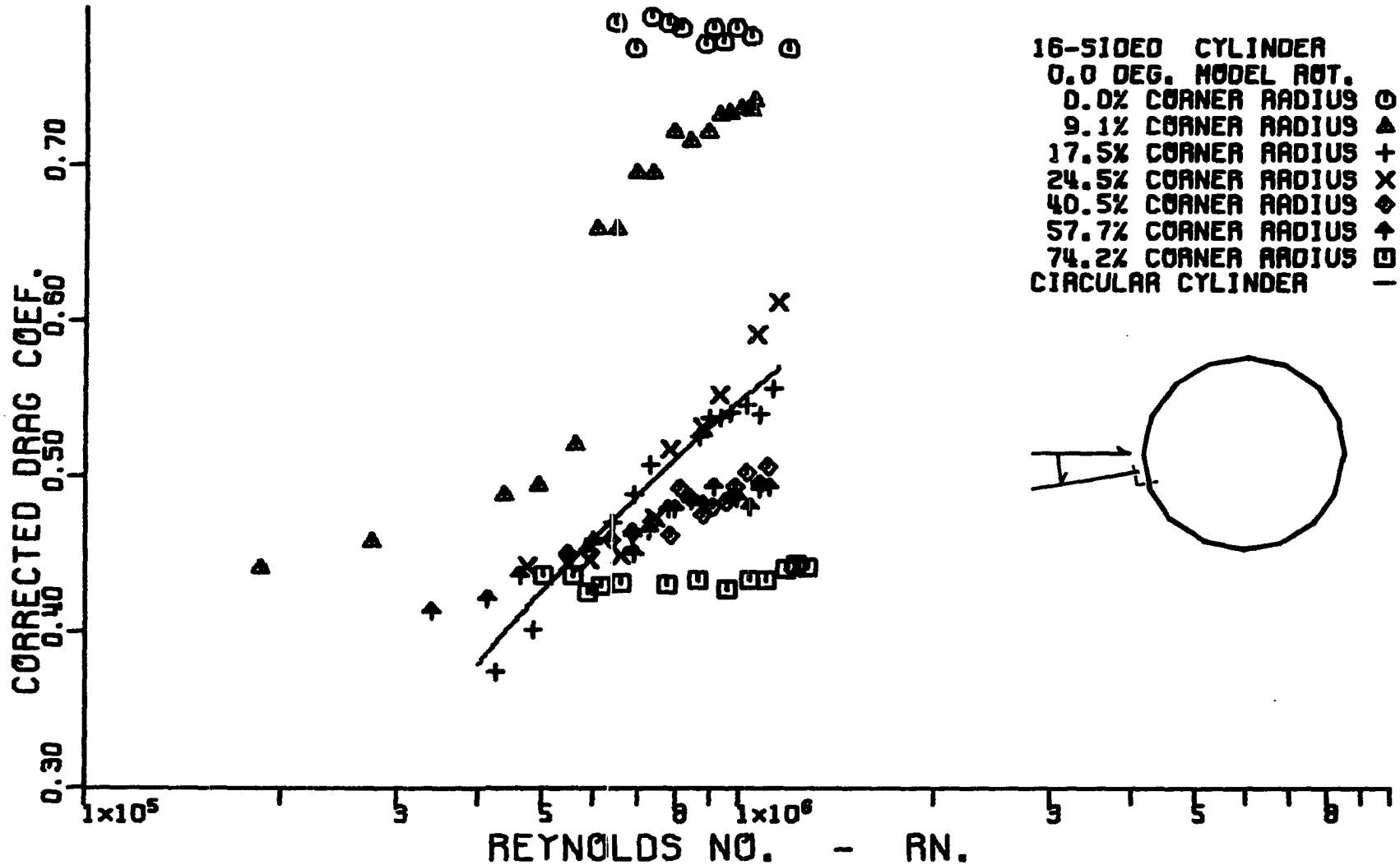

Figure 34. Variation of corrected cross-flow drag coefficient with corrected cross-flow Reynolds number for hexdecagonal cylinders. Models orientated at 0.0° with respect to the relative wind.

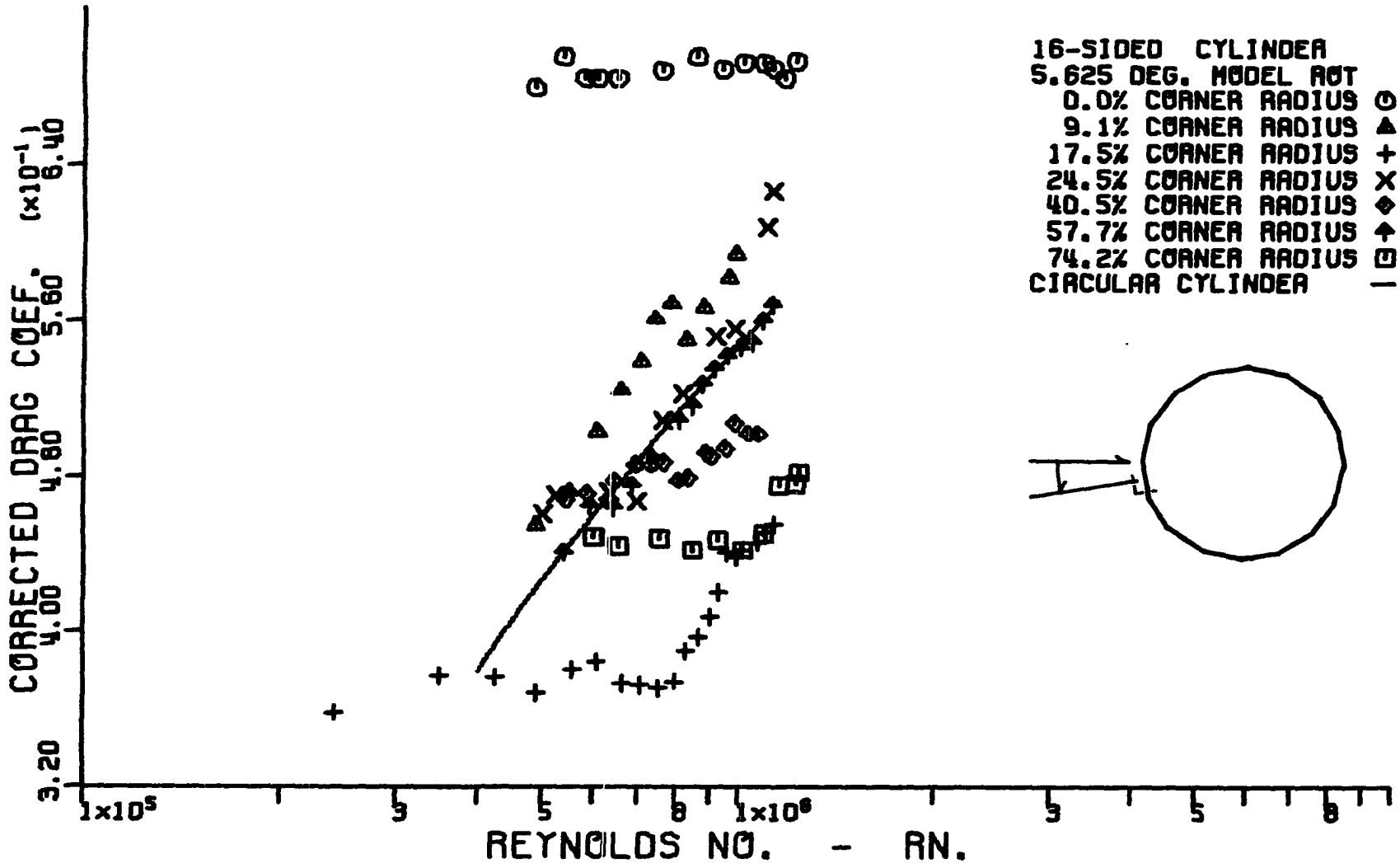

Figure 35. Variation of corrected cross-flow drag coefficient with corrected cross-flow Reynolds number for hexdecagonal cylinders. Models orientated at 5.6° with respect to the relative wind.

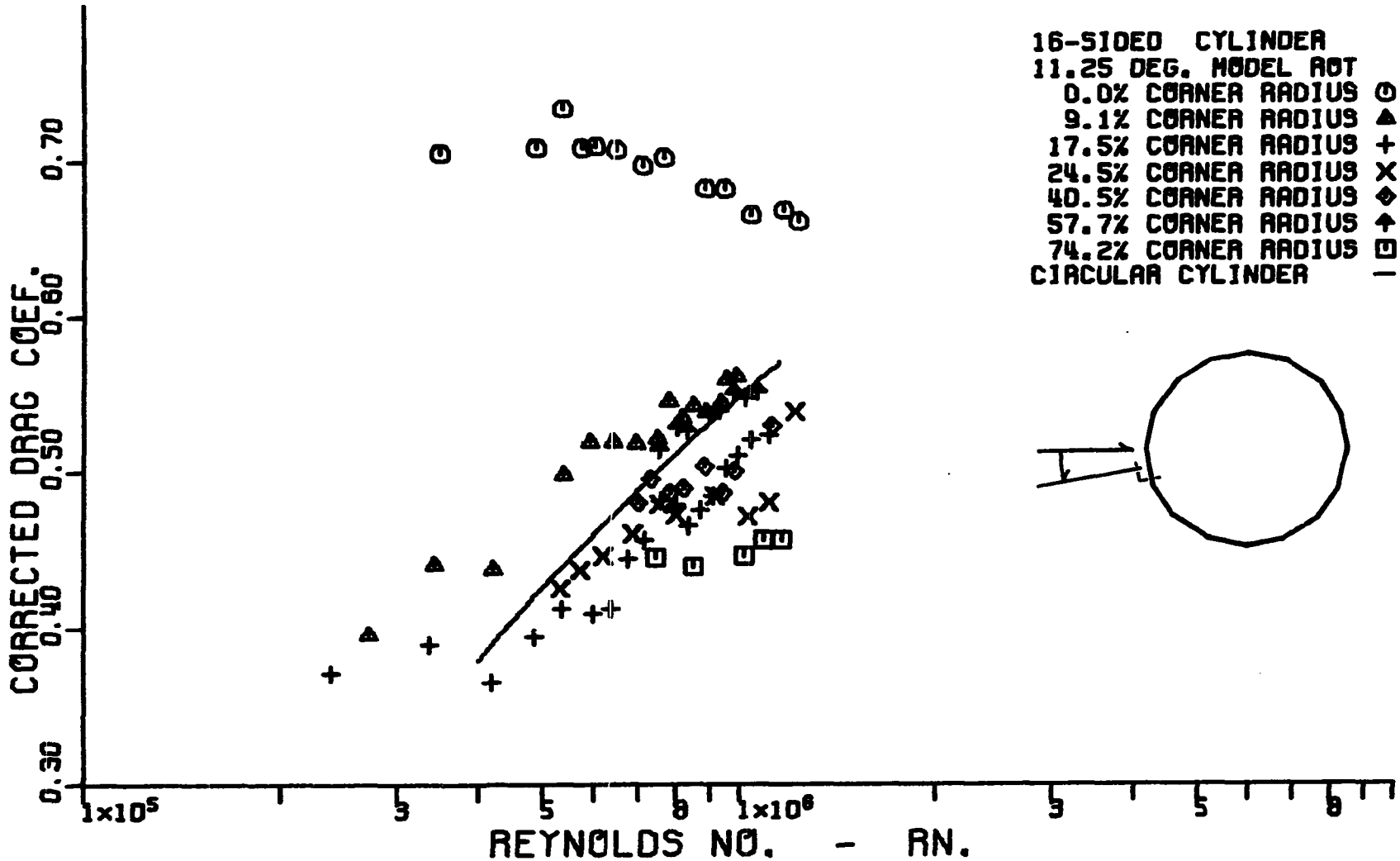

Figure 36. Variation of corrected cross-flow drag coefficient with corrected cross-flow Reynolds number for hexdecagonal cylinders. Models orientated at 11.25° with respect to the relative wind.

only for supercritical Reynolds numbers, those Reynolds numbers for which the boundary layer on the cylinder becomes turbulent before separation occurs. This change in the nature of the boundary layer causes a sudden significant decrease in the coefficient of drag and the Reynolds number at which the decrease occurs is called the critical Reynolds number. The complete drag coefficient plots are shown in Figures 37 to 57. Figures 26 to 36 show that for any fixed Reynolds number above the critical Reynolds number, for all cross-sections except the sharp-cornered cross-section, the maximum drag coefficient is experienced by the sharp-cornered models, 0.0 percent corner radius, and that, in general, as the corner radius increases the drag coefficient decreases.

Octagonal cylinders For the 8-sided cylinders the variation of drag coefficient with change in corner radius shows the following behavior. For the model rotations of 15° and 22.5°, Figures 28 and 29, as the radius of the corner increases toward the radius of the inscribed circular cylinder, the value of the drag coefficient approaches the value of drag coefficient for the circular cylinder. In the 15° case they approach asymptotically while in the 22.5° case the 74.2 percent corner radius has a drag coefficient less than that of the circular cylinder. At a Reynolds number of 10^6 the drag coefficient for the 74.2 percent polygonal

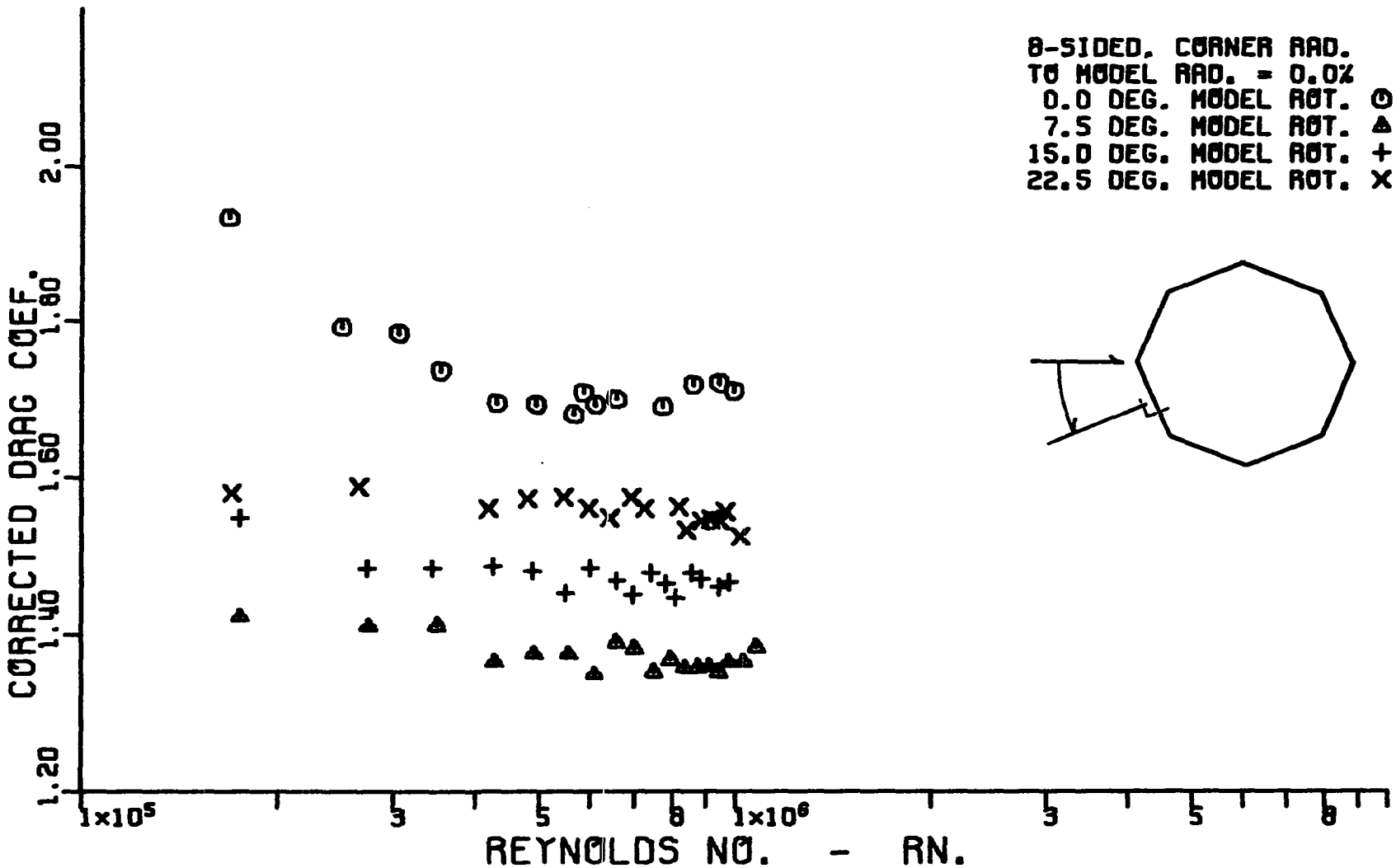

Figure 37. Variation of corrected cross-flow drag coefficient with corrected cross-flow Reynolds number for an octagonal cylinder having a corner radius equal to 0.0 percent of the radius of the inscribed circular cylinder.

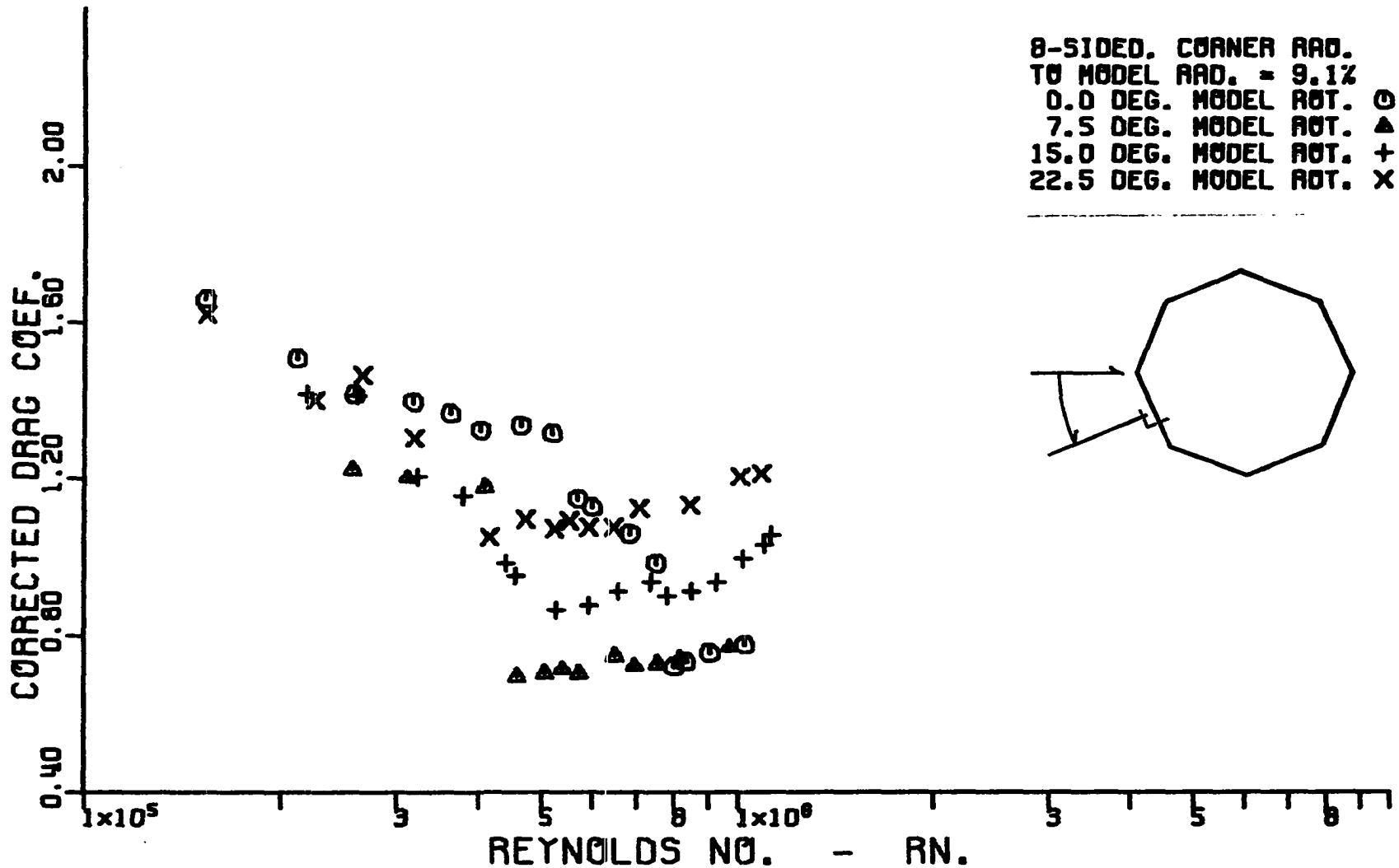

Figure 38. Variation of corrected cross-flow drag coefficient with corrected cross-flow Reynolds number for an octagonal cylinder having a corner radius equal to 9.1 percent of the radius of the inscribed circular cylinder.

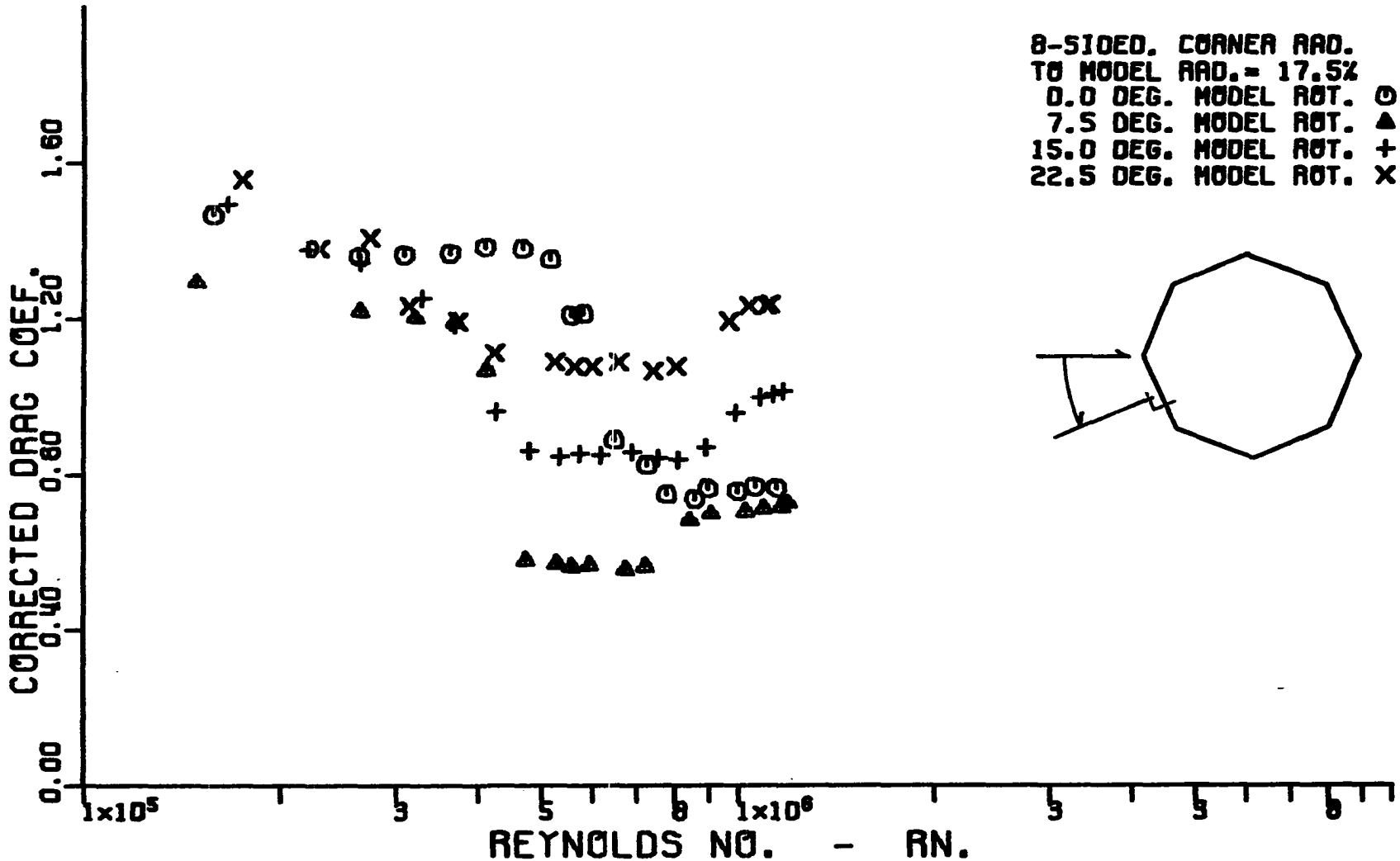

Figure 39. Variation of corrected cross-flow drag coefficient with corrected cross-flow Reynolds number for an octagonal cylinder having a corner radius equal to 17.5 percent of the radius of the inscribed circular cylinder.

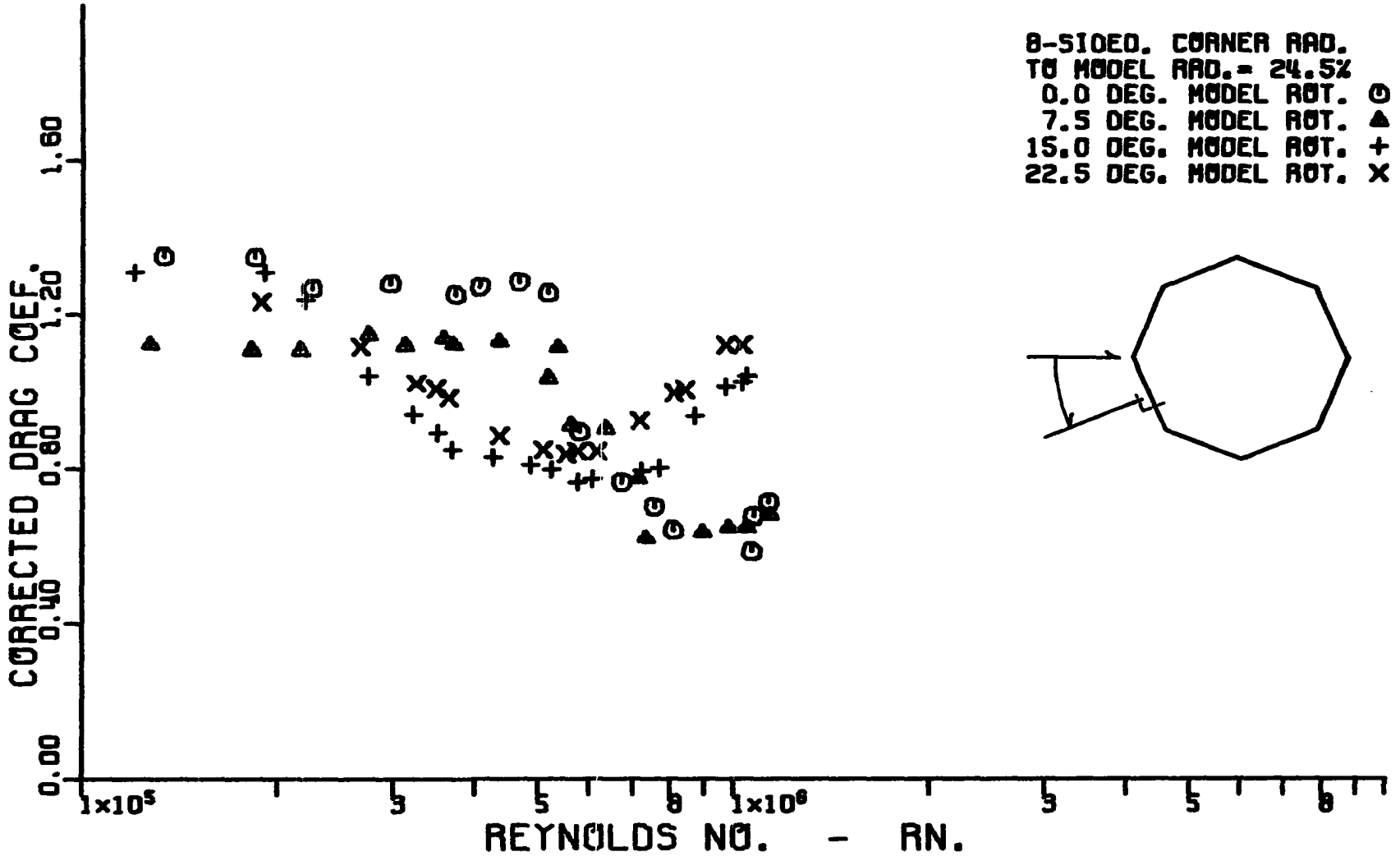

Figure 40. Variation of corrected cross-flow drag coefficient with corrected cross-flow Reynolds number for an octagonal cylinder having a corner radius equal to 24.5 percent of the radius of the inscribed circular cylinder.

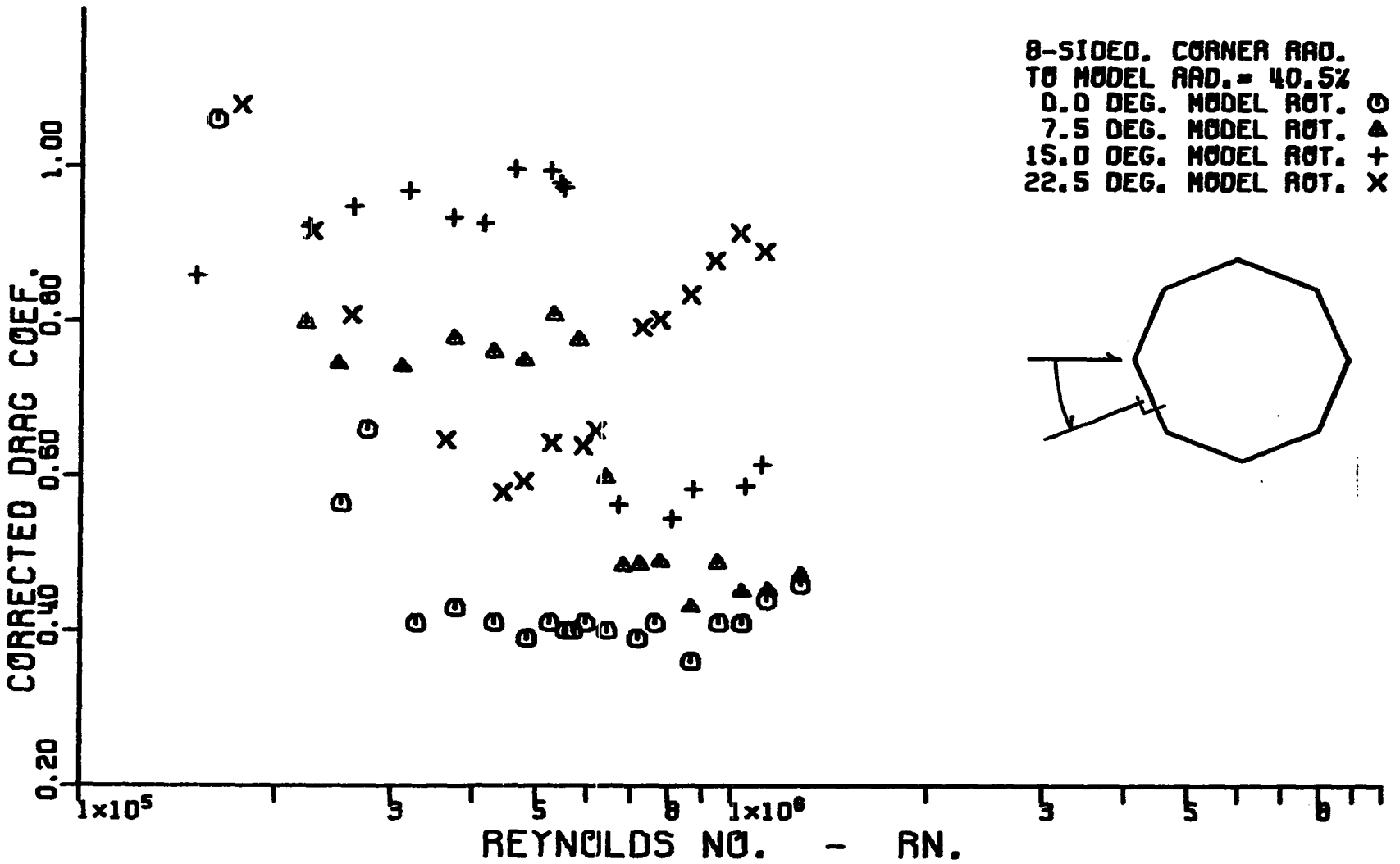

Figure 41. Variation of corrected cross-flow drag coefficient with corrected cross-flow Reynolds number for an octagonal cylinder having a corner radius equal to 40.5 percent of the radius of the inscribed circular cylinder.

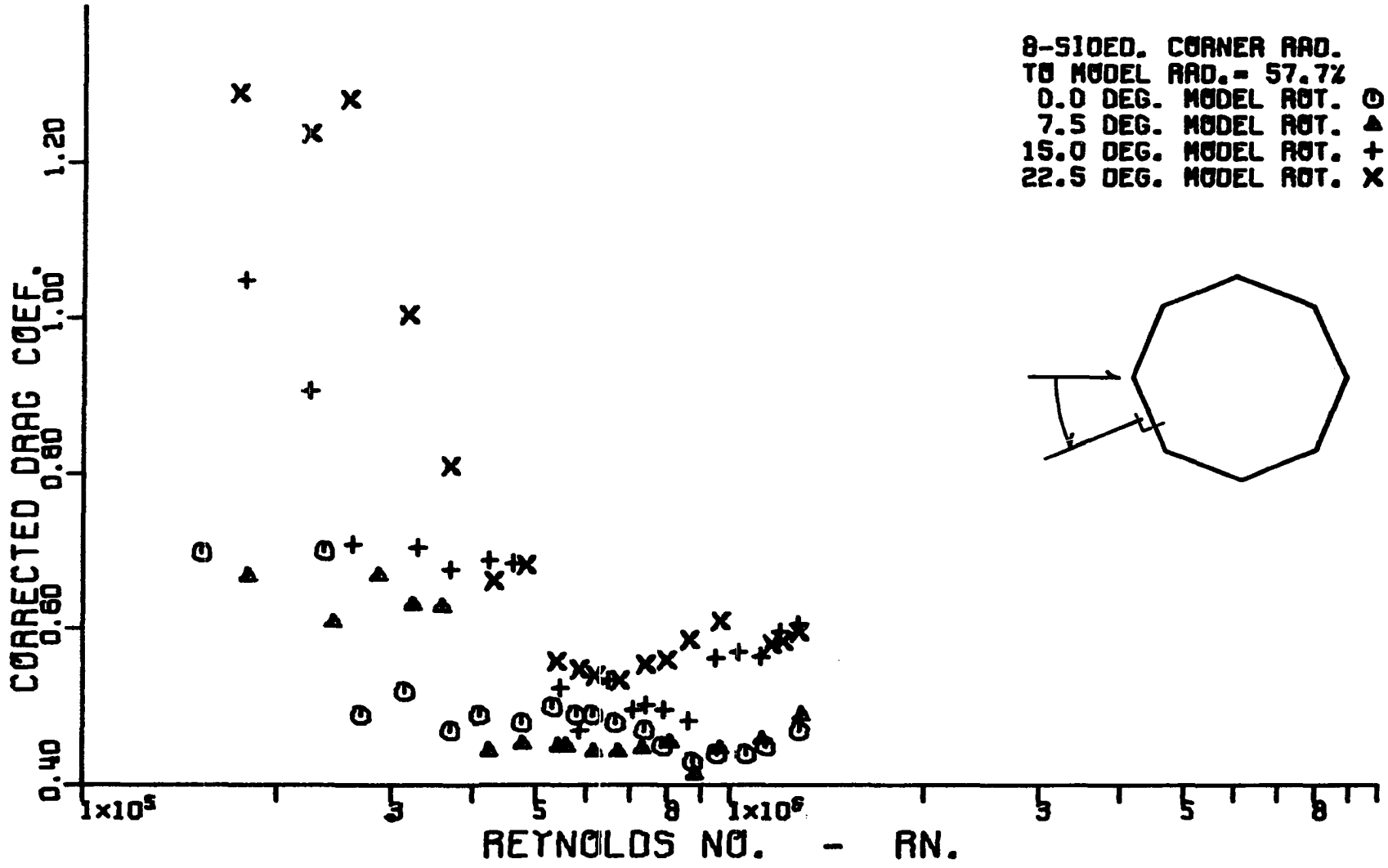

Figure 42. Variation of corrected cross-flow drag coefficient with corrected cross-flow Reynolds number for an octagonal cylinder having a corner radius equal to 57.7 percent of the radius of the inscribed circular cylinder.

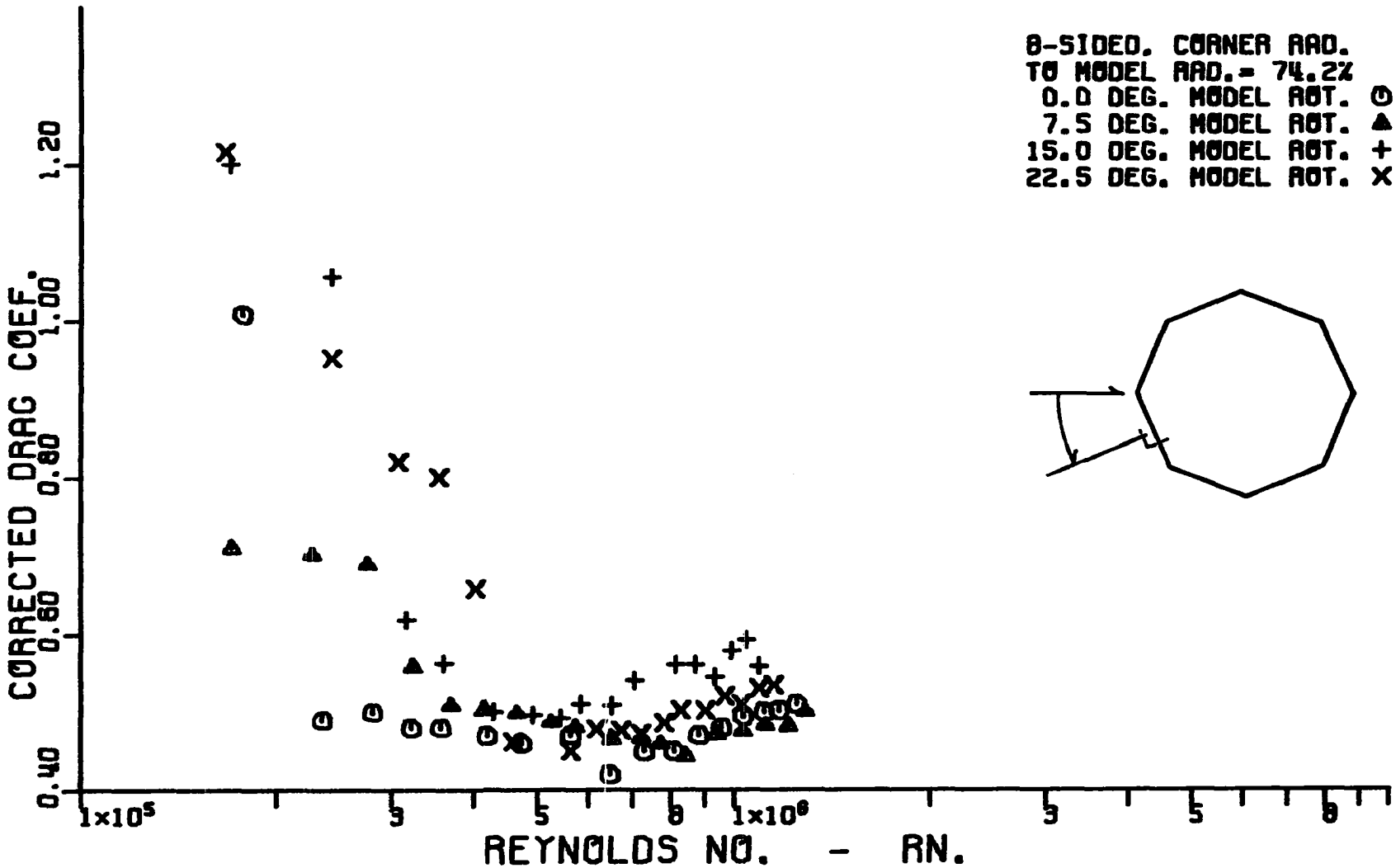

Figure 43. Variation of corrected cross-flow drag coefficient with corrected cross-flow Reynolds number for an octagonal cylinder having a corner radius equal to 74.2 percent of the radius of the inscribed circular cylinder.

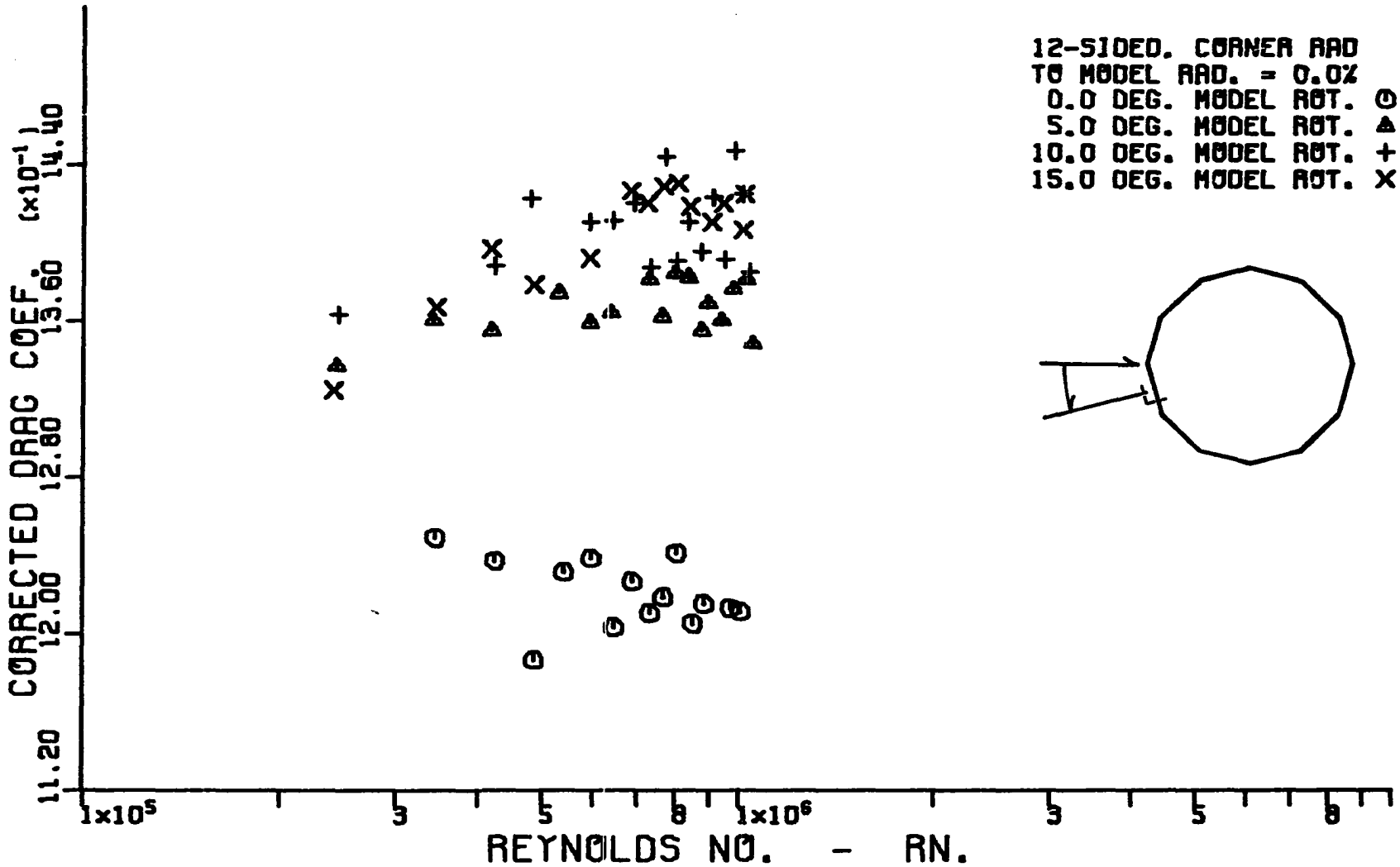

Figure 44. Variation of corrected cross-flow drag coefficient with corrected cross-flow Reynolds number for a dodecagonal cylinder having a corner radius equal to 0.0 percent of the radius of the inscribed circular cylinder.

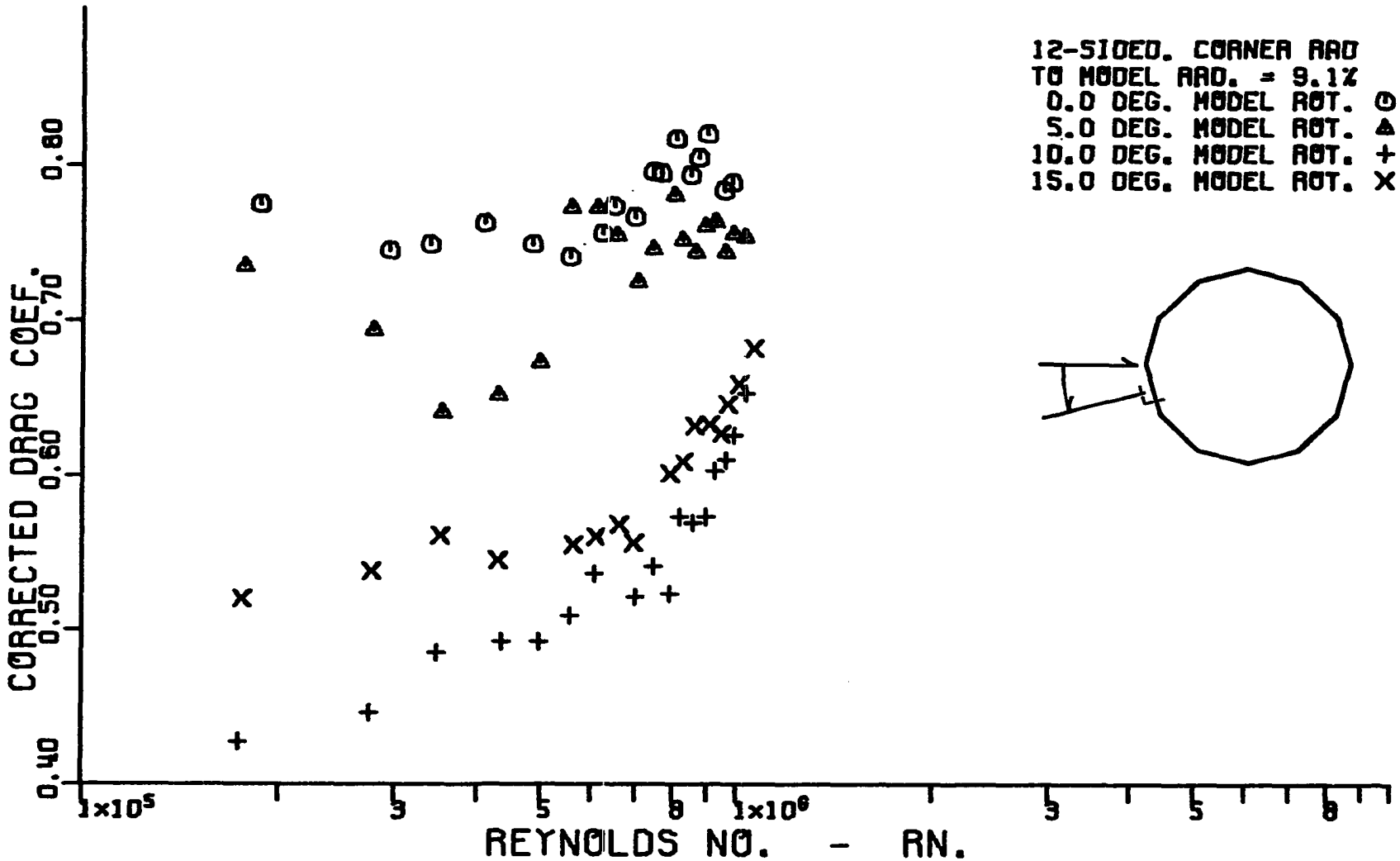

Figure 45. Variation of corrected cross-flow drag coefficient with corrected cross-flow Reynolds number for a dodecagonal cylinder having a corner radius equal to 9.1 percent of the radius of the inscribed circular cylinder.

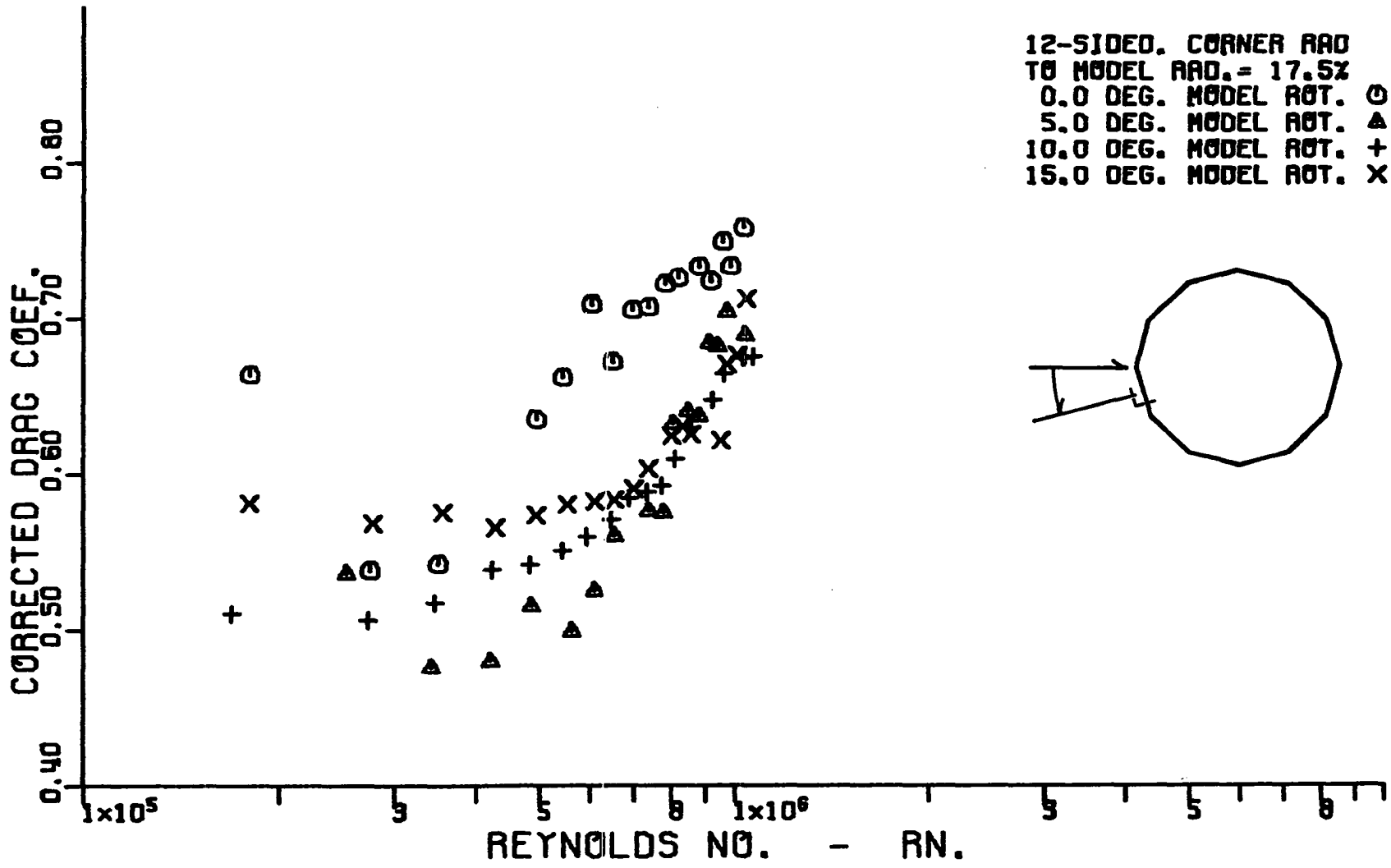

Figure 46. Variation of corrected cross-flow drag coefficient with corrected cross-flow Reynolds number for a dodecagonal cylinder having a corner radius equal to 17.5 percent of the radius of the inscribed circular cylinder.

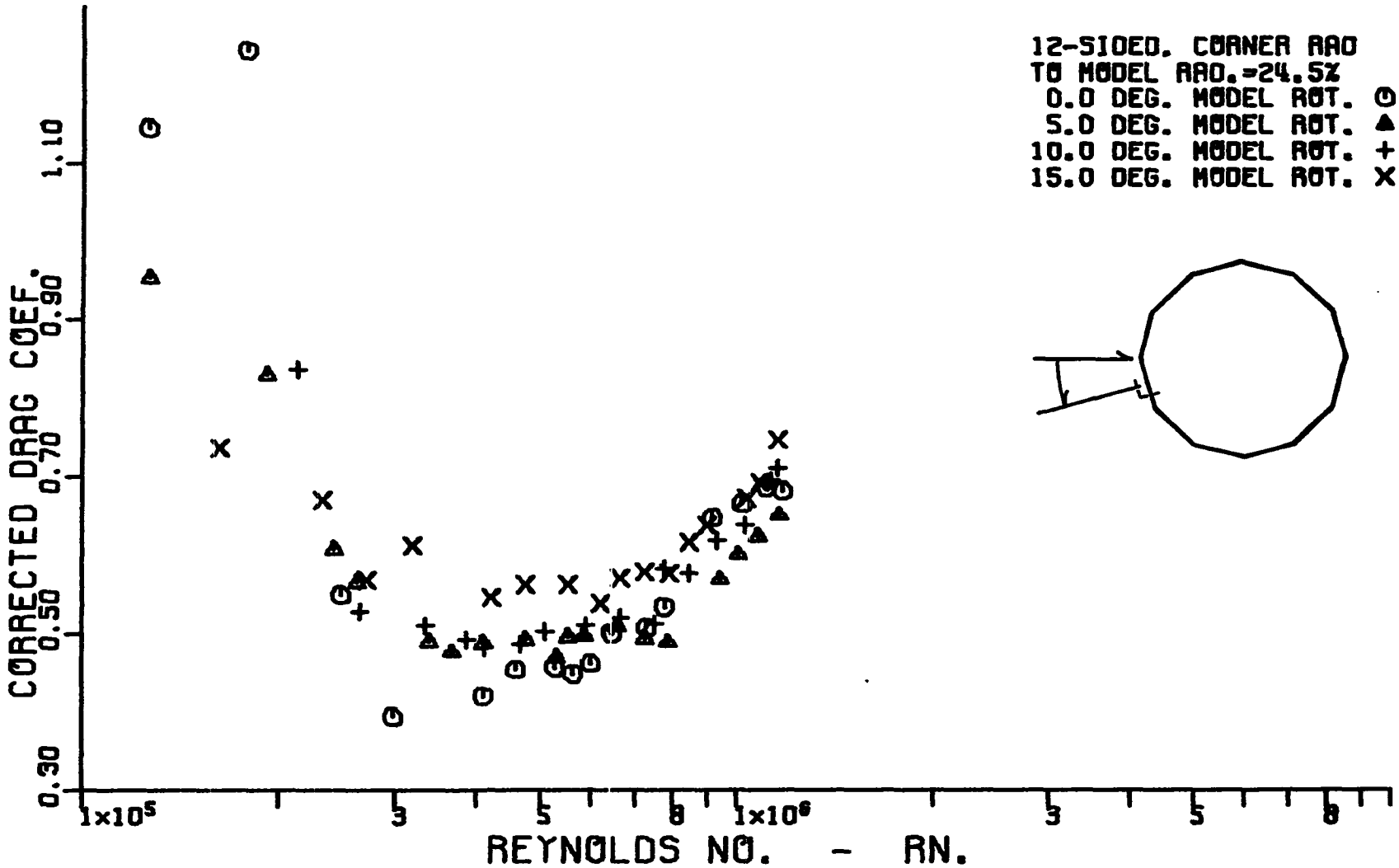

Figure 47. Variation of corrected cross-flow drag coefficient with corrected cross-flow Reynolds number for a dodecagonal cylinder having a corner radius equal to 24.5 percent of the radius of the inscribed circular cylinder.

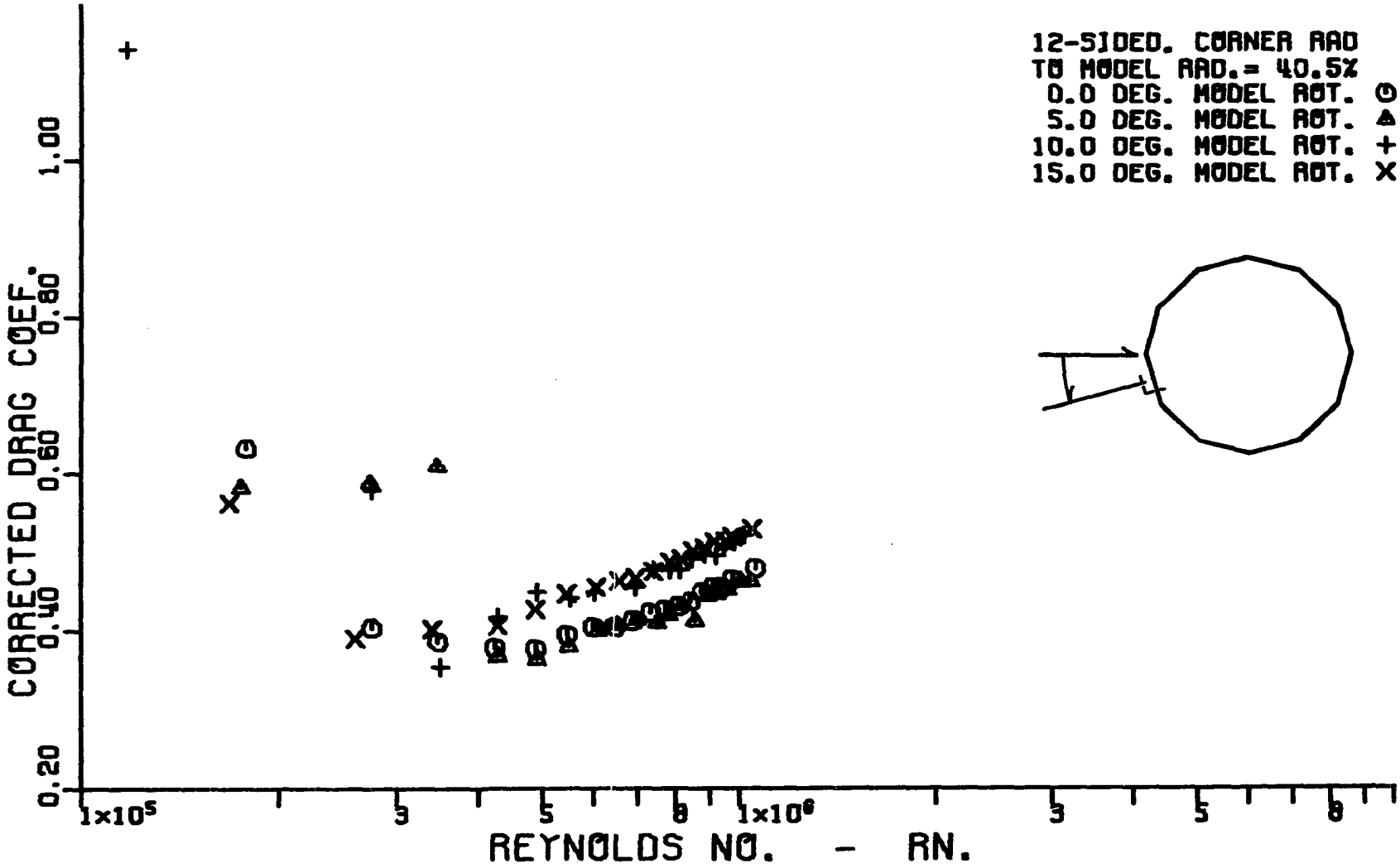

Figure 48. Variation of corrected cross-flow drag coefficient with corrected cross-flow Reynolds number for a dodecagonal cylinder having a corner radius equal to 40.5 percent of the radius of the inscribed circular cylinder.

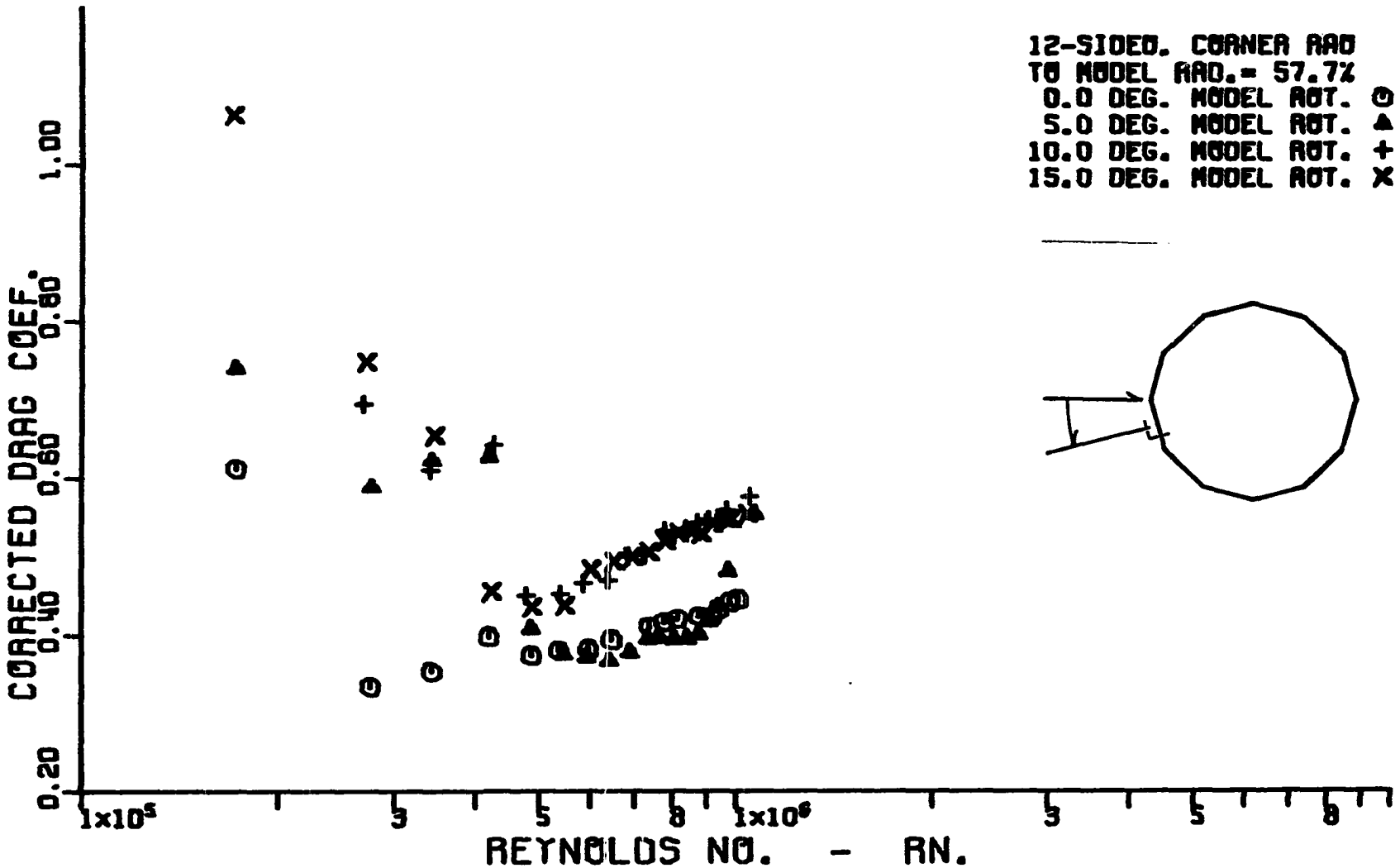

Figure 49. Variation of corrected cross-flow drag coefficient with corrected cross-flow Reynolds number for a dodecagonal cylinder having a corner radius equal to 57.7 percent of the radius of the inscribed circular cylinder.

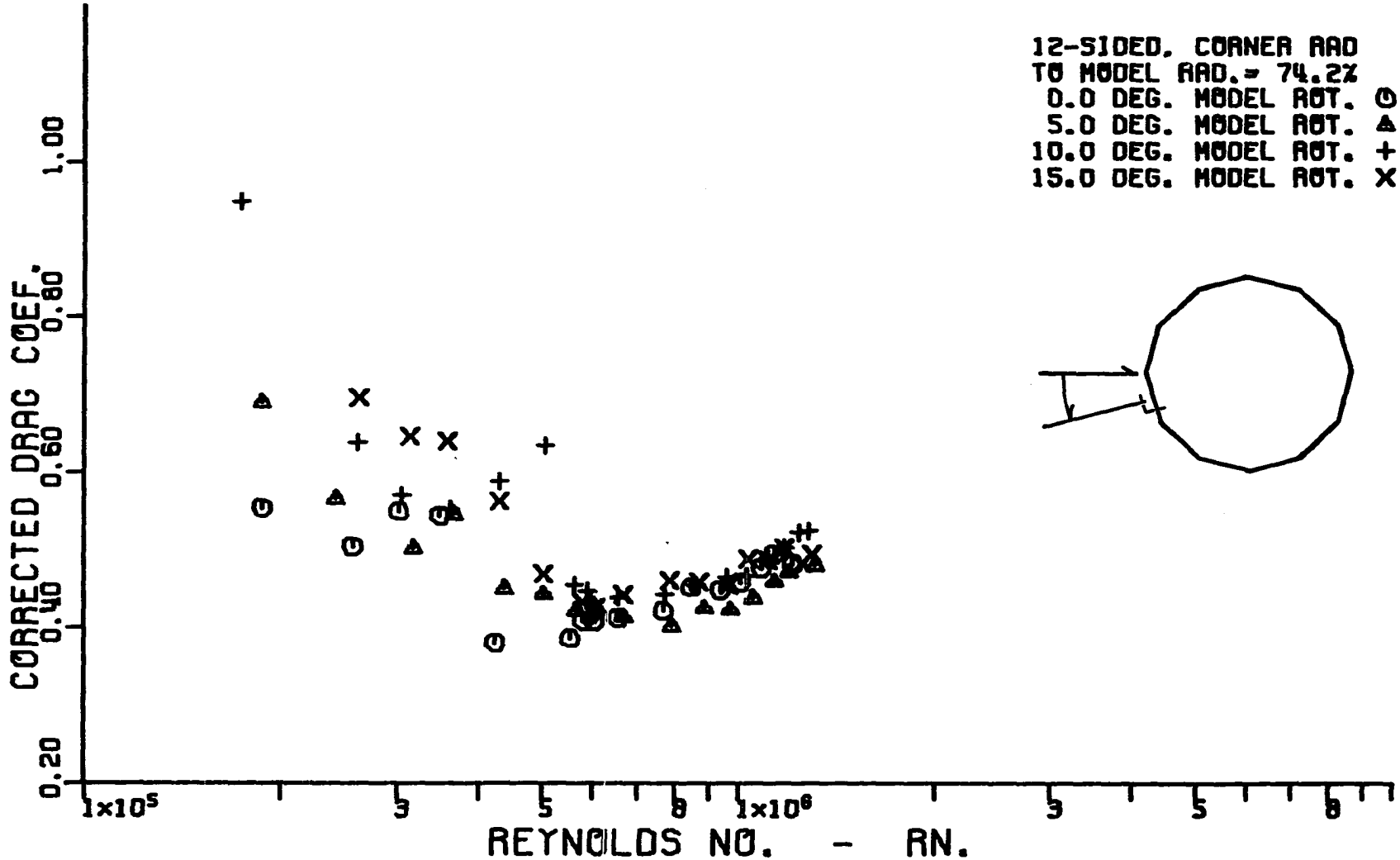

Figure 50. Variation of corrected cross-flow drag coefficient with corrected cross-flow Reynolds number for a dodecagonal cylinder having a corner radius equal to 74.2 percent of the radius of the inscribed circular cylinder.

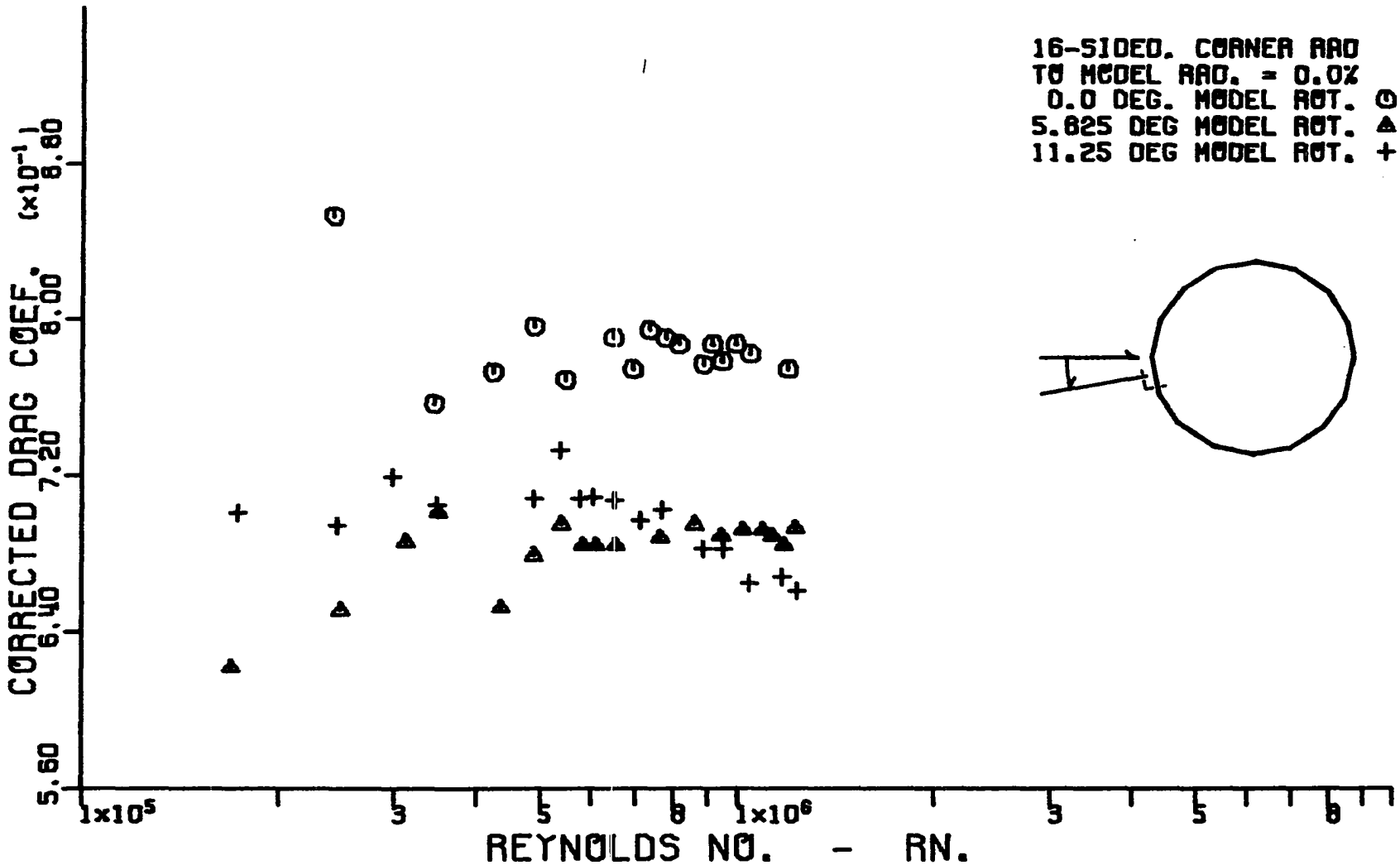

Figure 51. Variation of corrected cross-flow drag coefficient with corrected cross-flow Reynolds number for a hexdecagonal cylinder having a corner radius equal to 0.0 percent of the radius of the inscribed circular cylinder.

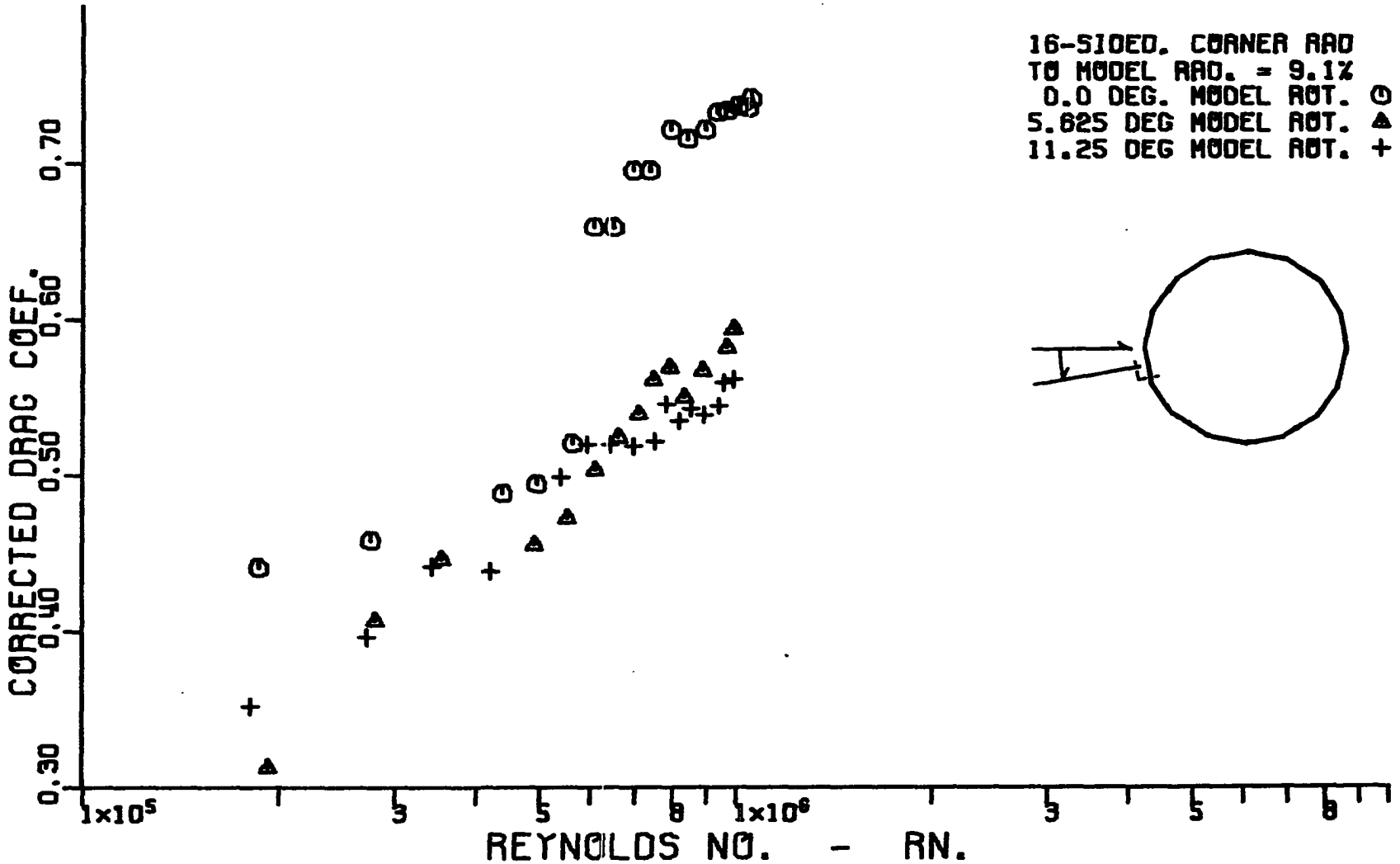

Figure 52. Variation of corrected cross-flow drag coefficient with corrected cross-flow Reynolds number for a hexdecagonal cylinder having a corner radius equal to 9.1 percent of the radius of the inscribed circular cylinder.

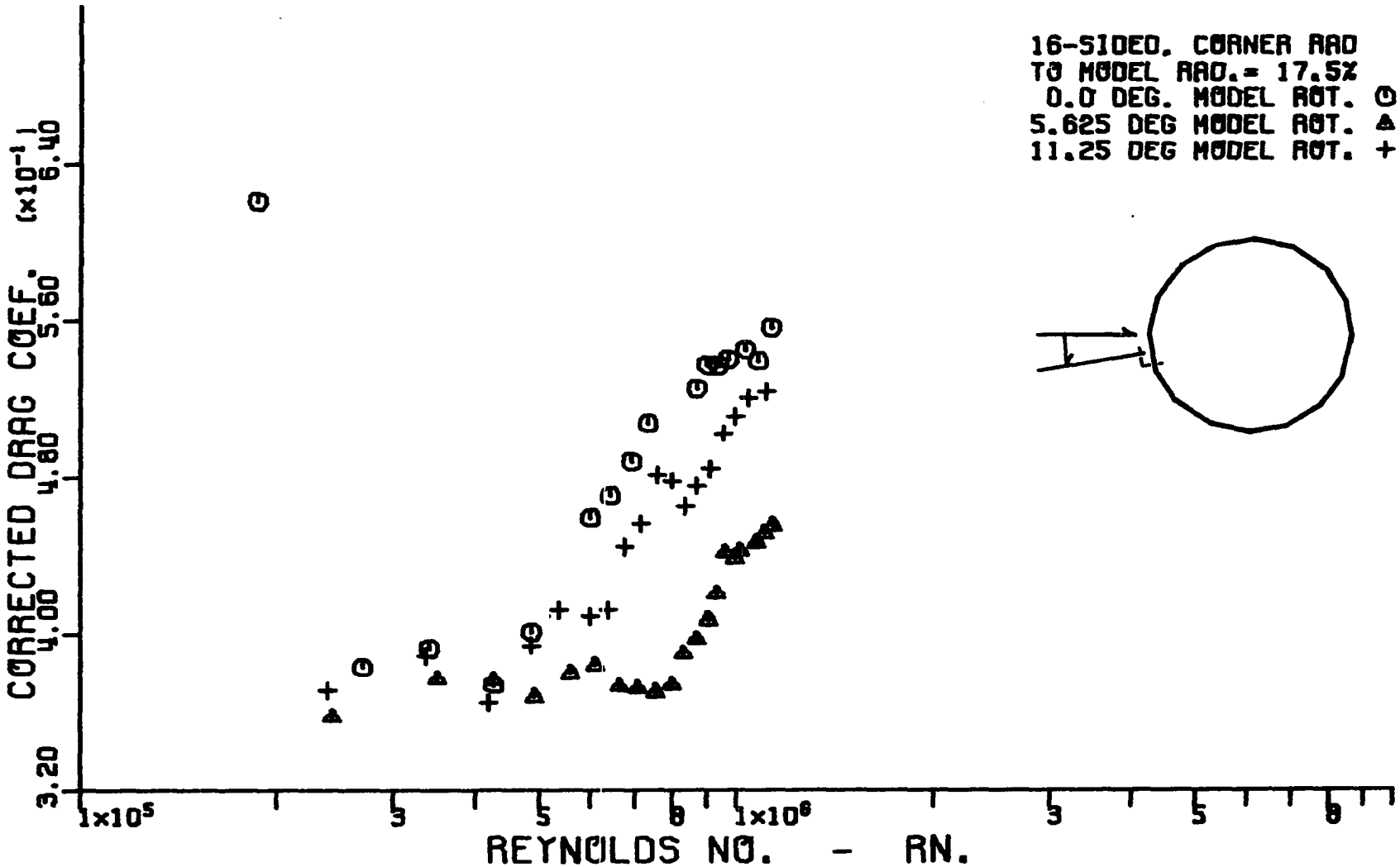

Figure 53. Variation of corrected cross-flow drag coefficient with corrected cross-flow Reynolds number for a hexdecagonal cylinder having a corner radius equal to 17.5 percent of the radius of the inscribed circular cylinder.

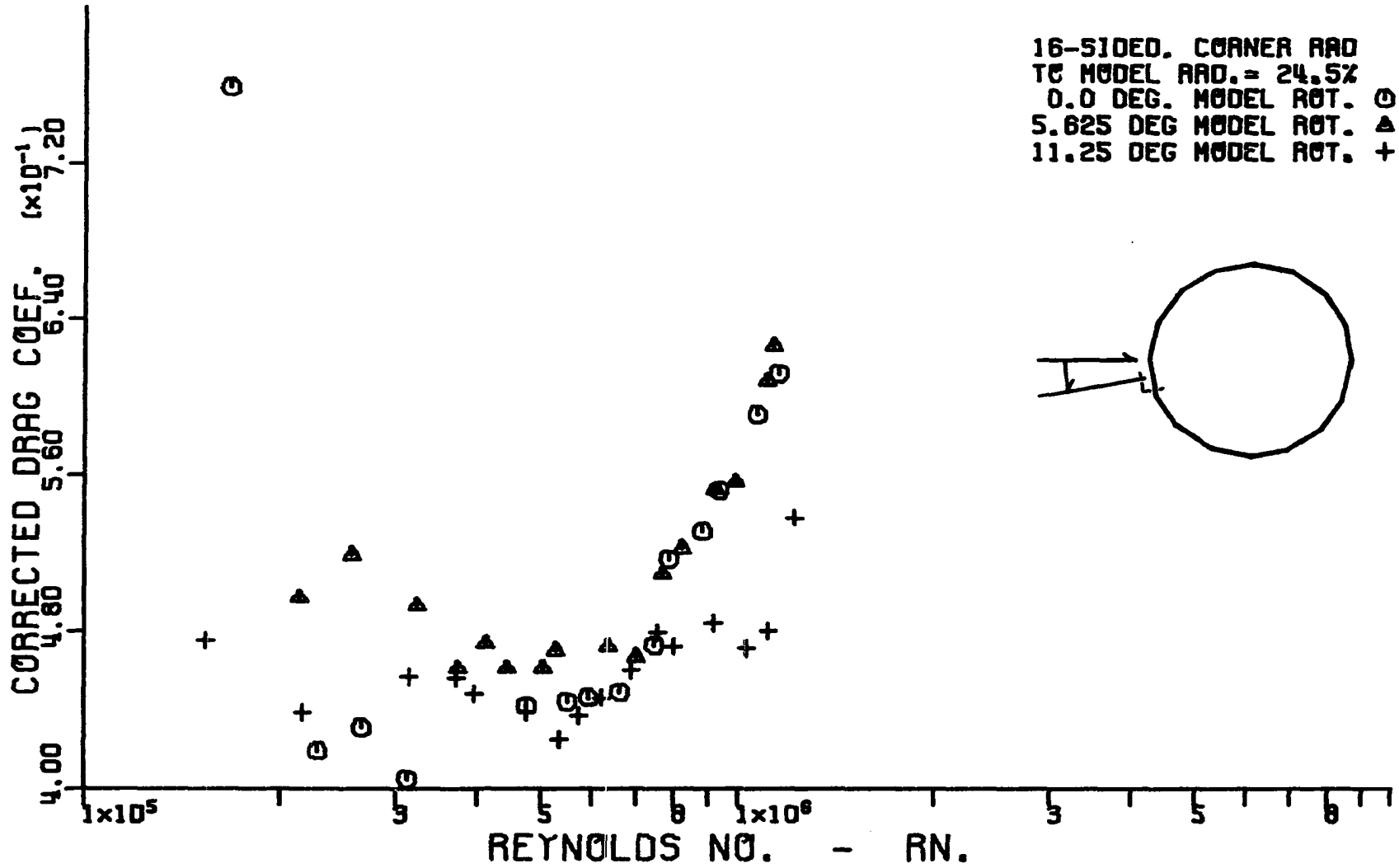

Figure 54. Variation of corrected cross-flow drag coefficient with corrected cross-flow Reynolds number for a hexdecagonal cylinder having a corner radius equal to 24.5 percent of the radius of the inscribed circular cylinder.

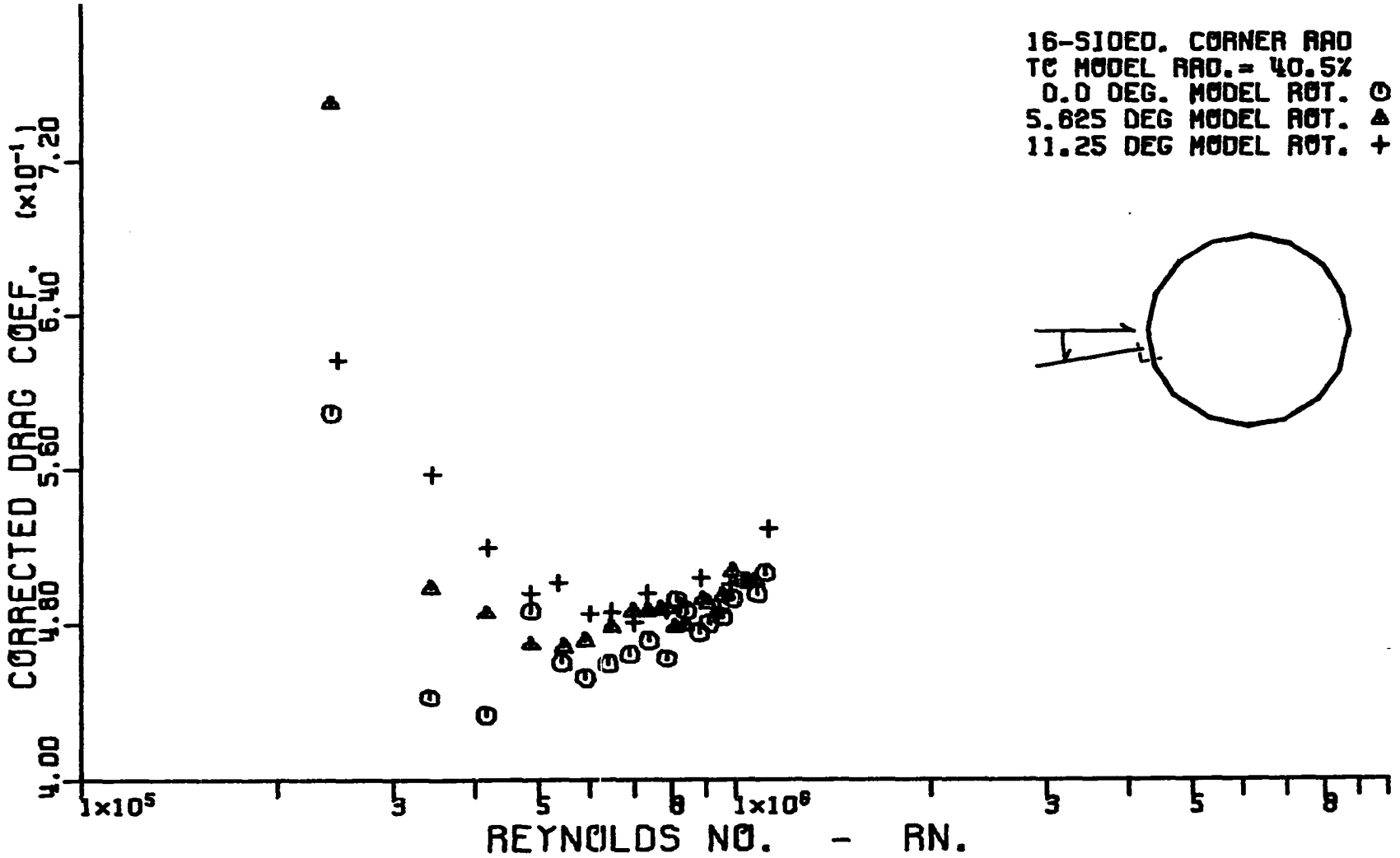

Figure 55. Variation of corrected cross-flow drag coefficient with corrected cross-flow Reynolds number for a hexdecagonal cylinder having a corner radius equal to 40.5 percent of the radius of the inscribed circular cylinder.

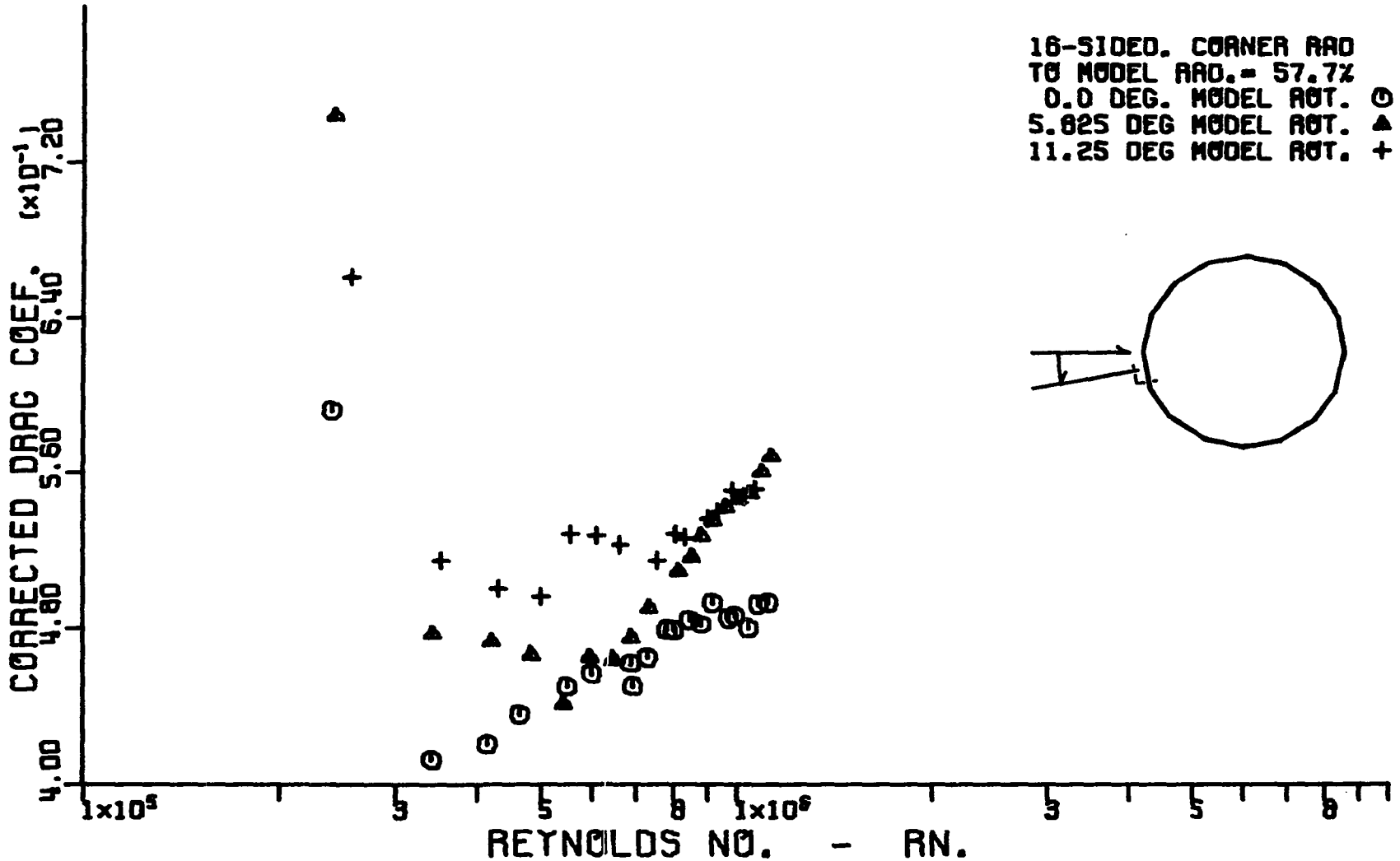

Figure 56. Variation of corrected cross-flow drag coefficient with corrected cross-flow Reynolds number for a hexdecagonal cylinder having a corner radius equal to 57.7 percent of the radius of the inscribed circular cylinder.

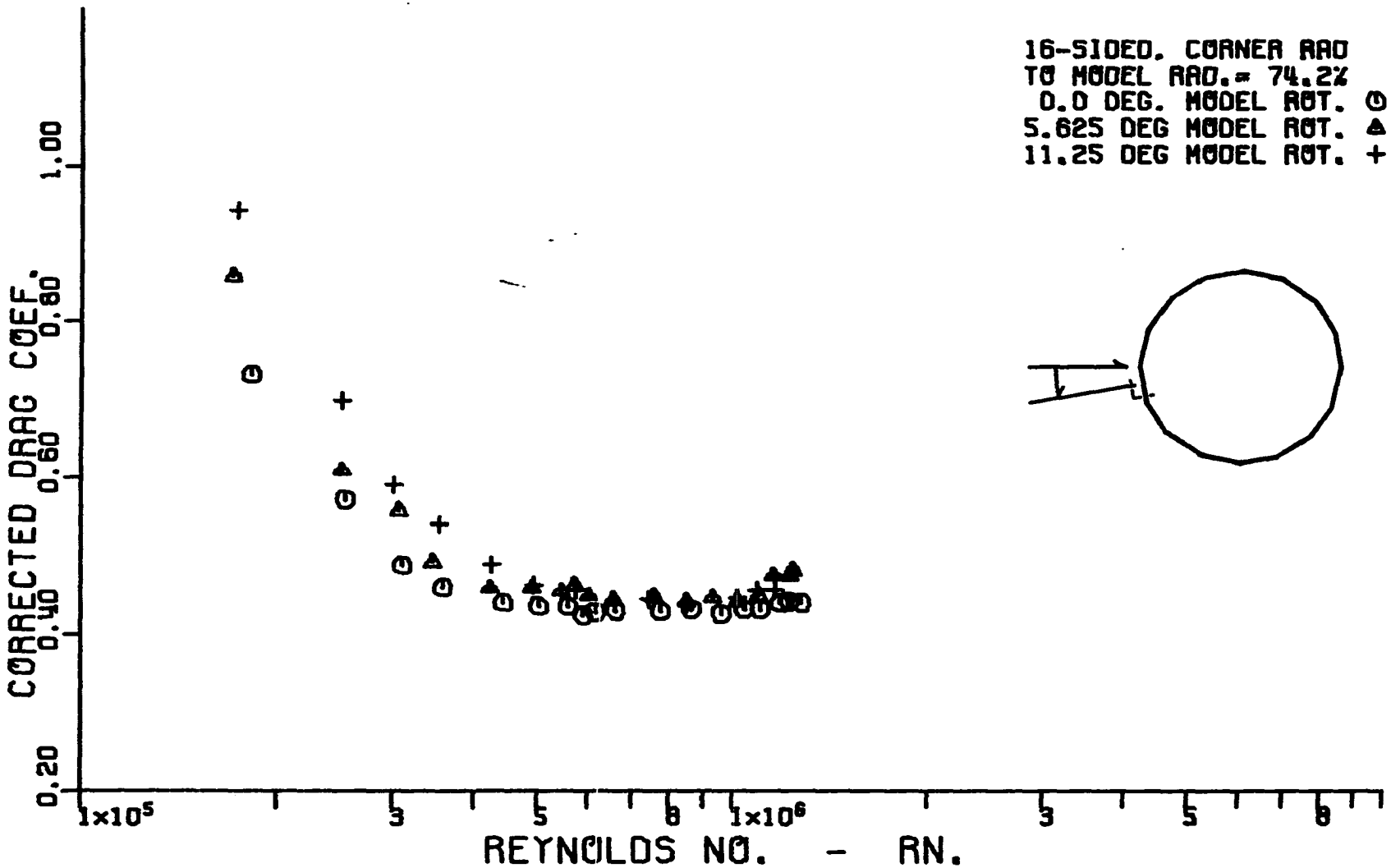

Figure 57. Variation of corrected cross-flow drag coefficient with corrected cross-flow Reynolds number for a hexdecagonal cylinder having a corner radius equal to 74.2 percent of the radius of the inscribed circular cylinder.

cylinder is 4.7 percent less than that for the circular cylinder and the percentage increases for increasing Reynolds number. The percentage difference is large enough to indicate a slight improvement by the 74.2 percent octagonal cylinder over the circular cylinder at high Reynolds numbers.

For the 0° and 7.5° model rotations, Figures 26 and 27, the behavior of the drag coefficient decrease is somewhat different. In these cases the drag coefficients reach the level of those for the circular cylinder at a corner radius somewhere between 24.5 percent and 40.5 percent of the radius of the inscribed circular cylinder, around 33 percent, and then continue to decrease, reaching a minimum value of drag coefficient some 20 percent less than the corresponding value for a circular cylinder at a corner radius of approximately 40.5 percent of the radius of the inscribed circular cylinder. The actual difference between the coefficients of drag for the circular cylinder and the octagonal cylinder with 40.5 percent corners is approximately constant for increasing Reynolds numbers. As the corner radii continue to increase the drag coefficients of the octagonal cylinders approach those of the circular cylinder from below.

Dodecagonal cylinders The same behavior can be seen for the 12-sided models. Figure 30 shows 0° orientation, flat side perpendicular to the relative wind, where the trend shown is identical to the 0° orientation for the 8-sided

cylinders. The only noticeable difference between the 8- and 12-sided cases is that the radius for the minimum drag has increased from 40.5 percent, minimum drag for the octagonal cylinders, to 57.7 percent for the dodecagonal cylinders. Figure 31 shows the first intermediate orientation, 5°, and its behavior is that just described. Again it matches the behavior of the first intermediate orientation for the octagonal cylinders, that of 7.5°.

For the 10° and 15° model-relative wind orientations, Figures 32 and 33, the same behavior just described again occurs with two differences. First, at these orientations the percentage difference between the circular and polygonal drag coefficients is less and second, the best corner shape appears to be the 74.2 percent radius. Again it should be noted that the curves are essentially parallel. The difference between the behaviors of the 8- and 12-sided cylinders at this second intermediate and corner forward orientations can probably be attributed to the basic shape. Due to its greater number of sides the dodecagonal cylinder is a more streamlined shape than the octagonal cylinder at these larger rotations where the corners are at the extremes of the model and should therefore be expected to have less drag.

Hexdecagonal cylinders This variation in basic shape also explains the behavior of the 16-sided cylinders shown in

Figures 34 to 36. A hexdecagonal cylinder is almost circular except for the sharp-cornered model and because of this it would be expected that the values of drag coefficient should be close to those of a circular cylinder for all orientations and corner radii. This shows up in the figures where the data for the various corner radii are grouped in one band. This is unlike the 8- and 12-sided cases where, in general, the sharper corners were grouped together at a drag coefficient somewhere between that of the sharp-cornered case and that of the circular cylinder, with the larger radii corners grouped either at, or just below, the circular cylinder. In the 16-sided case the data are grouped in a band located with its top just above the line of the circular cylinder. At the higher Reynolds numbers the boundaries of this band are approximately parallel, except for the 0° orientation where they are slightly divergent. At a Reynolds number of 10^6 the width of the band is approximately 20 percent of the value of the drag coefficient of the circular cylinder which puts the band's lower boundary approximately the same distance below the circular cylinder curve as that of the minimum line for the 8- and 12-sided models. The small variation in drag coefficient with variation in orientation is also obvious from the figures. Except for one or two exceptions the C_d curves remain in the same relative location as the model is

rotated.

Of the results shown in Figures 26-36, none are unexpected or unusual except for the smaller drag coefficients of the polygonal cylinders with large corner radii when compared with those for the circular cylinders. This behavior can be explained by examining the variation of surface static pressure about both the circular cylinder and a group of polygonal cylinders of the same family but with different corner radii. Data from the octagonal cylinders will be used to document this behavior but that from either the dodecagonal or hexdecagonal cylinders could have been used. The only difference would have been that the effect would be less pronounced had either the dodecagonal or hexdecagonal data been used because of their closer approximation of the circular shape.

Pressure distribution

Figures 58 to 65 show the static pressure distribution in the form of pressure coefficients around both circular and octagonal cylinders at a corrected Reynolds number of approximately 10^6 and at model rotations of 0°, 7.5°, 15° and 22.5°. The pressure coefficients are plotted against angular rotation from the forward stagnation point. Data for the 0.0 percent and 40.5 percent 8-sided models are compared with the data from the circular cylinder tested in the project

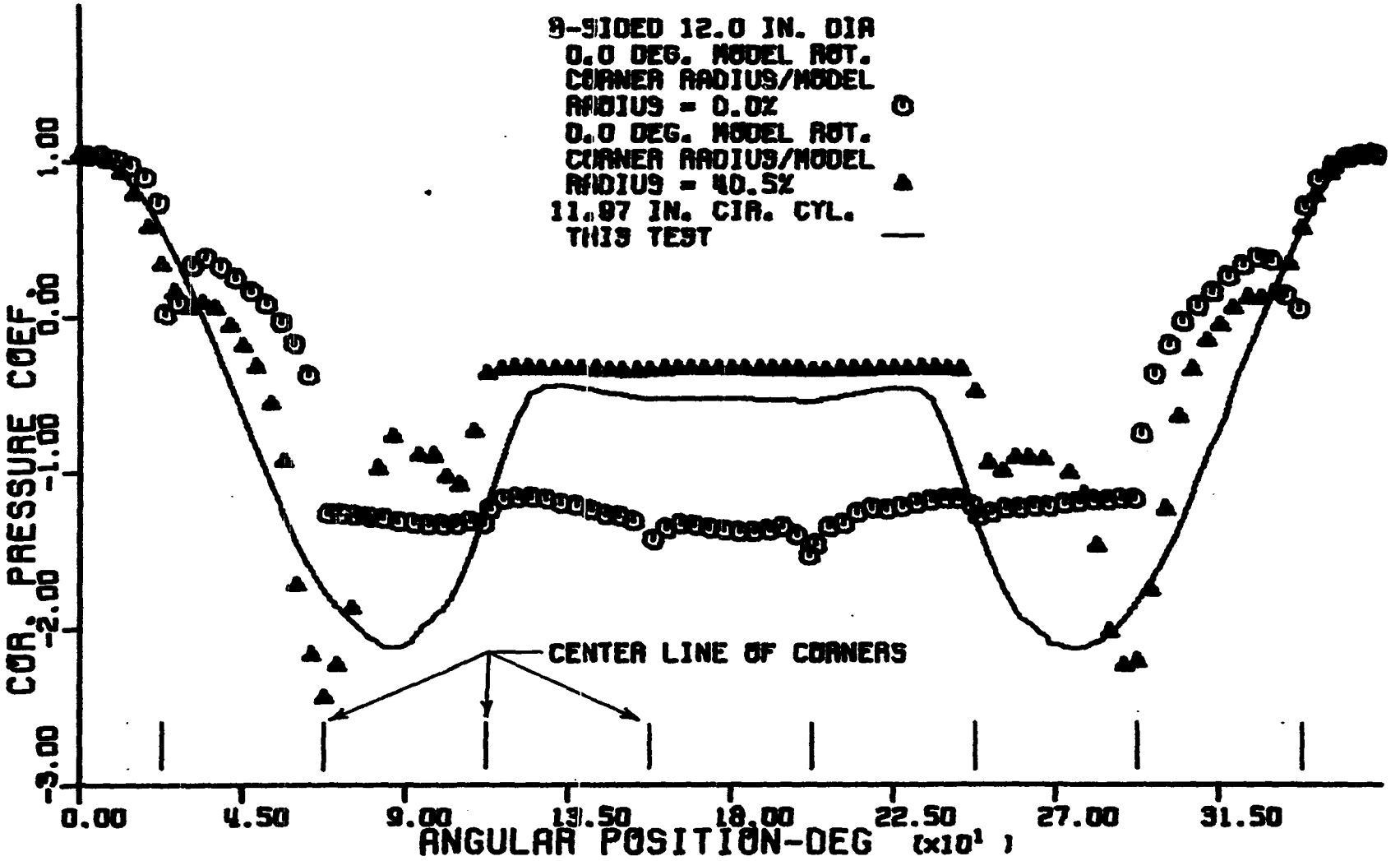

Figure 58. Variation of corrected pressure coefficient with change in angular position from the forward stagnation point for a circular cylinder and two octagonal cylinders, 0.0 and 40.5 percent corner radii at 0.0° model rotation. Cylinders have corrected Reynolds numbers of 1,000,000.

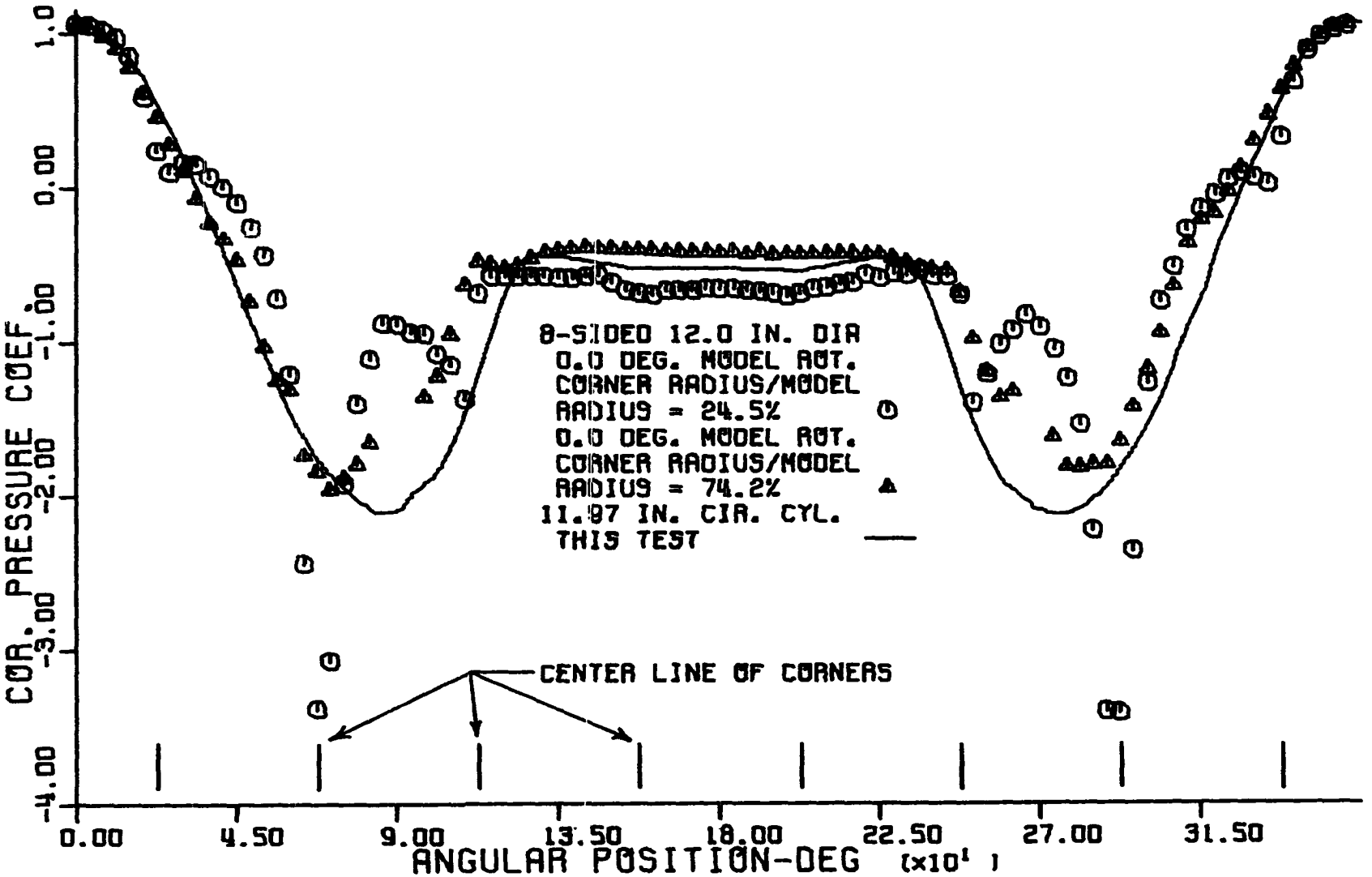

Figure 59. Variation of corrected pressure coefficient with change in angular position from the forward stagnation point for a circular cylinder and two octagonal cylinders, 24.5 and 74.2 percent corner radii, at 0.0° model rotation. Cylinders have corrected Reynolds numbers of 1,000,000.

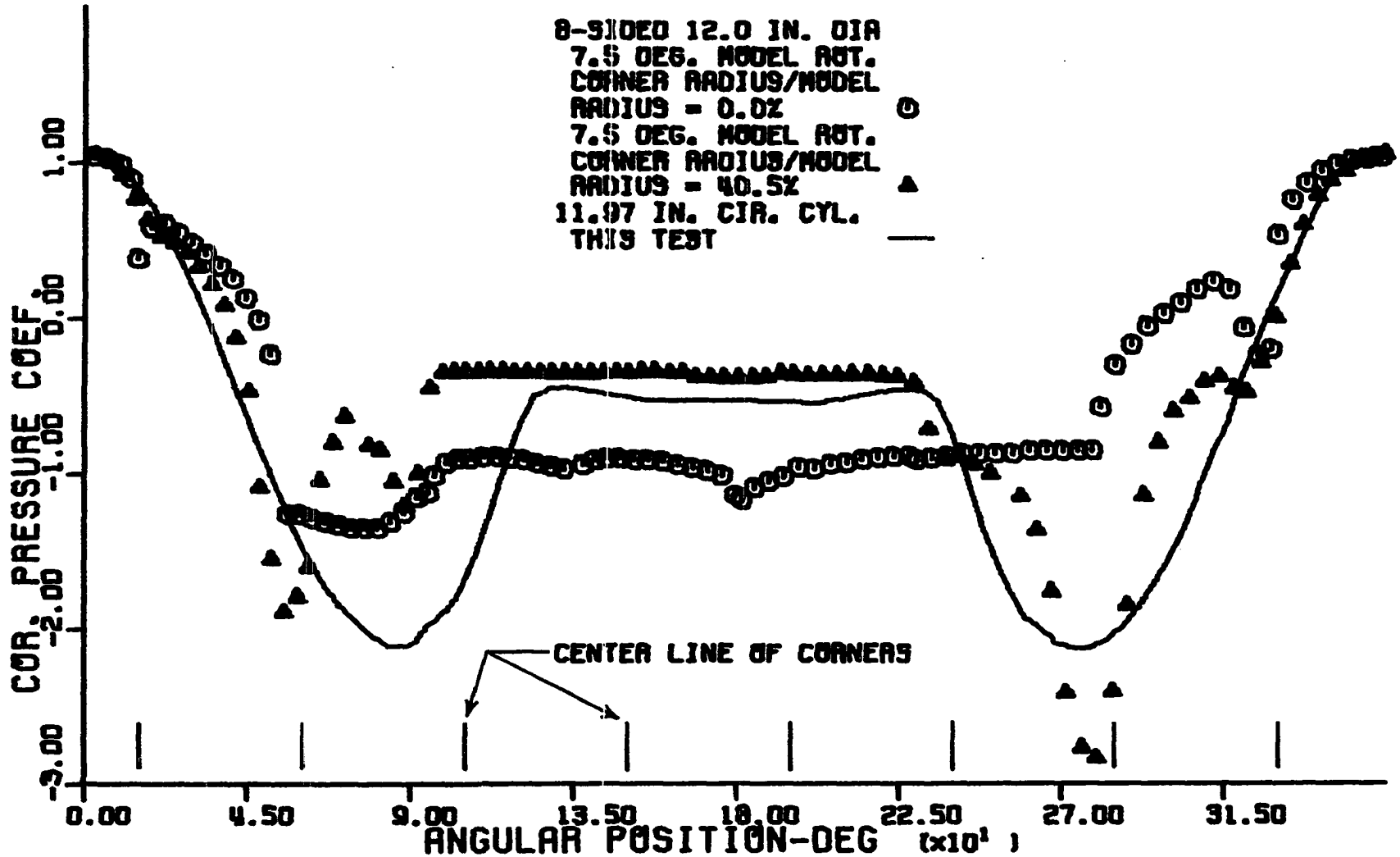

Figure 60. Variation of corrected pressure coefficient with change in angular position from the forward stagnation point for a circular cylinder and two octagonal cylinders, 0.0 and 40.5 percent corner radii, at 7.5° model rotation. Cylinders have corrected Reynolds numbers of 1,000,000.

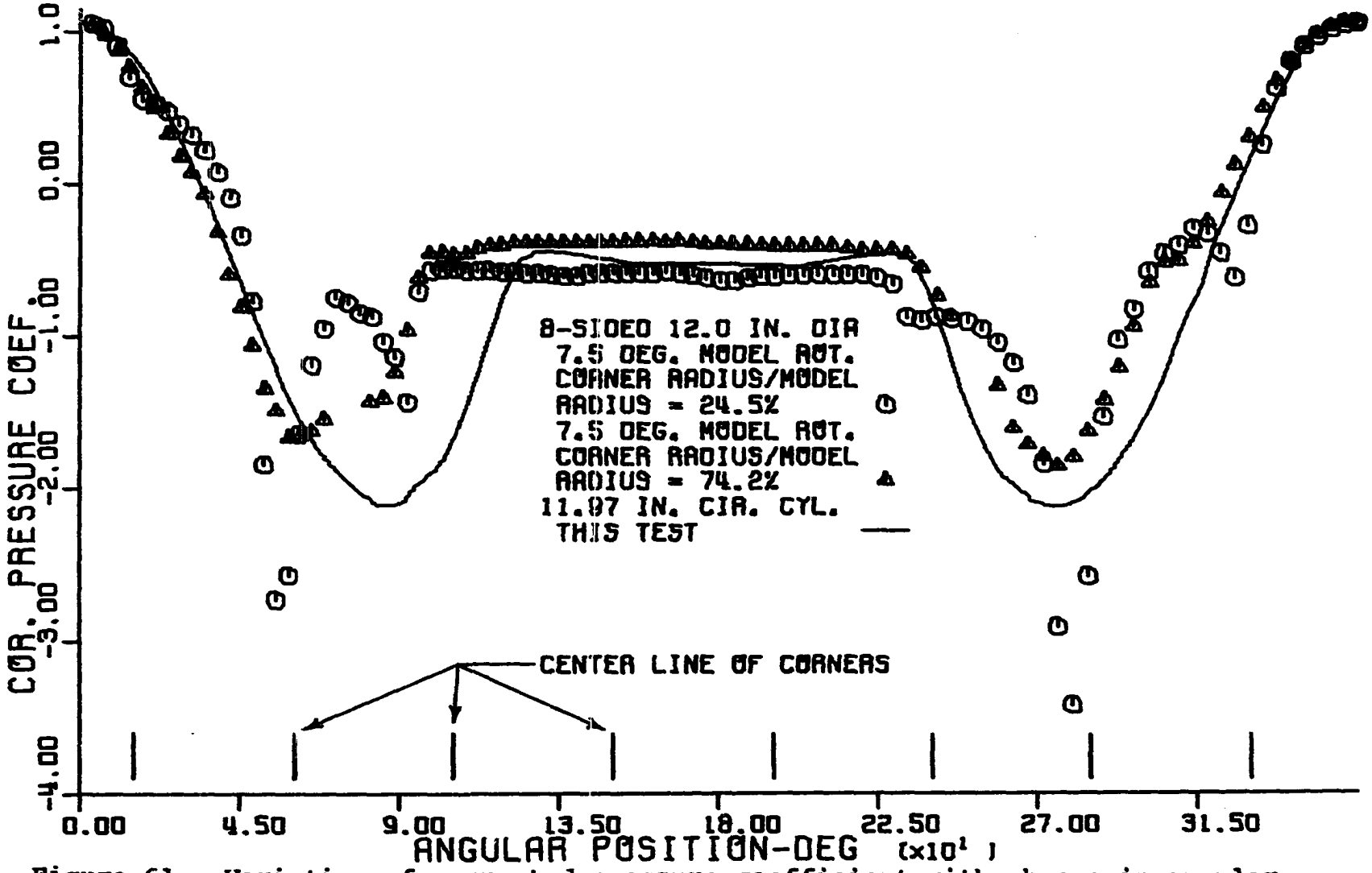

Figure 61. Variation of corrected pressure coefficient with change in angular position from the forward stagnation point for a circular cylinder and two octagonal cylinders, 24.5 and 74.2 percent corner radii, at 7.5° model rotation. Cylinders have corrected Reynolds numbers of 1,000,000.

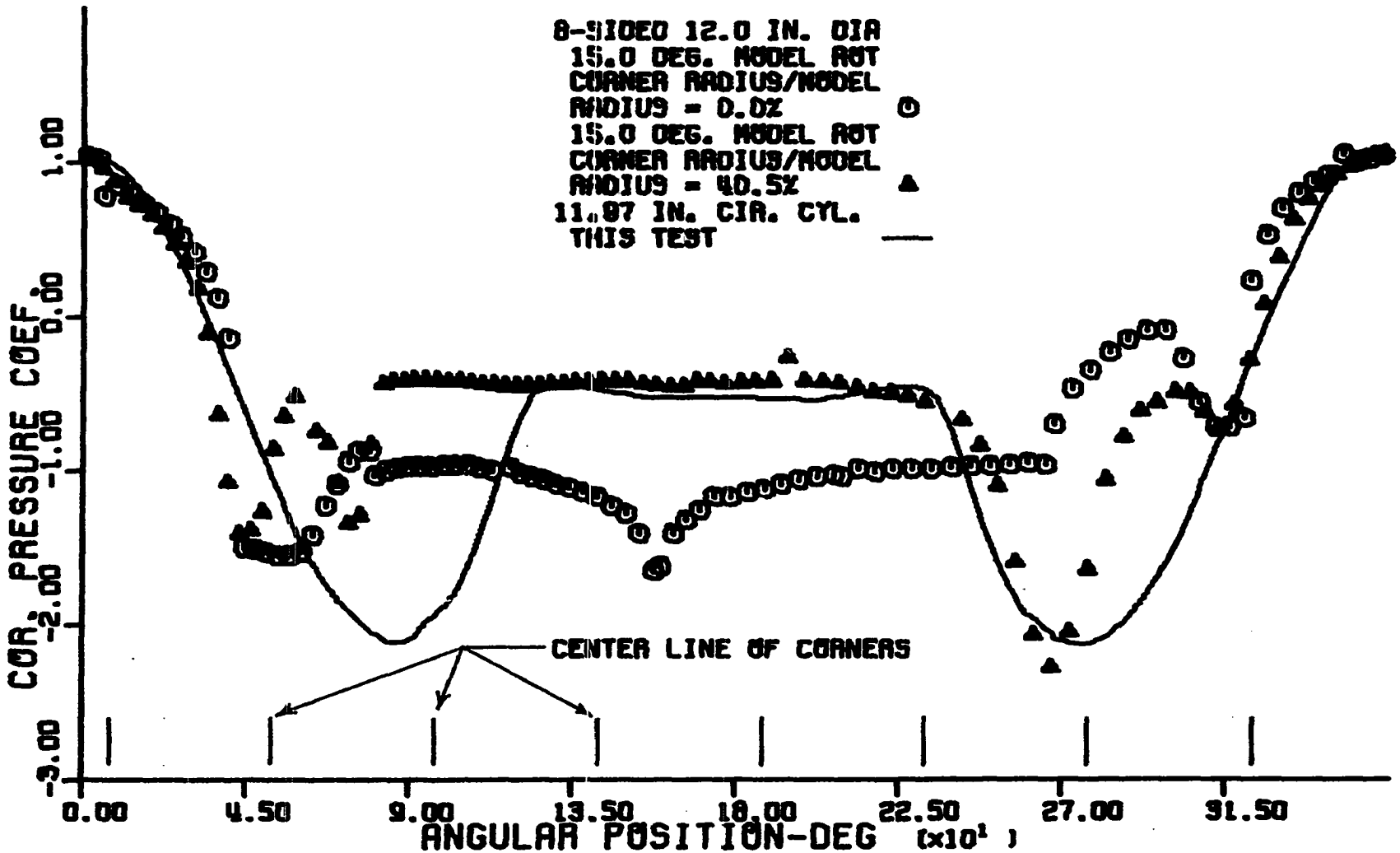

Figure 62. Variation of corrected pressure coefficient with change in angular position from the forward stagnation point for a circular cylinder and two octagonal cylinders, 0.0 and 40.5 percent corner radii, at 15.0° model rotation. Cylinders have corrected Reynolds numbers of 1,000,000.

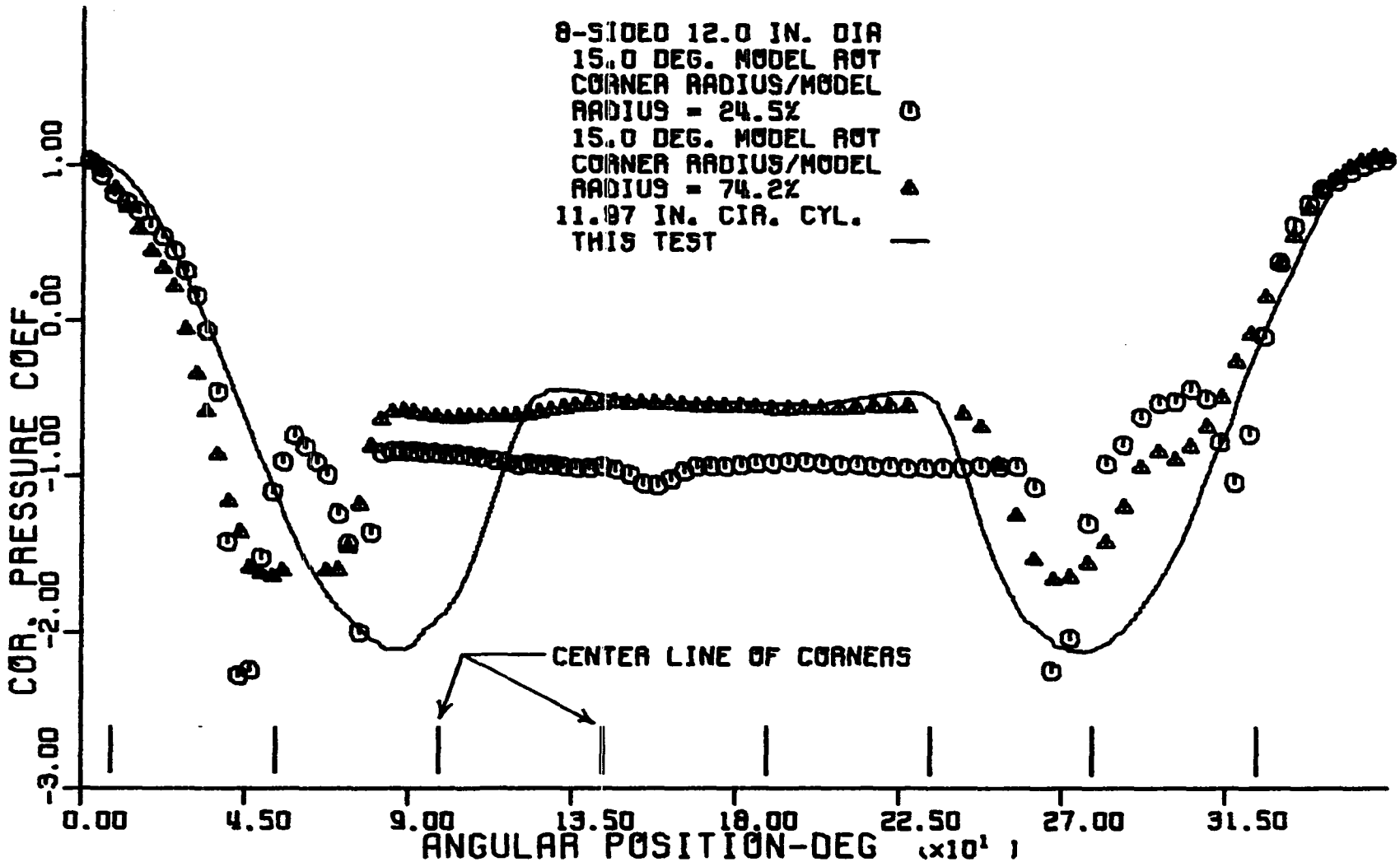

Figure 63. Variation of corrected pressure coefficient with change in angular position from the forward stagnation point for a circular cylinder and two octagonal cylinders, 24.5 and 74.2 percent corner radii, at 15.0° model rotation. Cylinders have corrected Reynolds numbers of 1,000,000.

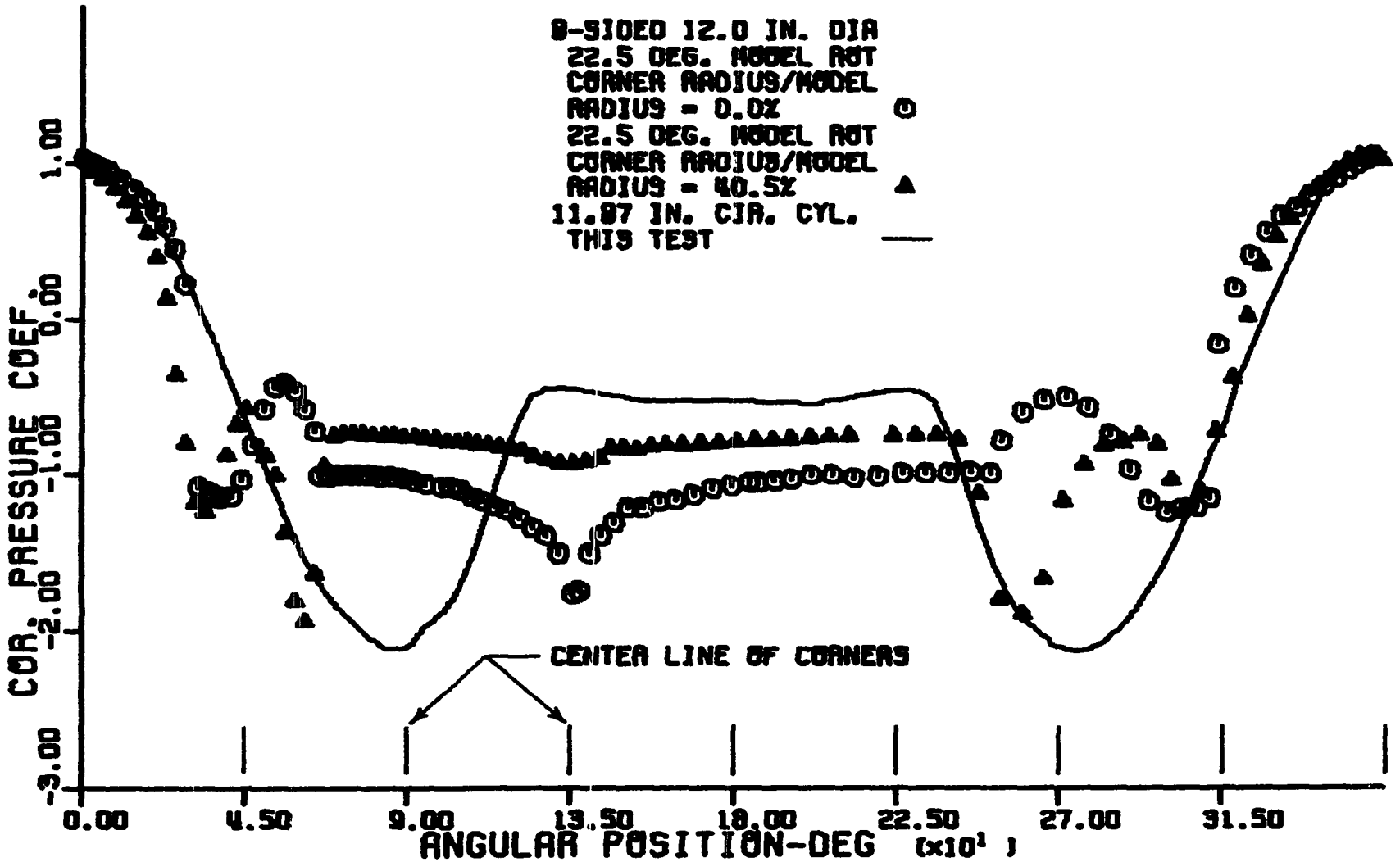

Figure 64. Variation of corrected pressure coefficient with change in angular position from the forward stagnation point for a circular cylinder and two octagonal cylinders, 0.0 and 40.5 percent corner radii, at 22.5° model rotation. Cylinders have corrected Reynolds numbers of 1,000,000.

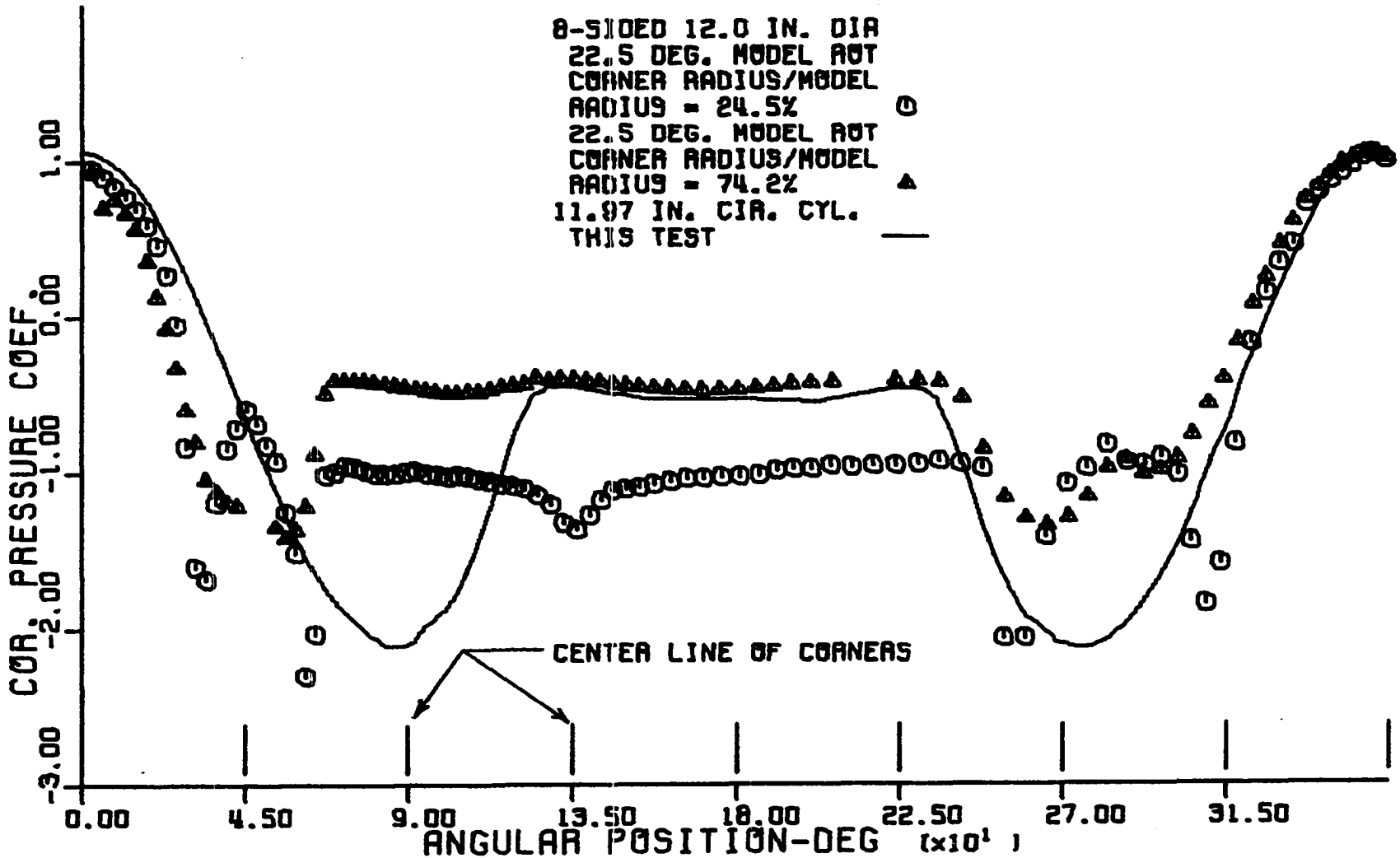

Figure 65. Variation of corrected pressure coefficient with change in angular position from the forward stagnation point for a circular cylinder and two octagonal cylinders, 24.5 and 74.2 percent corner radii, at 22.5° model rotation. Cylinders have corrected Reynolds numbers of 1,000,000.

in Figures 58, 60, 62 and 64 and the 24.5 percent and 74.2 percent 8-sided models are likewise compared in Figures 59, 61, 63 and 65. From these figures it is seen that the wide variation in drag coefficient for the polygonal cylinders results from the variation in static pressure distributions set up by the flow as it passes around the corners of the body. The net result is an interplay of two effects, the first being the form drag caused by the base pressure in the wake region being less than the pressure acting on the corresponding forward position of the body and the second being a small "thrust" effect on the rest of the body caused by the location of the minimum pressure point forward of 90°.

In the case of a circular cylinder the point of minimum pressure can be seen from Figure 9 to be located at approximately 86° from the forward stagnation point. Because of this the surface pressures acting at corresponding angular positions on either side of 90° are larger on the back or downwind side of the model than on the forward side and thus, the net force is in the thrust, or forward direction. This behavior occurs from approximately 42° to 138° or over the outer 25 percent of the body. However two effects combine to make this thrust force small. First the average pressure difference is less than one-half the pressure difference causing drag over the wake region and second, and more importantly, the model surface between 42° to 138° is very

close to parallel with the free-stream relative wind. The usual result is that this thrust force is generally small and the total force is dominated by the pressure imbalance acting in the wake region.

Considering first the 0° rotation, Figures 58 and 69, the decreased drag of the polygonal cylinders as compared to the circular cylinder comes about mainly because of the ability of the polygonal cylinders with the larger corner radii, greater than 40.5 percent, to produce a larger pressure recovery in the base region behind the model than can the circular cylinder. This pressure recovery leads to a reduced form or pressure drag which, as just pointed out, is the major component of the total drag. In addition to an improved base pressure recovery, the corners create a surface pressure on the front surface consisting of a series of relative pressure minima at the corners and pressure maxima on the flat sides between these corners. The location of the mid-point of the corners is indicated in Figures 58 to 65. The net effect of this pressure variation is to increase the thrust effect relative to that acting on a circular cylinder. This increase is due both to a larger pressure difference between the pressures acting on the front and rear surfaces of the body and to the fact that the outer surfaces of an octagonal shape are inclined at 45° to the flow which is more nearly normal to the free-stream velocity than are the outer

surfaces of a circular cylinder. This combination of a larger pressure difference acting on surfaces more nearly perpendicular to the relative wind makes this thrust effect much more important for the octagonal cylinders at 0° than for the circular cylinder. For the 0° rotation the thrust effect helps reduce the overall drag but this is not always the case, as the gain or loss in drag depends on the model orientation which determines the magnitude of the pressure relative to that on a circular cylinder.

Pressure distributions for the 7.5° rotation are shown in Figures 60 and 61. Again the base pressure recovery is greater than that of the circular cylinders and as a result the octagonal cylinder again has less drag than the circular cylinder. The effect of rotating the body is also evident in these figures. As the corners on a surface move forward the negative pressure spikes at these corners become smaller, while on the surface that moves toward the rear the peaks become more negative. This will be discussed in greater detail when the lift or side force is covered. The base pressure recovery continues to decrease for model rotations of 15° and 22.5°, Figures 62 to 65, giving rise to larger drags. At these orientations the drag of the octagonal cylinders is greater than the circular cylinder except for the 74.2 percent model at 22.5°.

The importance of the pressure distribution over the

surface reaches its maximum for cases where the base pressures of the polygonal and circular cylinder are about equal, such as the case of the 40.5 percent model at a 15° rotation. In this case consideration of the base pressure alone would lead to the erroneous conclusion that the drag of the octagonal cylinder was less than that of the circular cylinder. However, due to a decrease in the thrust effect over the outer parts of the octagonal cylinder relative to that acting on a circular cylinder the drag of the octagonal cylinder is slightly greater than that of the circular cylinder. As the reader studies Figures 58 to 65 he must remember that the surface of the polygonal cylinder consists of a series of flat walls between the corners, so that just because a point is between 90° and 270°, it does not mean it is on the leeward or back side of the model. It depends on the orientation of the model.

The magnitude of the base pressure appears to be tied to the minimum pressure acting on the last corner before separation on the surface that has rotated forward, in this report the upper surface as shown in Figure 1. As this pressure becomes more negative, as it does with sharper corners corners, so does the base pressure which yields an increasing drag.

Coefficient of lift

The lift forces being produced on the cylinders are shown in Figures 68 to 81 for the octagonal cylinders, Figures 82 to 95 for the dodecagonal cylinders and Figures 96 to 102 for the hexdecagonal cylinders. In these figures the corrected lift coefficient or side force coefficient is plotted versus corrected Reynolds number. It will be remembered from Equation 14 that the blockage correction for both the lift and drag coefficients are the same. The magnitude of this correction can be seen by comparing the uncorrected lift coefficients for the sharp-cornered octagonal cylinder shown in Figures 66 and 67 with the corrected lift coefficients shown in Figures 68 and 69. As with drag the correction decreased the magnitude of the coefficients for the same model. At Reynolds numbers below critical, the lift coefficient is rather unsteady, producing nonzero values for all model orientations. This is to be expected since at these Reynolds numbers the flow is very unsteady, with flow patterns showing large changes. At Reynolds numbers above critical, out of the range of rapidly changing drag, this unsteadiness disappears and the flow becomes much more predictable. Here the side force essentially disappears for model orientations of 0° and 22.5° for the 8-sided bodies, 0° and 15° for the 12-sided bodies and 0° and 11.25° for the 16-sided bodies since at these orientations the upper and

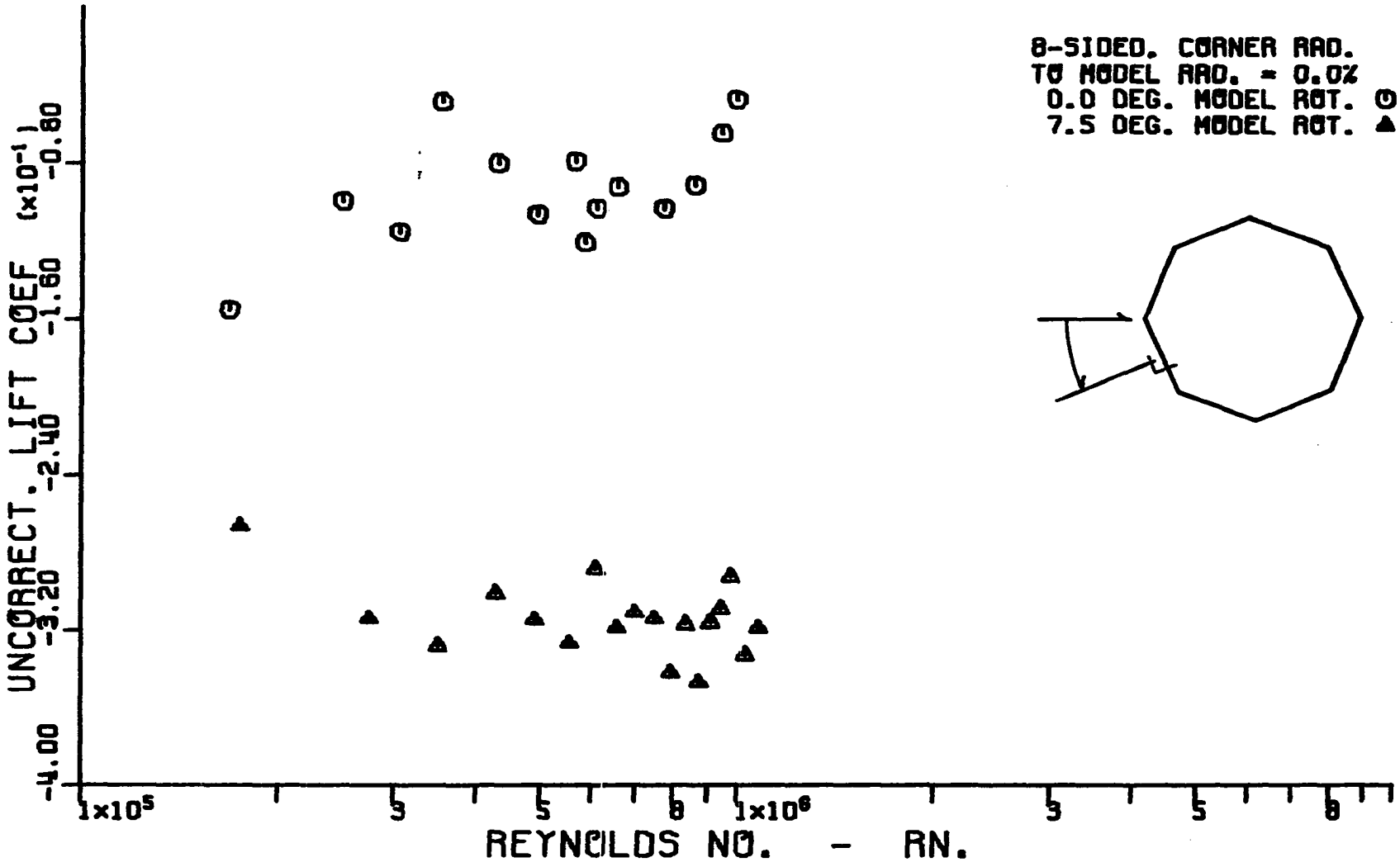

Figure 66. Variation of uncorrected cross-flow lift coefficient with uncorrected cross-flow Reynolds number for an octagonal cylinder having a corner radius equal to 0.0 percent of the radius of the inscribed circular cylinder.

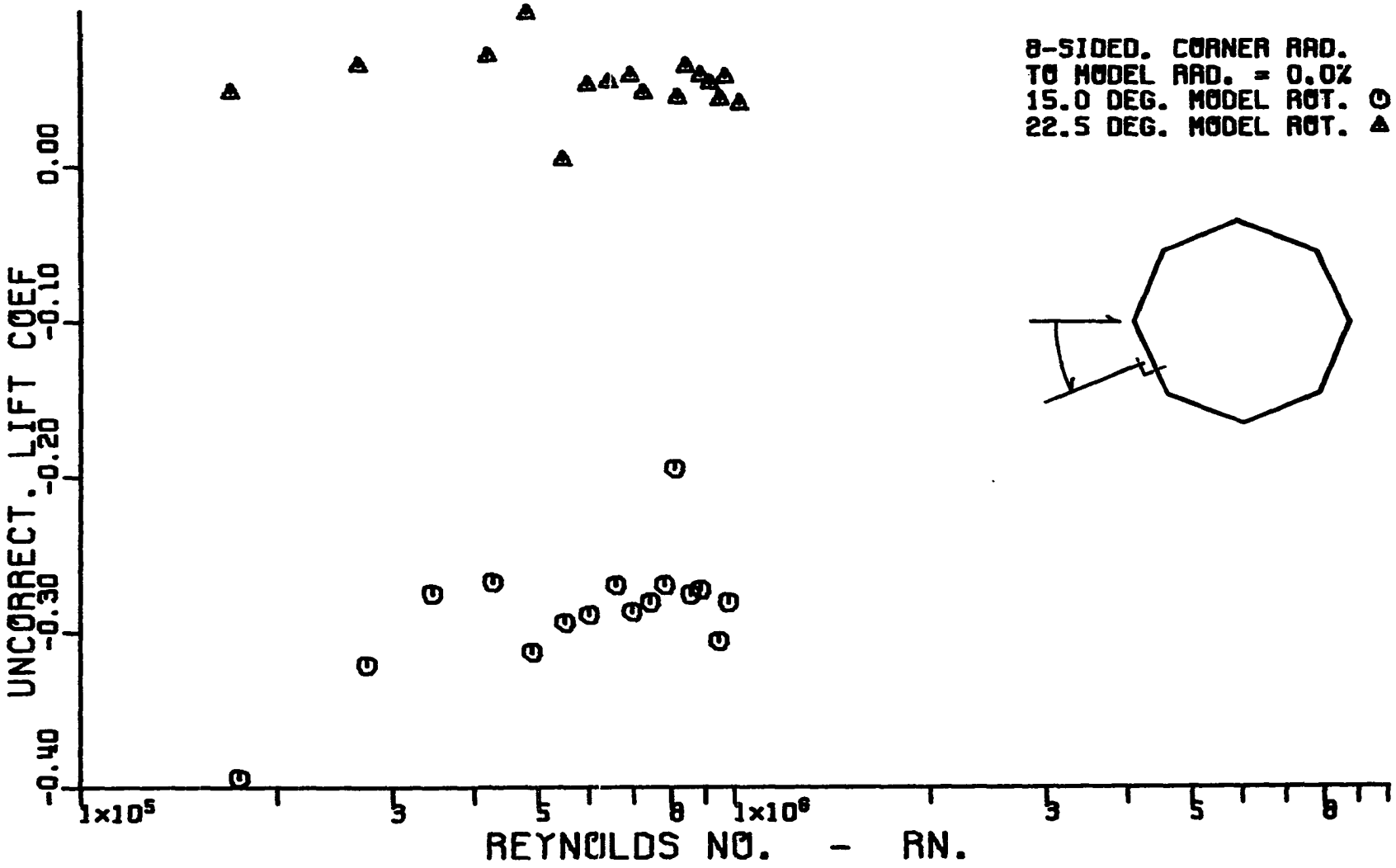

Figure 67. Variation of uncorrected cross-flow lift coefficient with uncorrected cross-flow Reynolds number for an octagonal cylinder having a corner radius equal to 0.0 percent of the radius of the inscribed circular cylinder.

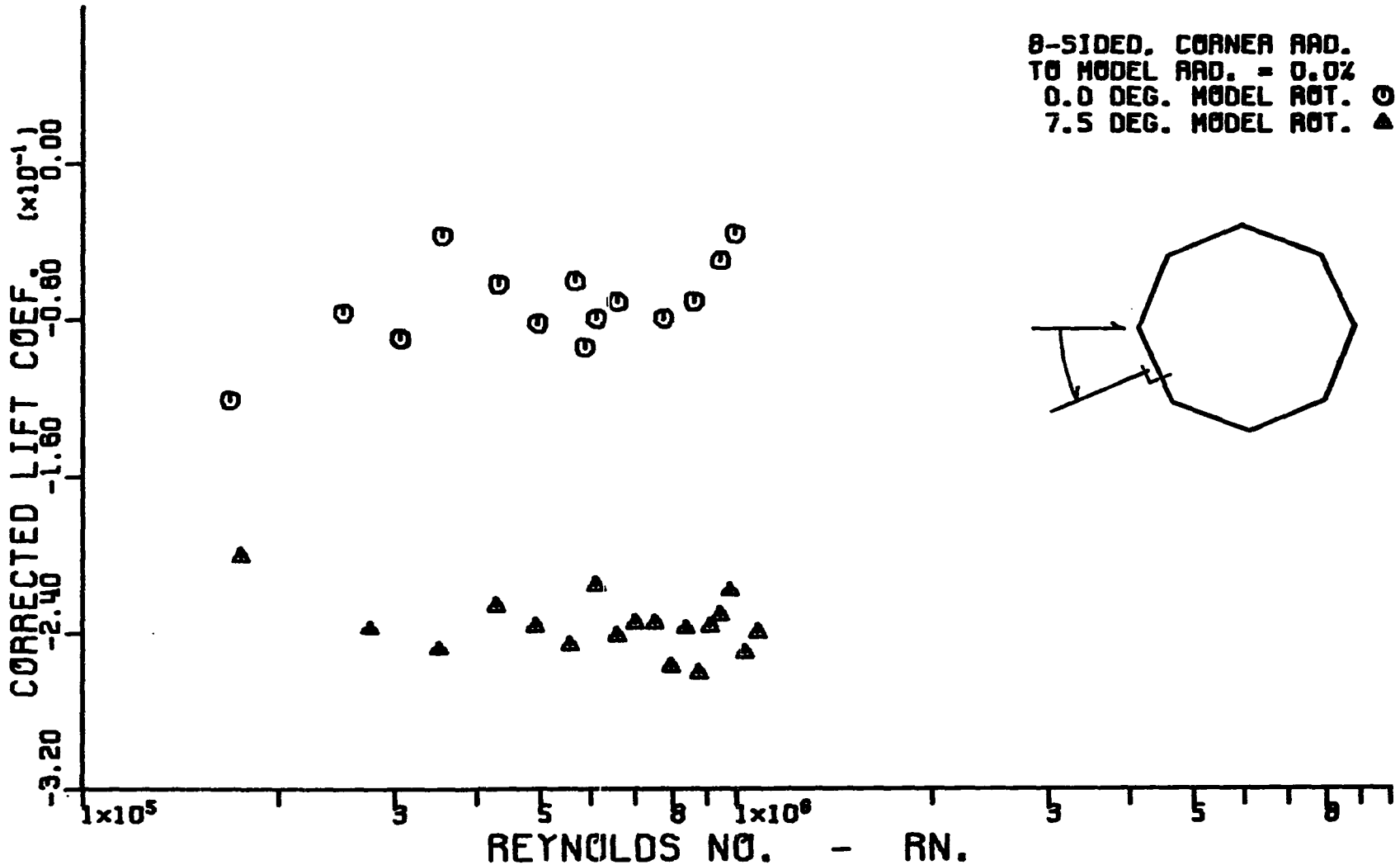

Figure 68. Variation of corrected cross-flow lift coefficient with corrected cross-flow Reynolds number for an octagonal cylinder having a corner radius equal to 0.0 percent of the radius of the inscribed circular cylinder.

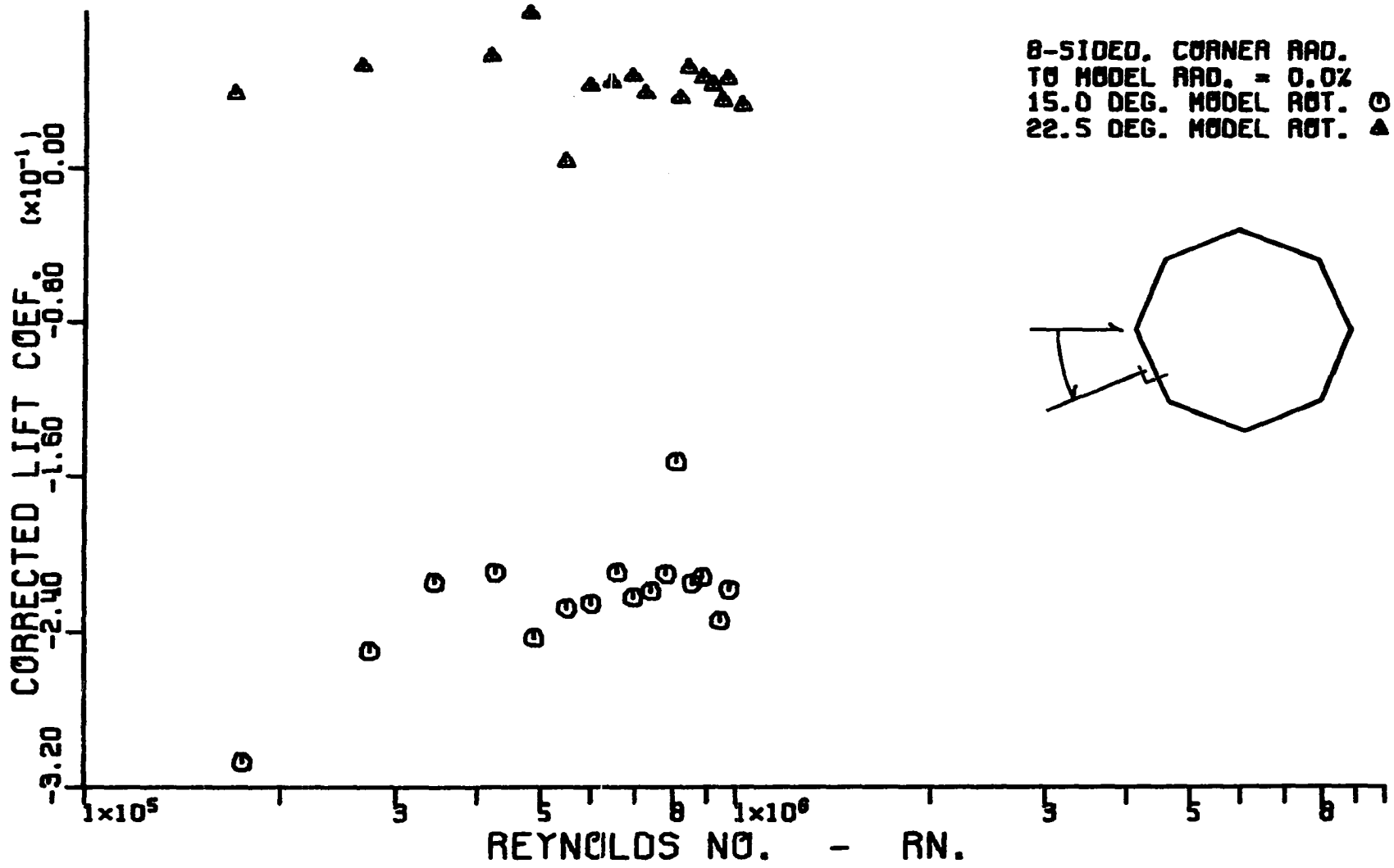

Figure 69. Variation of corrected cross-flow lift coefficient with corrected cross-flow Reynolds number for an octagonal cylinder having a corner radius equal to 0.0 percent of the radius of the inscribed circular cylinder.

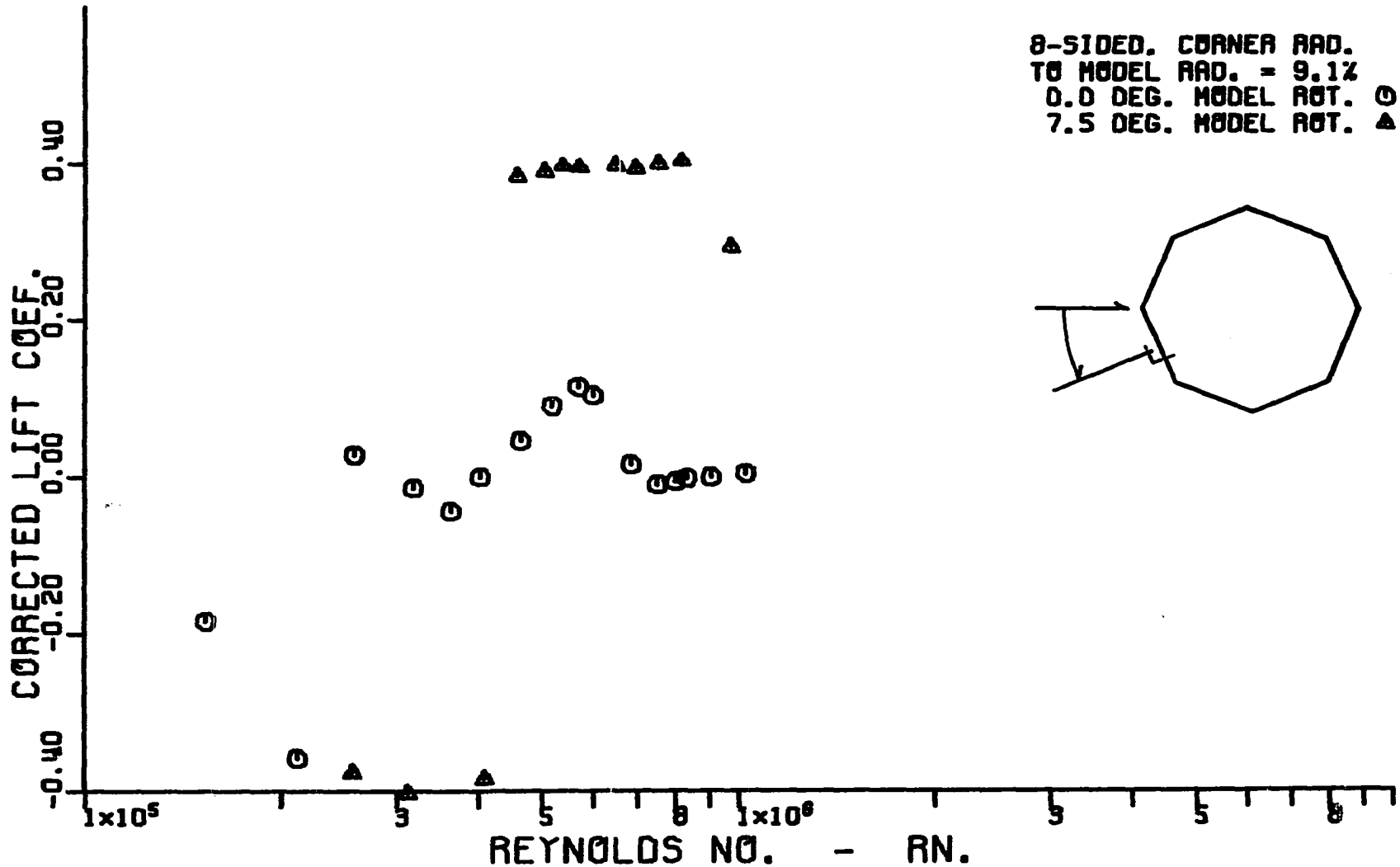

Figure 70. Variation of corrected cross-flow lift coefficient with corrected cross-flow Reynolds number for an octagonal cylinder having a corner radius equal to 9.1 percent of the radius of the inscribed circular cylinder.

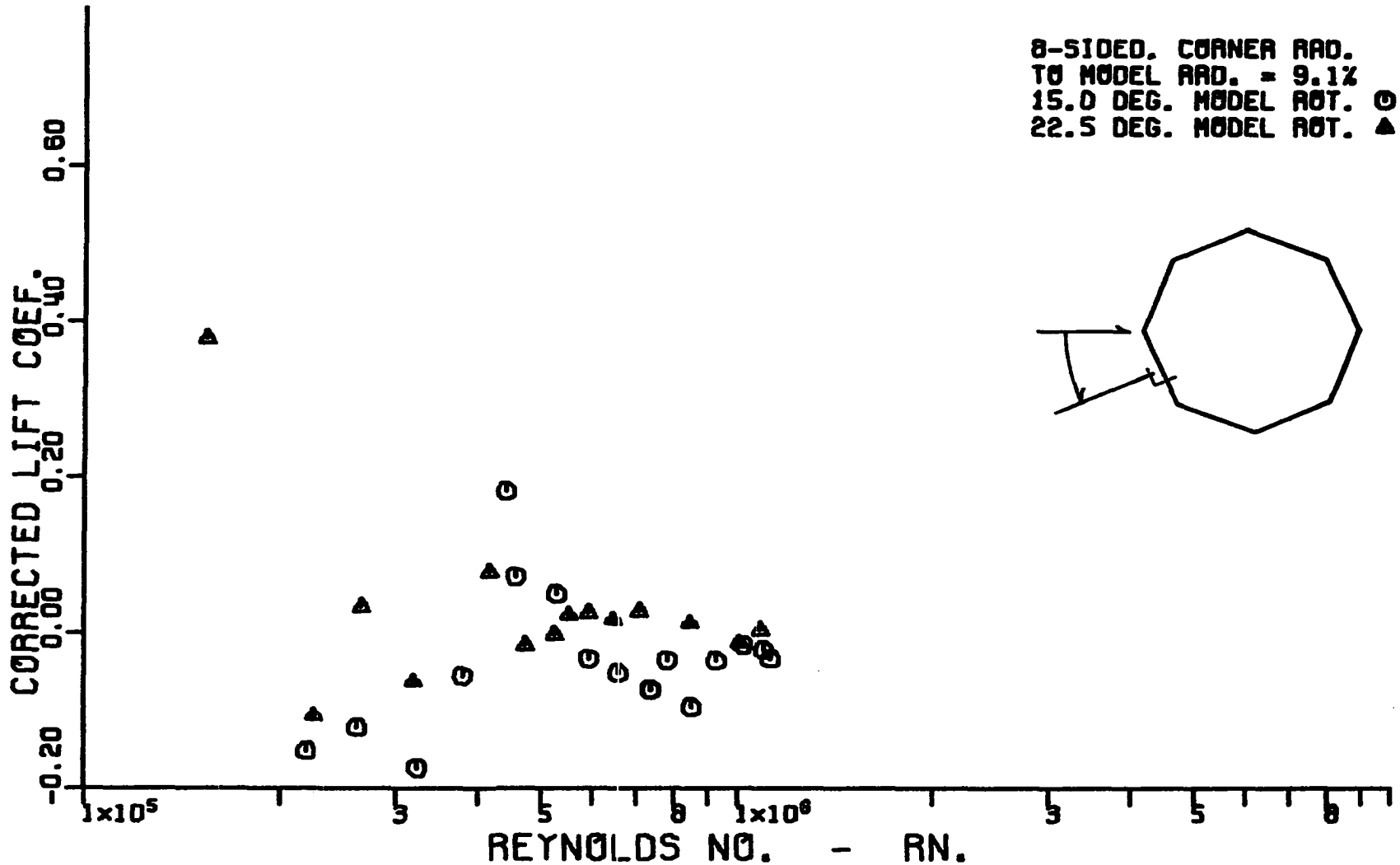

Figure 71. Variation of corrected cross-flow lift coefficient with corrected cross-flow Reynolds number for an octagonal cylinder having a corner radius equal to 9.1 percent of the radius of the inscribed circular cylinder.

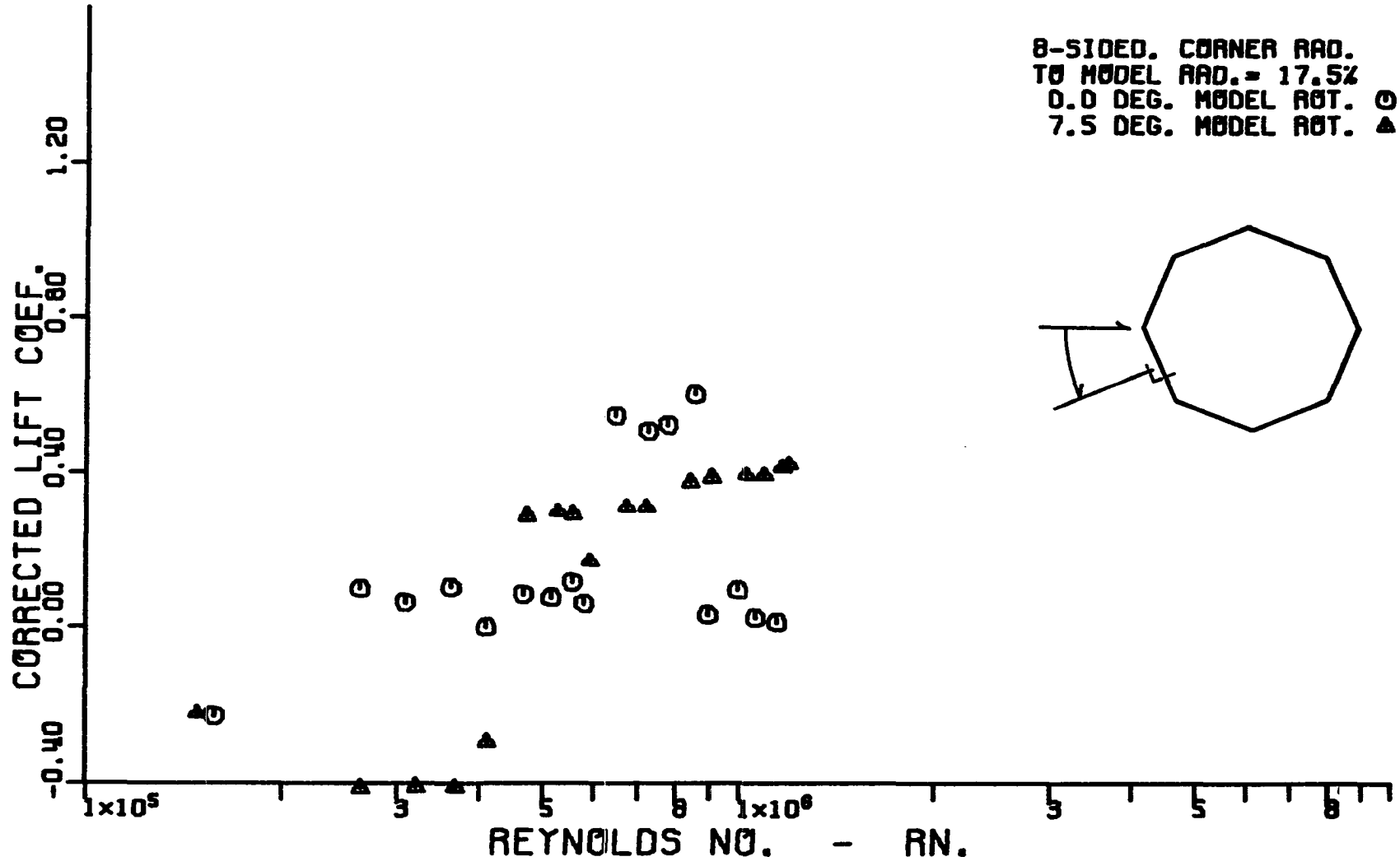

Figure 72. Variation of corrected cross-flow lift coefficient with corrected cross-flow Reynolds number for an octagonal cylinder having a corner radius equal to 17.5 percent of the radius of the inscribed circular cylinder.

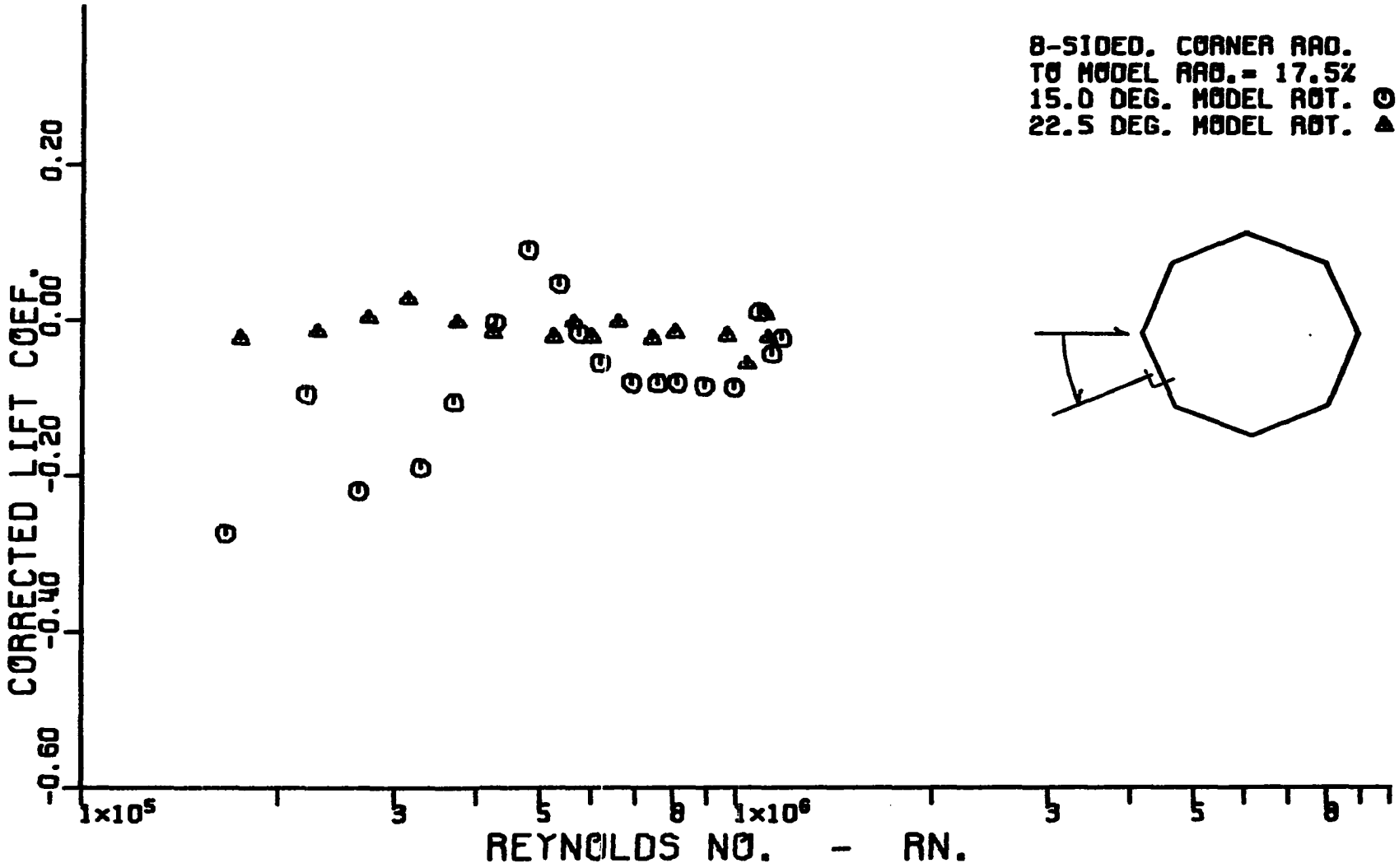

Figure 73. Variation of corrected cross-flow lift coefficient with corrected cross-flow Reynolds number for an octagonal cylinder having a corner radius equal to 17.5 percent of the radius of the inscribed circular cylinder.

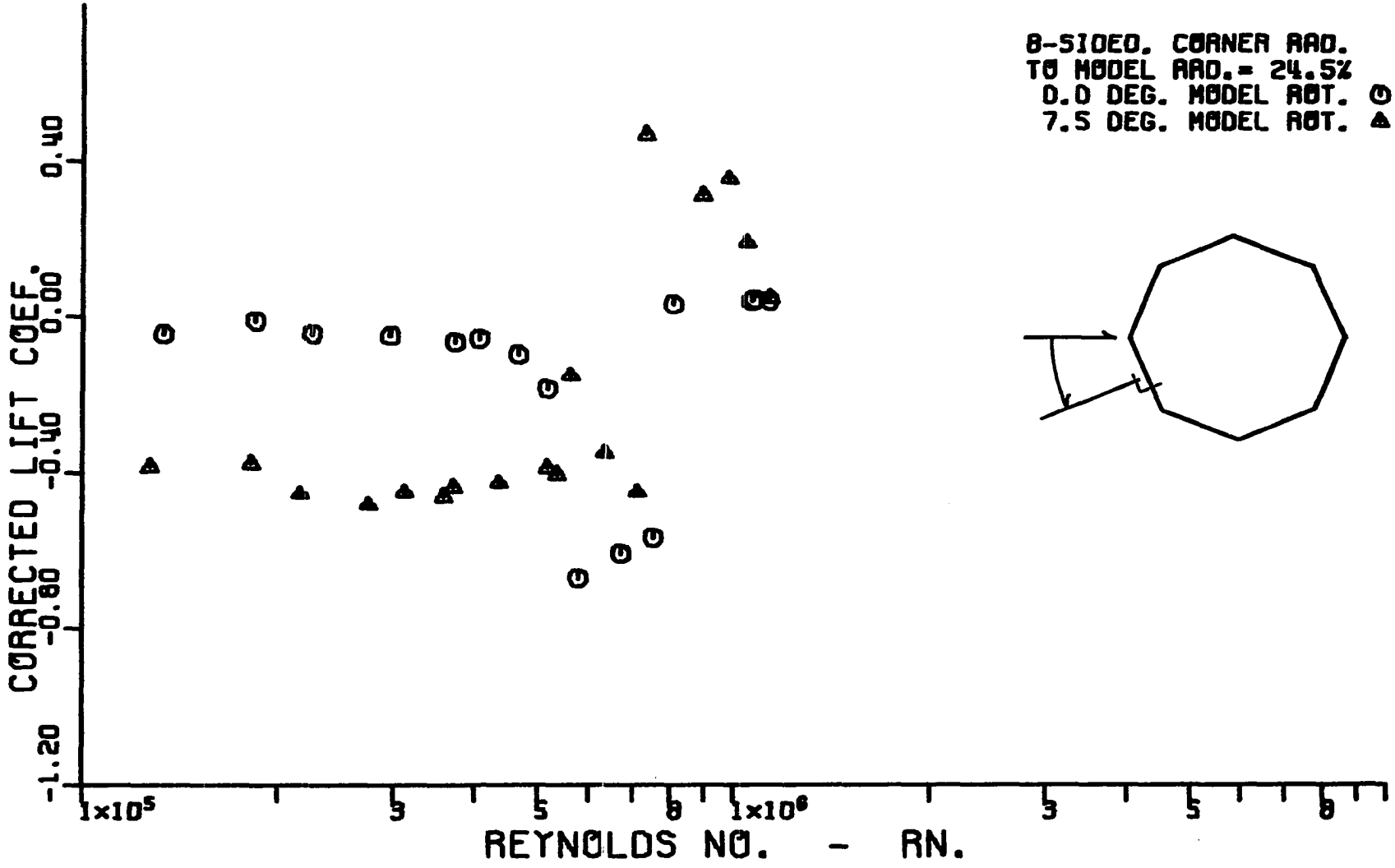

Figure 74. Variation of corrected cross-flow lift coefficient with corrected cross-flow Reynolds number for an octagonal cylinder having a corner radius equal to 24.5 percent of the radius of the inscribed circular cylinder.

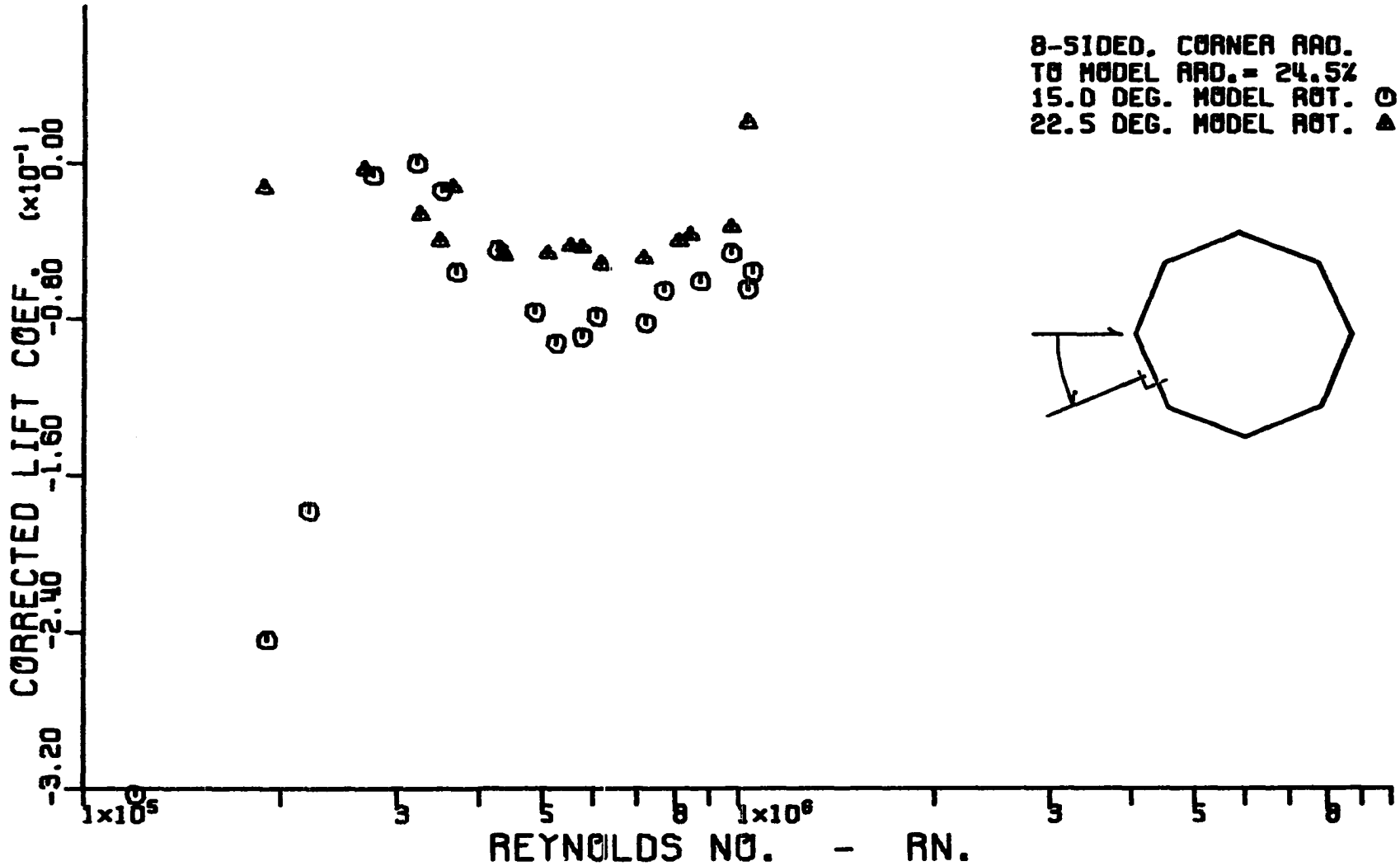

Figure 75. Variation of corrected cross-flow lift coefficient with corrected cross-flow Reynolds number for an octagonal cylinder having a corner radius equal to 24.5 percent of the radius of the inscribed circular cylinder.

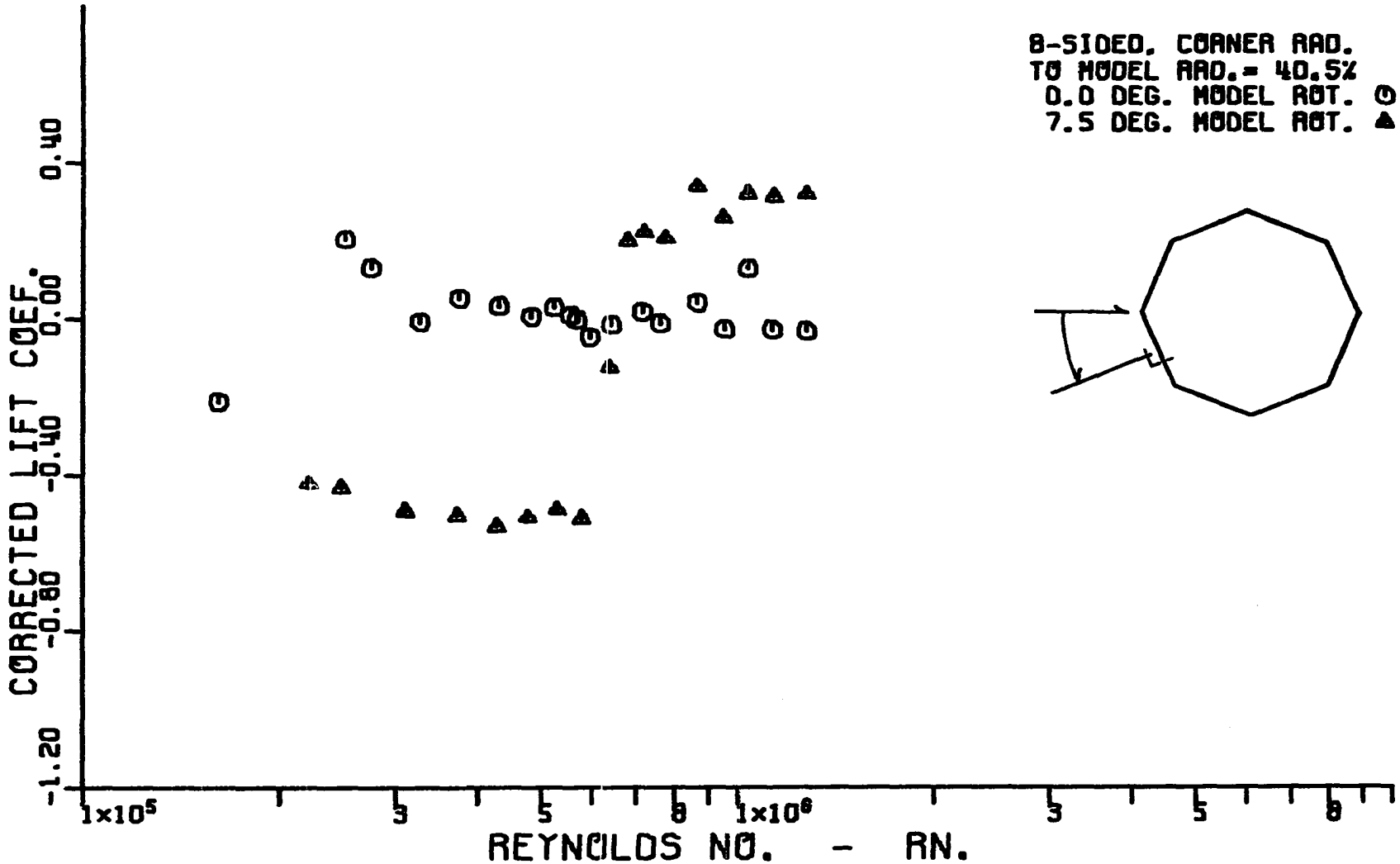

Figure 76. Variation of corrected cross-flow lift coefficient with corrected cross-flow Reynolds number for an octagonal cylinder having a corner radius equal to 40.5 percent of the radius of the inscribed circular cylinder.

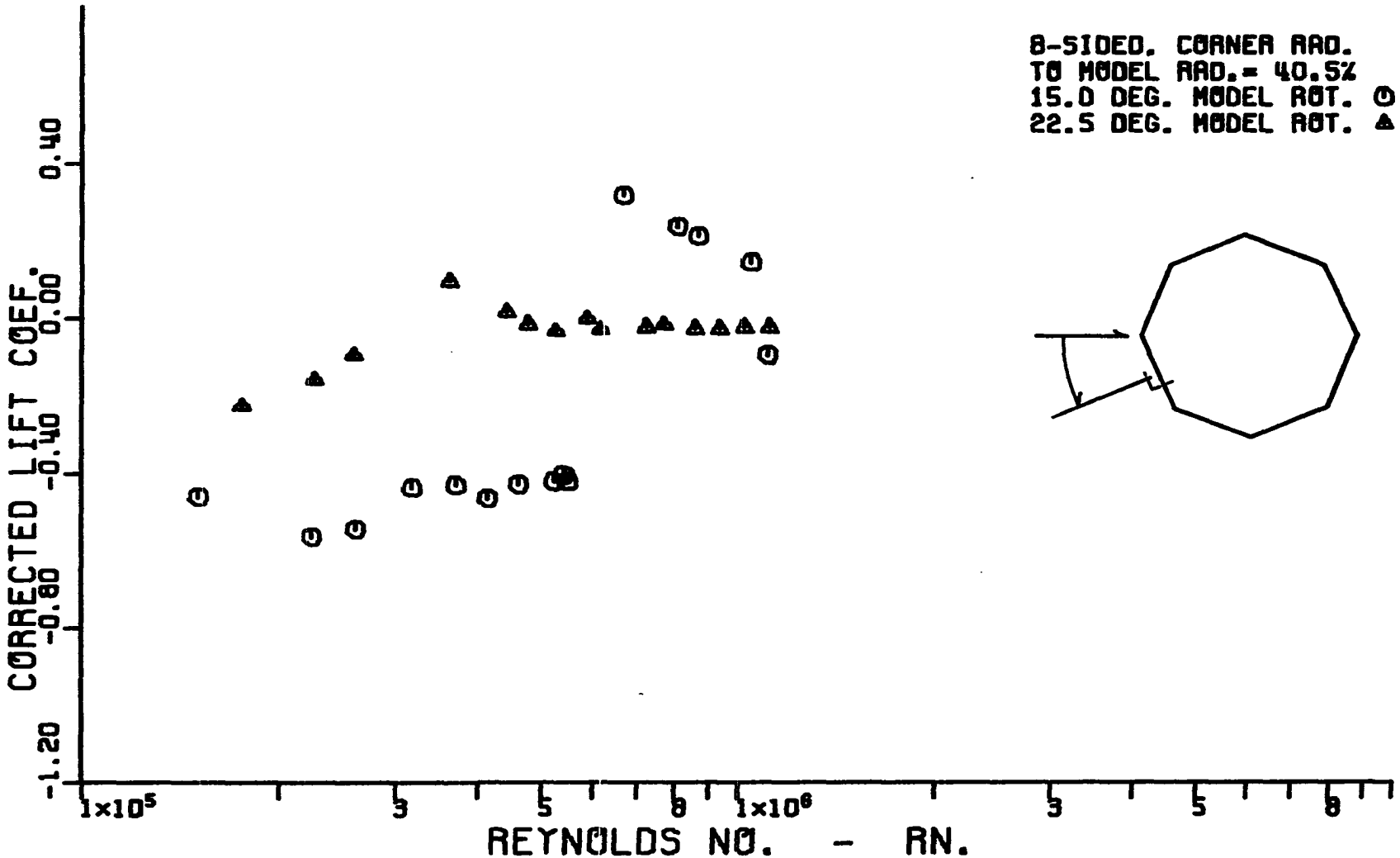

Figure 77. Variation of corrected cross-flow lift coefficient with corrected cross-flow Reynolds number for an octagonal cylinder having a corner radius equal to 40.5 percent of the radius of the inscribed circular cylinder.

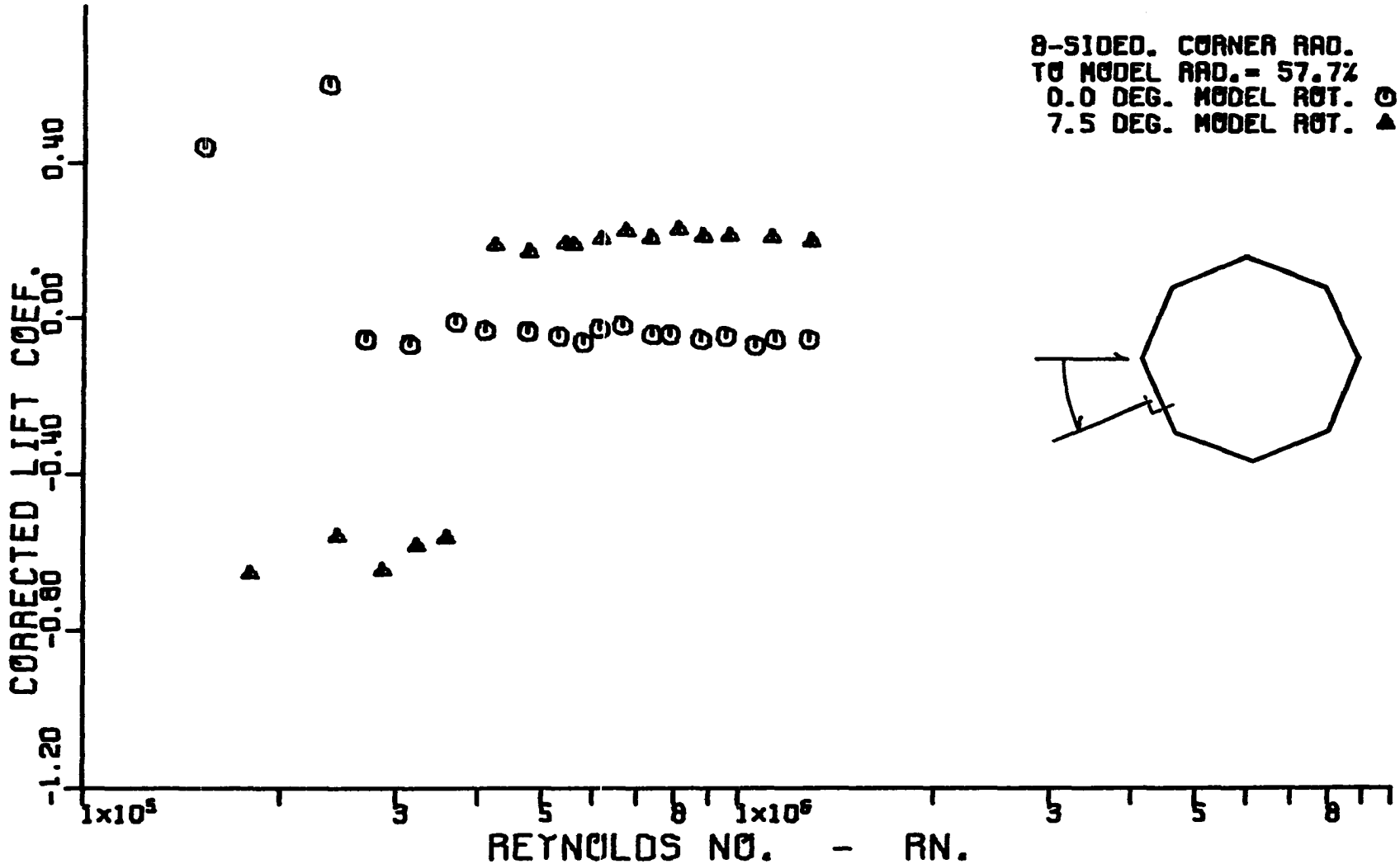

Figure 78. Variation of corrected cross-flow lift coefficient with corrected cross-flow Reynolds number for an octagonal cylinder having a corner radius equal to 57.7 percent of the radius of the inscribed circular cylinder.

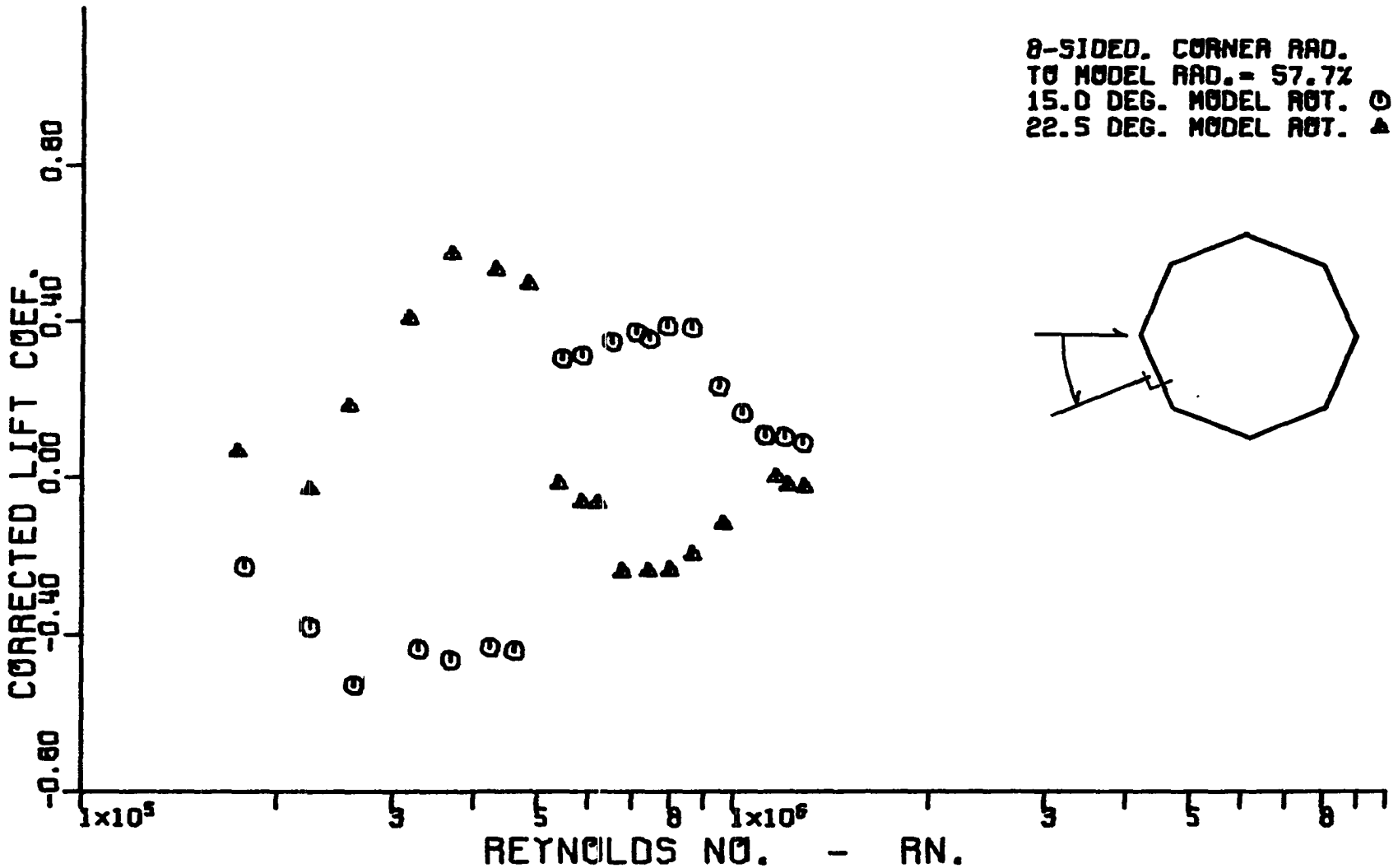

Figure 79. Variation of corrected cross-flow lift coefficient with corrected cross-flow Reynolds number for an octagonal cylinder having a corner radius equal to 57.7 percent of the radius of the inscribed circular cylinder.

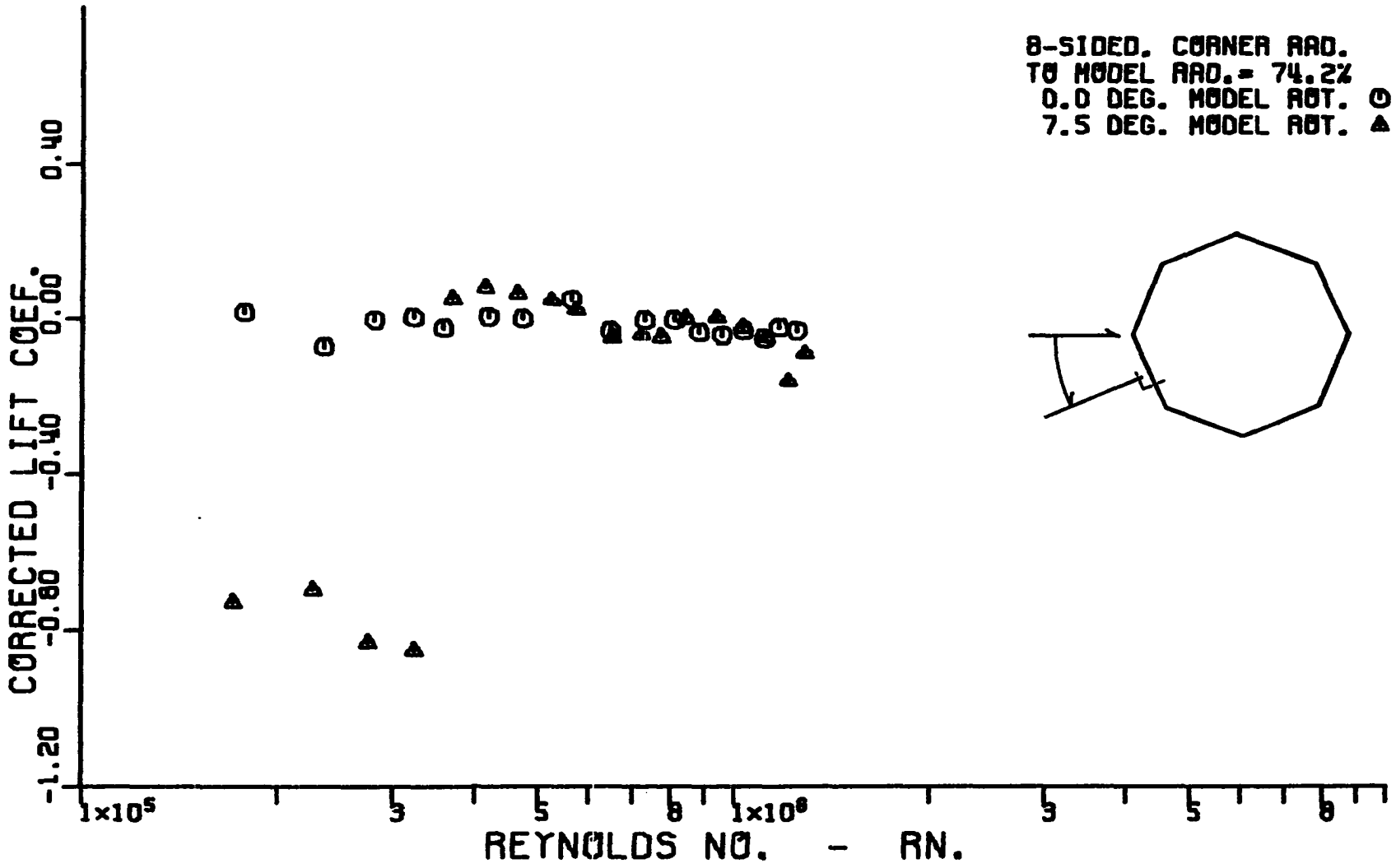

Figure 80. Variation of corrected cross-flow lift coefficient with corrected cross-flow Reynolds number for an octagonal cylinder having a corner radius equal to 74.2 percent of the radius of the inscribed circular cylinder.

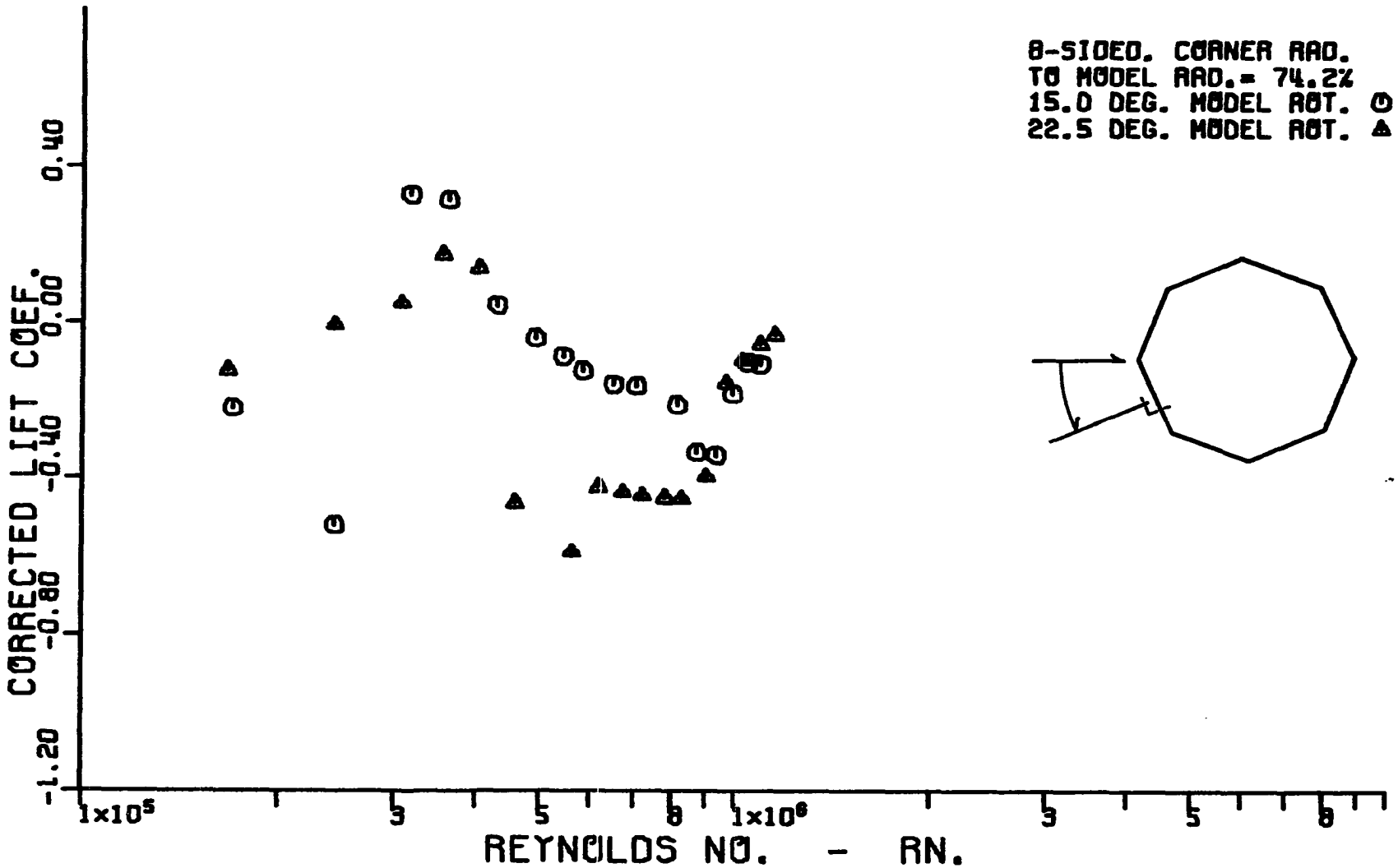

Figure 81. Variation of corrected cross-flow lift coefficient with corrected cross-flow Reynolds number for an octagonal cylinder having a corner radius equal to 74.2 percent of the radius of the inscribed circular cylinder.

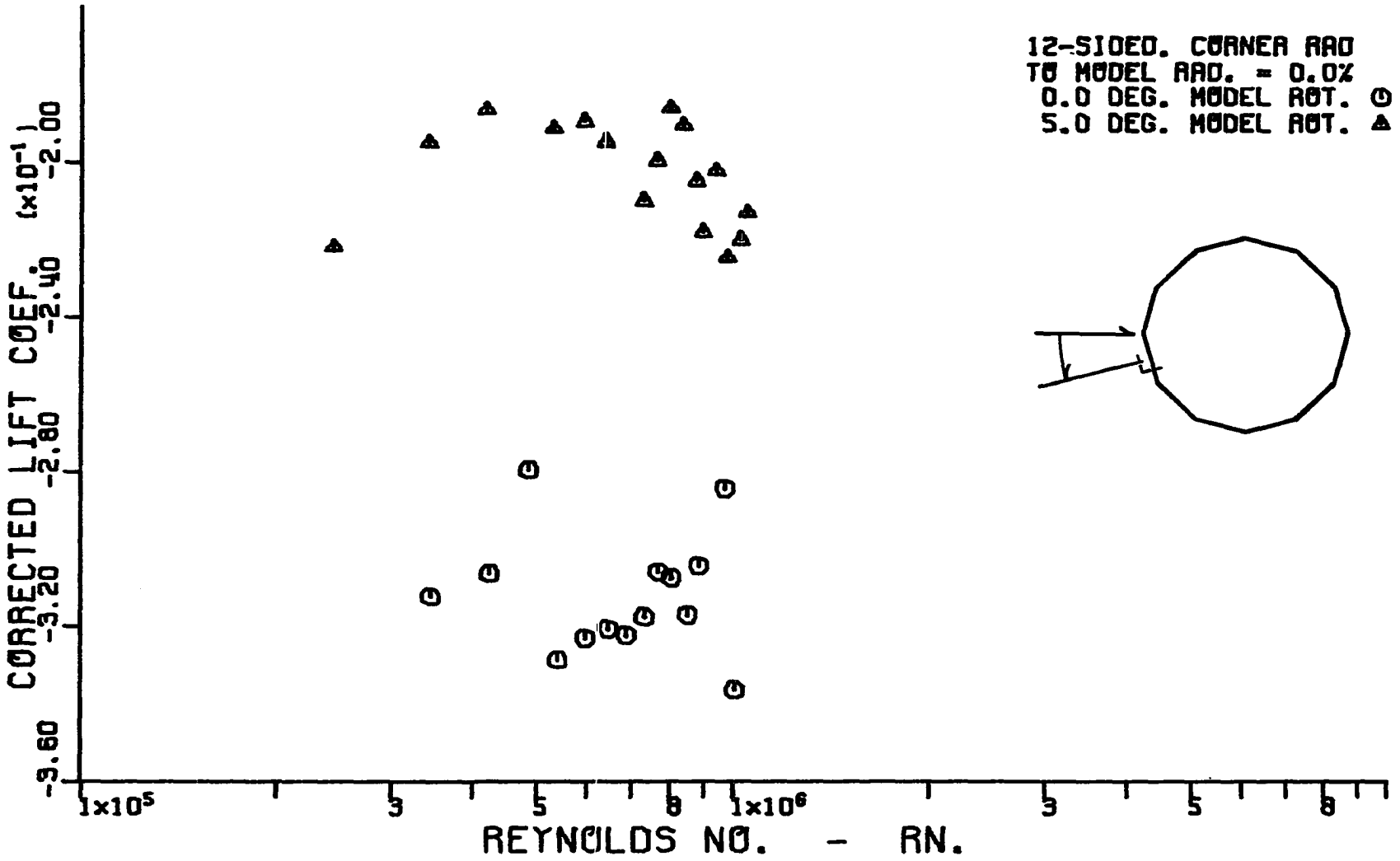

Figure 82. Variation of corrected cross-flow lift coefficient with corrected cross-flow Reynolds number for a dodecagonal cylinder having a corner radius equal to 0.0 percent of the radius of the inscribed circular cylinder.

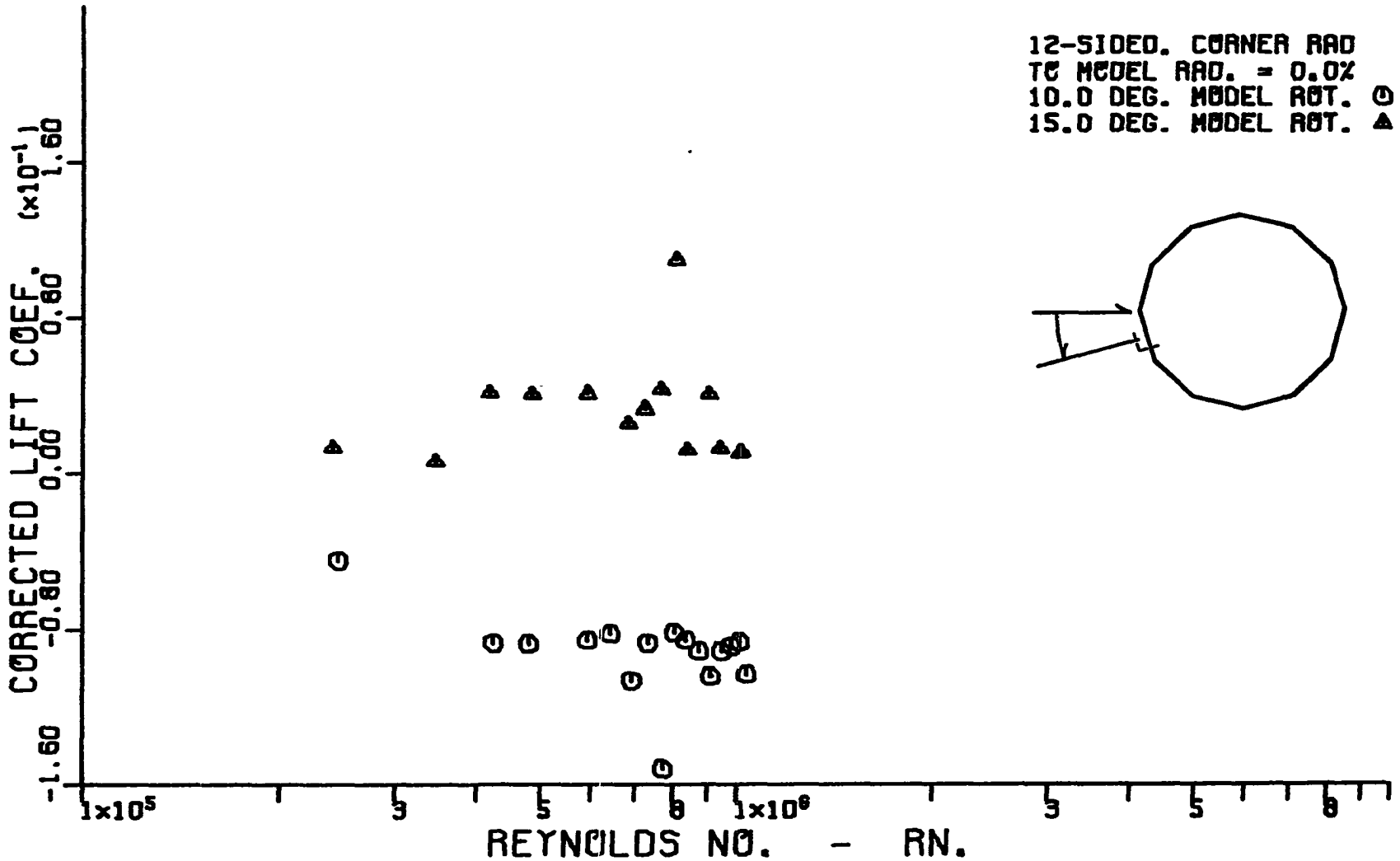

Figure 83. Variation of corrected cross-flow lift coefficient with corrected cross-flow Reynolds number for a dodecagonal cylinder having a corner radius equal to 0.0 percent of the radius of the inscribed circular cylinder.

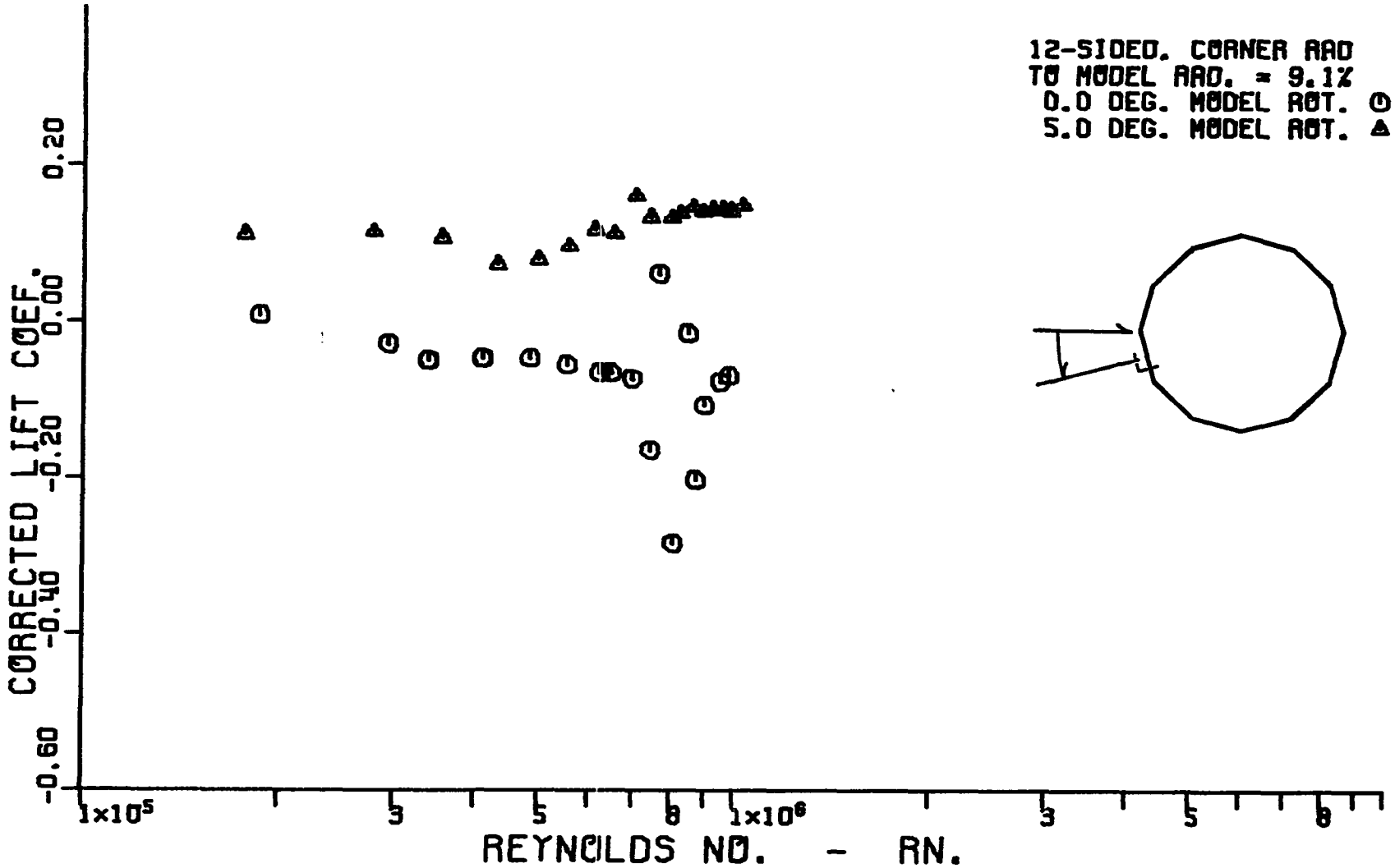

Figure 84. Variation of corrected cross-flow lift coefficient with corrected cross-flow Reynolds number for a dodecagonal cylinder having a corner radius equal to 9.1 percent of the radius of the inscribed circular cylinder.

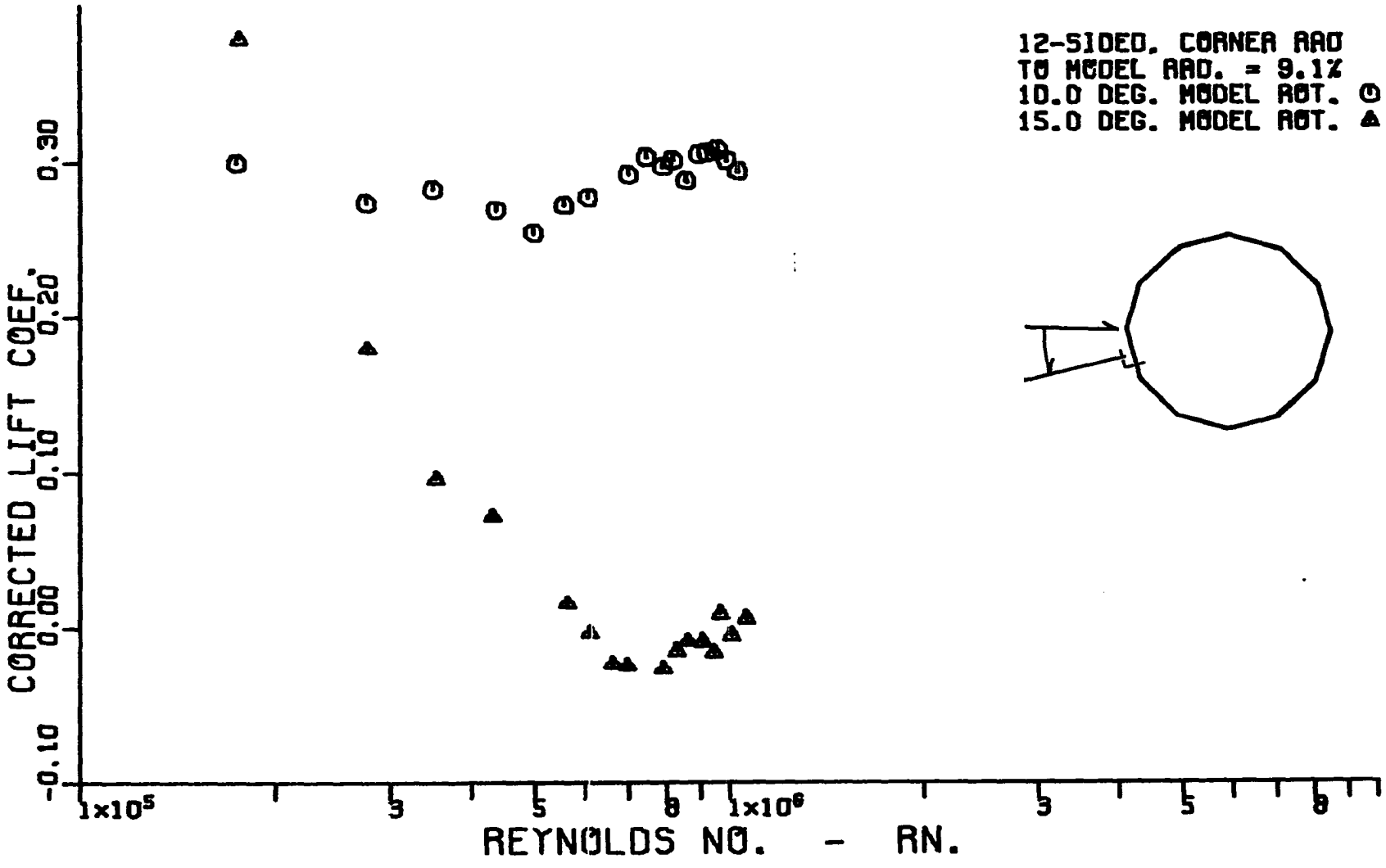

Figure 85. Variation of corrected cross-flow lift coefficient with corrected cross-flow Reynolds number for a dodecagonal cylinder having a corner radius equal to 9.1 percent of the radius of the inscribed circular cylinder.

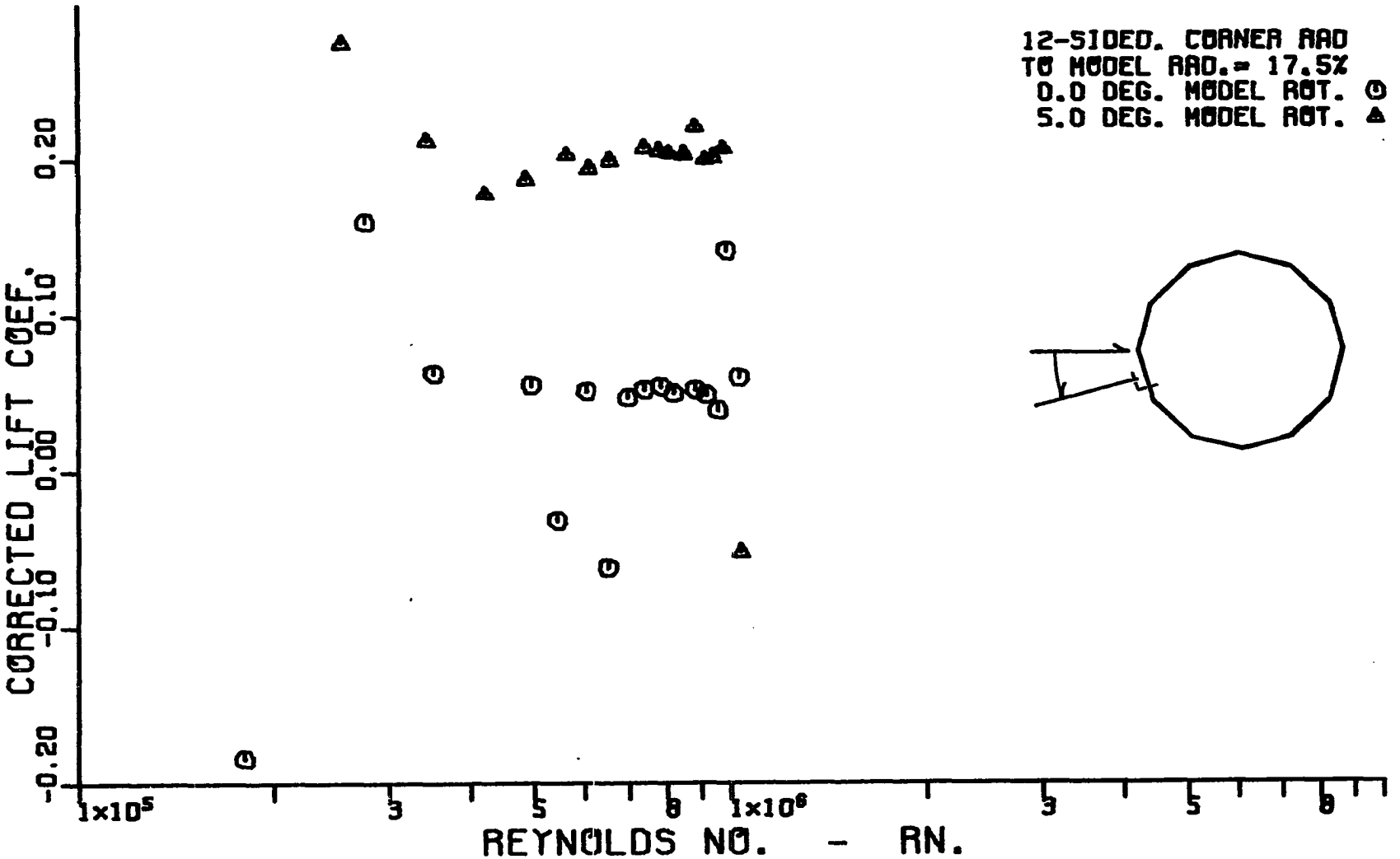

Figure 86. Variation of corrected cross-flow lift coefficient with corrected cross-flow Reynolds number for a dodecagonal cylinder having a corner radius equal to 17.5 percent of the radius of the inscribed circular cylinder.

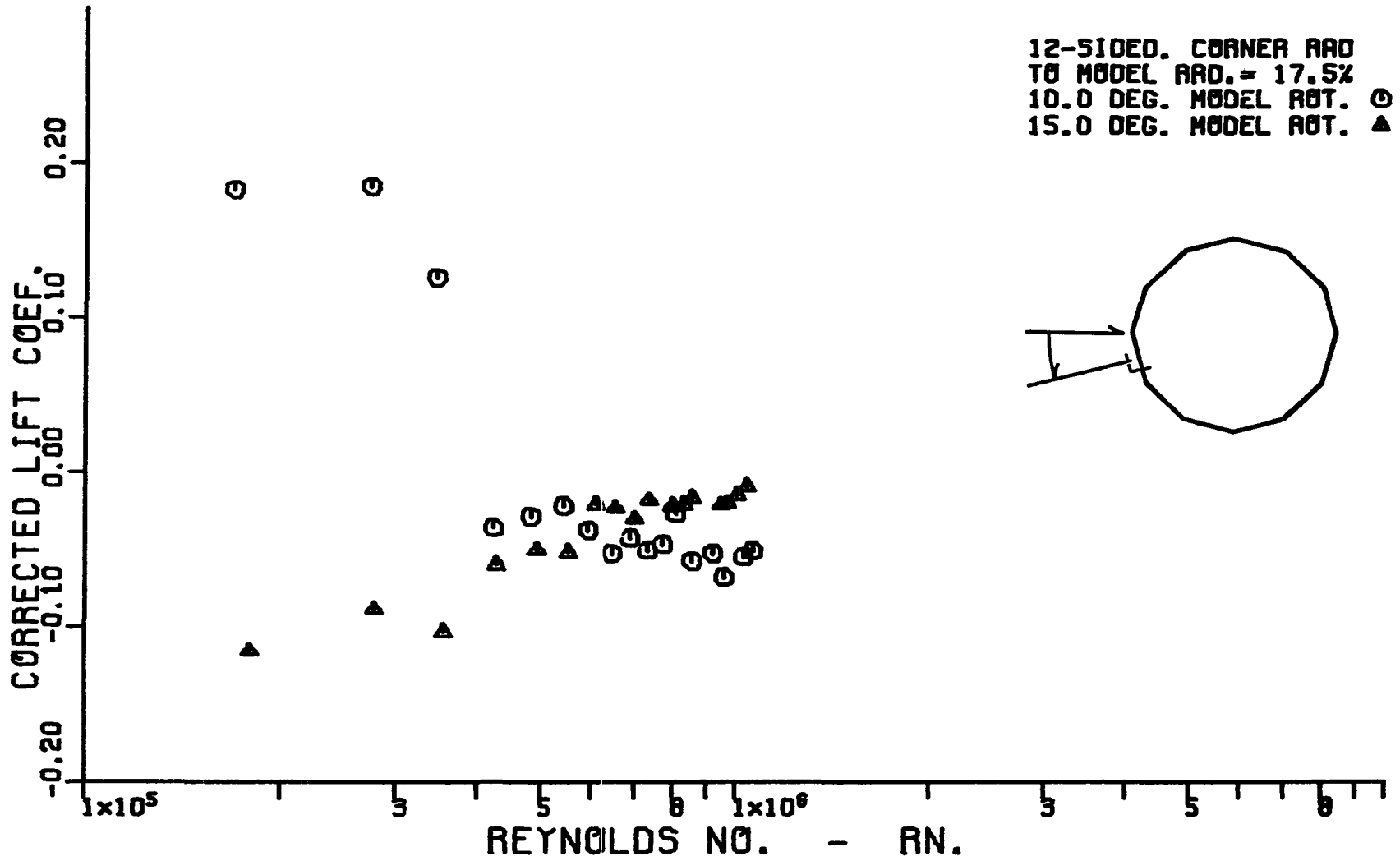

Figure 87. Variation of corrected cross-flow lift coefficient with corrected cross-flow Reynolds number for a dodecagonal cylinder having a corner radius equal to 17.5 percent of the radius of the inscribed circular cylinder.

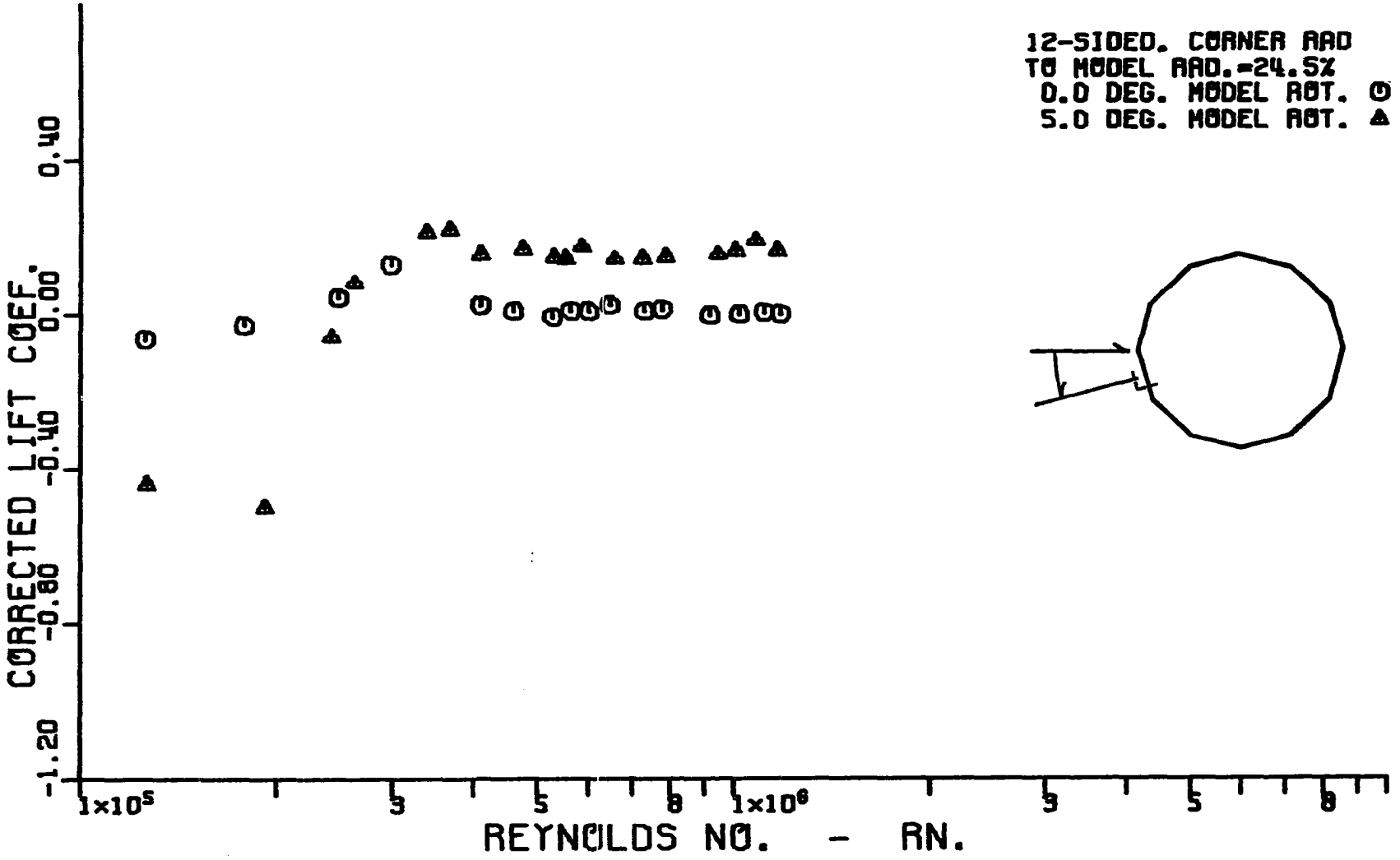

Figure 88. Variation of corrected cross-flow lift coefficient with corrected cross-flow Reynolds number for a dodecagonal cylinder having a corner radius equal to 24.5 percent of the radius of the inscribed circular cylinder.

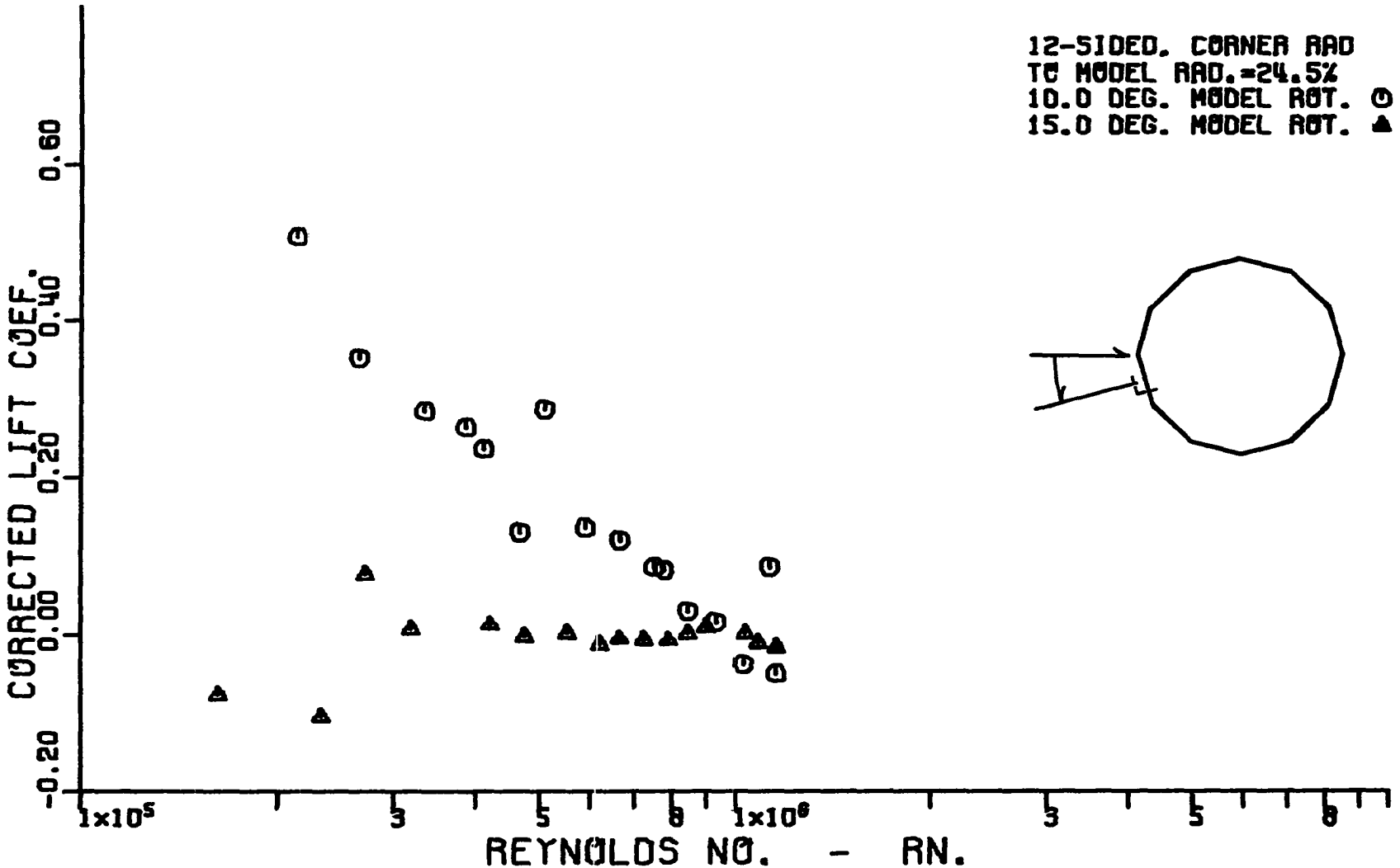

Figure 89. Variation of corrected cross-flow lift coefficient with corrected cross-flow Reynolds number for a dodecagonal cylinder having a corner radius equal to 24.5 precent of the radius of the inscribed circular cylinder.

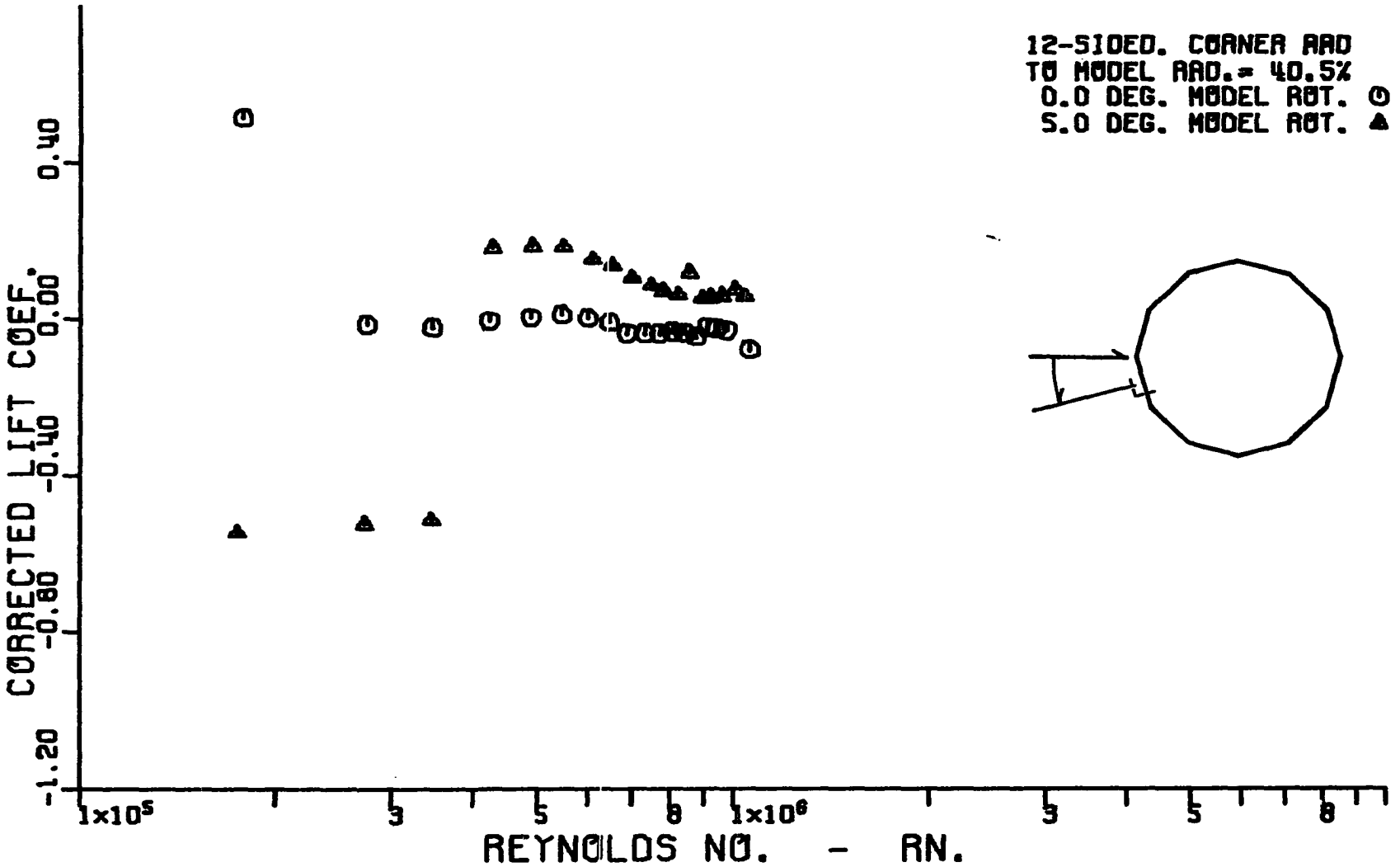

Figure 90. Variation of corrected cross-flow lift coefficient with corrected cross-flow Reynolds number for a dodecagonal cylinder having a corner radius equal to 40.5 percent of the radius of the inscribed circular cylinder.

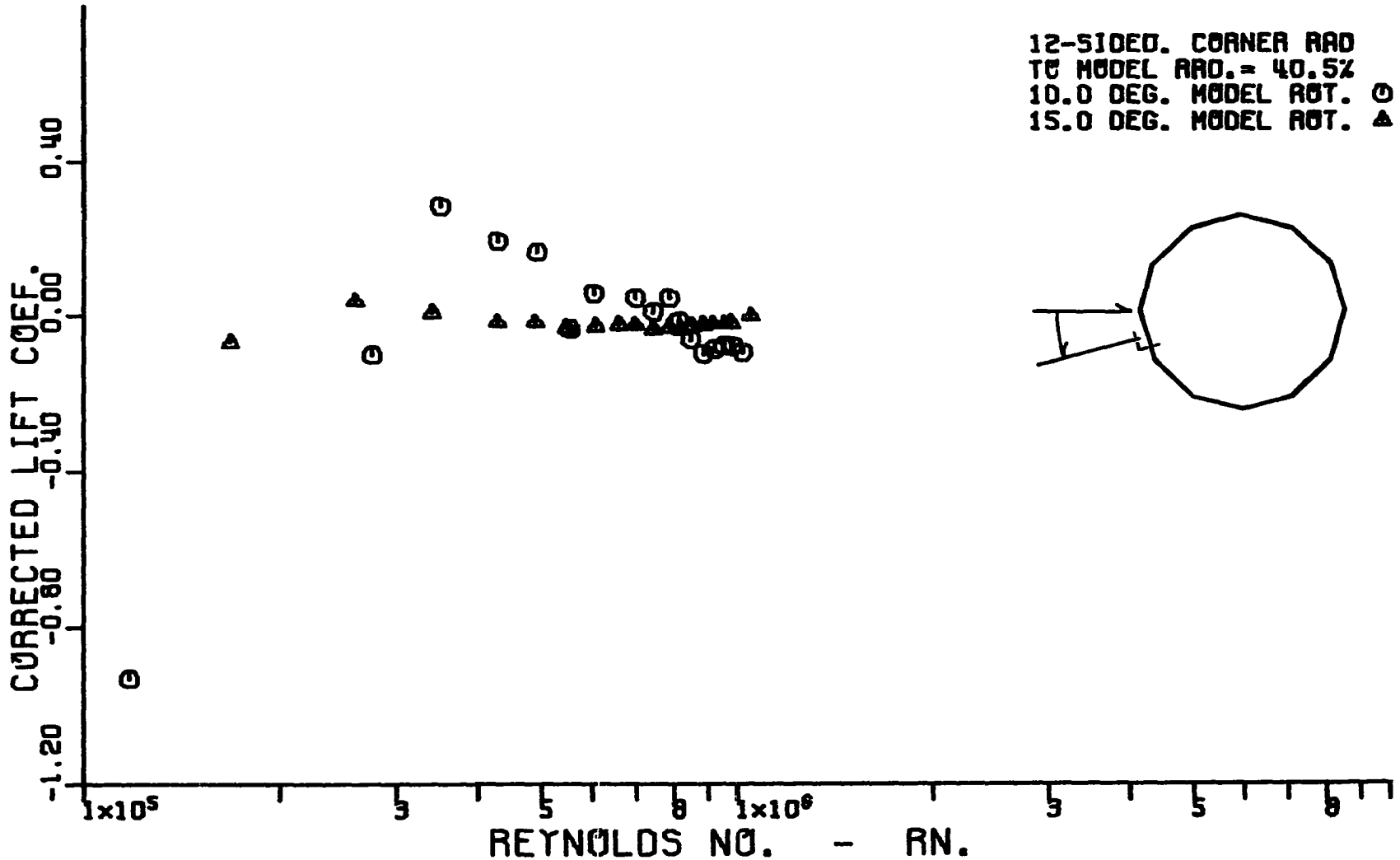

Figure 91. Variation of corrected cross-flow lift coefficient with corrected cross-flow Reynolds number for a dodecagonal cylinder having a corner radius equal to 40.5 percent of the radius of the inscribed circular cylinder.

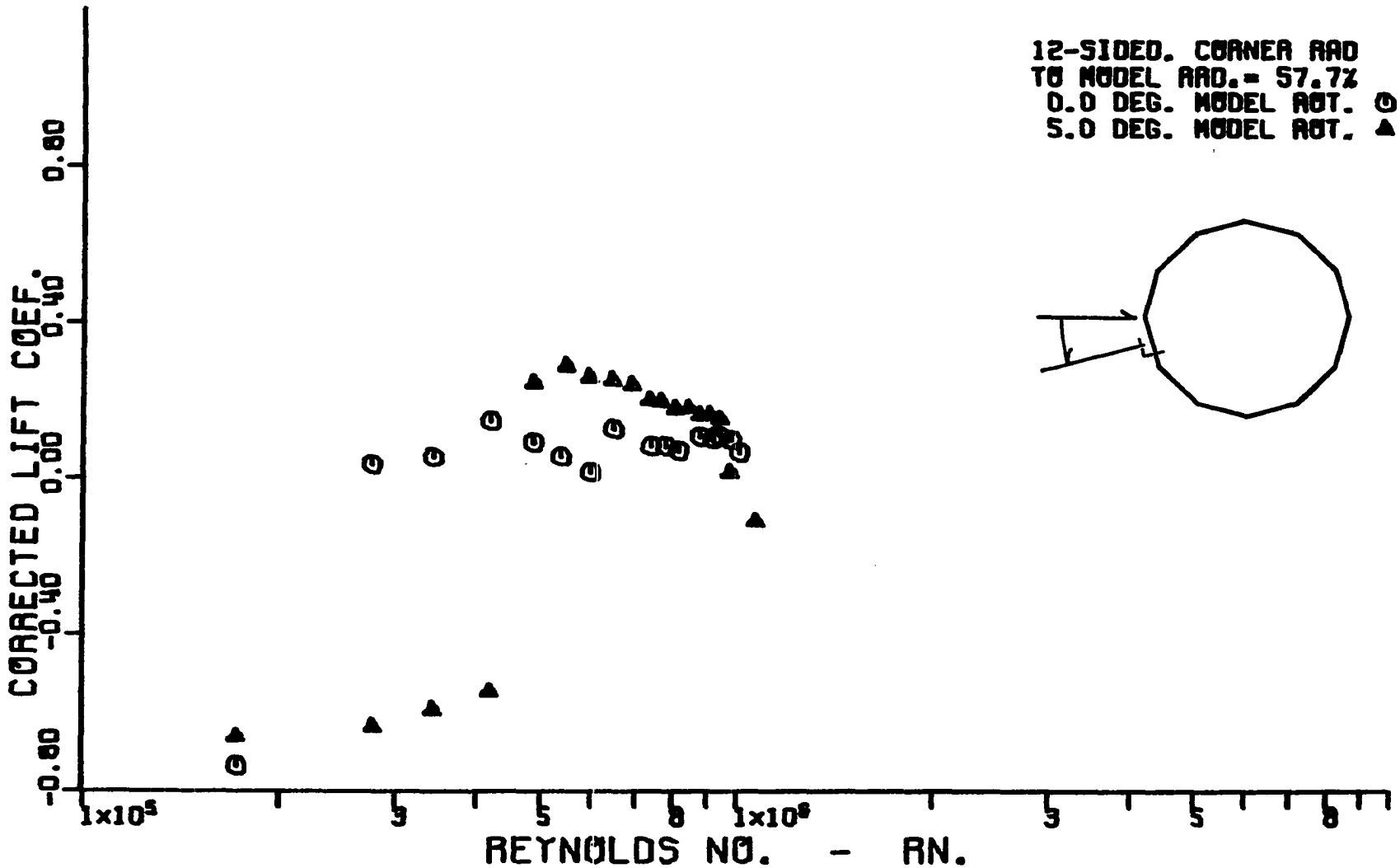

Figure 92. Variation of corrected cross-flow lift coefficient with corrected cross-flow Reynolds number for a dodecagonal cylinder having a corner radius equal to 57.7 percent of the radius of the inscribed circular cylinder.

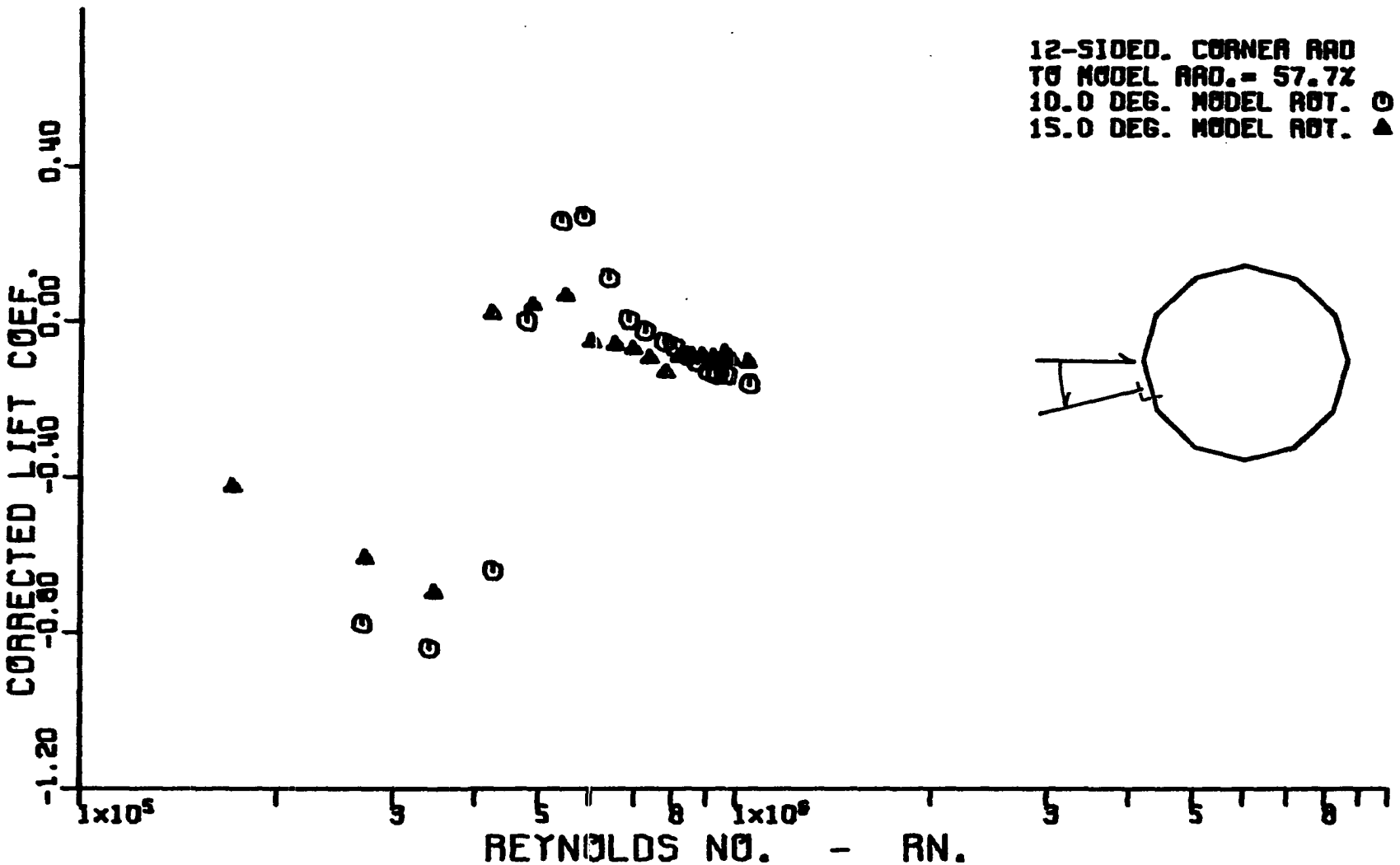

Figure 93. Variation of corrected cross-flow lift coefficient with corrected cross-flow Reynolds number for a dodecagonal cylinder having a corner radius equal to 57.7 percent of the radius of the inscribed circular cylinder.

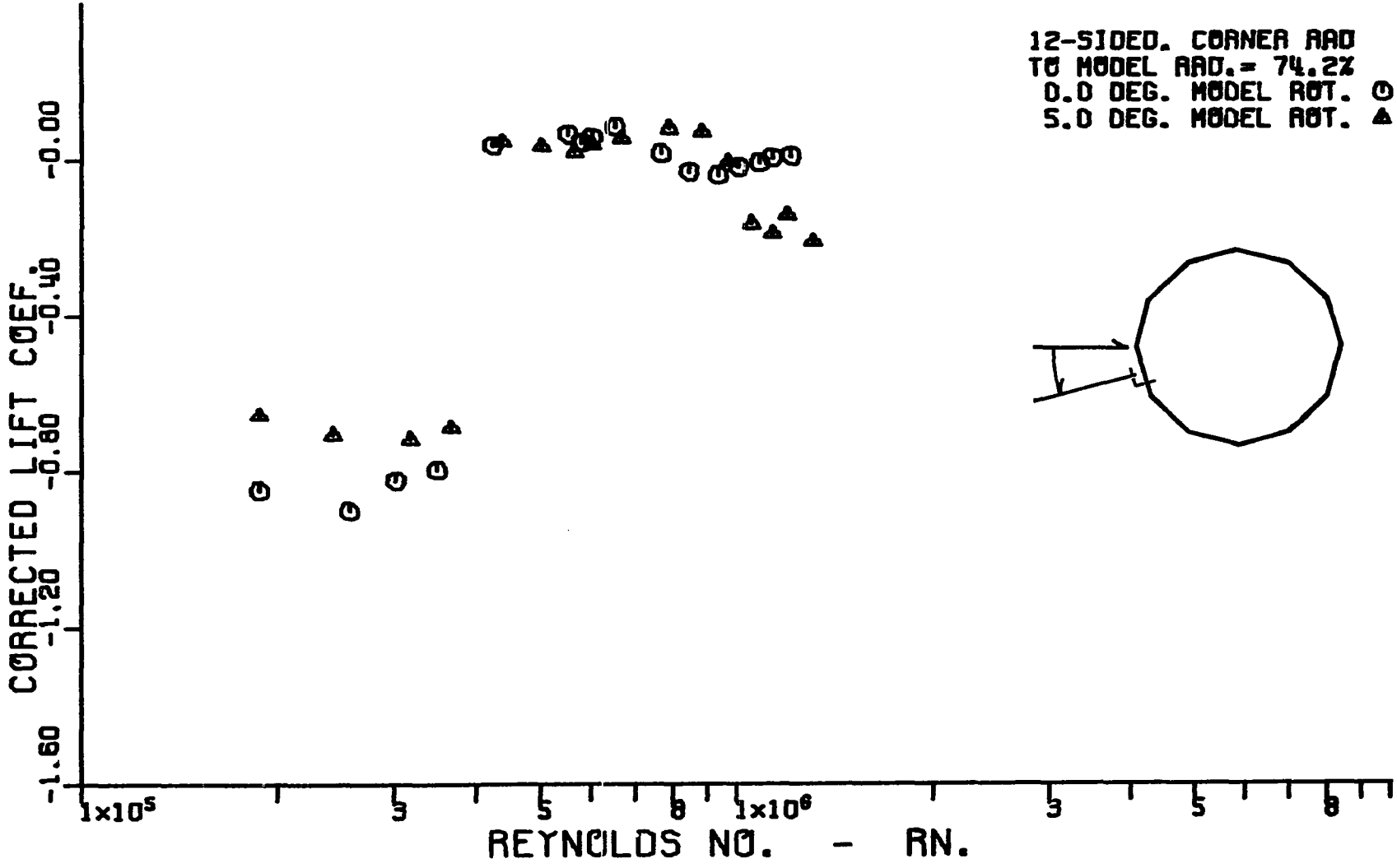

Figure 94. Variation of corrected cross-flow lift coefficient with corrected cross-flow Reynolds number for a dodecagonal cylinder having a corner radius equal to 74.2 percent of the radius of the inscribed circular cylinder.

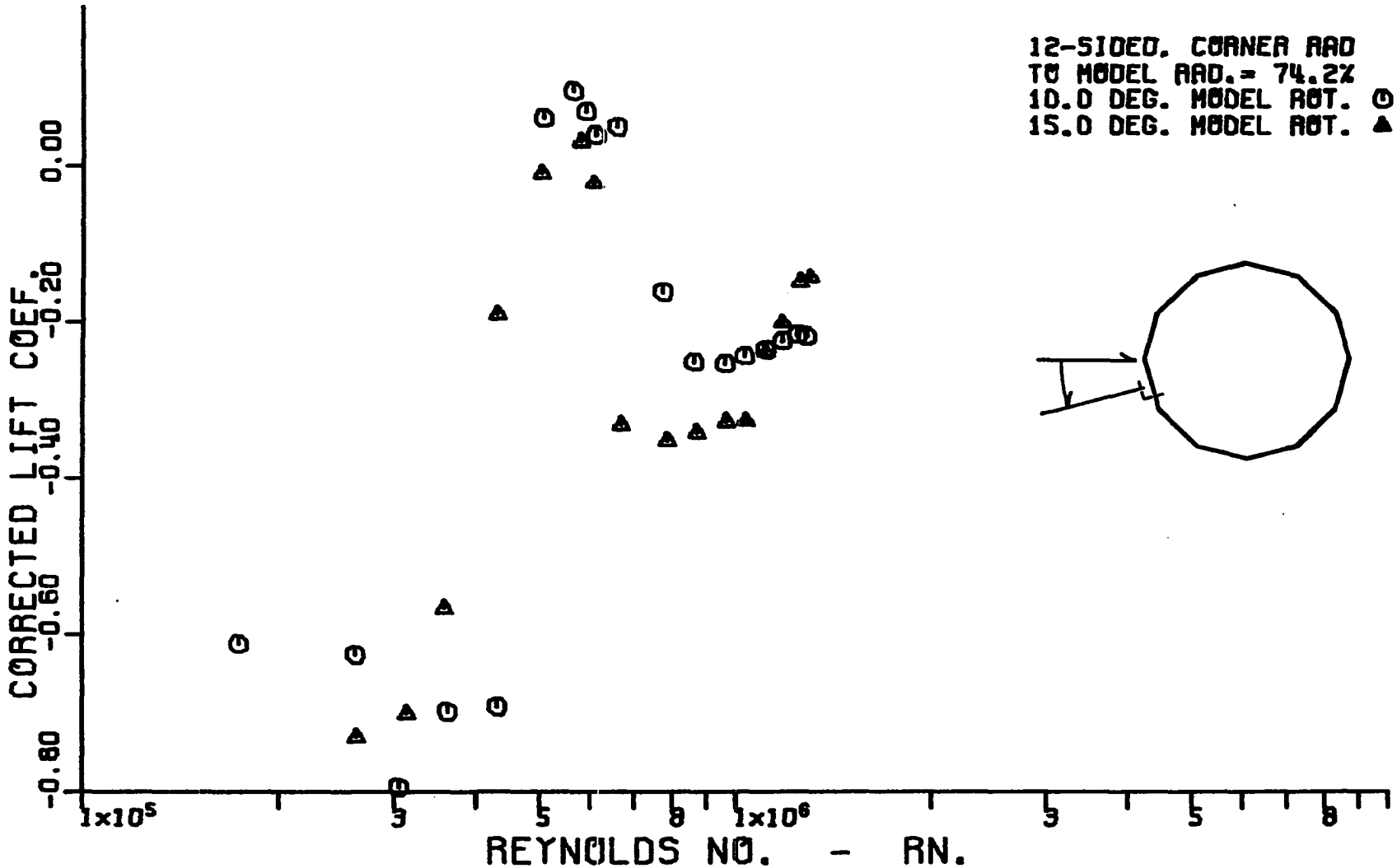

Figure 95. Variation of corrected cross-flow lift coefficient with corrected cross-flow Reynolds number for a dodecagonal cylinder having a corner radius equal to 74.2 percent of the radius of the inscribed circular cylinder.

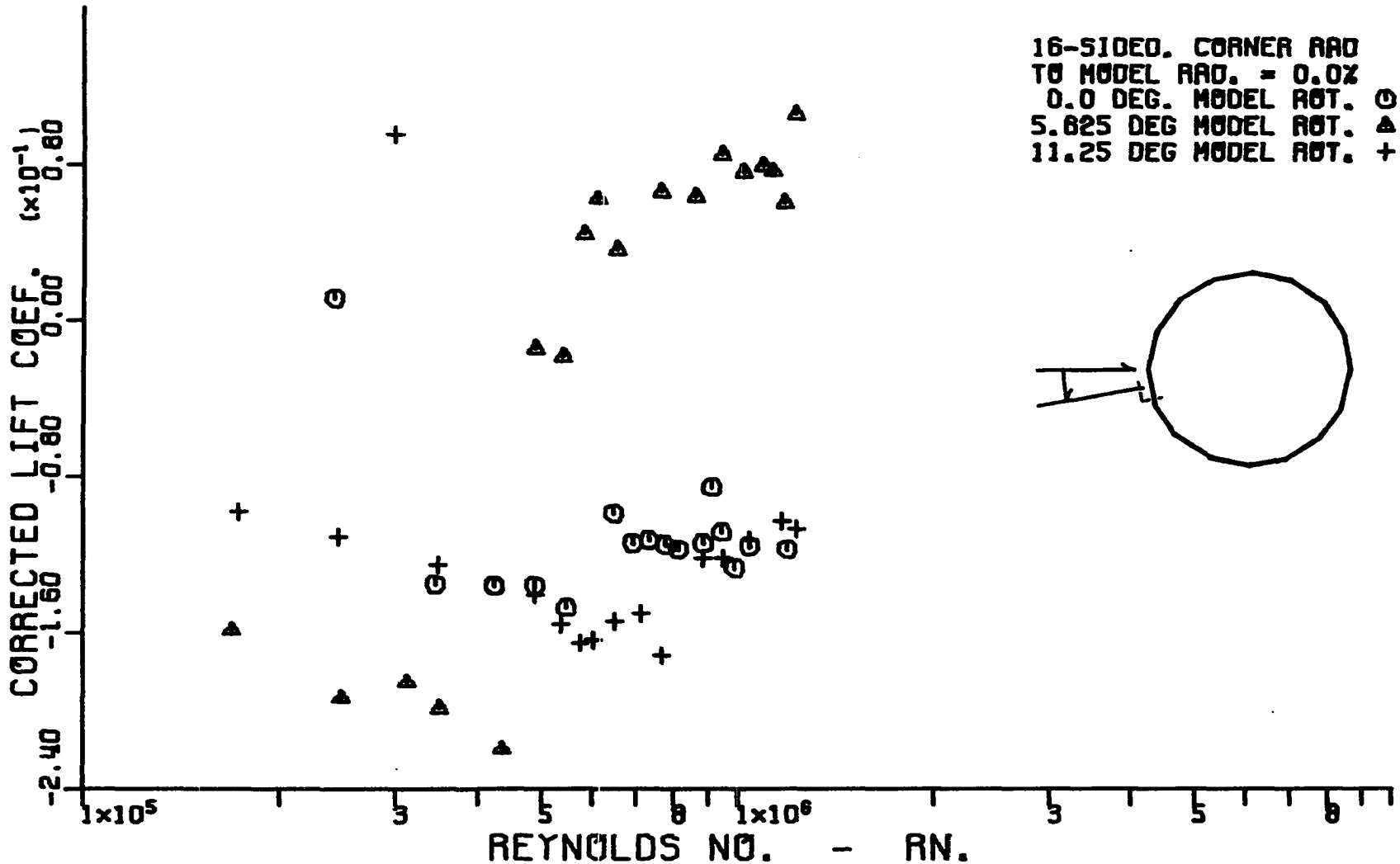

Figure 96. Variation of corrected cross-flow lift coefficient with corrected cross-flow Reynolds number for a hexdecagonal cylinder having a corner radius equal to 0.0 percent of the radius of the inscribed circular cylinder.

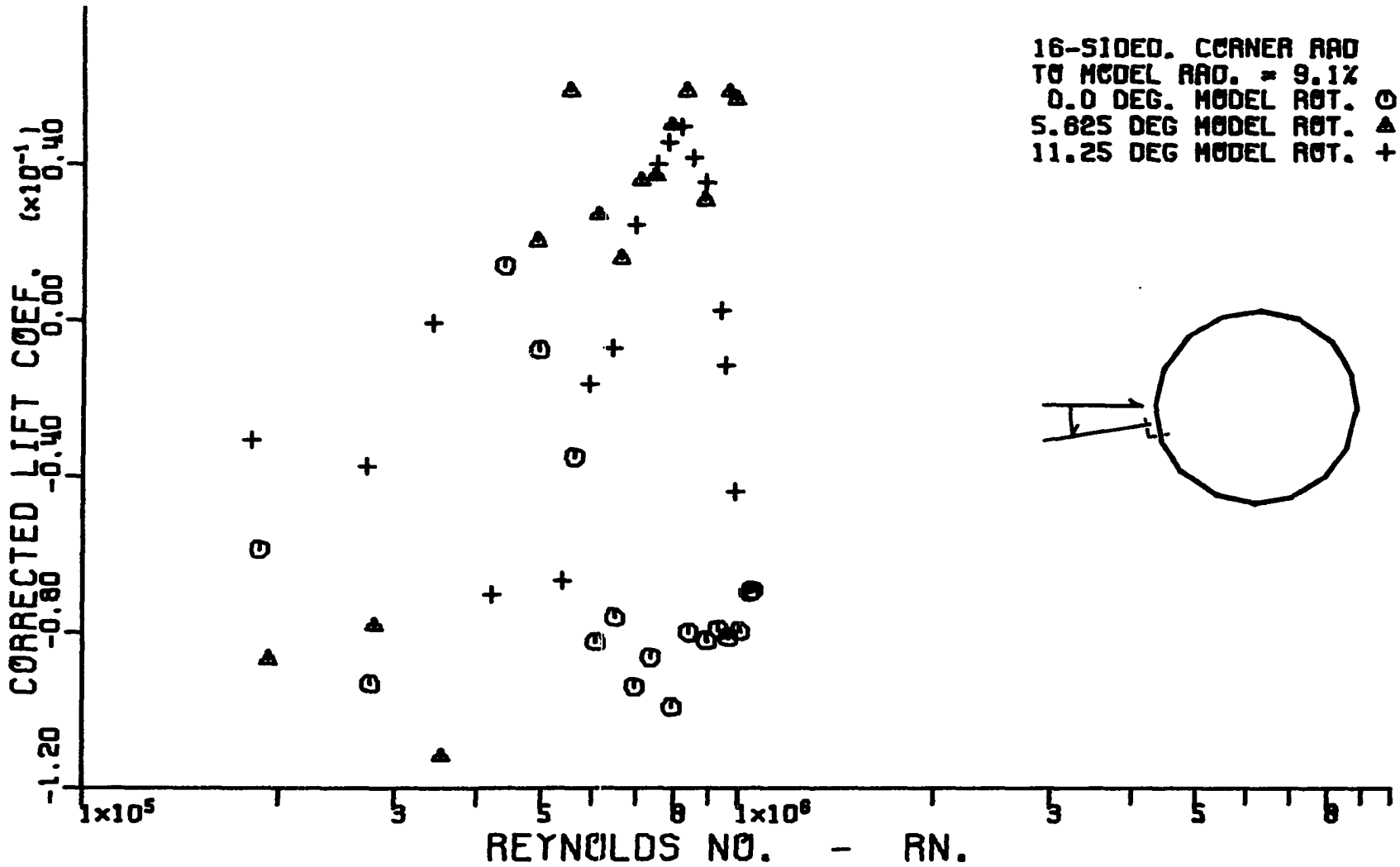

Figure 97. Variation of corrected cross-flow lift coefficient with corrected cross-flow Reynolds number for a hexdecagonal cylinder having a corner radius equal to 9.1 percent of the radius of the inscribed circular cylinder.

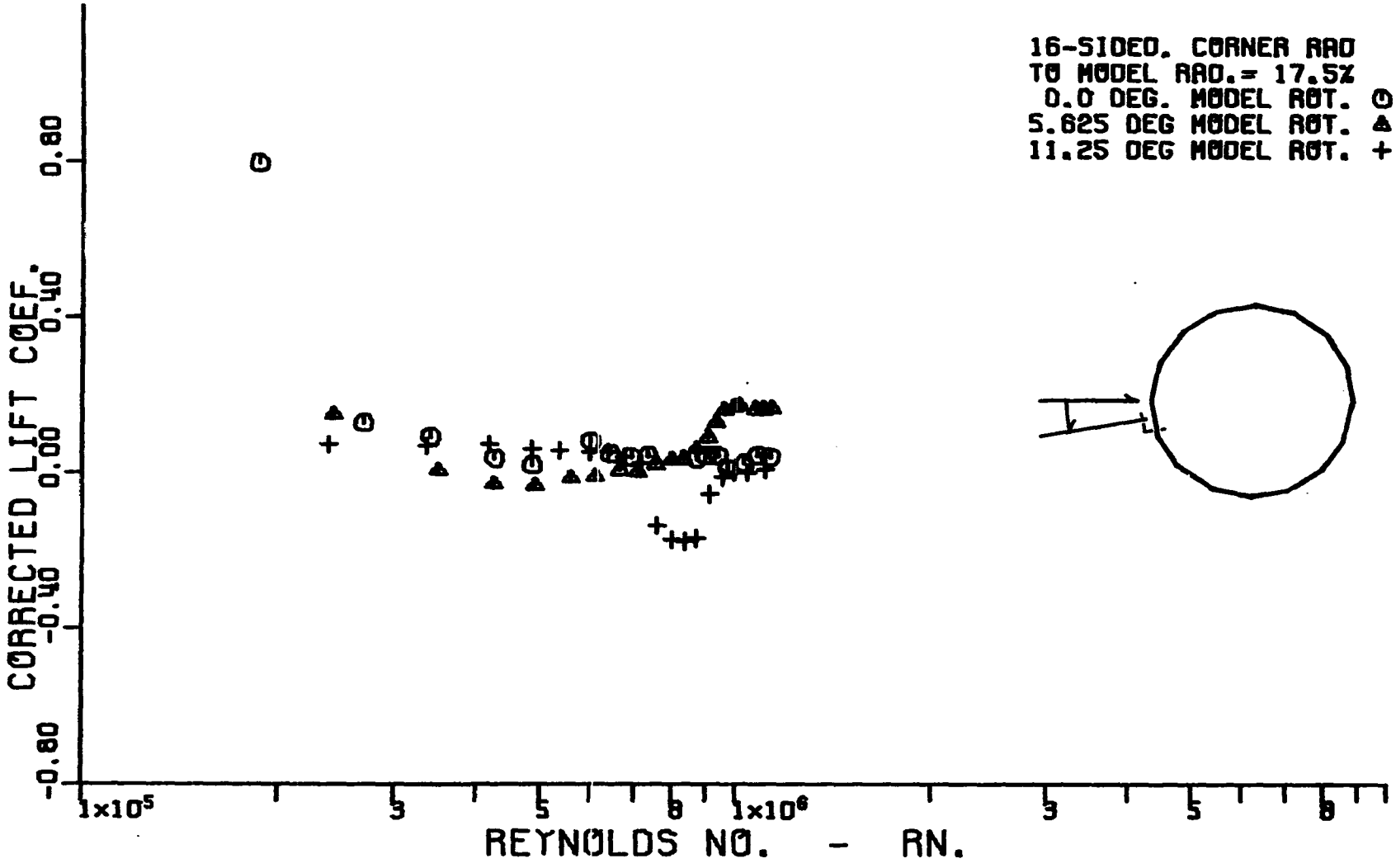

Figure 98. Variation of corrected cross-flow lift coefficient with corrected cross-flow Reynolds number for a hexdecagonal cylinder having a corner radius equal to 17.5 percent of the radius of the inscribed circular cylinder.

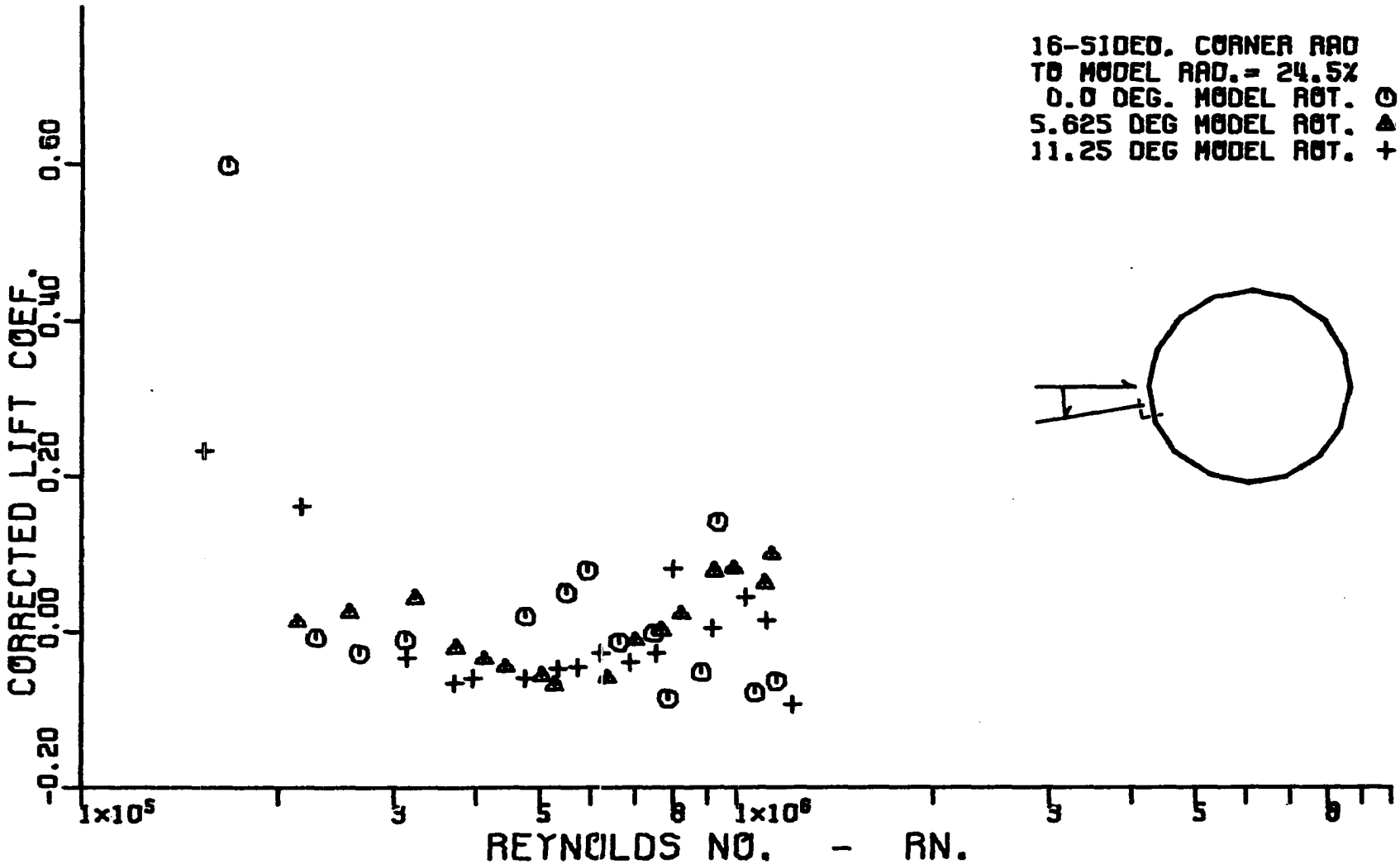

Figure 99. Variation of corrected cross-flow lift coefficient with corrected cross-flow Reynolds number for a hexdecagonal cylinder having a corner radius equal to 24.5 percent of the radius of the inscribed circular cylinder.

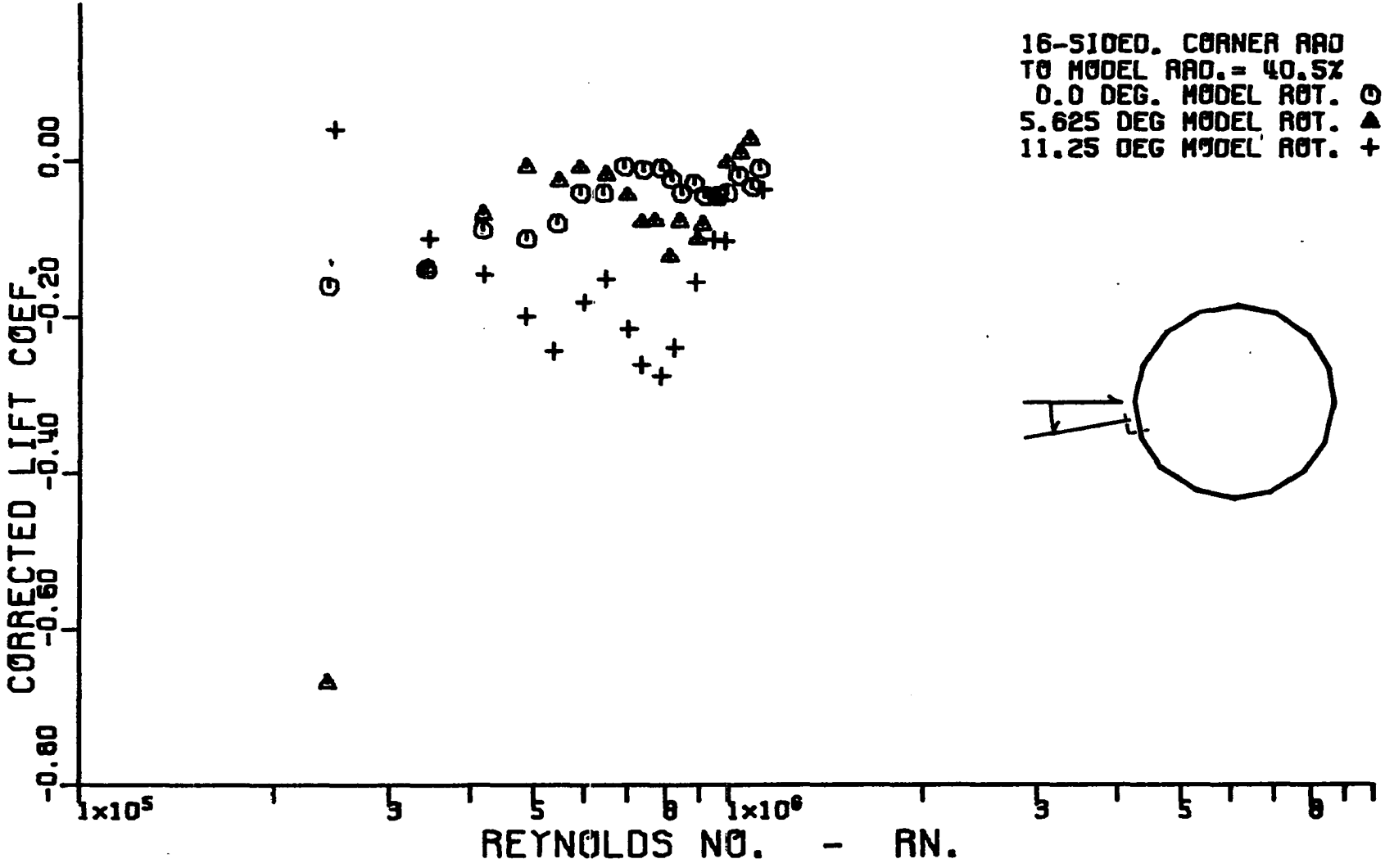

Figure 100. Variation of corrected cross-flow lift coefficient with corrected cross-flow Reynolds number for a hexdecagonal cylinder having a corner radius equal to 40.5 percent of the radius of the inscribed circular cylinder.

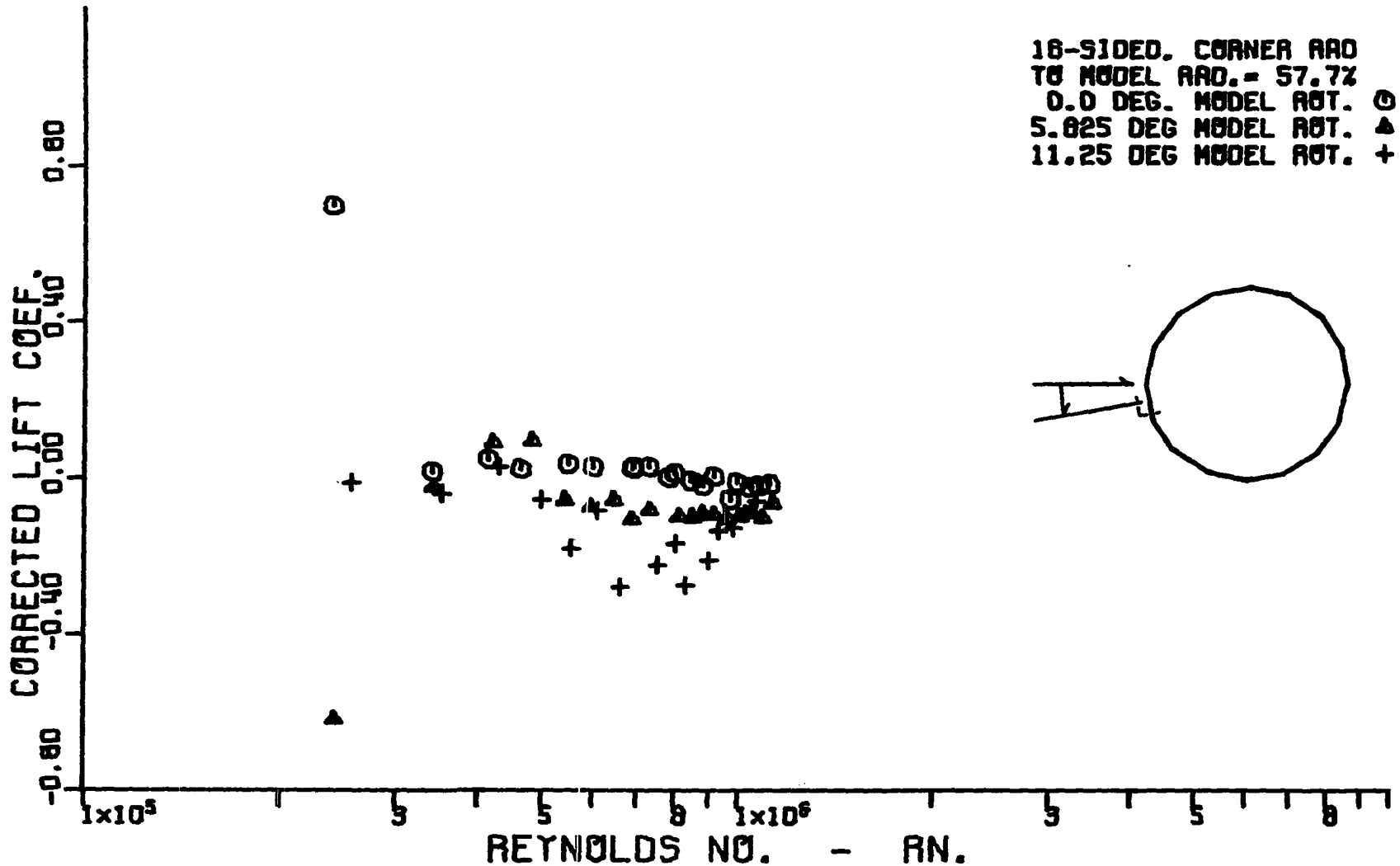

Figure 101. Variation of corrected cross-flow lift coefficient with corrected cross-flow Reynolds number for a hexdecagonal cylinder having a corner radius equal to 57.7 percent of the radius of the inscribed circular cylinder.

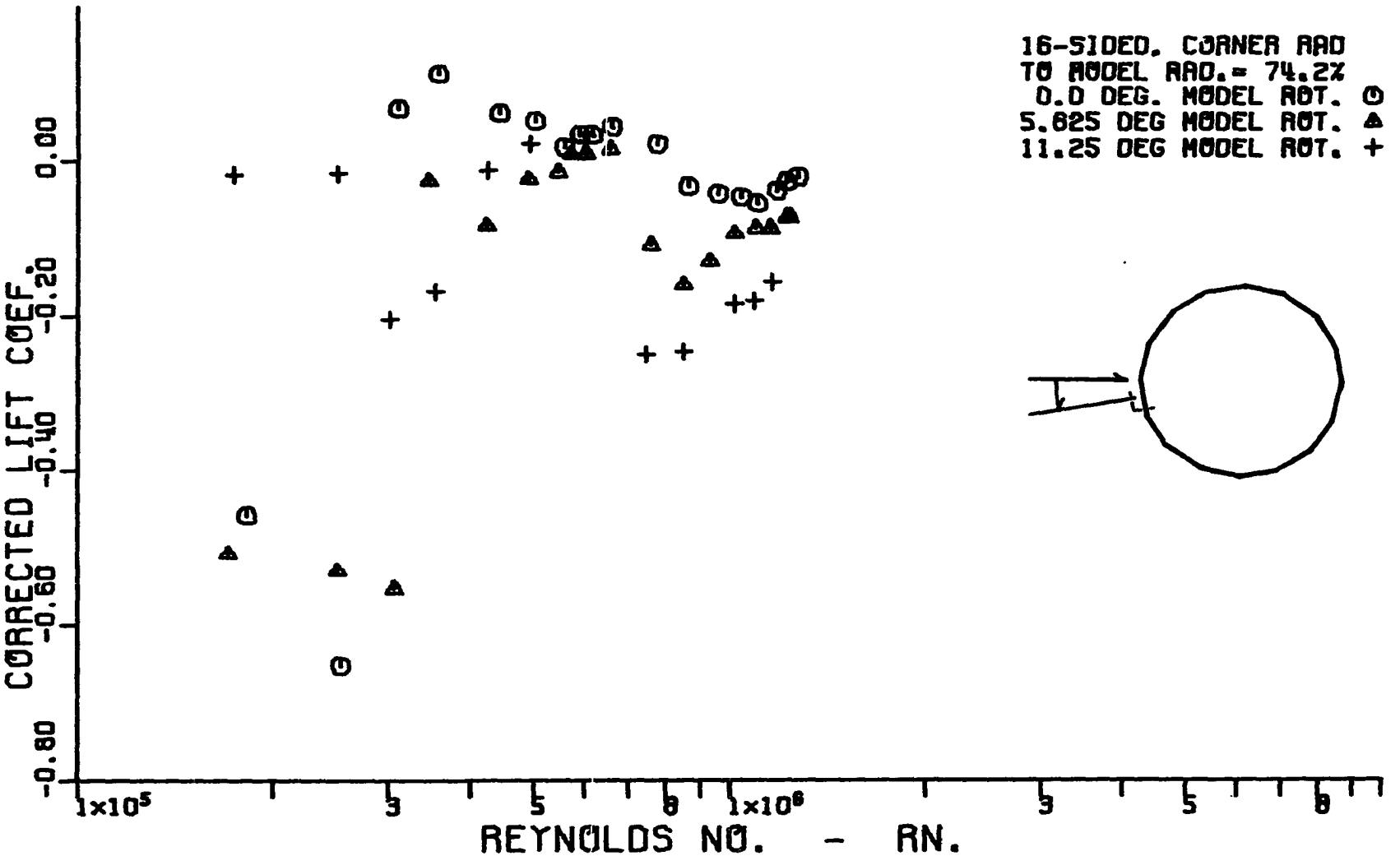

Figure 102. Variation of corrected cross-flow lift coefficient with corrected cross-flow Reynolds number for a hexdecagonal cylinder having a corner radius equal to 74.2 percent of the radius of the inscribed circular cylinder.

lower surfaces of the body are similar. At the intermediate orientations this similarity is no longer present and side forces arise that in general act toward the side of the cylinder rotated downwind.

Consider the octagonal cylinder at some intermediate orientation as shown in Figure 103. As the flow goes over the surface rotated downwind, referred to henceforth as the lower surface, it reaches the point of maximum body thickness and hence its minimum pressure before it has traveled one-half way around the side. If the orientation is the first intermediate angle in the 8- or 12-sided case, or the middle intermediate angle as in the 16-sided case the flow is able to turn the corner and remain attached on the leeward surface. This attachment is accompanied by a low pressure which covers a wide area of the lower surface. On the surface rotated upwind, the upper surface in this project, the flow must travel around an additional corner and more than one-half way around the side before it reaches the corner located at the point of maximum thickness. Because of this the flow behaves as it does on a circular cylinder and reaches its minimum pressure before the corner, undergoes laminar separation with a following turbulent reattachment, and is increasing in pressure by the time it goes around the corner. Because of this the pressures on the upper surface remain larger than those on the lower surface and a lift force or

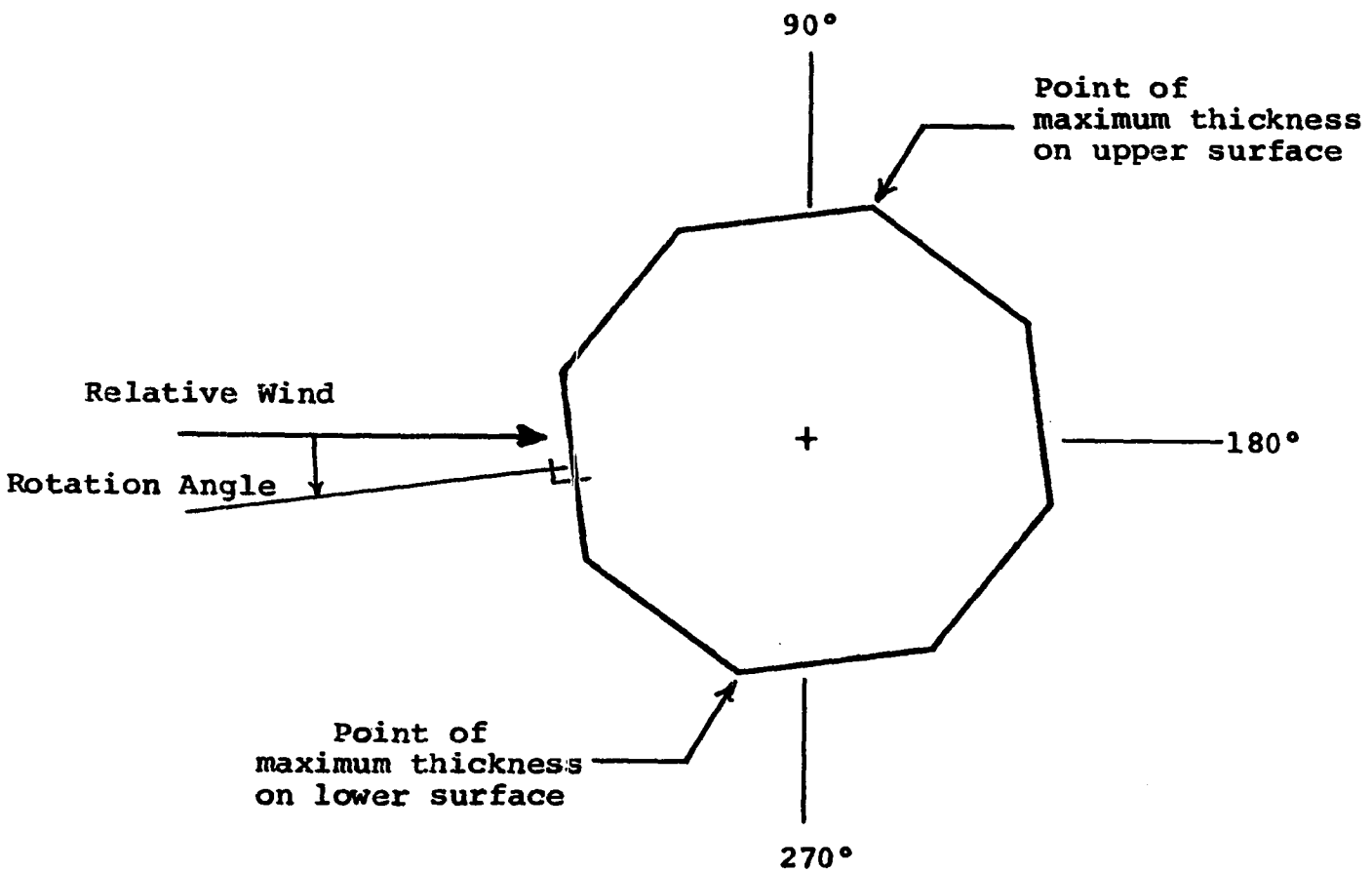

Figure 103. Octagonal cylinder near first intermediate angle, 7.5°, showing relative positions of the points of maximum thickness for upper and lower surfaces.

side force is produced acting toward the surface that was rotated in the downwind direction.

As the model is rolled toward the second intermediate orientation, the distance to the lower extreme increases while that to the upper extreme decreases. A review of the lift data shows that when this occurs, the lift force acts toward the surface rotated upwind for corners having the smaller radii and the largest included angle. A review of the pressure data indicates that when this happens, the flow on the lower surface behaves like the flow on the upper surface, reaching its minimum pressure before the corner located at the point of maximum thickness, and is increasing in pressure as it passes around that corner. When this occurs the higher pressure wake region is reached sooner on the lower surface than on the upper surface with the result that the net force now acts toward the upper surface.

Separation just before the extreme corners on both the upper and lower surfaces always occurs for the sharp-cornered models, 0.0 percent corners, at all orientations for both the 8- and 12-sided cylinders as would be expected. As above, this yields a force in the upward direction. The same is also true of the 74.2 percent corner models which are beginning to closely approximate a circular cylinder both in shape and behavior.

Total force coefficients and force phase angles

The magnitude of the lift or side force for the intermediate angles can be one-half as large as the drag force for the 8-sided cylinder, decreasing as the number of sides increase to a value of approximately 20 percent of the drag for the 16-sided models. Because of this the actual steady force acting on the cross-section can be as much as 10 percent greater than the drag force alone. Since this can be a significant increase, the corrected total force coefficient, the vector sum of the lift and drag coefficients, was plotted versus corrected Reynolds number along with the force phase angle of that force. The angle was taken positive for a clockwise rotation in Figure 1. This information is shown in Figures 104 to 117 for the 8-sided cylinders, Figures 118 to 131 for the 12-sided cylinders and Figures 132 to 145 for the 16-sided cylinders. The variation of the force coefficients with corner radius is similar to that of the drag coefficient while the force phase angle varies in much the same way as the coefficient of lift.

Empirical equation relating force and corner radius

Since the total aerodynamic force acting on the model was significantly larger than the drag force alone for certain model-relative wind orientations, it was

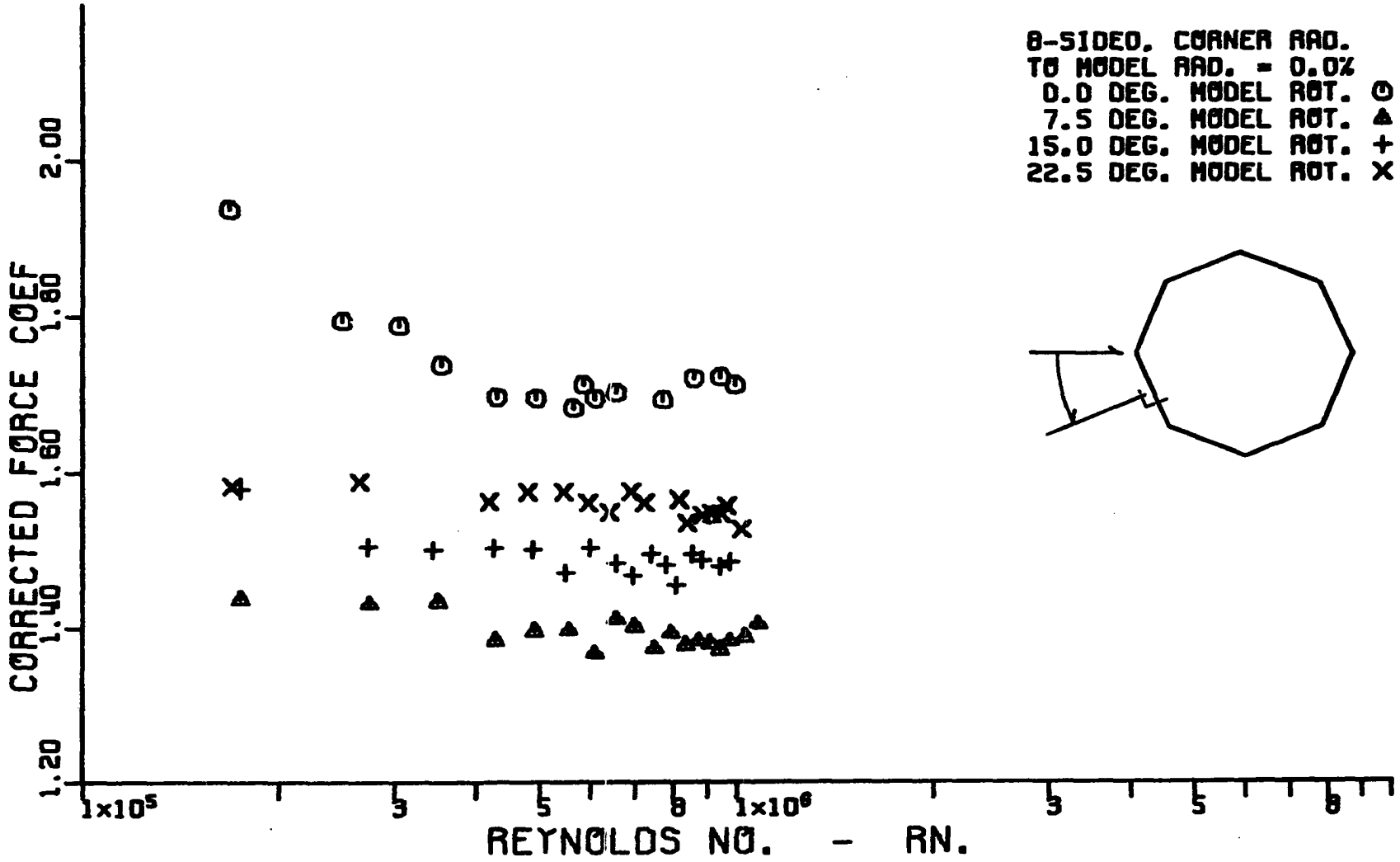

Figure 104. Variation of corrected cross-flow force coefficient with corrected cross-flow Reynolds number for an octagonal cylinder having a corner radius equal to 0.0 percent of the radius of the inscribed circular cylinder.

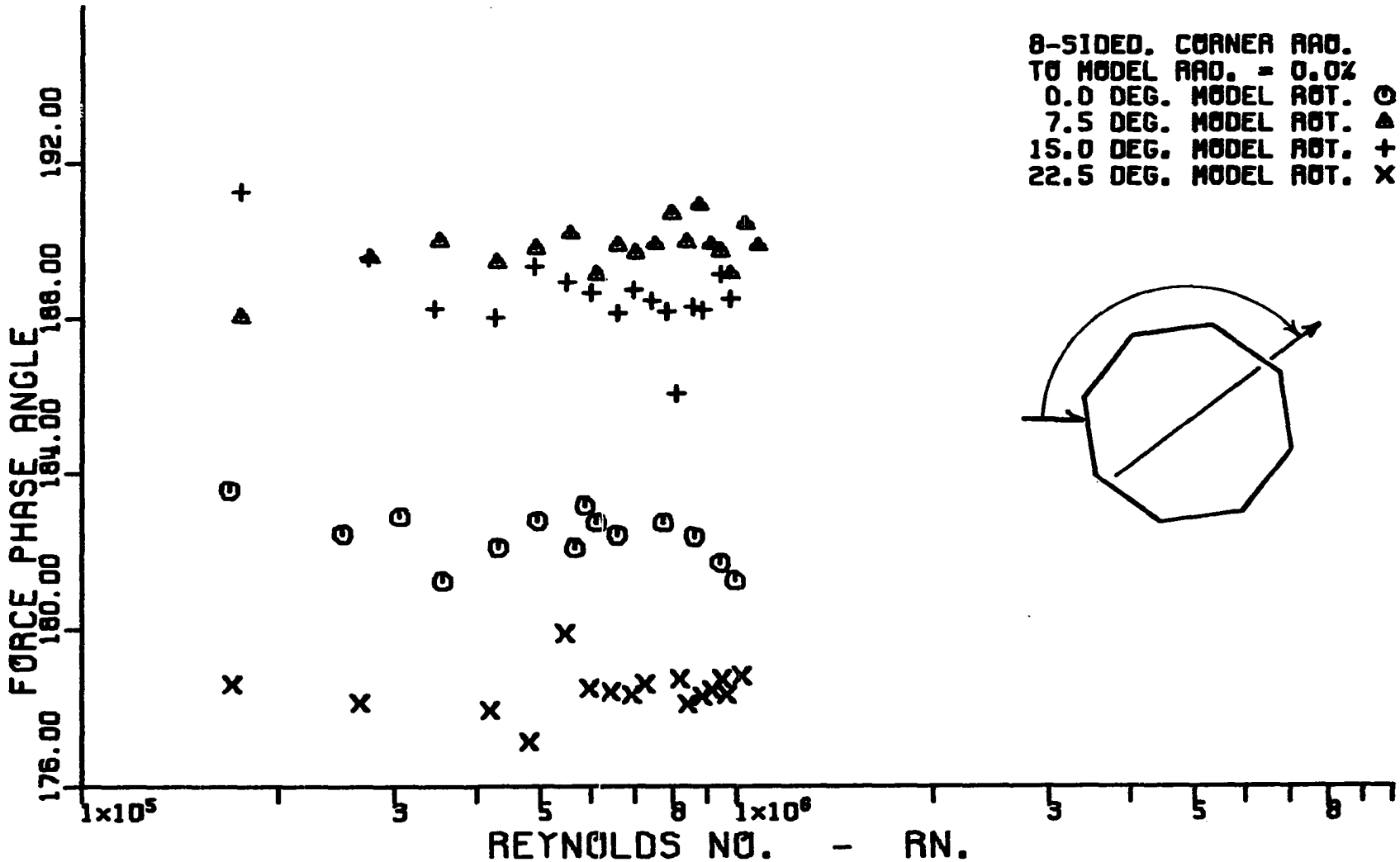

Figure 105. Variation of corrected cross-flow force phase angle with corrected cross-flow Reynolds number for an octagonal cylinder having a corner radius equal to 0.0 percent of the radius of the inscribed circular cylinder.

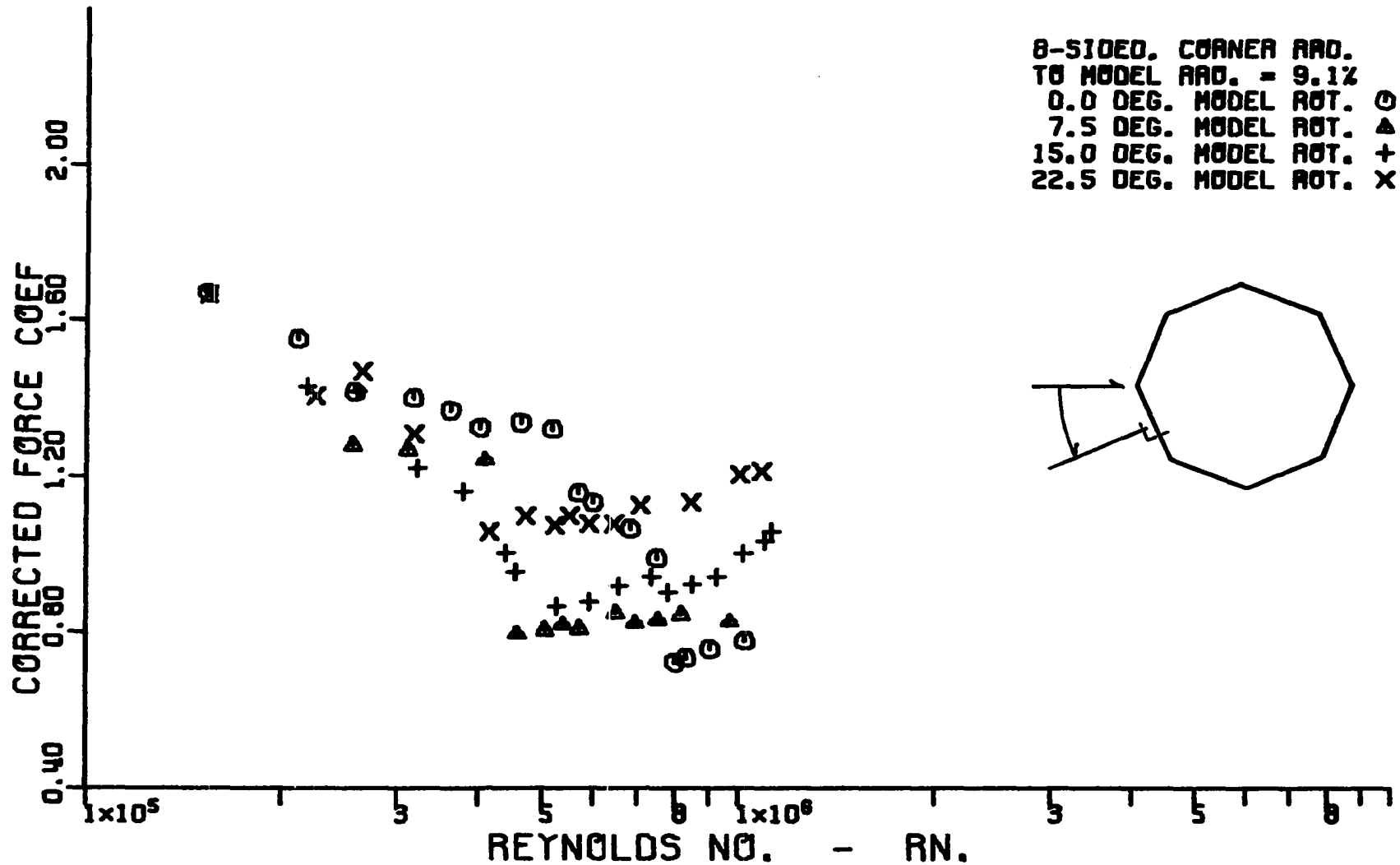

Figure 106. Variation of corrected cross-flow force coefficient with corrected cross-flow Reynolds number for an octagonal cylinder having a corner radius equal to 9.1 percent of the radius of the inscribed circular cylinder.

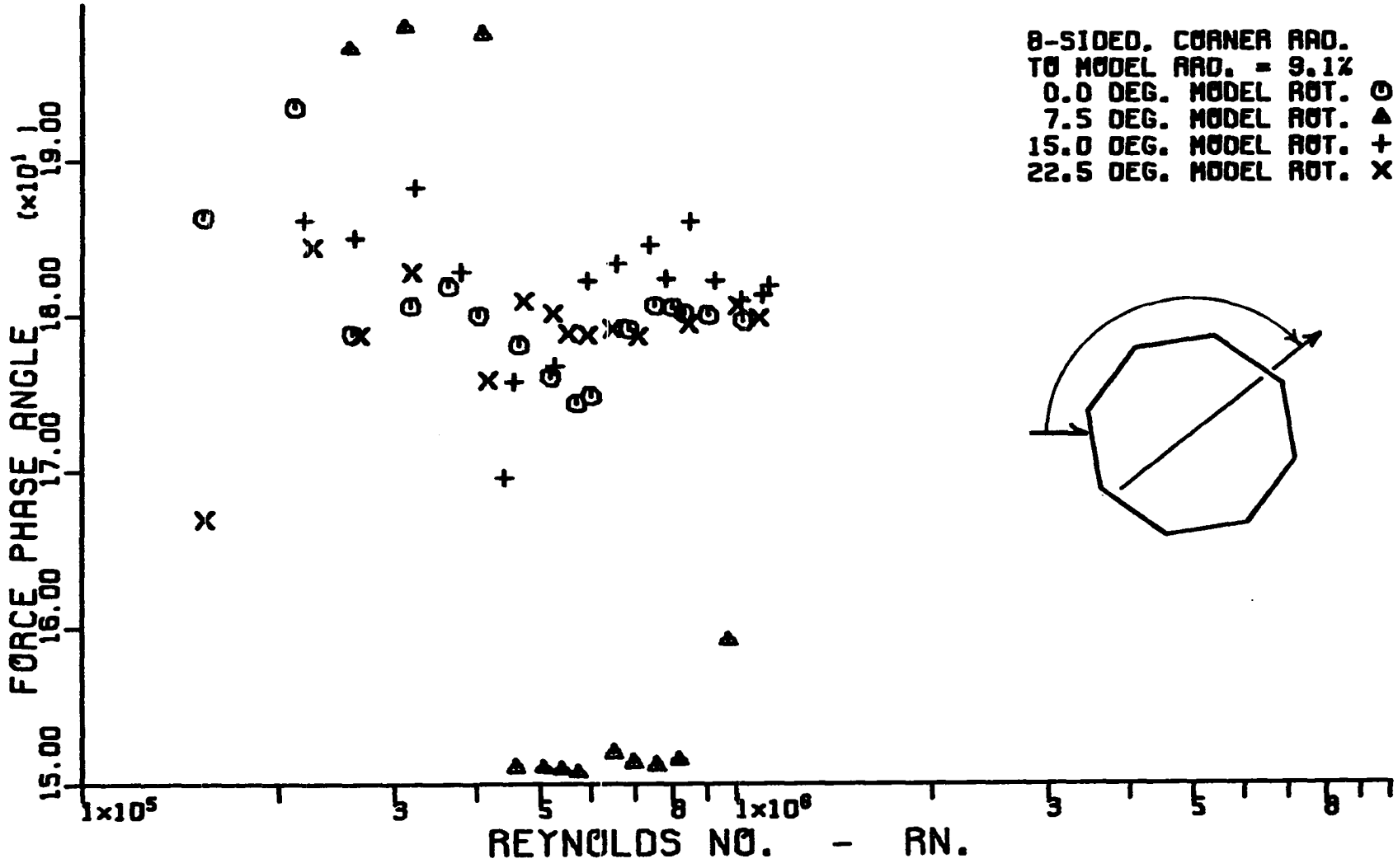

Figure 107. Variation of corrected cross-flow force phase angle with corrected cross-flow Reynolds number for an octagonal cylinder having a corner radius equal to 9.1 percent of the radius of the inscribed circular cylinder.

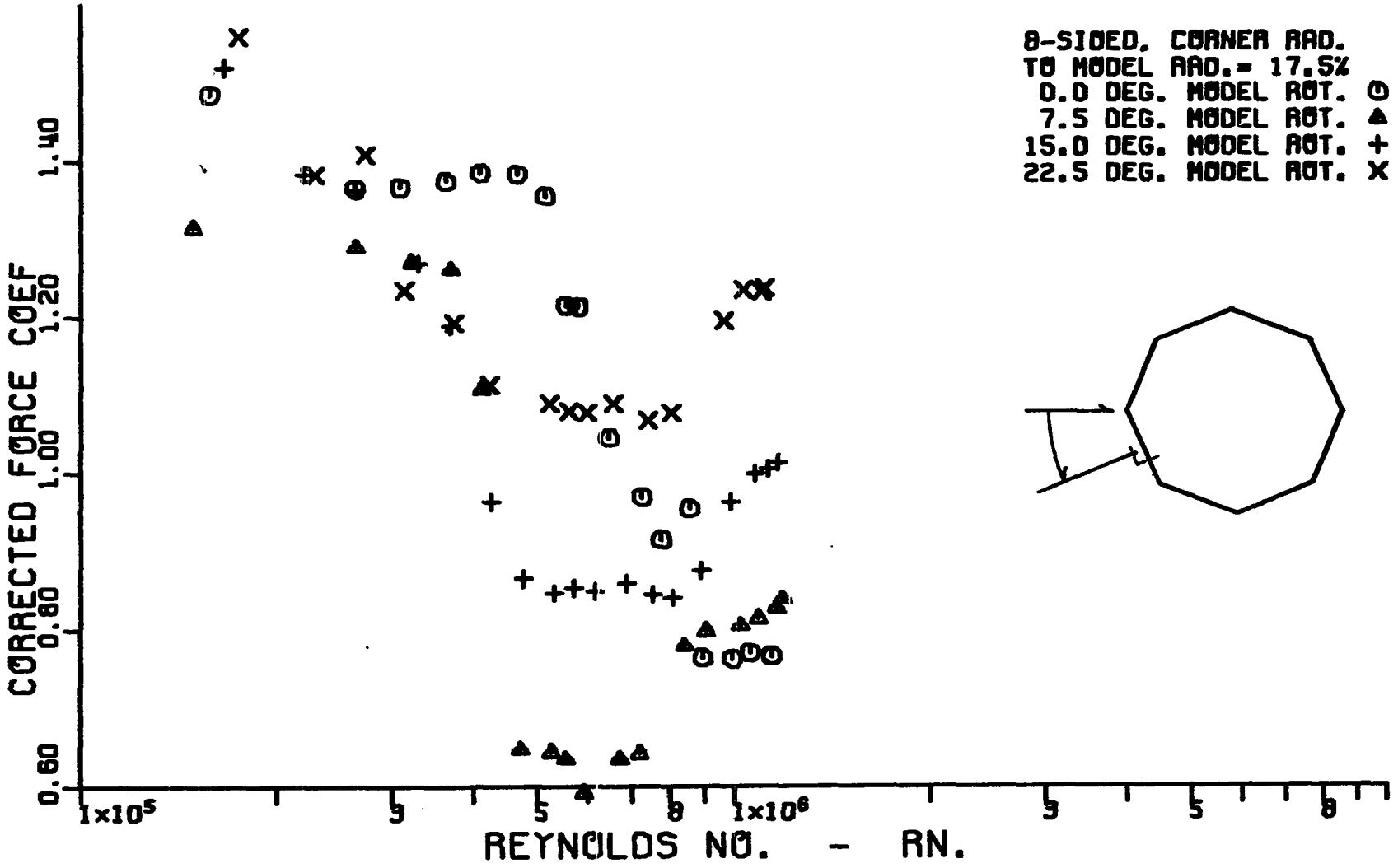

Figure 108. Variation of corrected cross-flow force coefficient with corrected cross-flow Reynolds number for an octagonal cylinder having a corner radius equal to 17.5 percent of the radius of the inscribed circular cylinder.

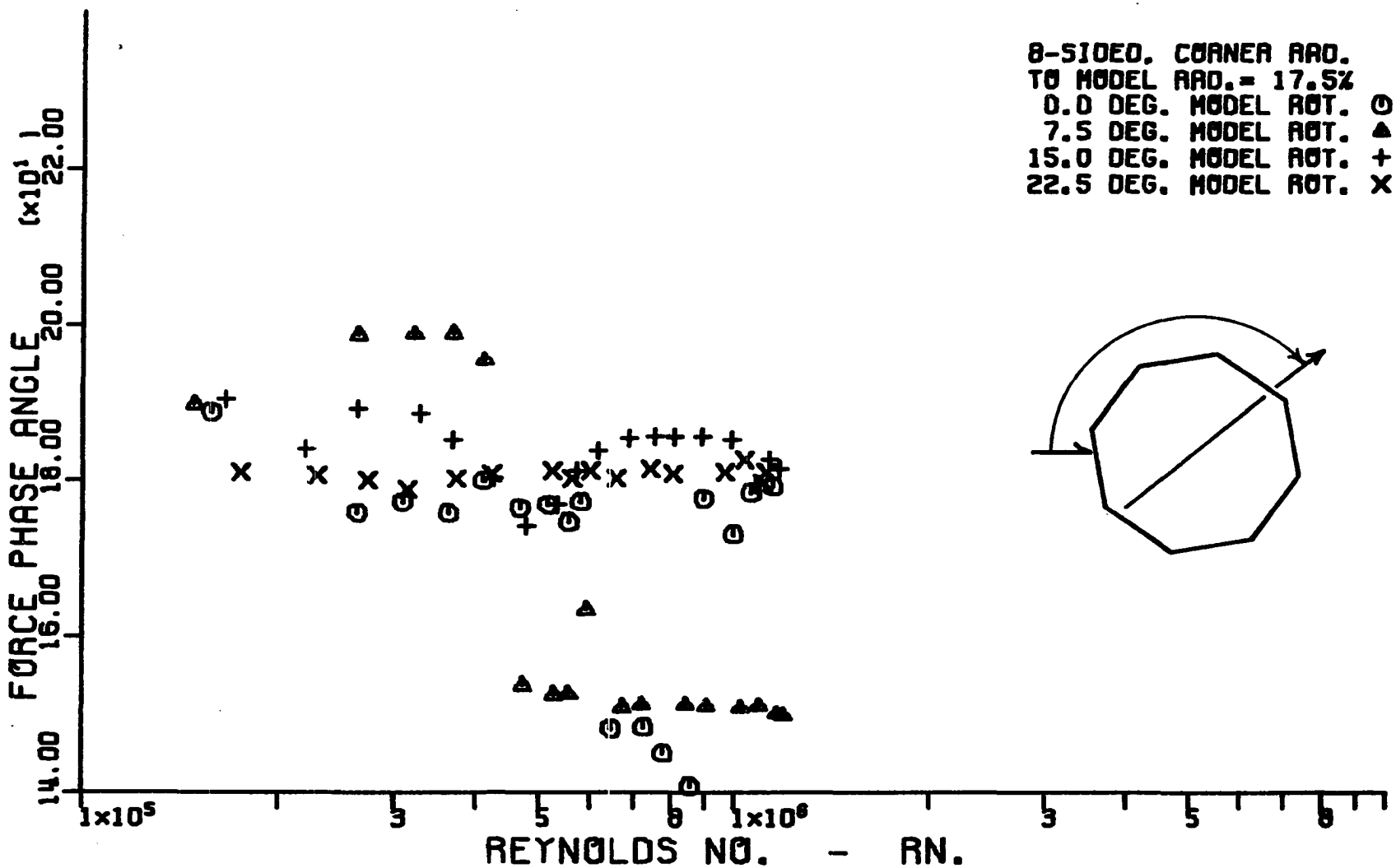

Figure 109. Variation of corrected cross-flow force phase angle with corrected cross-flow Reynolds number for an octagonal cylinder having a corner radius equal to 17.5 percent of the radius of the inscribed circular cylinder.

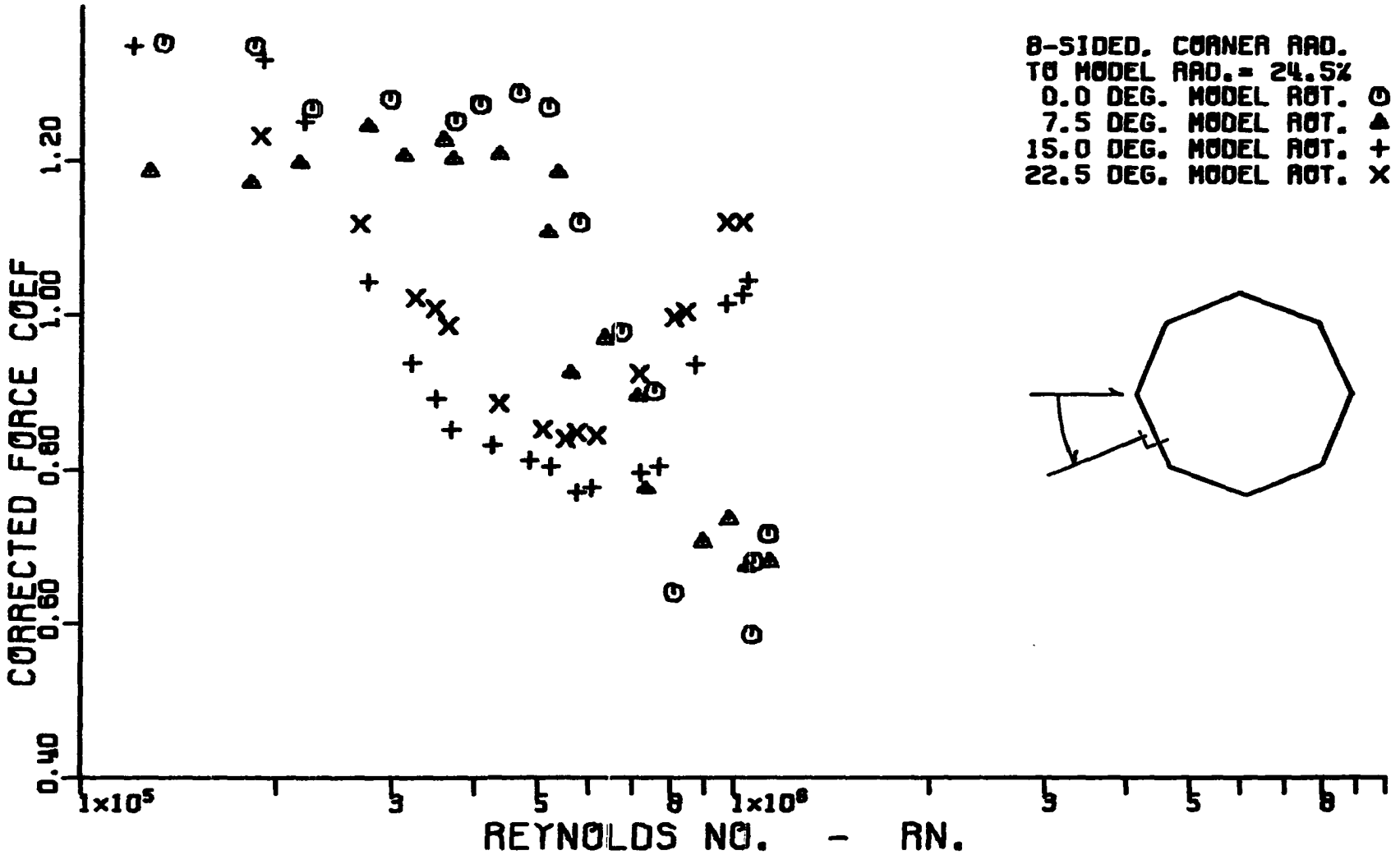

Figure 110. Variation of corrected cross-flow force coefficient with corrected cross-flow Reynolds number for an octagonal cylinder having a corner radius equal to 24.5 percent of the radius of the inscribed circular cylinder.

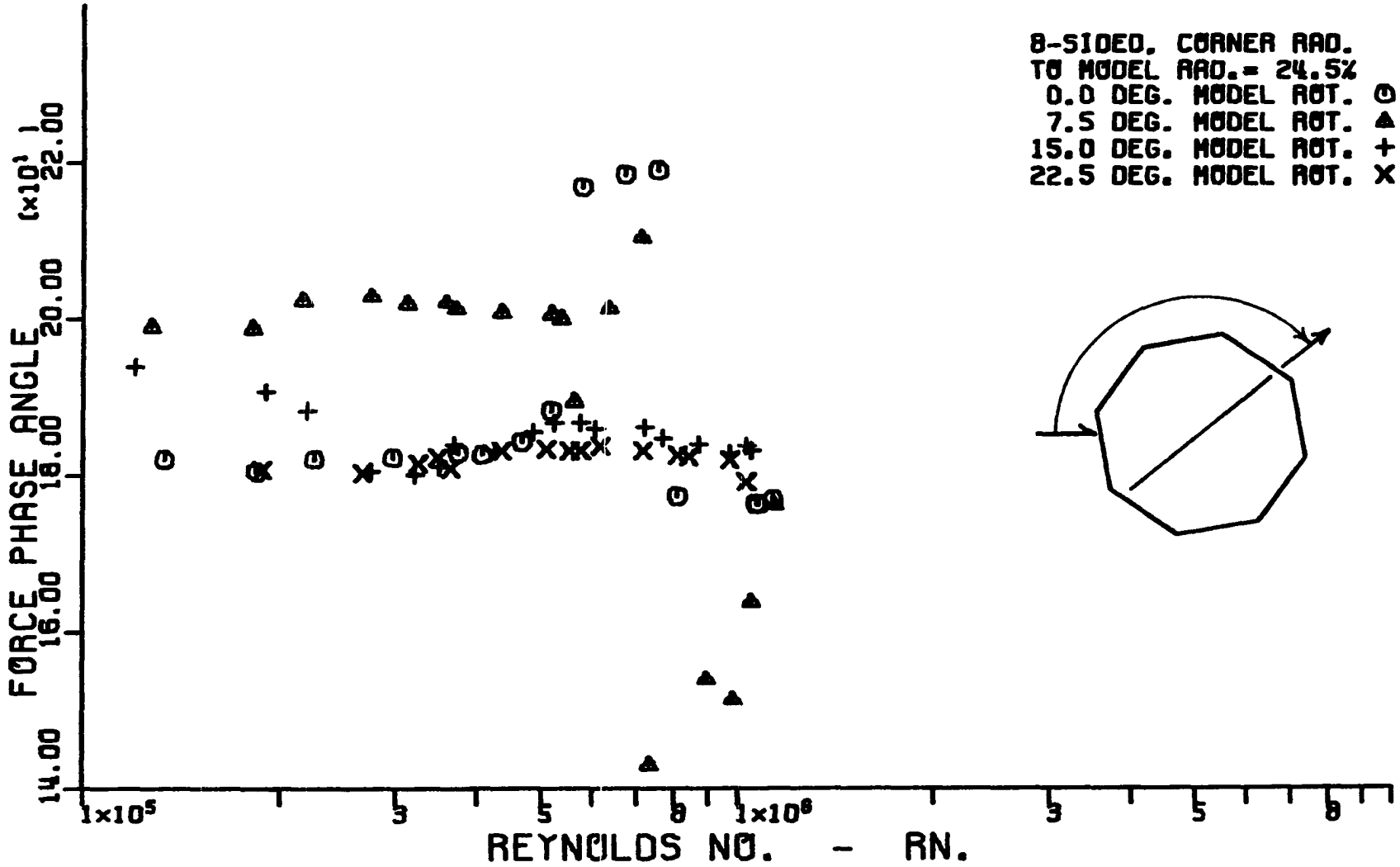

Figure 111. Variation of corrected cross-flow force phase angle with corrected cross-flow Reynolds number for an octagonal cylinder having a corner radius equal to 24.5 percent of the radius of the inscribed circular cylinder.

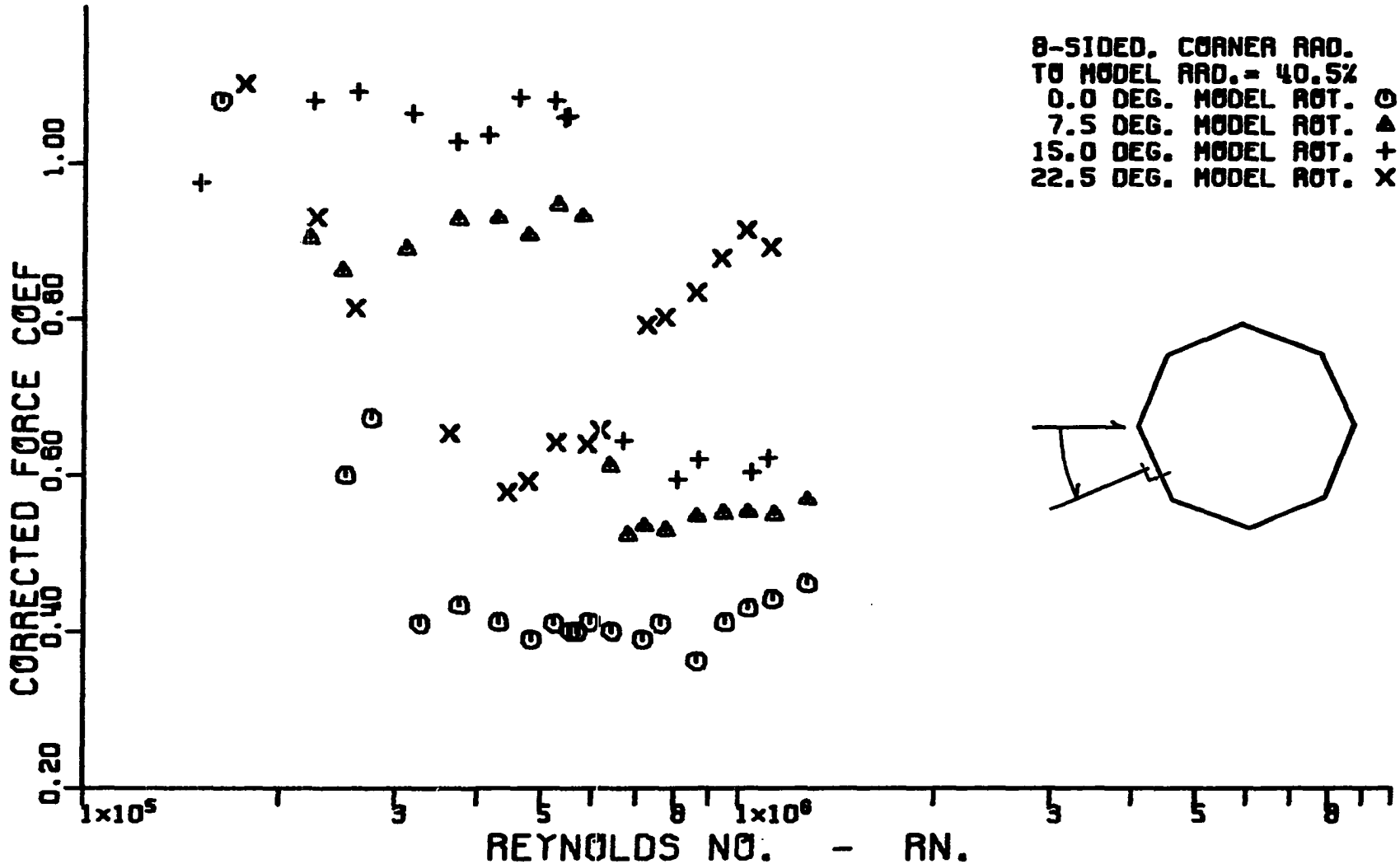

Figure 112. Variation of corrected cross-flow force coefficient with corrected cross-flow Reynolds number for an octagonal cylinder having a corner radius equal to 40.5 percent of the radius of the inscribed circular cylinder.

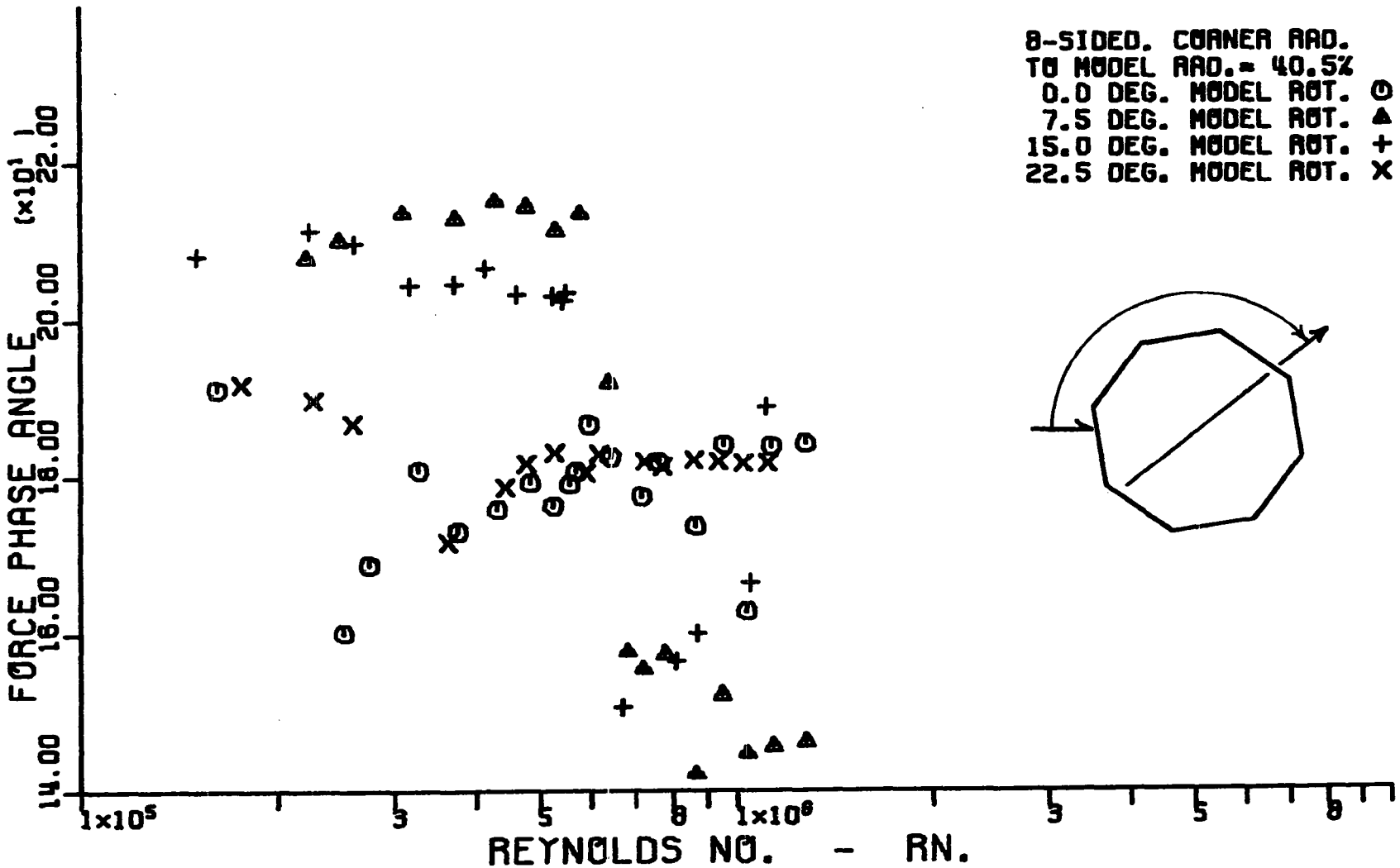

Figure 113. Variation of corrected cross-flow force phase angle with corrected cross-flow Reynolds number for an octagonal cylinder having a corner radius equal to 40.5 percent of the radius of the inscribed circular cylinder.

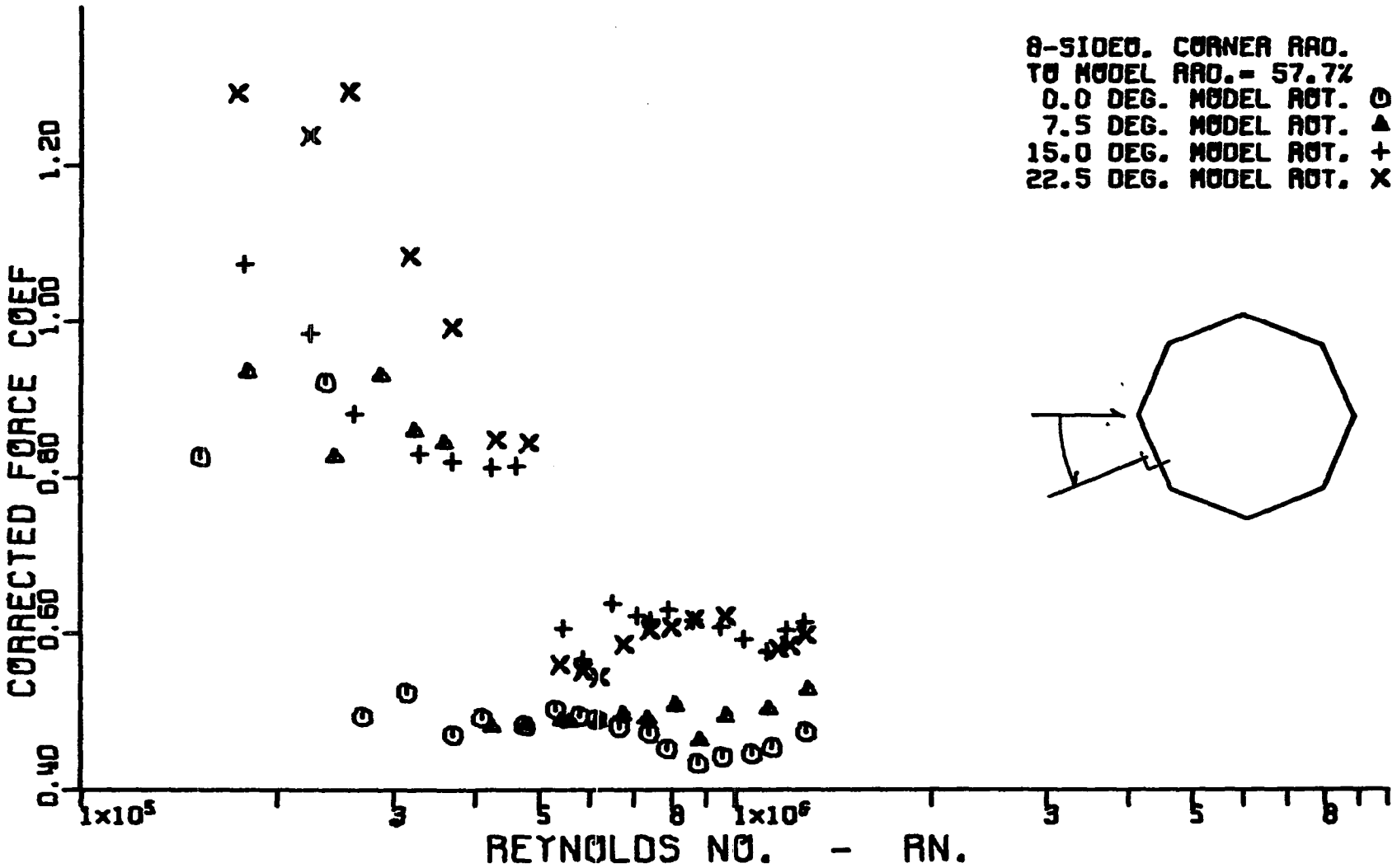

Figure 114. Variation of corrected cross-flow force coefficient with corrected cross-flow Reynolds number for an octagonal cylinder having a corner radius equal to 57.7 percent of the radius of the inscribed circular cylinder.

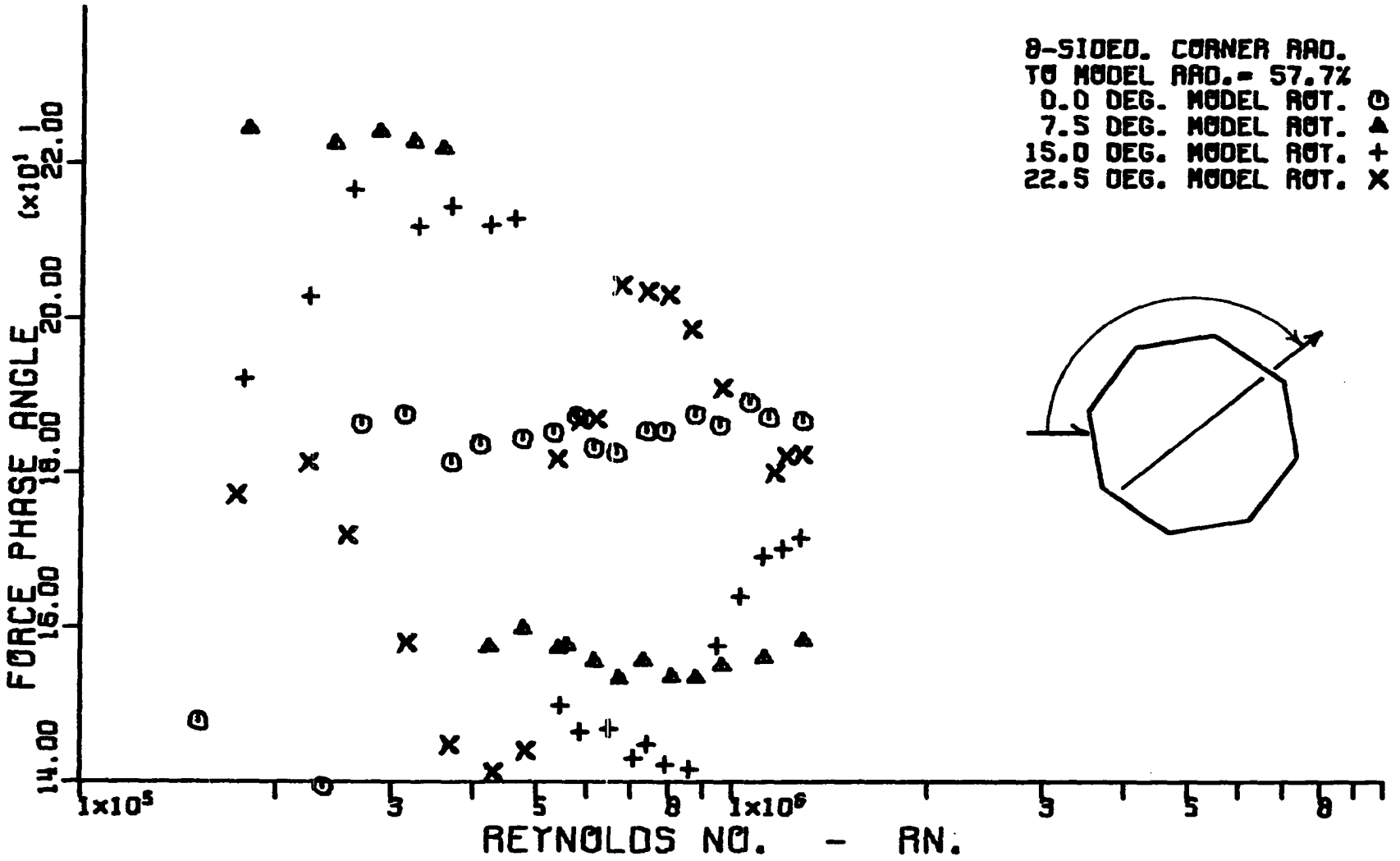

Figure 115. Variation of corrected cross-flow force phase angle with corrected cross-flow Reynolds number for an octagonal cylinder having a corner radius equal to 57.7 percent of the radius of the inscribed circular cylinder.

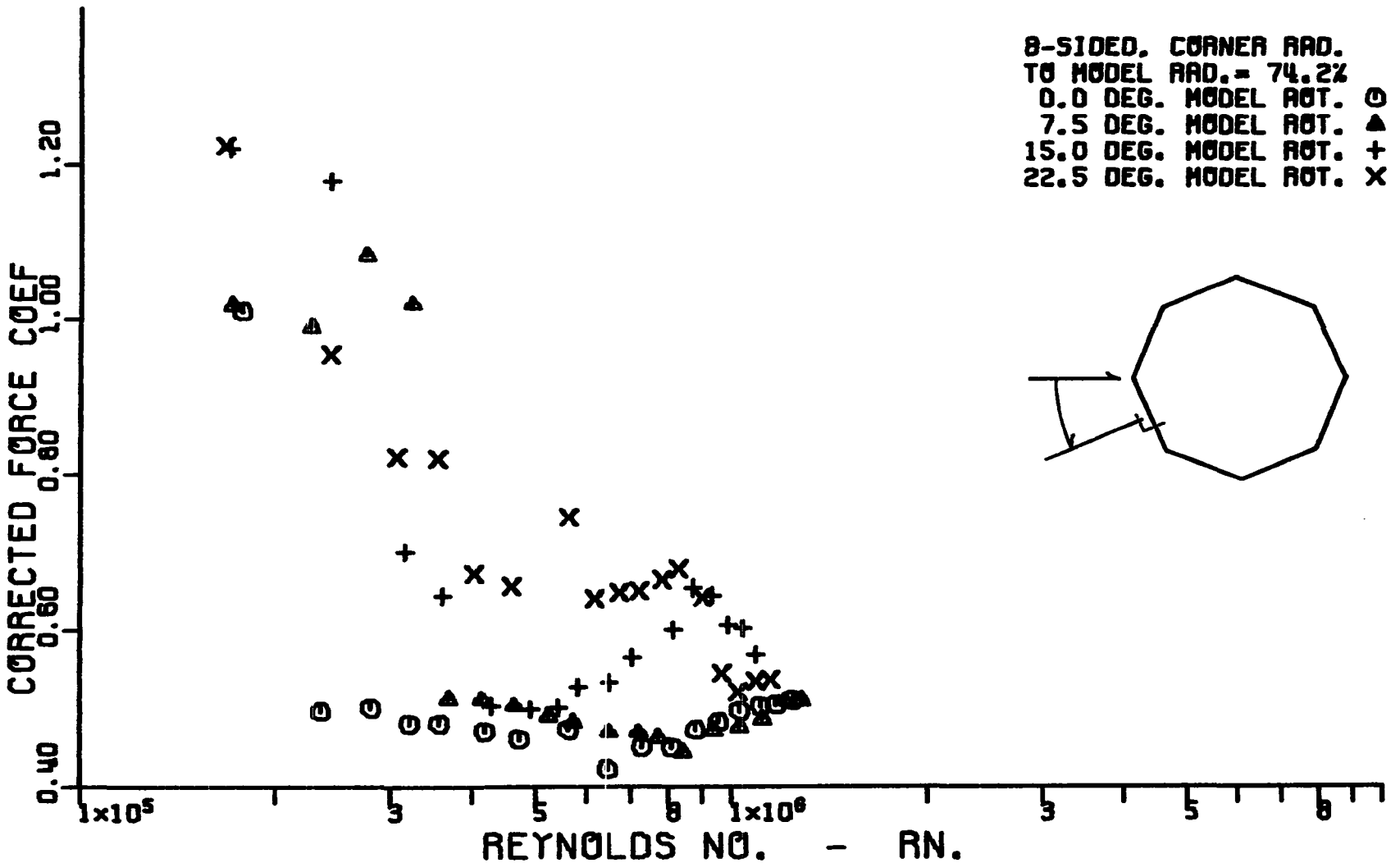

Figure 116. Variation of corrected cross-flow force coefficient with corrected cross-flow Reynolds number for an octagonal cylinder having a corner radius equal to 74.2 percent of the radius of the inscribed circular cylinder.

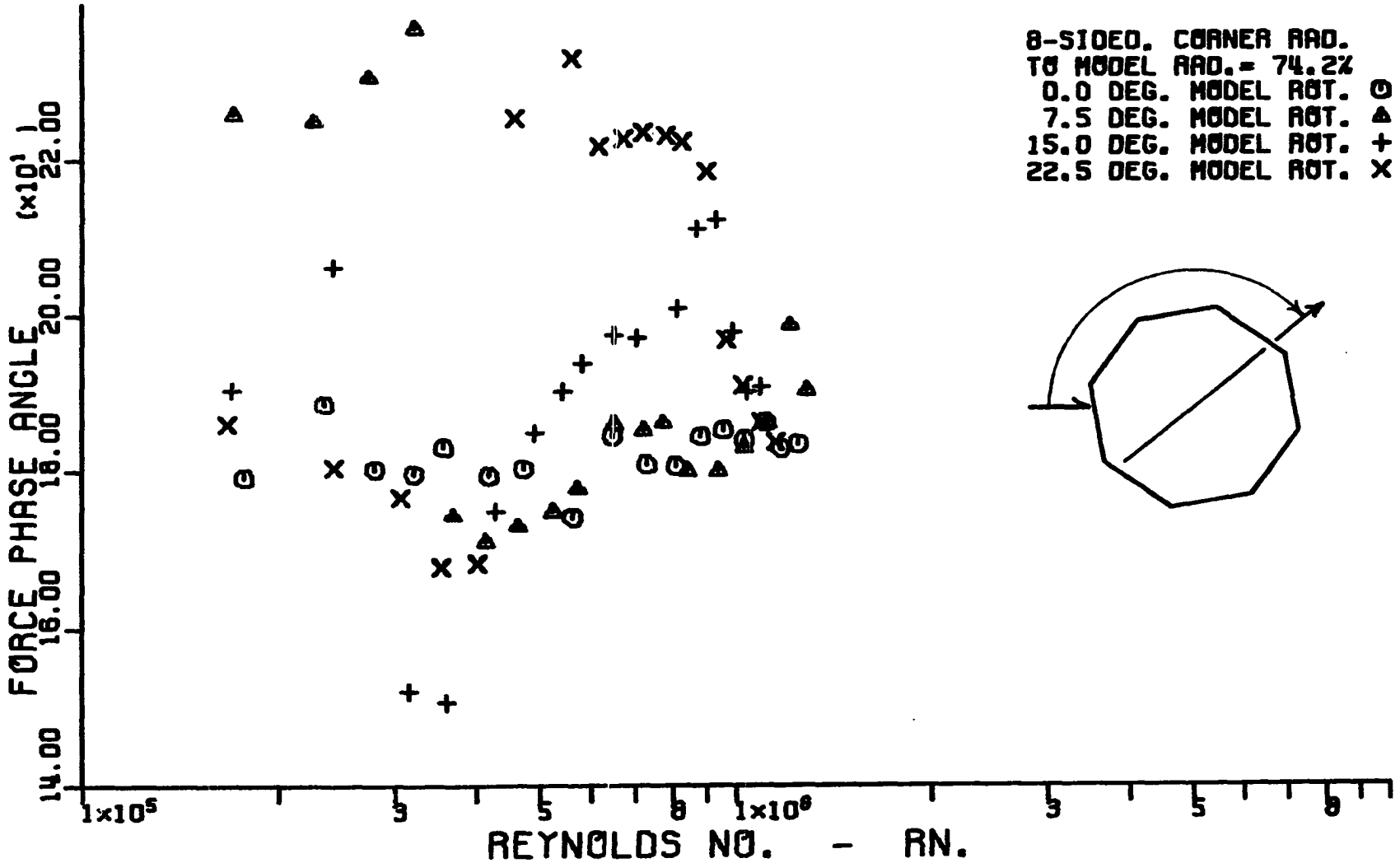

Figure 117. Variation of corrected cross-flow force phase angle with corrected cross-flow Reynolds number for an octagonal cylinder having a corner radius equal to 74.2 percent of the radius of the inscribed circular cylinder.

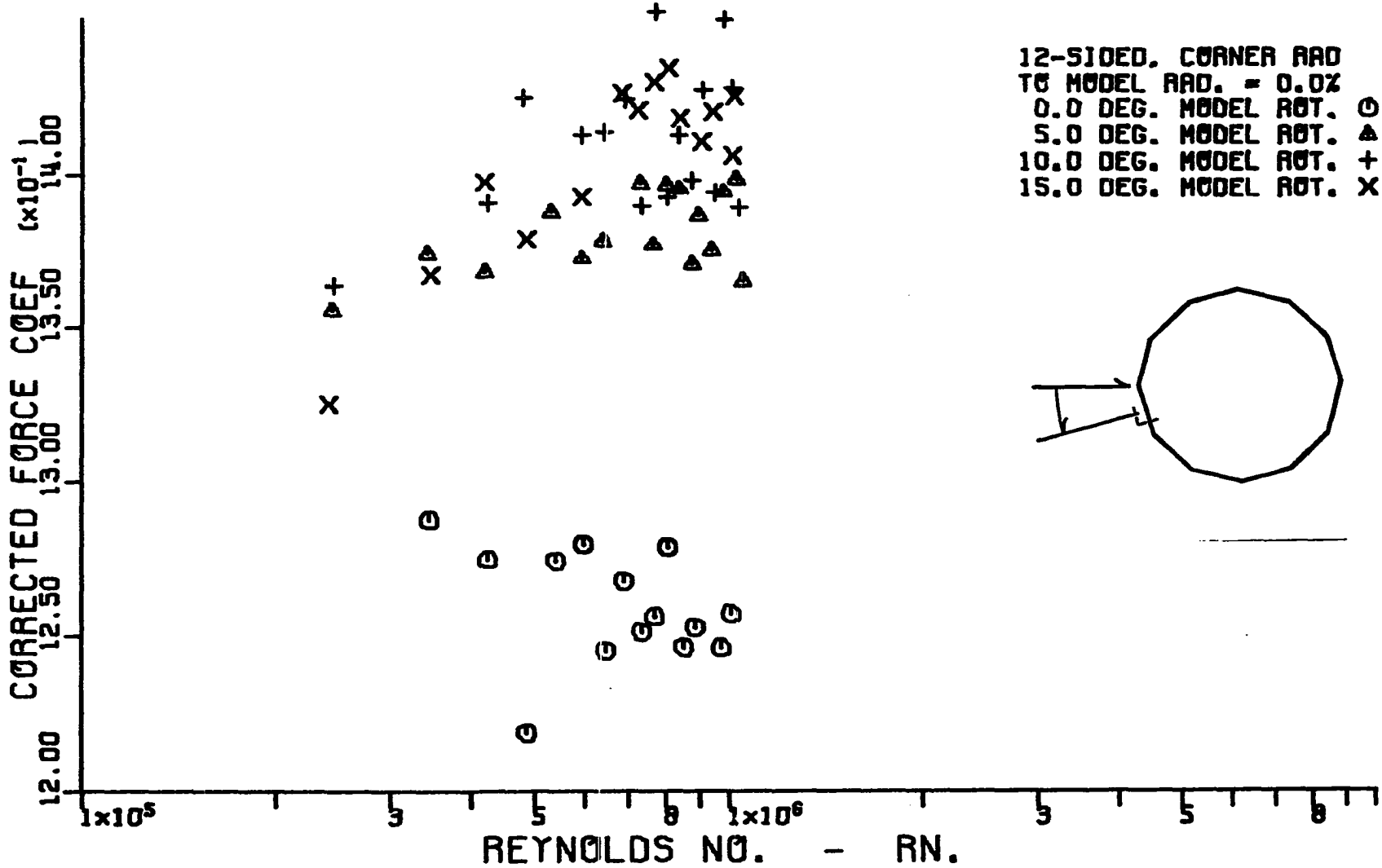

Figure 118. Variation of corrected cross-flow force coefficient with corrected cross-flow Reynolds number for a dodecagonal cylinder having a corner radius equal to 0.0 percent of the radius of the inscribed circular cylinder.

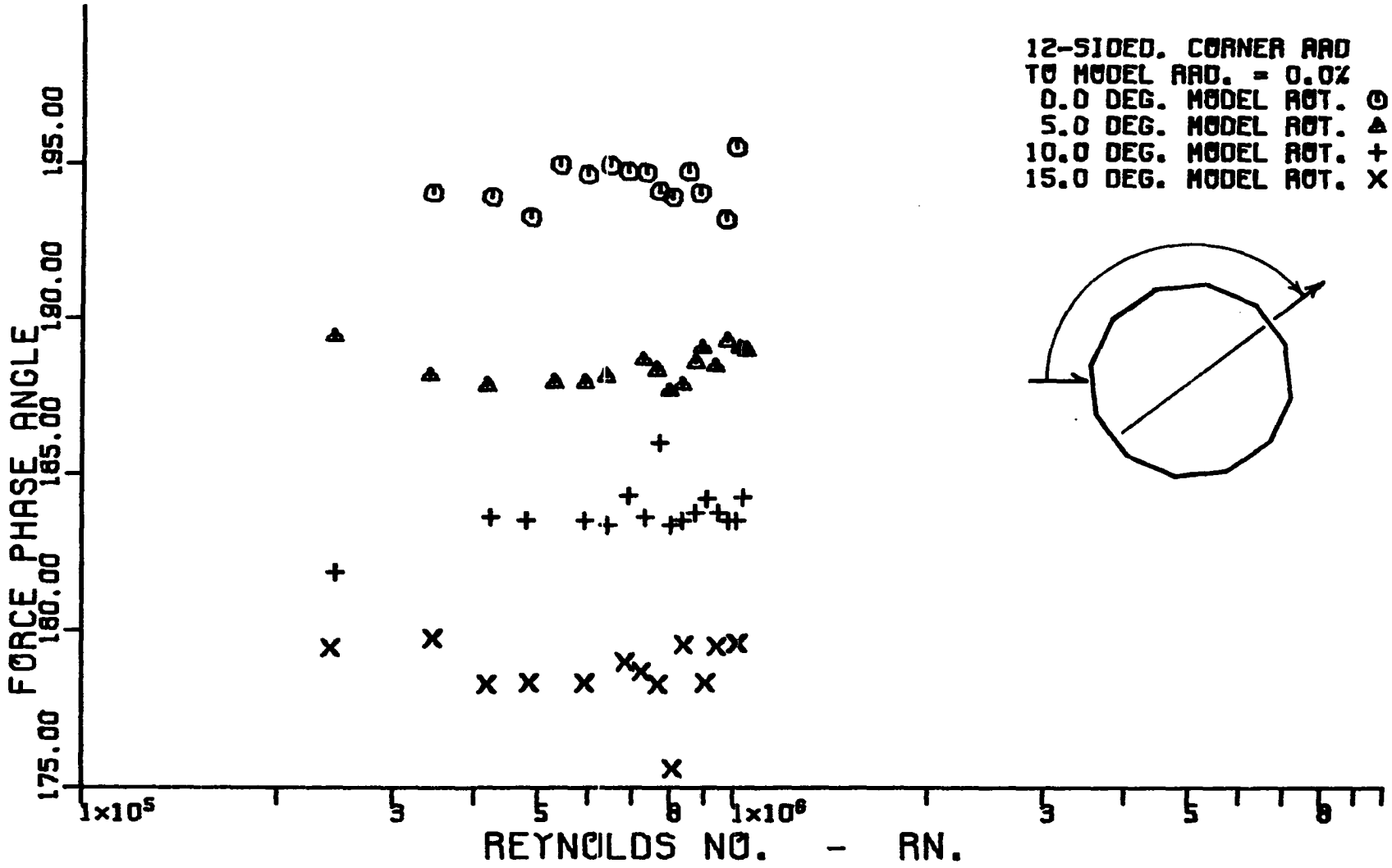

Figure 119. Variation of corrected cross-flow force phase angle with corrected cross-flow Reynolds number for a dodecagonal cylinder having a corner radius equal to 0.0 percent of the radius of the inscribed circular cylinder.

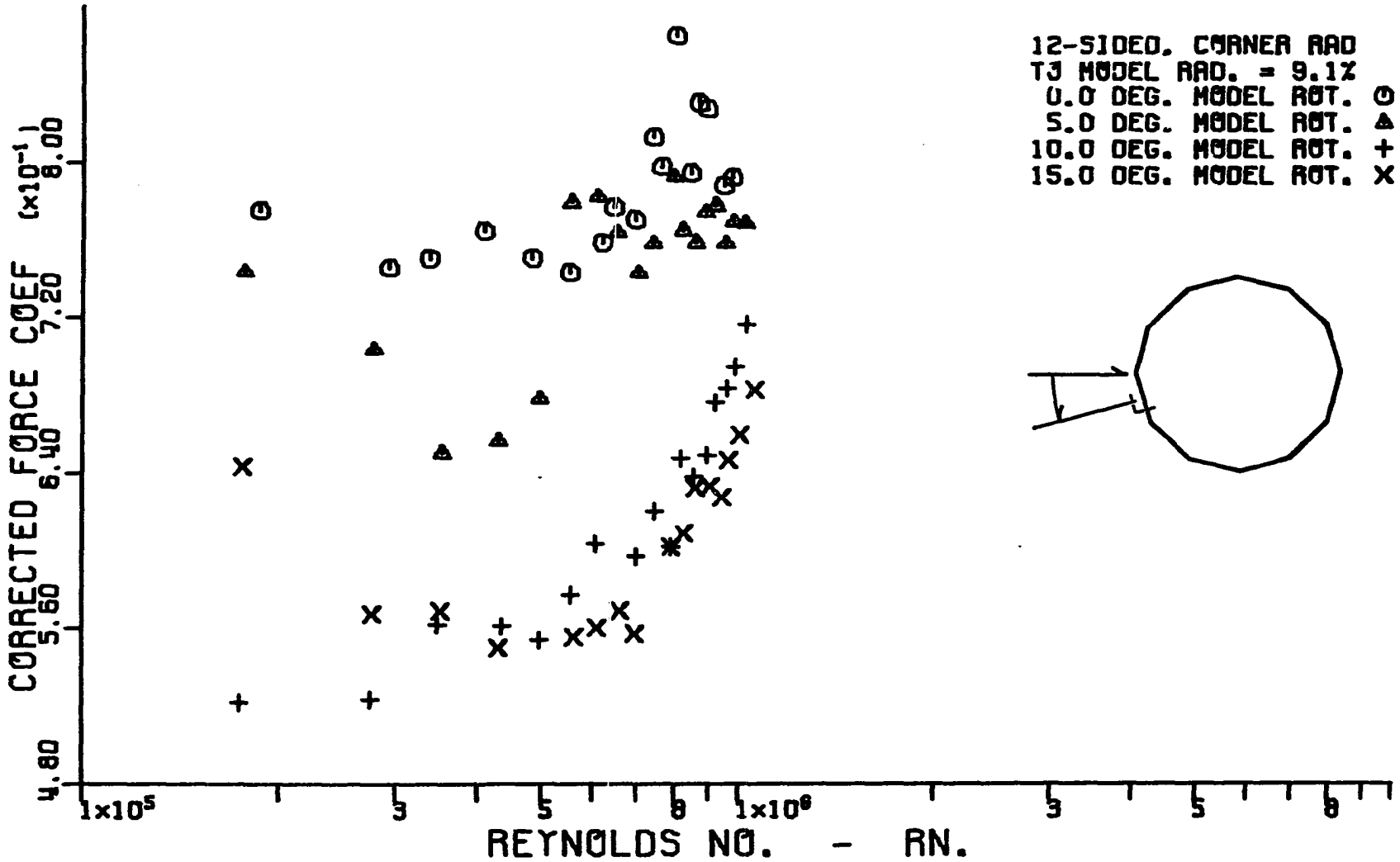

Figure 120. Variation of corrected cross-flow force coefficient with corrected cross-flow Reynolds number for a dodecagonal cylinder having a corner radius equal to 9.1 percent of the radius of the inscribed circular cylinder.

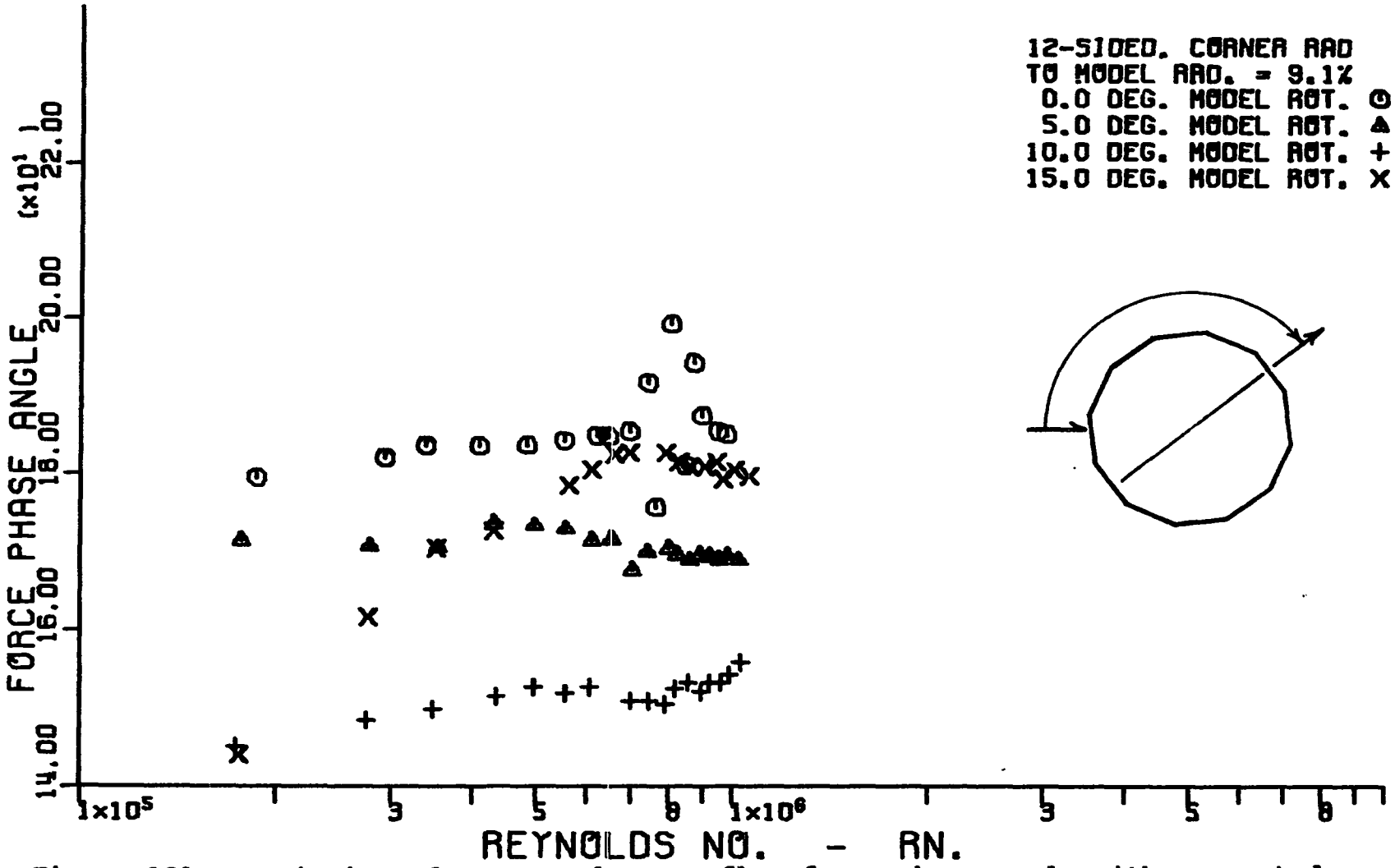

Figure 121. Variation of corrected cross-flow force phase angle with corrected cross-flow Reynolds number for a dodecagonal cylinder having a corner radius equal to 9.1 percent of the radius of the inscribed circular cylinder.

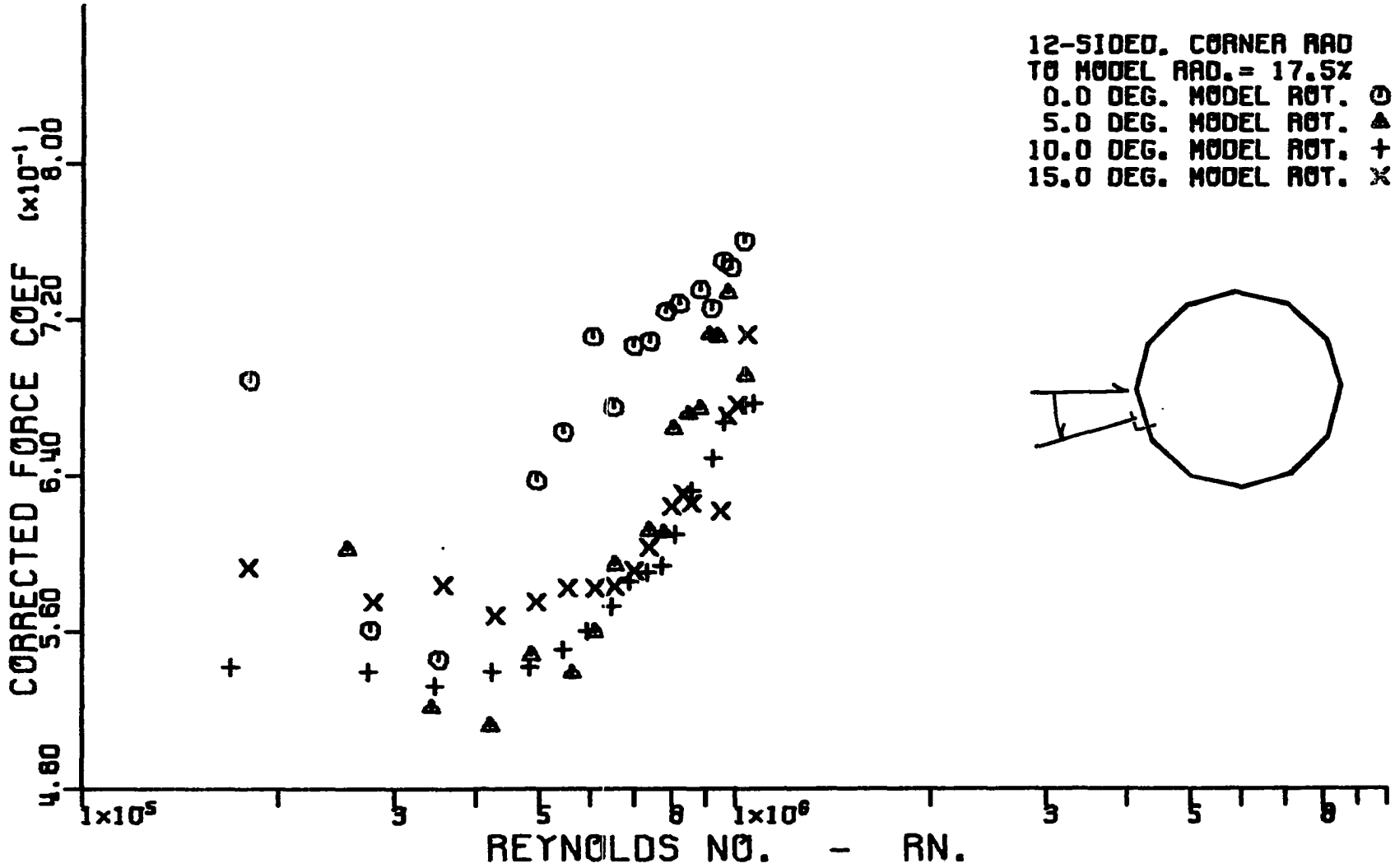

Figure 122. Variation of corrected cross-flow force coefficient with corrected cross-flow Reynolds number for a dodecagonal cylinder having a corner radius equal to 17.5 percent of the radius of the inscribed circular cylinder.

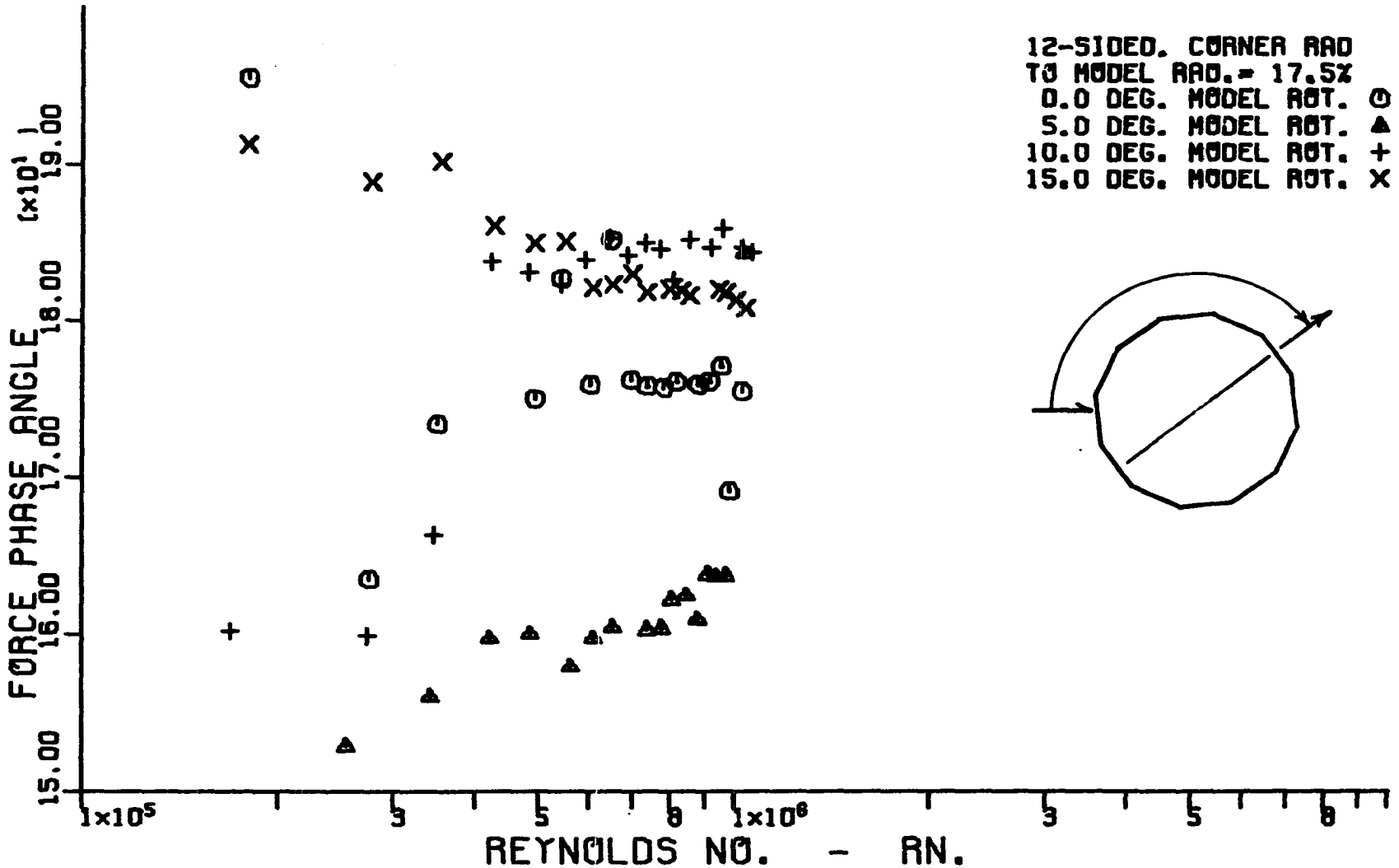

Figure 123. Variation of corrected cross-flow force phase angle with corrected cross-flow Reynolds number for a dodecagonal cylinder having a corner radius equal to 17.5 percent of the radius of the inscribed circular cylinder.

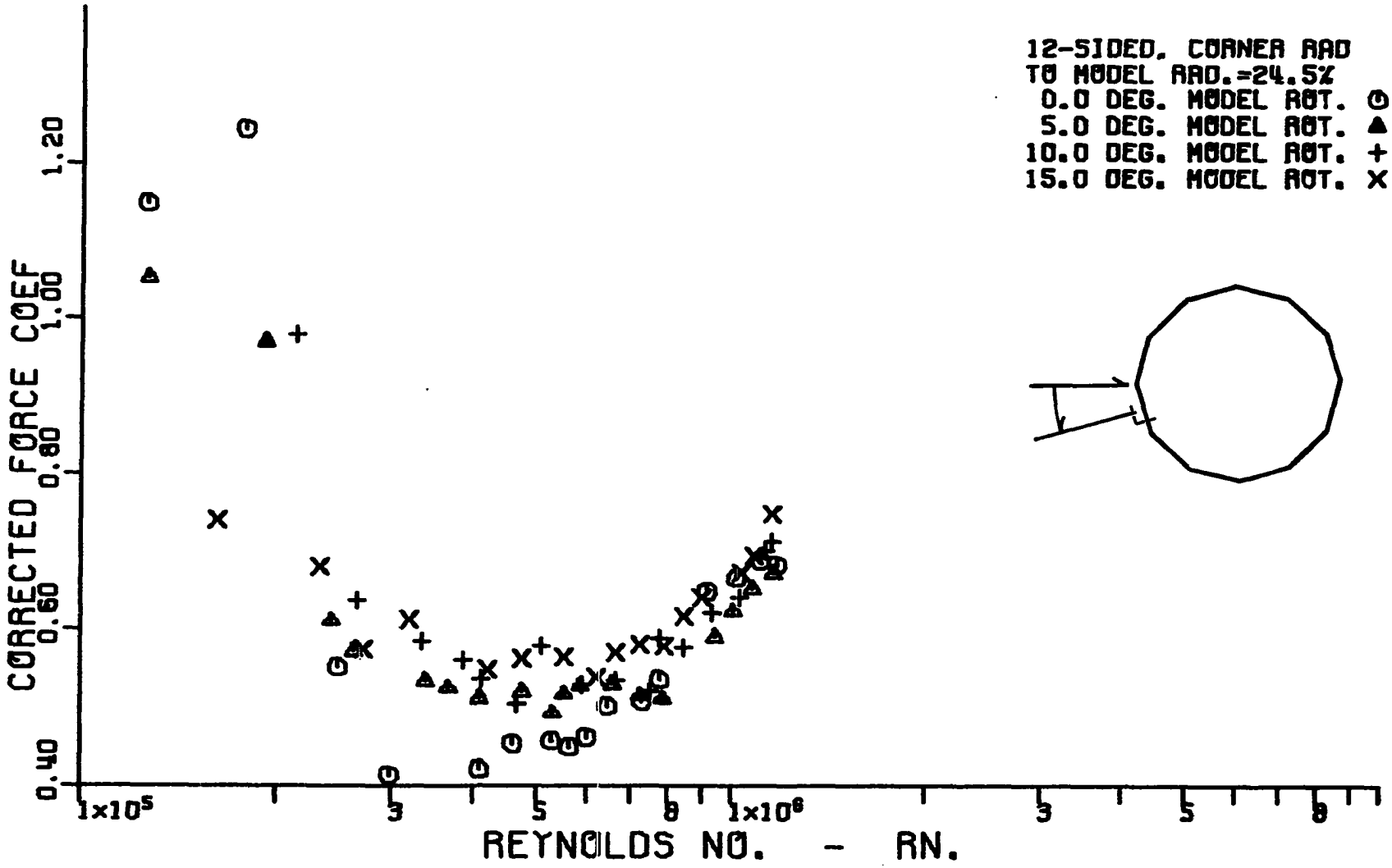

Figure 124. Variation of corrected cross-flow force coefficient with corrected cross-flow Reynolds number for a dodecagonal cylinder having a corner radius equal to 24.5 percent of the radius of the inscribed circular cylinder.

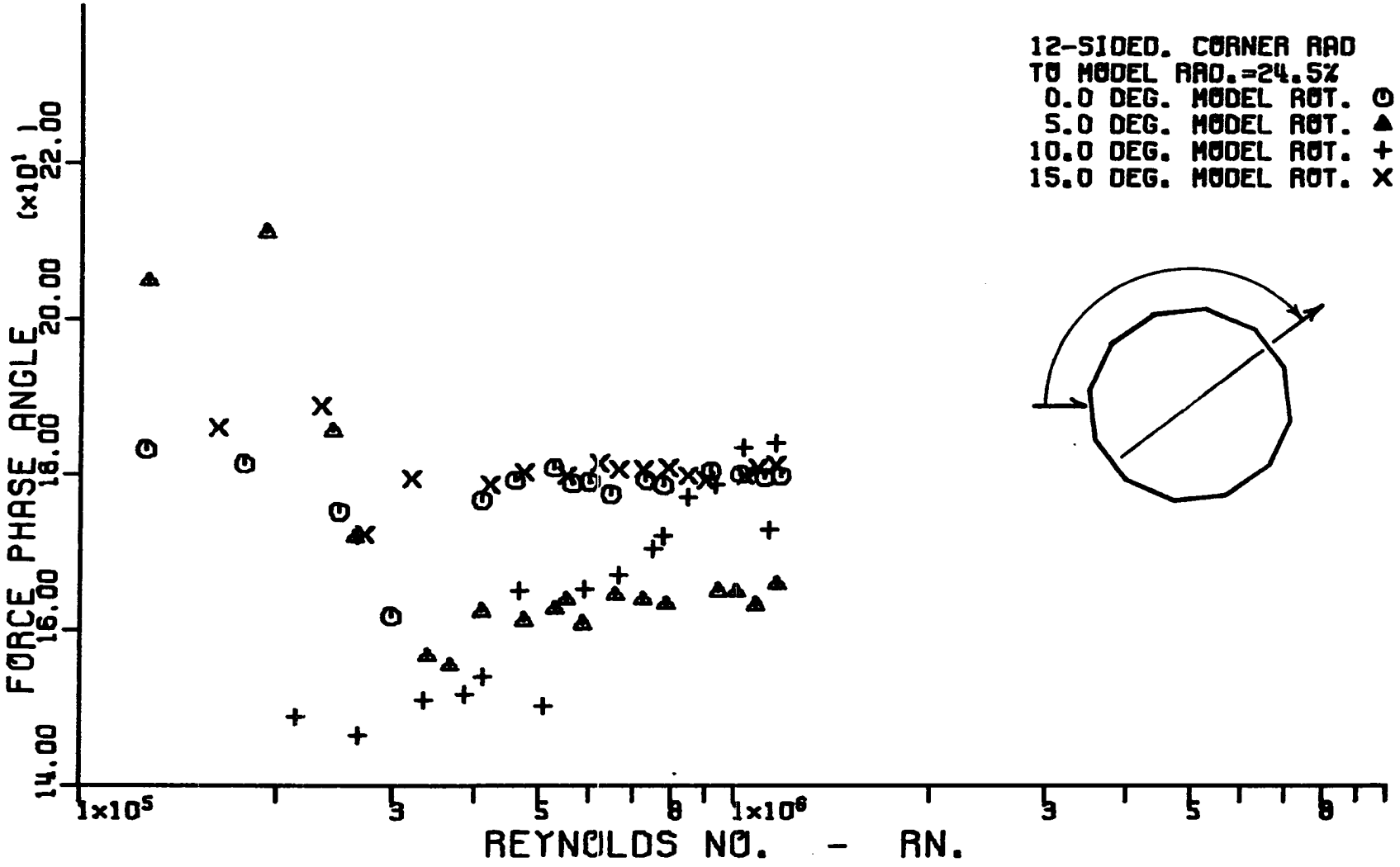

Figure 125. Variation of corrected cross-flow force phase angle with corrected cross-flow Reynolds number for a dodecagonal cylinder having a corner radius equal to 24.5 percent of the radius of the inscribed circular cylinder.

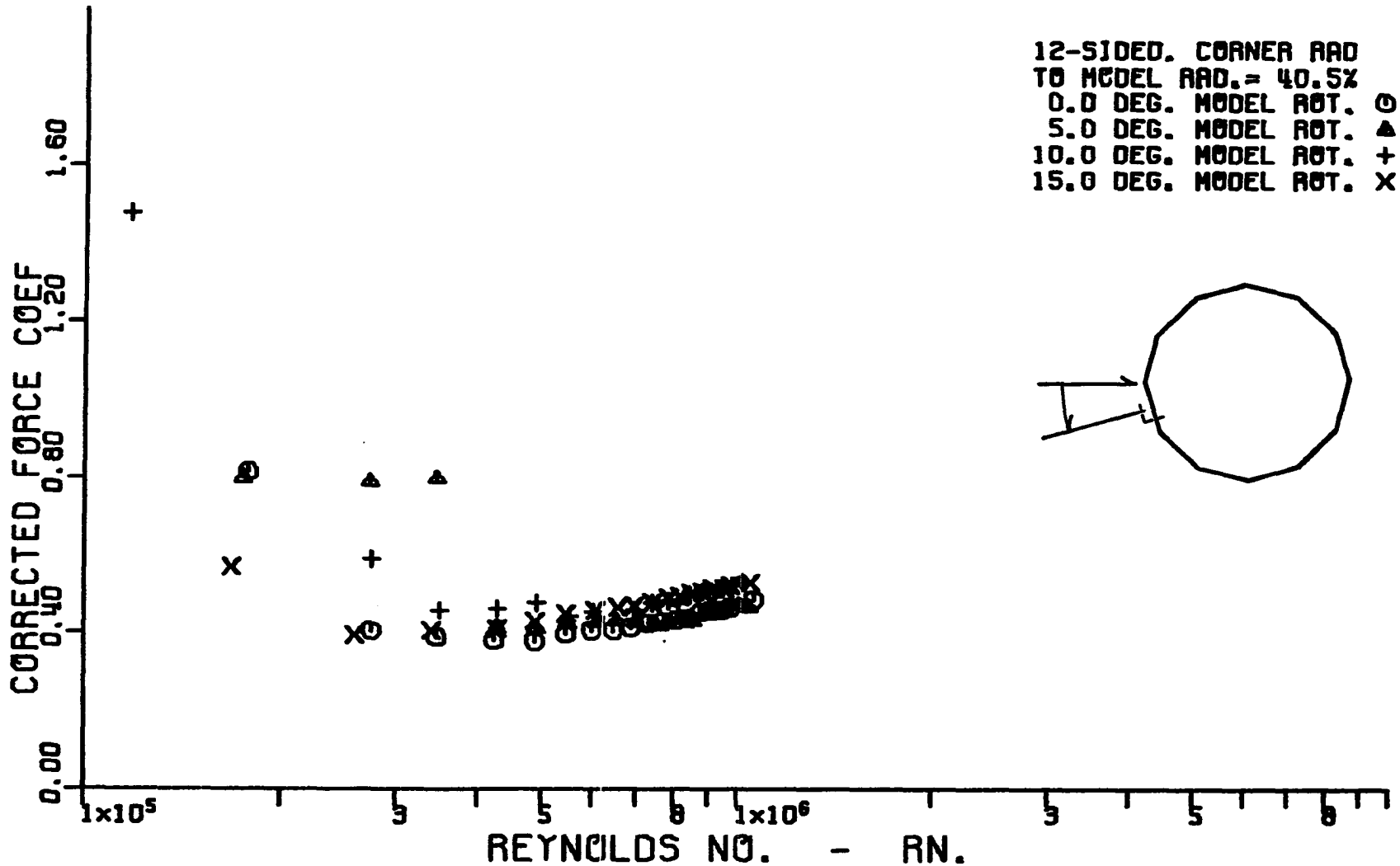

Figure 126. Variation of corrected cross-flow force coefficient with corrected cross-flow Reynolds number for a dodecagonal cylinder having a corner radius equal to 40.5 percent of the radius of the inscribed circular cylinder.

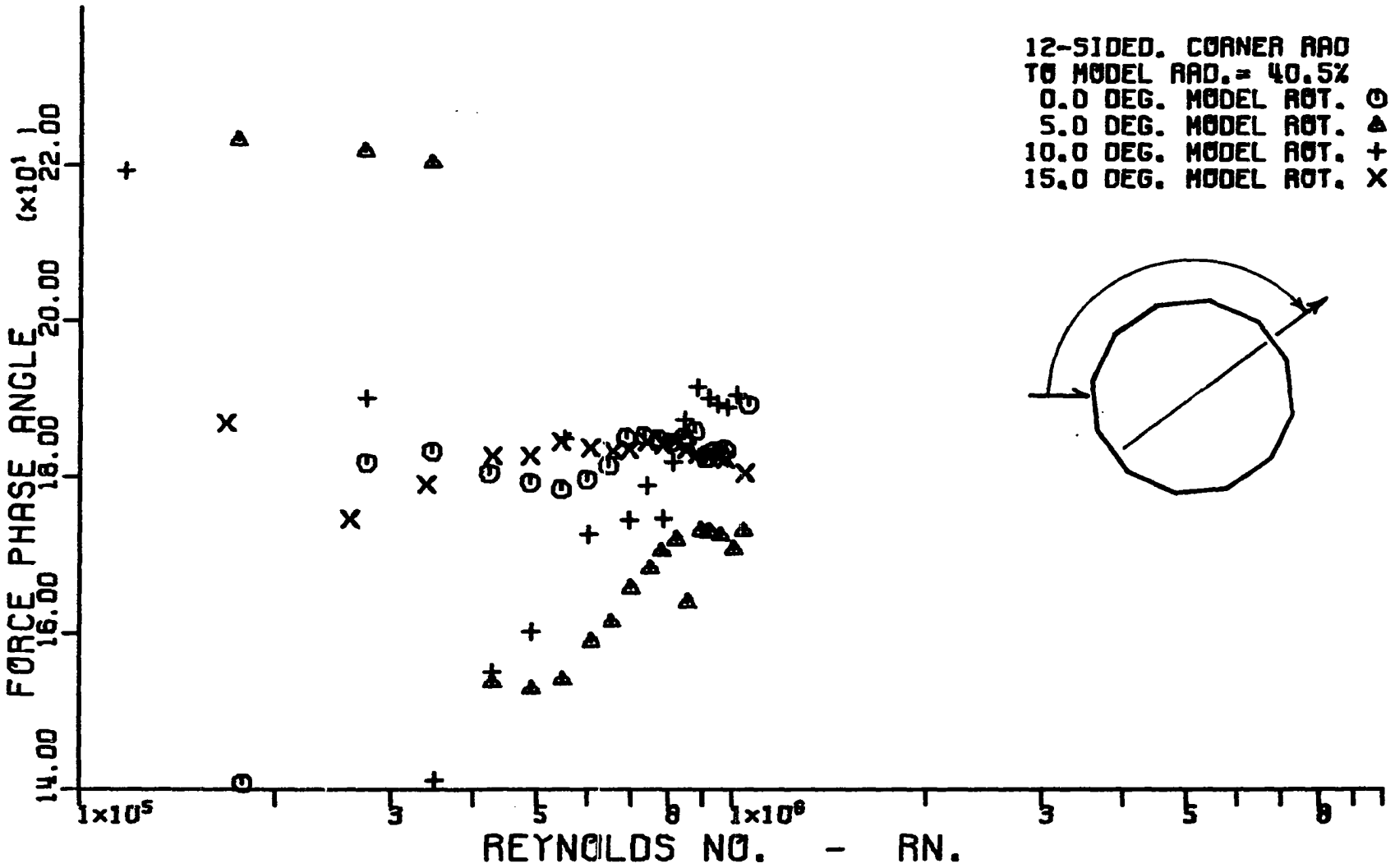

Figure 127. Variation of corrected cross-flow force phase angle with corrected cross-flow Reynolds number for a dodecagonal cylinder having a corner radius equal to 40.5 percent of the radius of the inscribed circular cylinder.

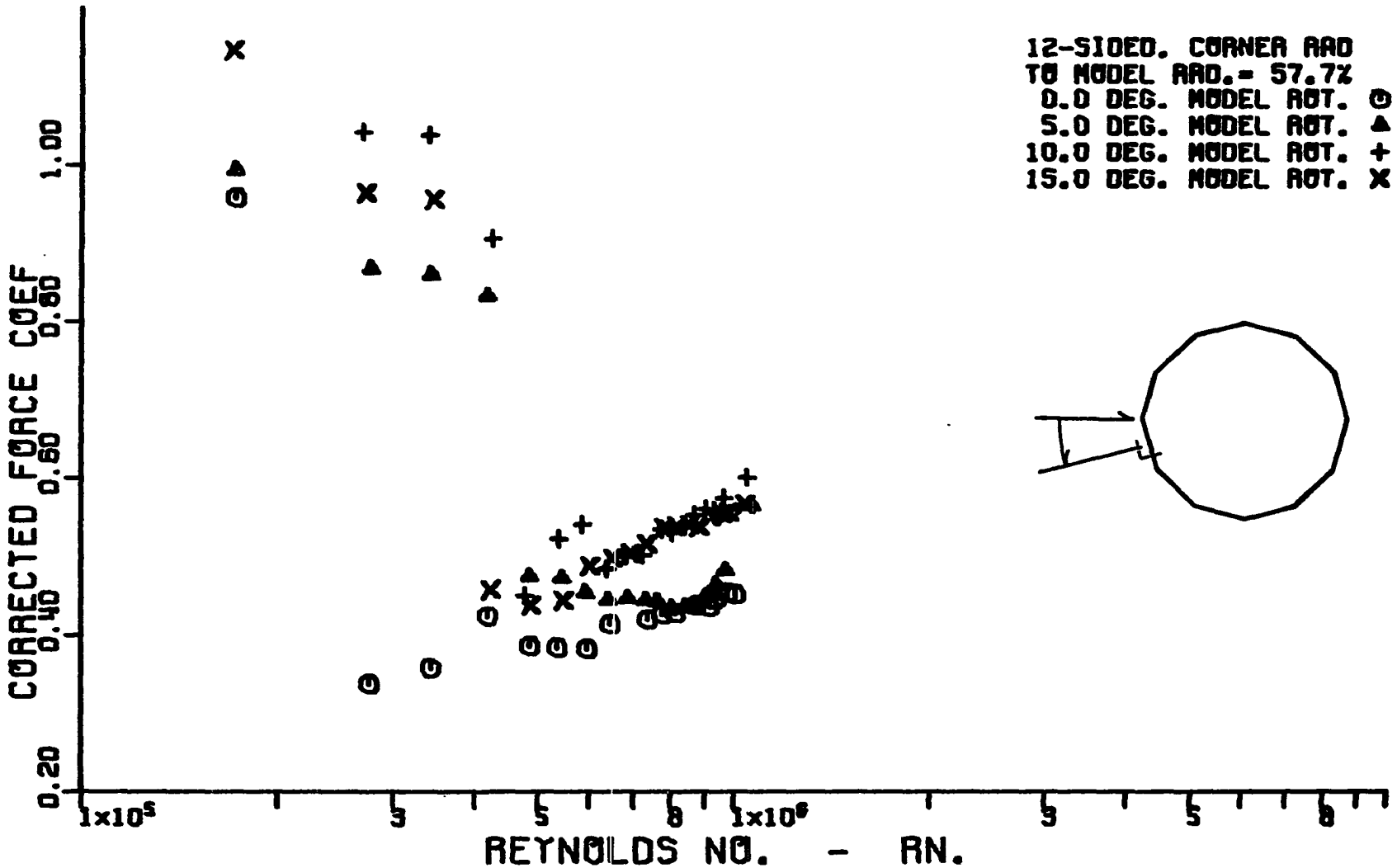

Figure 128. Variation of corrected cross-flow force coefficient with corrected cross-flow Reynolds number for a dodecagonal cylinder having a corner radius equal to 57.7 percent of the radius of the inscribed circular cylinder.

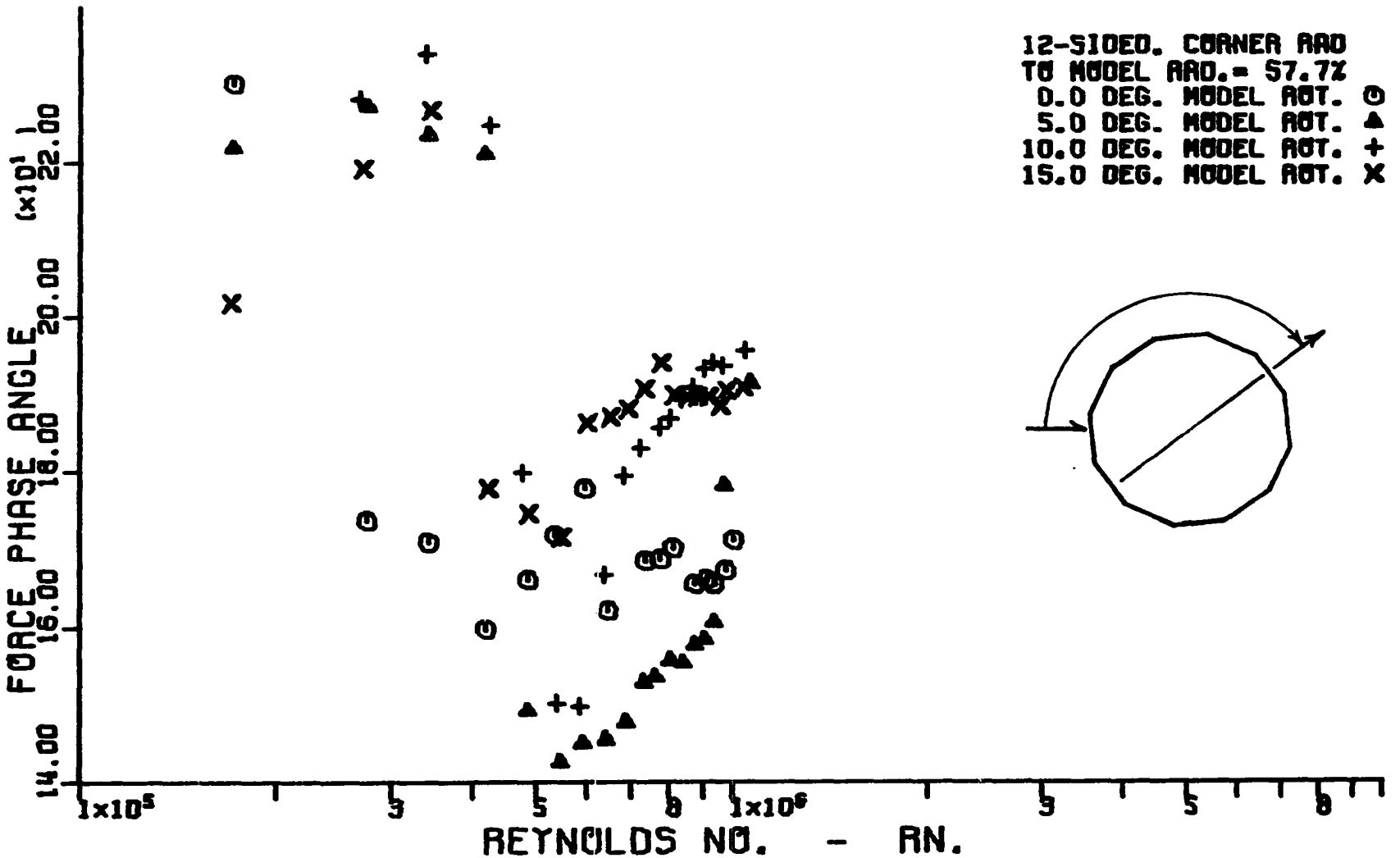

Figure 129. Variation of corrected cross-flow force phase angle with corrected cross-flow Reynolds number for a dodecagonal cylinder having a corner radius equal to 57.7 percent of the radius of the inscribed circular cylinder.

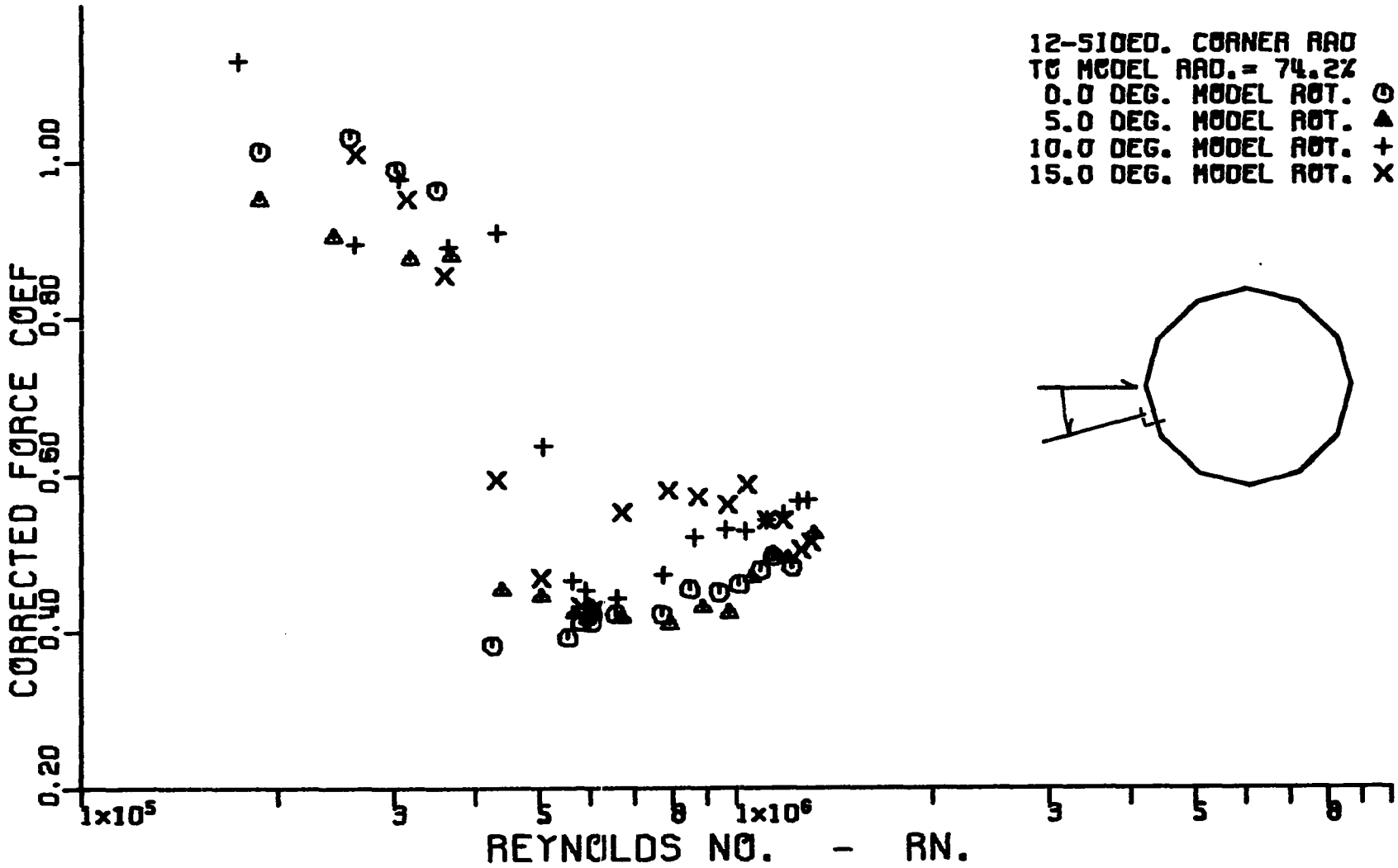

Figure 130. Variation of corrected cross-flow force coefficient with corrected cross-flow Reynolds number for a dodecagonal cylinder having a corner radius equal to 74.2 percent of the radius of the inscribed circular cylinder.

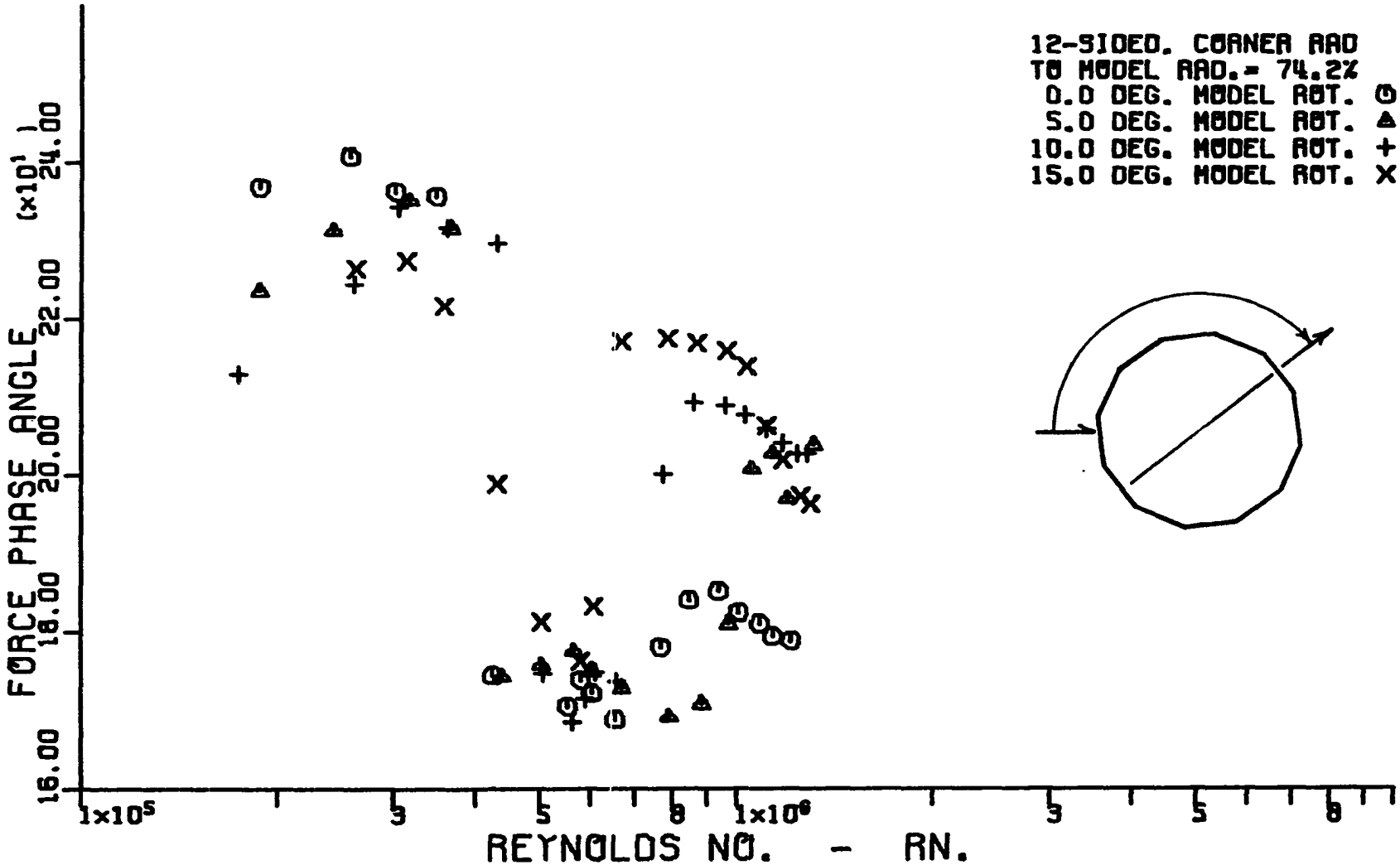

Figure 131. Variation of corrected cross-flow force phase angle with corrected cross-flow Reynolds number for a dodecagonal cylinder having a corner radius equal to 74.2 percent of the radius of the inscribed circular cylinder.

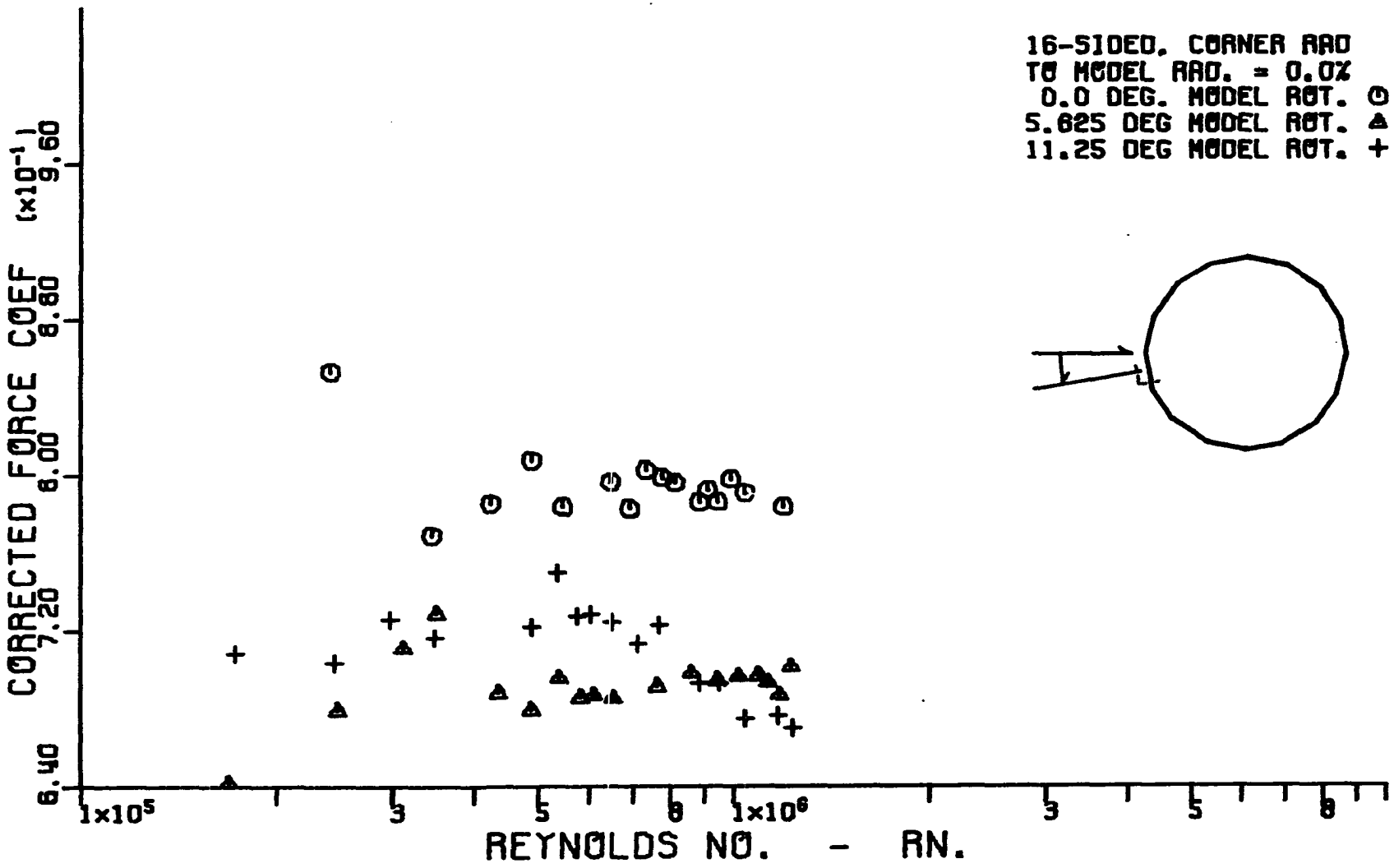

Figure 132. Variation of corrected cross-flow force coefficient with corrected cross-flow Reynolds number for a hexdecagonal cylinder having a corner radius equal to 0.0 percent of the radius of the inscribed circular cylinder.

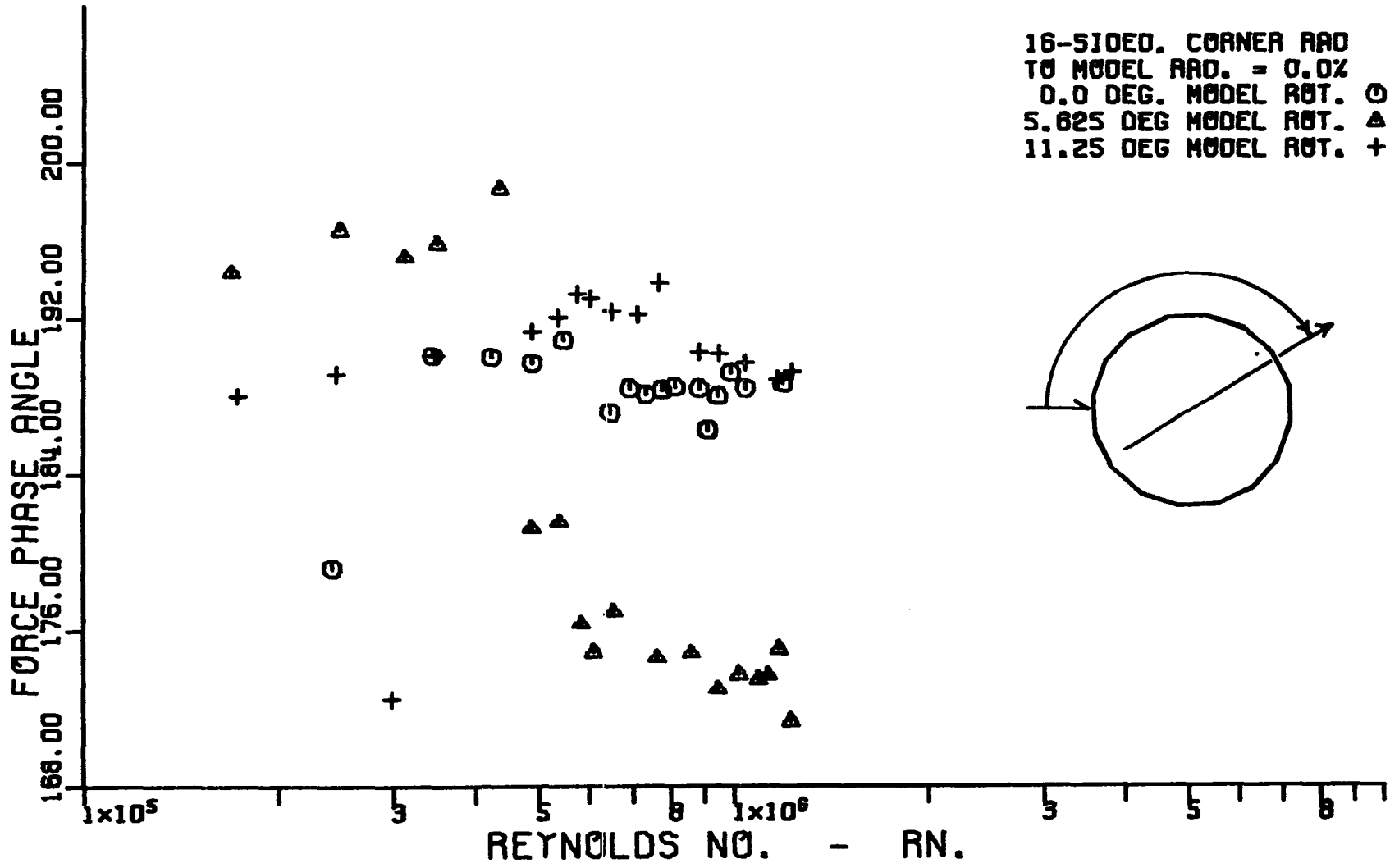

Figure 133. Variation of corrected cross-flow phase angle with corrected cross-flow Reynolds number for a hexdecagonal cylinder having a corner radius equal to 0.0 percent of the radius of the inscribed circular cylinder.

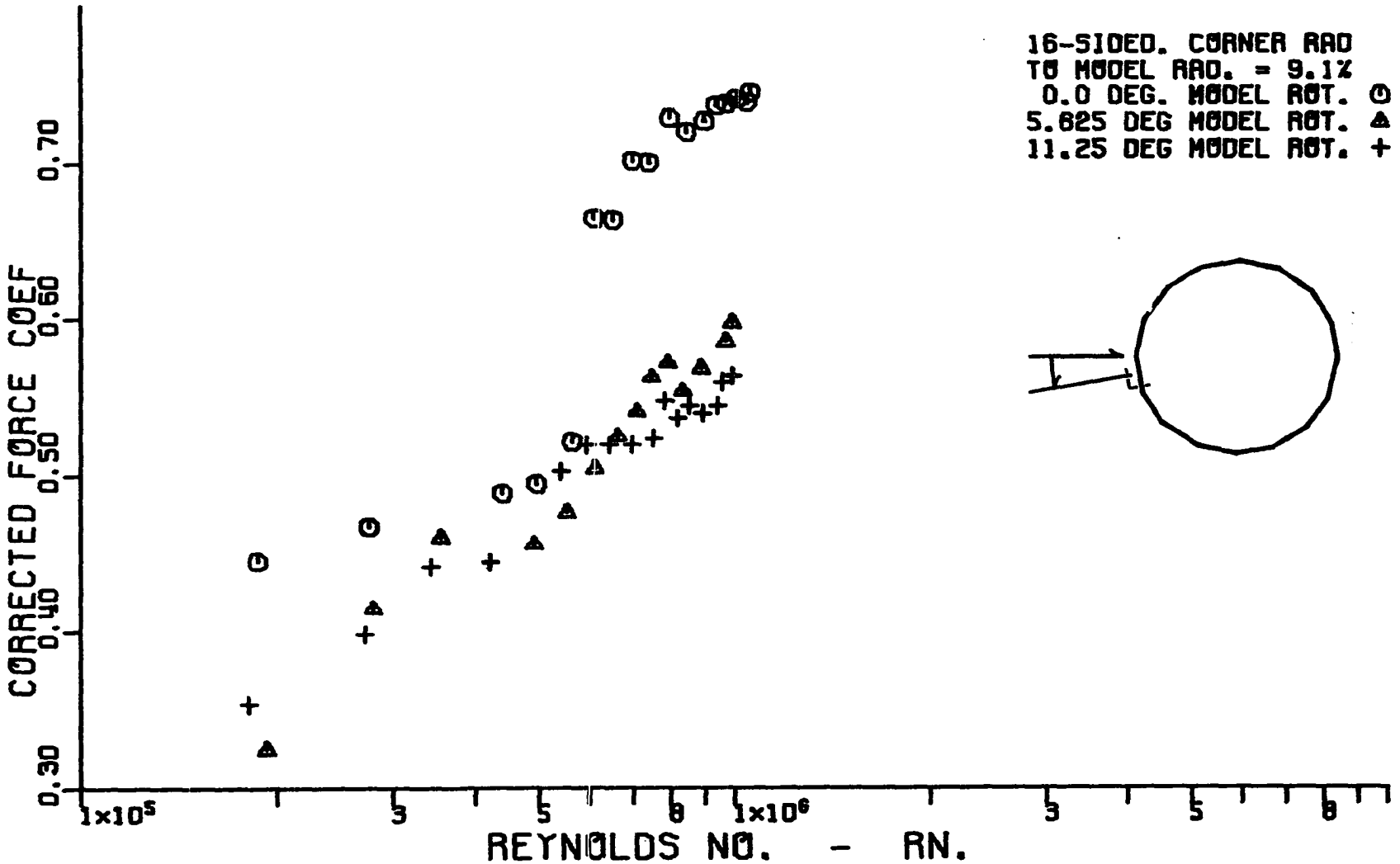

Figure 134. Variation of corrected cross-flow force coefficient with corrected cross-flow Reynolds number for a hexdecagonal cylinder having a corner radius equal to 9.1 percent of the radius of the inscribed circular cylinder.

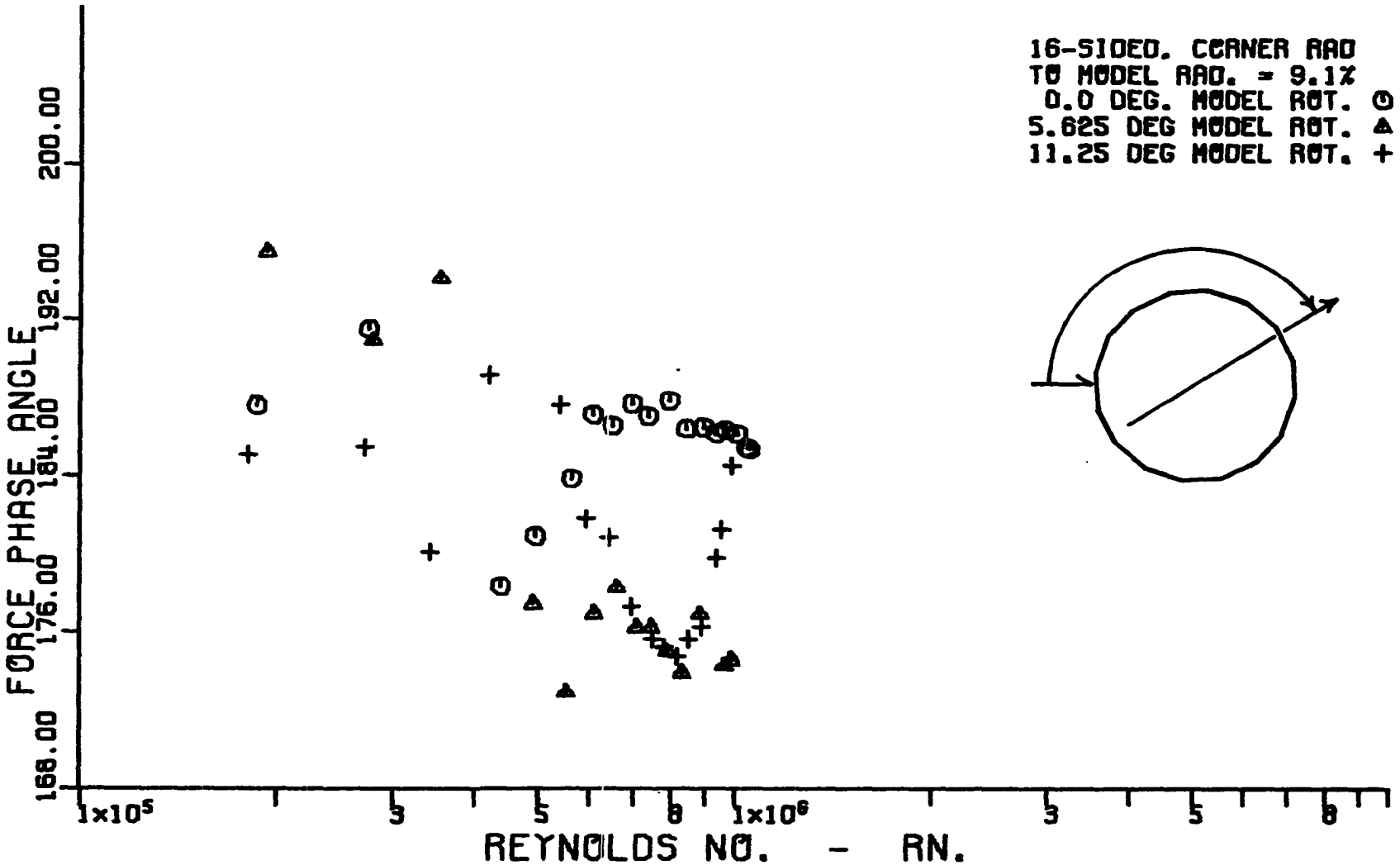

Figure 135. Variation of corrected cross-flow force phase angle with corrected cross-flow Reynolds number for a hexdecagonal cylinder having a corner radius equal to 9.1 percent of the radius of the inscribed circular cylinder.

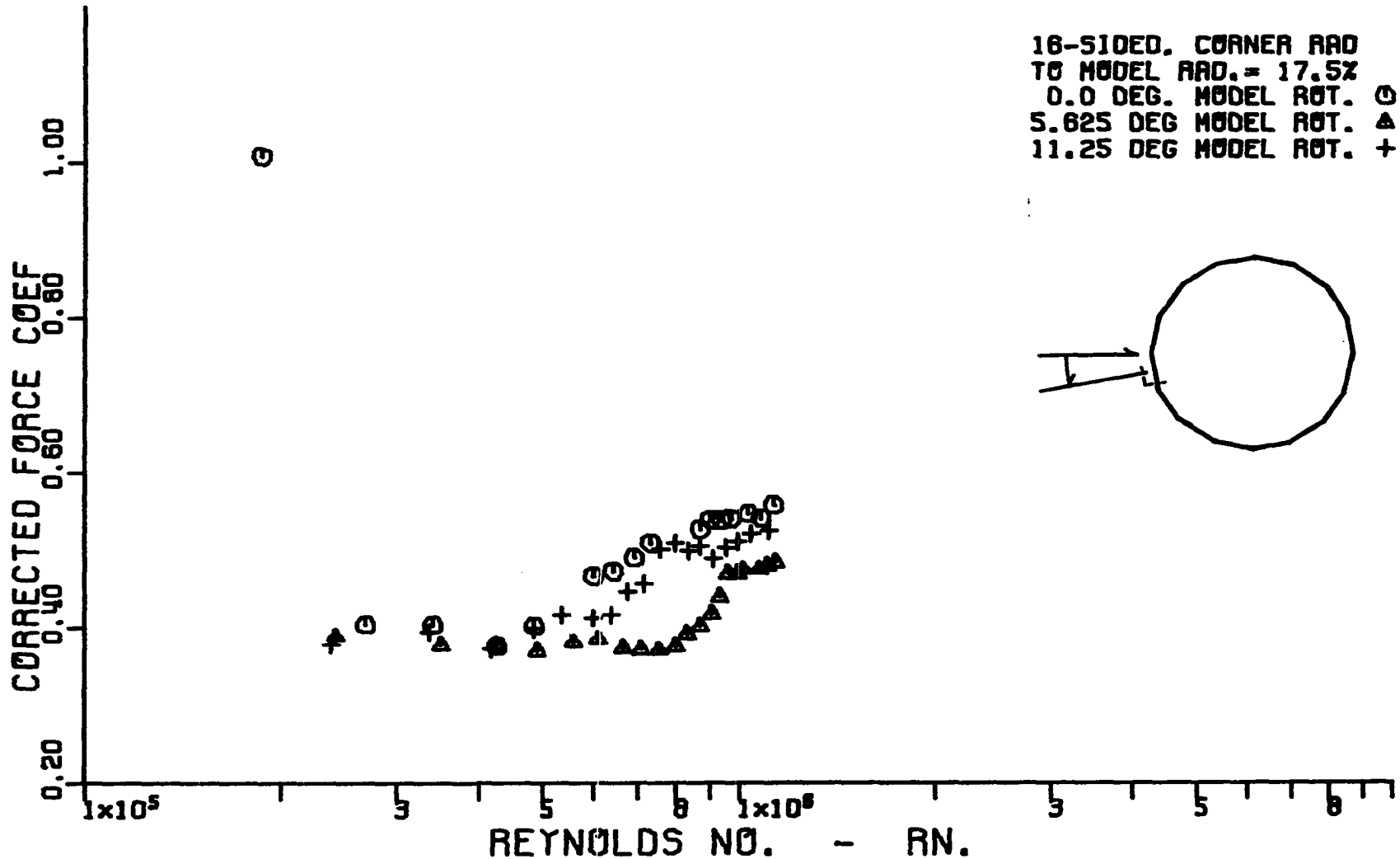

Figure 136. Variation of corrected cross-flow force coefficient with corrected cross-flow Reynolds number for a hexdecagonal cylinder having a corner radius equal to 17.5 percent of the radius of the inscribed circular cylinder.

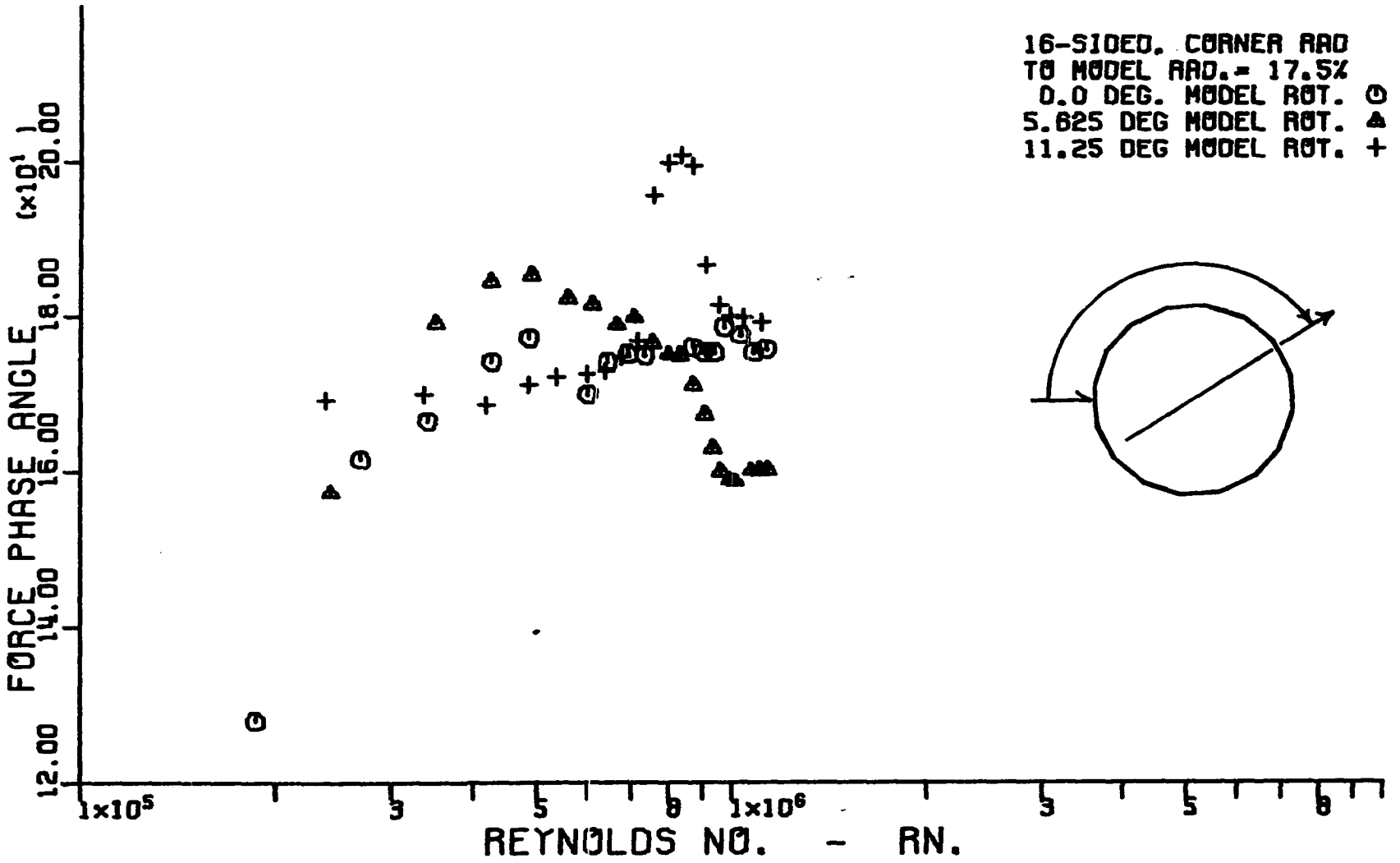

Figure 137. Variation of corrected cross-flow force phase angle with corrected cross-flow Reynolds number for a hexdecagonal cylinder having a corner radius equal to 17.5 percent of the radius of the inscribed circular cylinder.

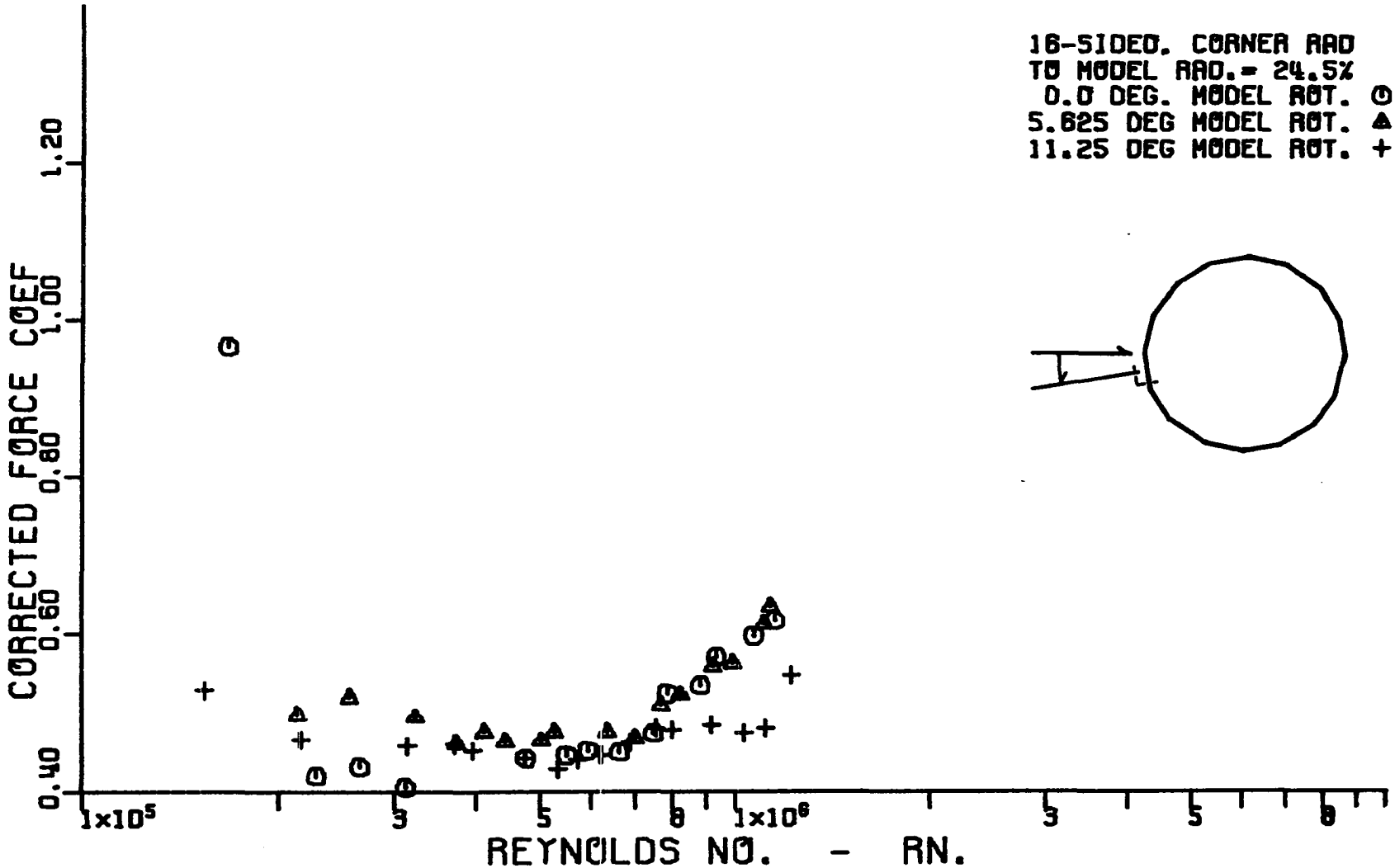

Figure 138. Variation of corrected cross-flow force coefficient with corrected cross-flow Reynolds number for a hexdecagonal cylinder having a corner radius equal to 24.5 percent of the radius of the inscribed circular cylinder.

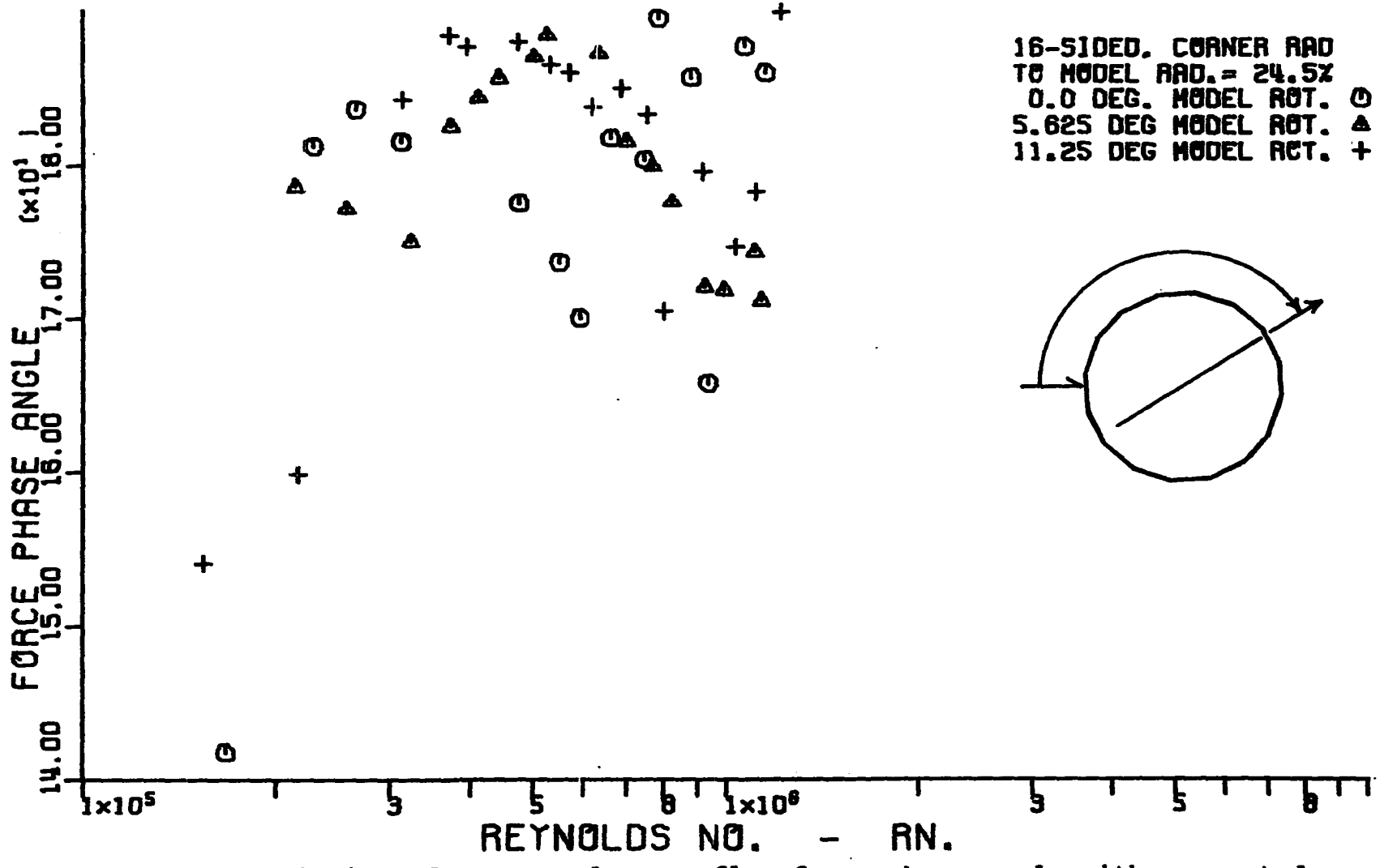

Figure 139. Variation of corrected cross-flow force phase angle with corrected cross-flow Reynolds number for a hexdecagonal cylinder having a corner radius equal to 24.5 percent of the radius of the inscribed circular cylinder.

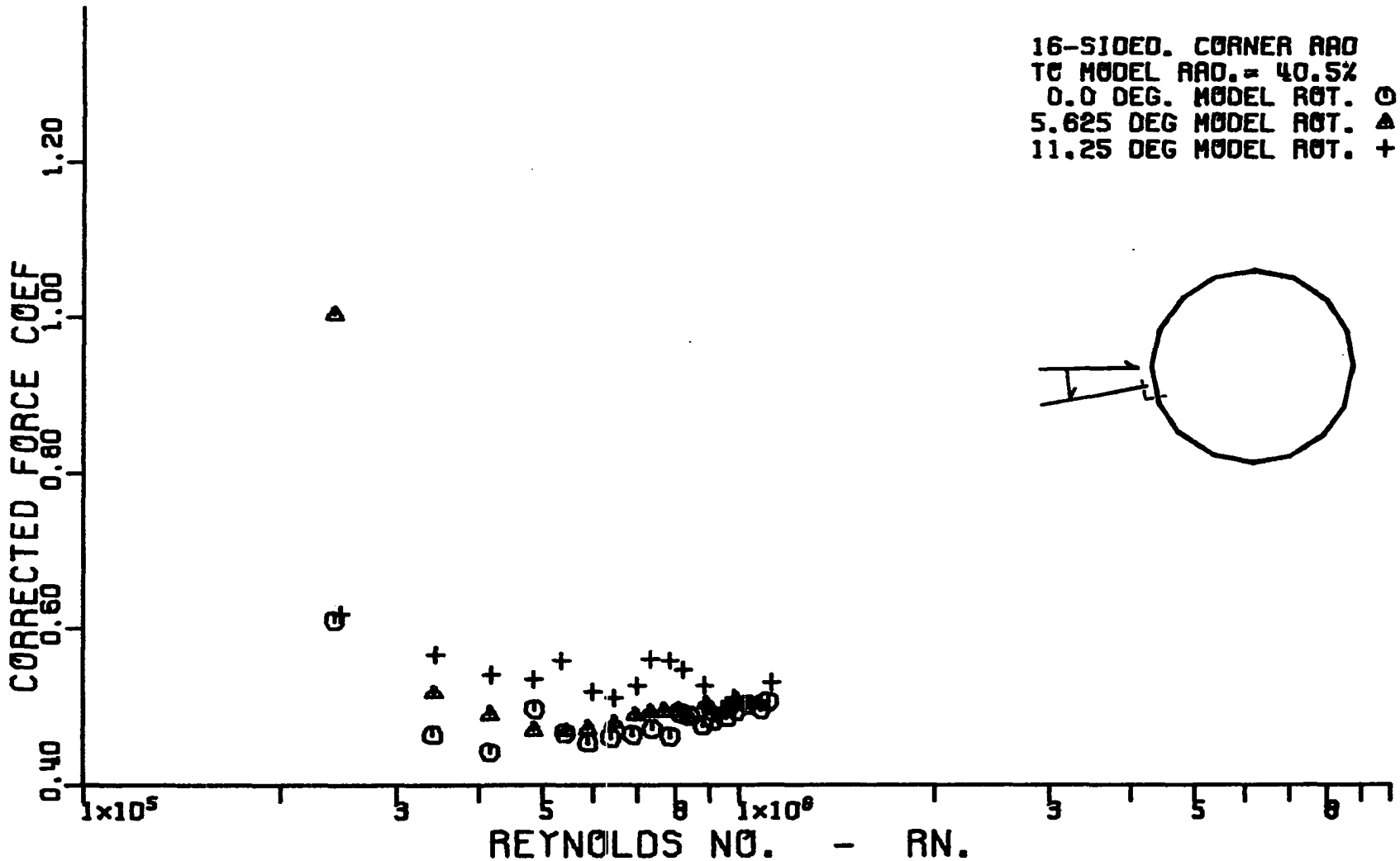

Figure 140. Variation of corrected cross-flow force coefficient with corrected cross-flow Reynolds number for a hexdecagonal cylinder having a corner radius equal to 40.5 percent of the radius of the inscribed circular cylinder.

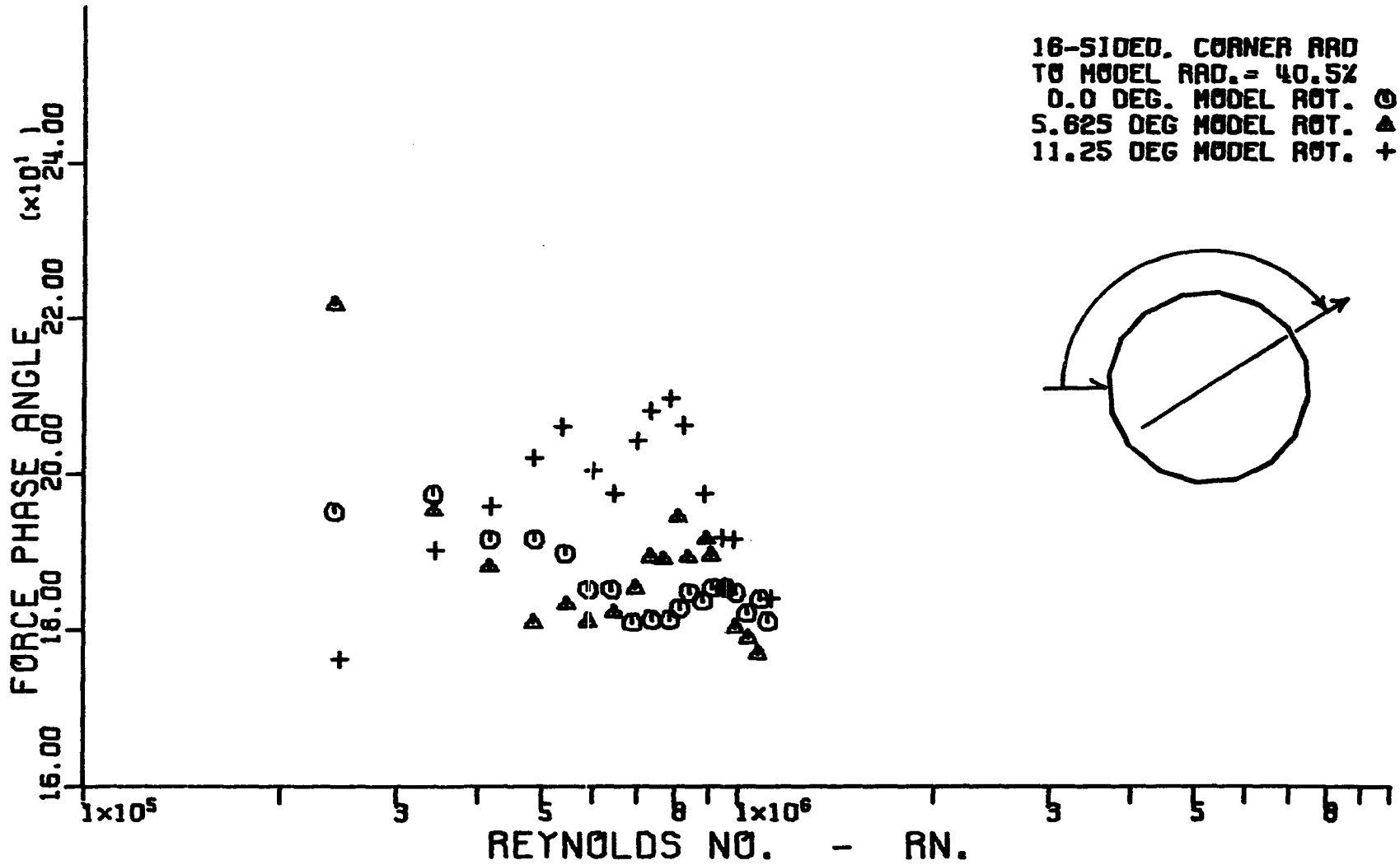

Figure 141. Variation of corrected cross-flow force phase angle with corrected cross-flow Reynolds number for a hexdecagonal cylinder having a corner radius equal to 40.5 percent of the radius of the inscribed circular cylinder.

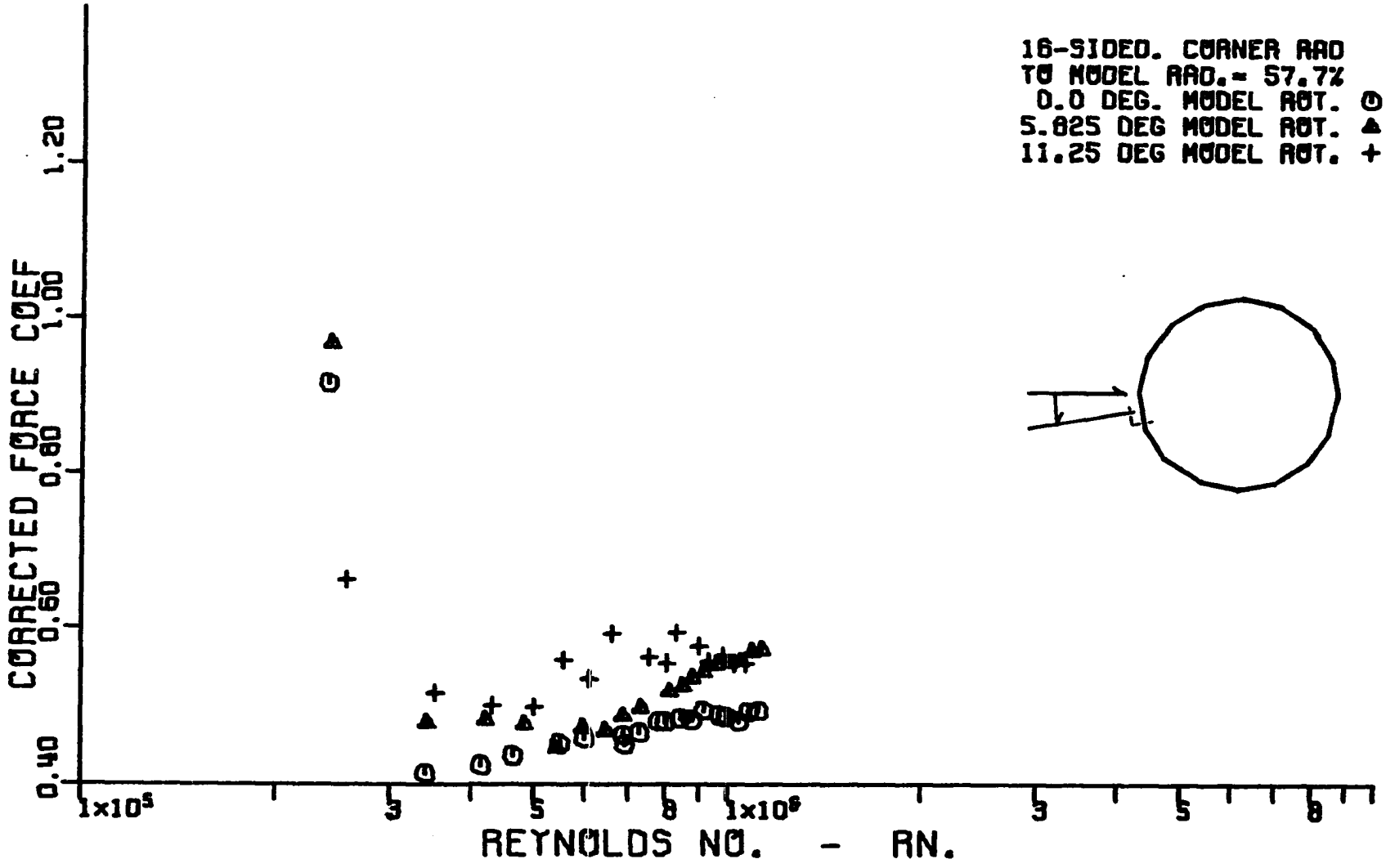

Figure 142. Variation of corrected cross-flow force coefficient with corrected cross-flow Reynolds number for a hexdecagonal cylinder having a corner radius equal to 57.7 percent of the radius of the inscribed circular cylinder.

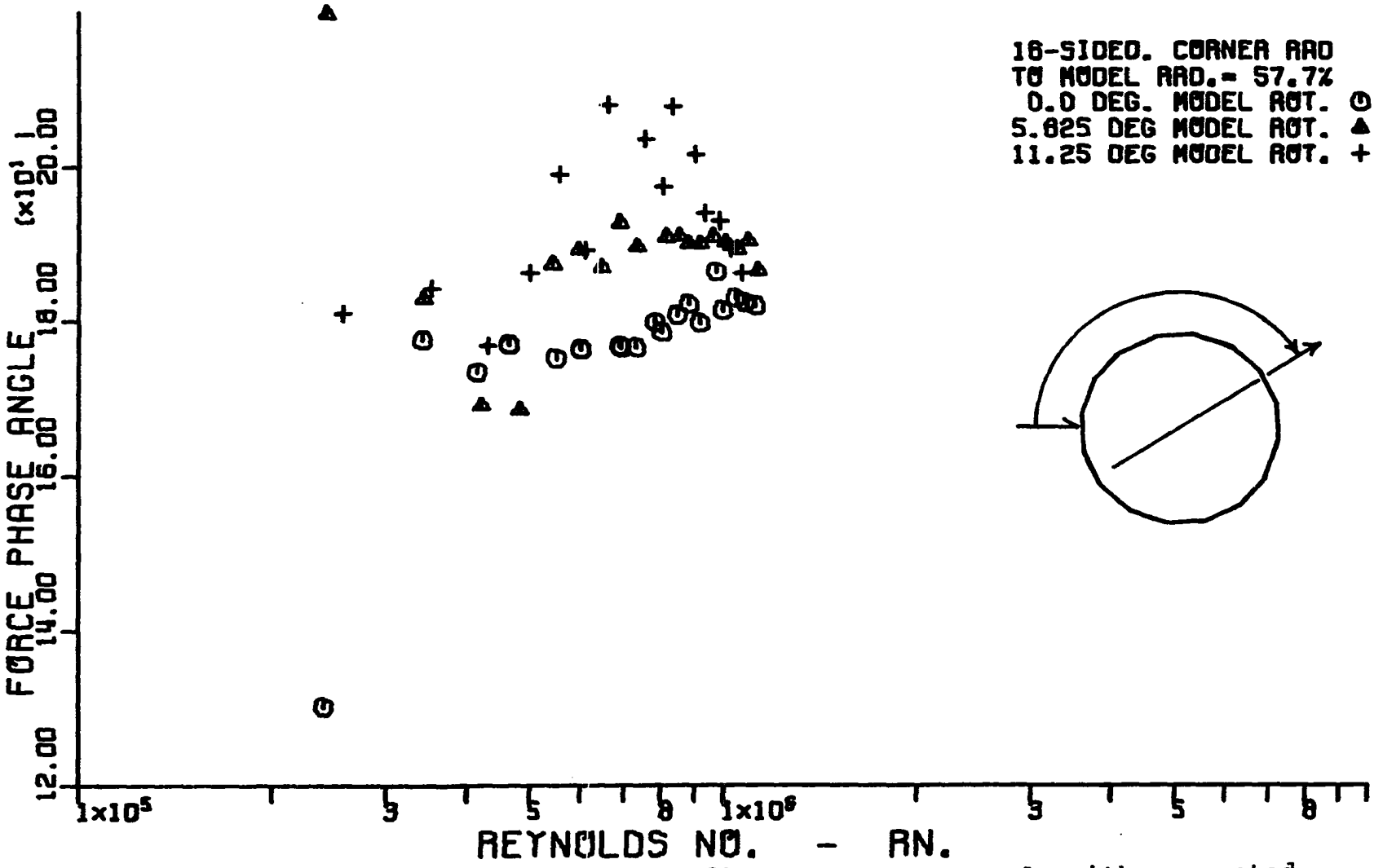

Figure 143. Variation of corrected cross-flow force phase angle with corrected cross-flow Reynolds number for a hexdecagonal cylinder having a corner radius equal to 57.7 percent of the radius of the inscribed circular cylinder.

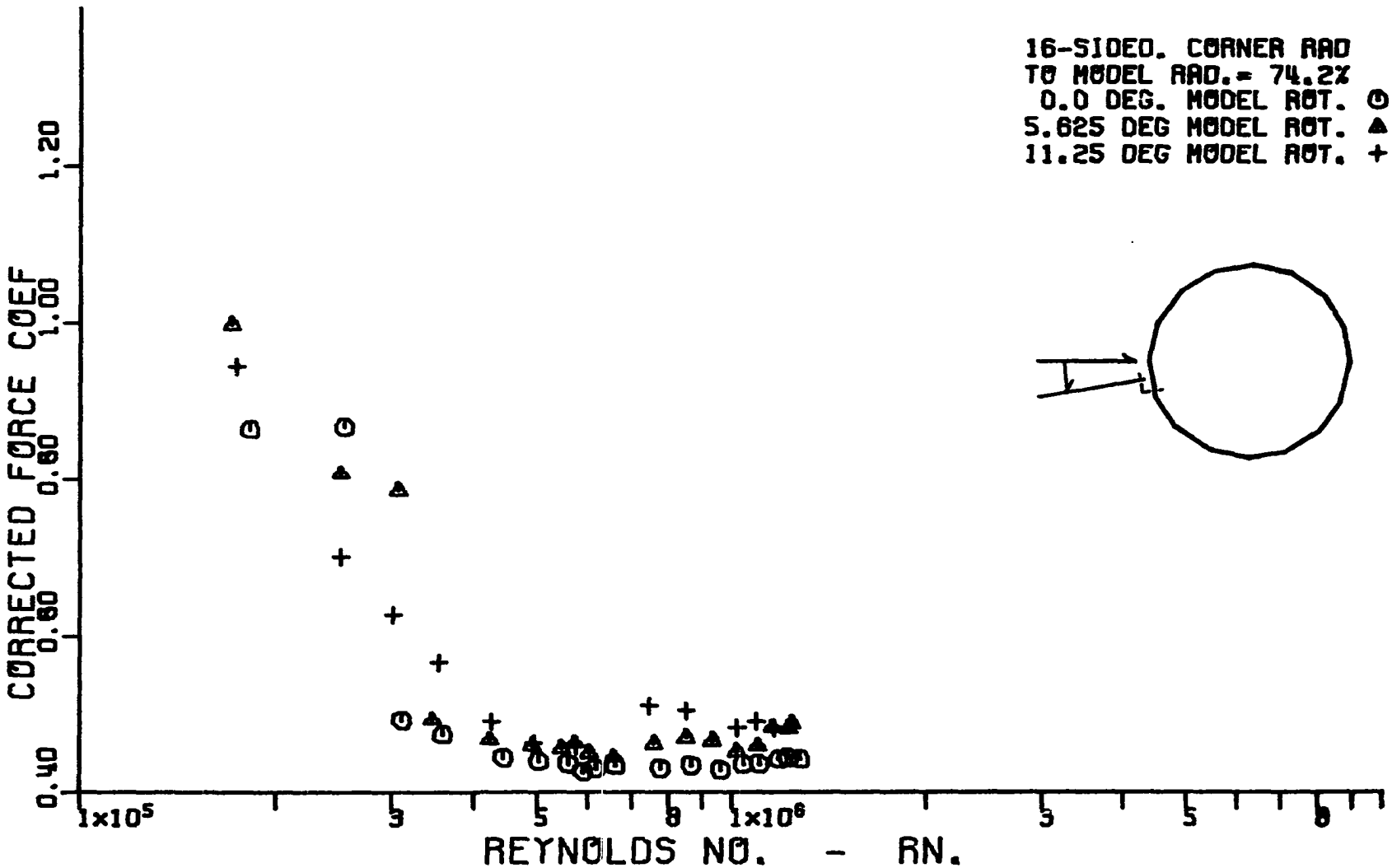

Figure 144. Variation of corrected cross-flow force coefficient with corrected cross-flow Reynolds number for a hexdecagonal cylinder having a corner radius equal to 74.2 percent of the radius of the inscribed circular cylinder.

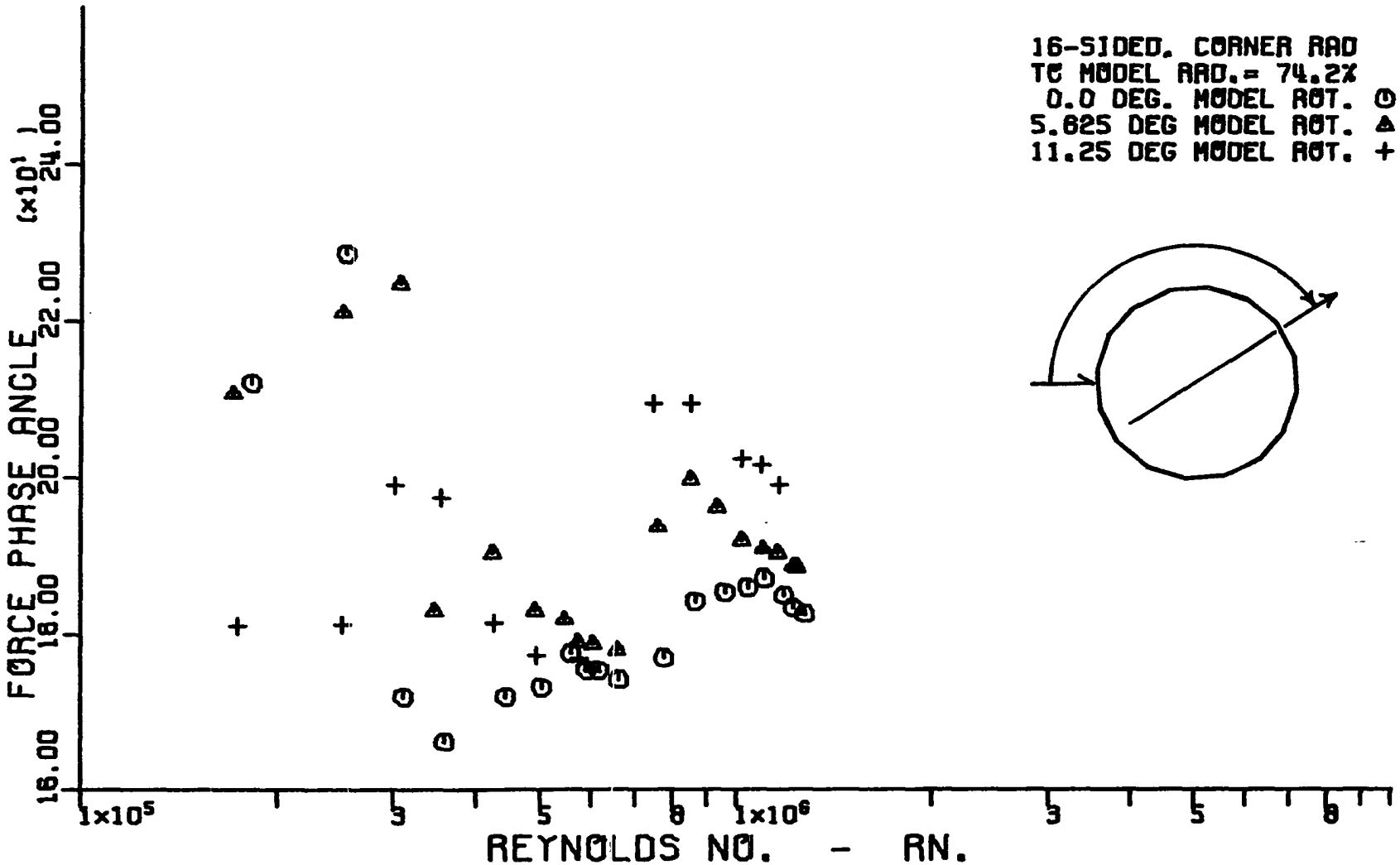

Figure 145. Variation of corrected cross-flow force phase angle with corrected cross-flow Reynolds number for a hexdecagonal cylinder having a corner radius equal to 74.2 percent of the radius of the inscribed circular cylinder.

decided to attempt to find an empirical equation relating the total aerodynamic force and the corner radius instead of just the drag and corner radius as was the original intention. Figures 146 to 148 show the variation of maximum aerodynamic force coefficient with change in corner radius, expressed as the ratio of corner radius to radius of the inscribed circular cylinder, for a constant Reynolds number of 10^6. This value of Reynolds number was chosen since it is in the range of maximum value of Reynolds number usually experienced by luminaire towers. For example, a tower 1.5 feet in diameter, experiencing an 80 mile per hour wind at sea level has a Reynolds number of 1,130,000. The value of force coefficient plotted versus corner radius is the maximum value obtained from all of the rotations tested. In general it was found that the maximum values occurred either at 0° or for the rotation with a corner pointing directly into the relative wind. Since at these rotations lift is close to zero, the force coefficients plotted are approximately equal to the drag coefficients. Because of this the equations obtained predict the variation of drag coefficient as well as total aerodynamic force coefficient.

As can be seen from Figures 146 to 148 the variation of force coefficient with corner radius is such that it would be difficult to fit a simple curve, an exponential or lower order polynomial, through the entire set of data points.

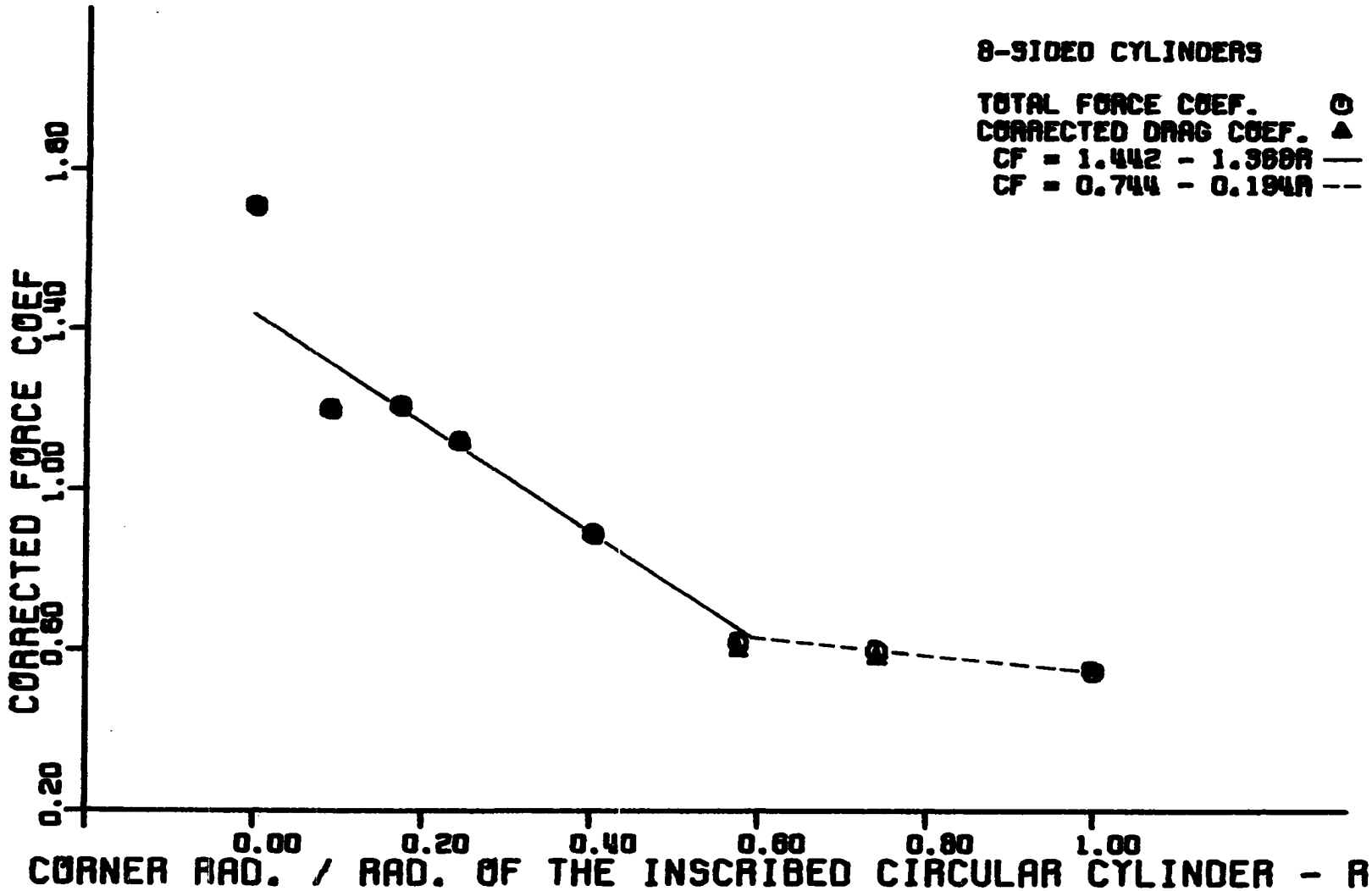

Figure 146. Variation of maximum corrected cross-flow force coefficient measured at any model orientation with ratio of corner radius to radius of the inscribed circular cylinder for octagonal cylinders.

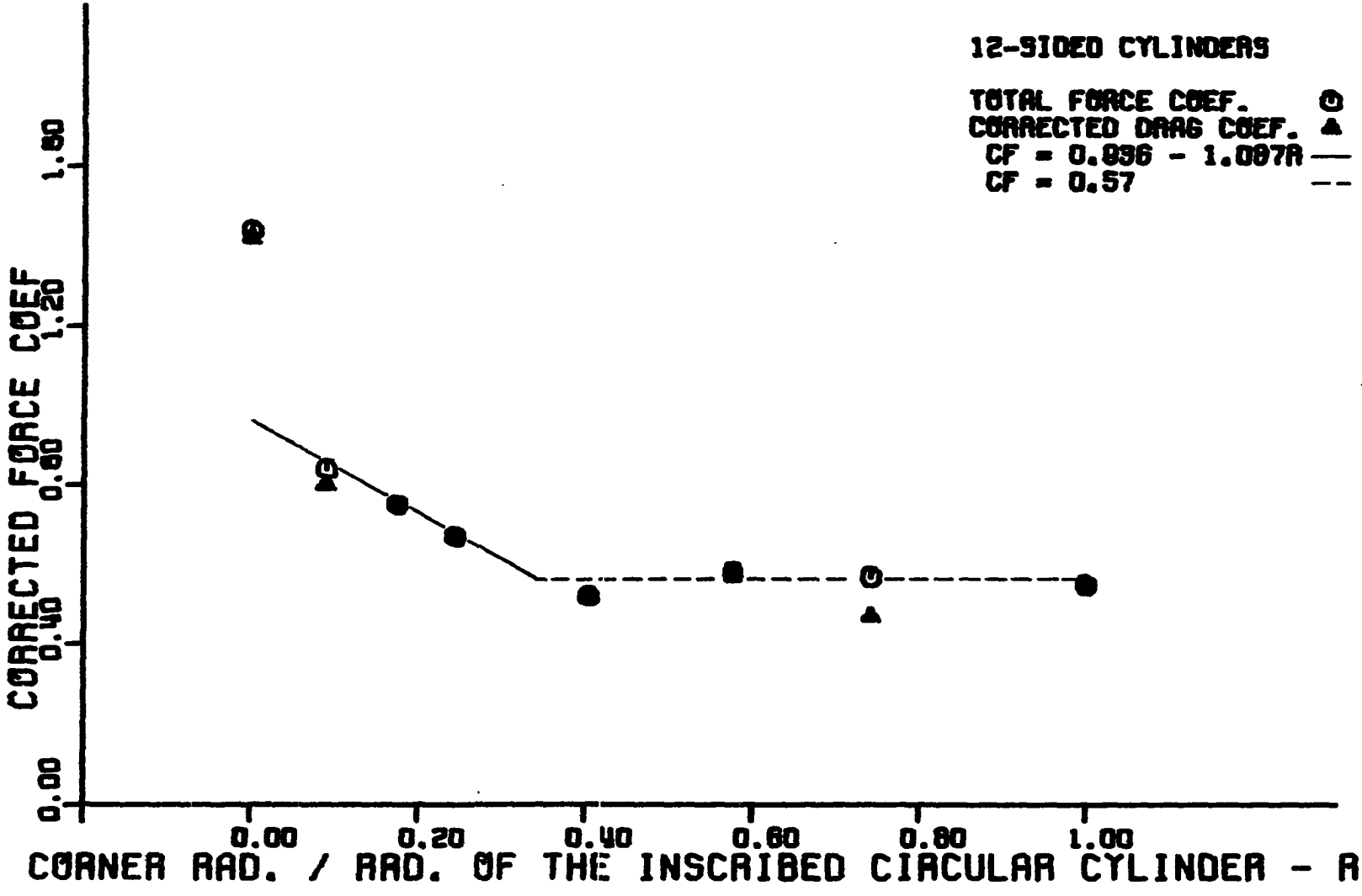

Figure 147. Variation of maximum corrected cross-flow force coefficient measured at any model orientation with ratio of corner radius to radius of the inscribed circular cylinder for dodecagonal cylinders.

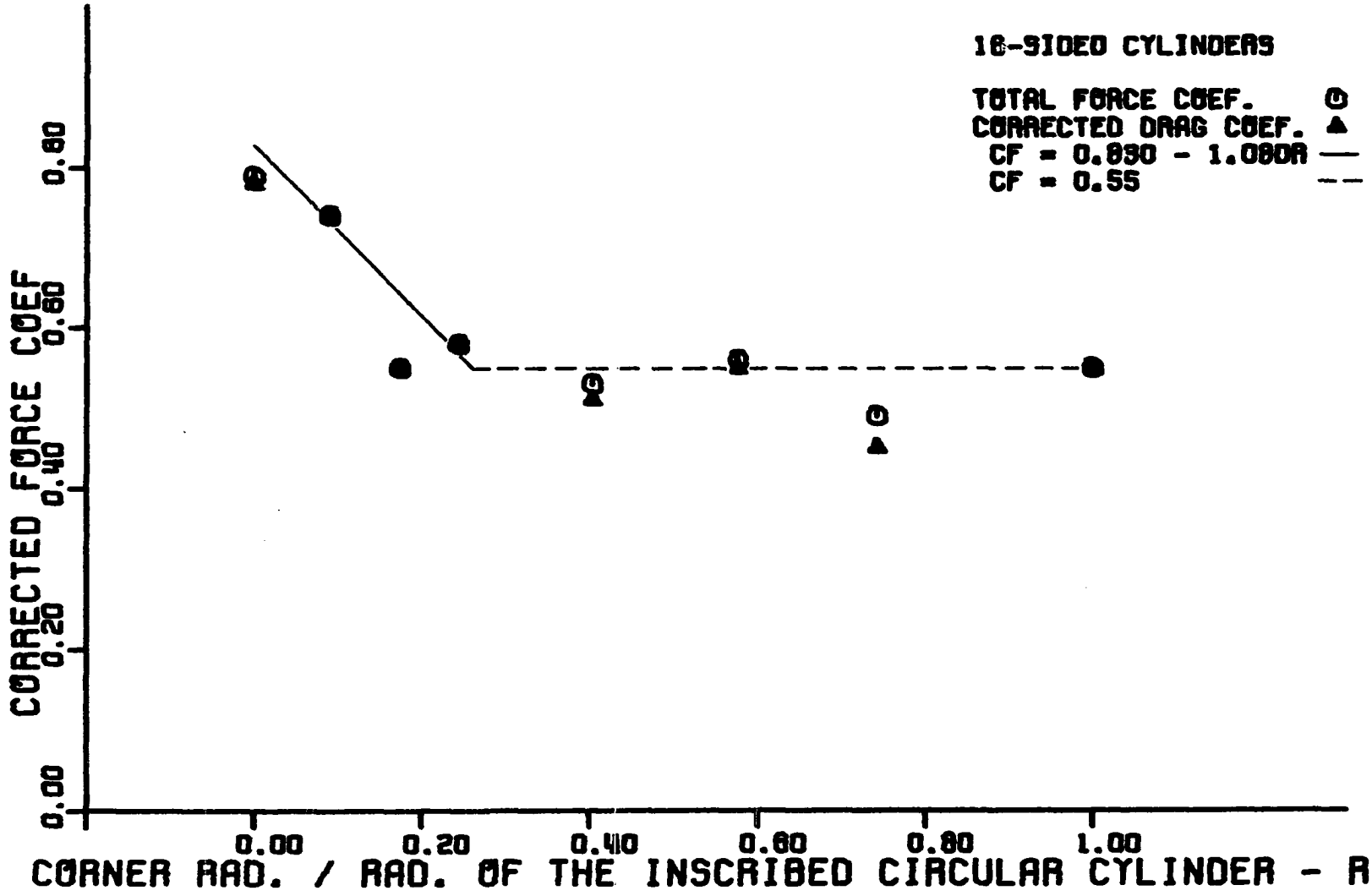

Figure 148. Variation of maximum corrected cross-flow force coefficient measured at any model orientation with ratio of corner radius to radius of the inscribed circular cylinder for hexdecagonal cylinders.

After many attempts failed, it was decided to take advantage of the linear segments of the curves and approximate each curve by two straight lines as shown. For the 8-sided cylinders the equations yielding the variation of force or drag coefficient with corner radius are

$$C_f = 1.422 - 1.368r \qquad 0.09 \leq r \leq 0.59$$

$$C_f = 0.744 - 0.194r \qquad 0.59 \leq r \leq 1.00 \tag{16}$$

where C_f is the total aerodynamic force coefficient and r is the ratio of corner radius to radius of the inscribed circular cylinder. For the 12-sided cylinders the equations are

$$C_f = 0.936 - 1.087r \qquad 0.09 \leq r \leq 0.34$$

$$C_f = 0.57 \qquad 0.34 \leq r \leq 1.00 \tag{17}$$

while for the 16-sided cylinders they become

$$C_f = 0.83 - 1.08r \qquad 0.0 \leq r \leq 0.26$$

$$C_f = 0.55 \qquad 0.26 \leq r \leq 1.00 \tag{18}$$

In general the deviation between the above curves and the data points is within ±5 percent, however for the sharp-cornered models the force coefficient is much larger than the

values predicted by Equations 16 to 18 except for the 16-sided models. Because of that, the range of validity for the above equations has been set at corner ratios of from 0.09 to 1.00 for the 8- and 12-sided cylinders and from 0.0 to 1.00 for the 16-sided models. Although it is possible to obtain expressions that fit shorter segments of the curve closer than do the straight lines given above, except for the sharp-corner data the deviation mentioned above is as close as the predicted accuracy of the data itself. Because of this, it is felt that the straight lines given by Equations 16 to 18 are sufficiently accurate to provide a good estimate of either the maximum total force or drag coefficient that can be expected at any model-relative wind orientation for a given corner radius.

Variation of Force Coefficients with Reynolds Number

The variation of the coefficient of drag can be seen in Figures 26 to 57 where the corrected drag coefficients have been plotted versus corrected Reynolds number. For all corner radii except that of 0.0 percent the variation of drag coefficient with Reynolds number follows the same pattern as does the circular cylinder. This variation of drag coefficient with Reynolds number for circular cylinders is due to the behavior of the boundary layer around the body.

Boundary layers are either laminar in nature, which limits the energy that can be transferred normal to the direction of the local flow, or turbulent in nature, in which case there is a large energy transfer normal to the local flow. The former is known as the laminar boundary layer and the latter as the turbulent boundary layer. Near the forward stagnation point, the point where the flow has been brought to rest, the boundary layer is always laminar. However, given a sufficient distance this laminar boundary layer will ultimately change into a turbulent boundary layer. The location at which this change takes place is known as the transition point. Transition takes place at a definite Reynolds number depending on the shape and surface roughness of the body and the turbulence of the free-stream, see Figure 12. Thus, as seen from Equation 1, as the free-stream velocity increases the transition point moves closer to the forward stagnation point. It is also known that due to the ability of the turbulent boundary layer to feed larger amounts of energy into the flow near the surface, a turbulent boundary layer will conform to the surface of a body in the face of skin friction and increasing wall pressures longer than will a laminar boundary layer. Separation, or failure to conform to the shape of the body, occurs when the kinetic energy of the flow near the surface becomes zero.

When the above knowledge is applied to a circular

cylinder, it is found that there is always a laminar boundary layer in the region near the forward stagnation point. At low Reynolds number, this laminar boundary layer separates from the surface of the cylinder before transition occurs. This is known as laminar separation and takes place about 80° behind the forward stagnation point. As the Reynolds number of the flow increases a point is reached where transition occurs before separation and the flow remains attached until around 120°, see Figures 9 and 10. As mentioned previously the Reynolds number at which this occurs is known as the critical Reynolds number. Upon passing the critical Reynolds number, two changes occur which are important. The first is that the flow remains attached until approximately 120° as was just mentioned. Because of this and the pressure distribution caused by it, the second change occurs: a significant decrease in drag coefficient. This change and the Reynolds number at which it occurs are shown in Figure 12 where the effects of surface roughness are demonstrated. As Reynolds number is further increased, the transition point continues to move forward with a resulting increase in drag coefficient. It is felt that transition continues to occur until a Reynolds number of approximately 3.5×10^6 is reached at which time a fully turbulent boundary layer has been established around most of the body (1,19). Test results indicate that beyond this Reynolds number the drag coefficient

remains essentially constant (1,11,19).

The flow around polygonal cylinders is controlled by the boundary layers just as in the case of the circular cylinder but with one difference, corners. Due to the tendency of subsonic flow to separate at corners because of the rapid pressure rise once the corner is passed, the critical Reynolds number for polygonal cylinders with small corner radii is larger than that for a circular cylinder. This is the major difference between circular and polygonal cylinders and is visible in Figures 37 to 57 where the variation of critical Reynolds number with corner radius can be seen. It is important to note that for the sharp-cornered bodies the critical Reynolds number is never reached. In addition it should also be noted that as the number of sides of the cylinder increases and thus the included angle in the corner goes down, the effect of corner radius becomes less important. Once the critical Reynolds number is reached the variation of drag coefficients with Reynolds number is once again similar to that of the circular cylinder.

The variation of lift coefficient with Reynolds number has already been covered. It will suffice here to simply restate the fact that once the critical Reynolds number is reached the value of the lift coefficient remains essentially constant.

CONCLUSIONS

The results of the research program presented herein point out several interesting and important facts pertaining to considerations and standards that should be used in the design of towers, both luminaire and others, when polygonal cylinders are to be used. They are as follows:

1. Hexdecagonal cylinders offer the smallest drag coefficient of the three shapes studied. They not only have the same force coefficient as a circular cylinder by the time the corner radius is 28 percent, but force coefficients as much as 10 percent less than those of a circular cylinder are reached for corner radii greater than 0.4.
2. Dodecagonal cylinders have a total aerodynamic force approximately equal to that of the circular cylinder for all corner ratios greater than 0.35. Thus if luminaire towers were constructed with corner radii of 35 percent instead of the present day 20 to 25 percent a force coefficient reduction of between 15 to 20 percent could be obtained.
3. The variation between the maximum forces acting on a dodecagonal cylinder and those acting on hexdecagonal cylinders is approximately 13 percent at corner ratios below 0.35. For corner ratios

greater than this they differ by only a few percent.

4. The maximum aerodynamic force acting on an octagonal cylinder is significantly greater than that acting on either a dodecagonal or hexdecagonal cylinder for all corner ratios up to 60 percent.

5. A set of useful empirical equations relating the maximum force coefficient to corner ratio for the cylinders studied were obtained. For the octagonal cylinders they are

$$\begin{aligned} C_f &= 1.422 - 1.368r \qquad 0.09 \leq r \leq 0.59 \\ C_f &= 0.744 - 0.194r \qquad 0.59 \leq r \leq 1.00 \end{aligned} \tag{16}$$

while for the dodecagonal cylinders they become

$$\begin{aligned} C_f &= 0.936 - 1.087r \qquad 0.09 \leq r \leq 0.34 \\ C_f &= 0.57 \qquad\qquad\quad 0.34 \leq r \leq 1.00 \end{aligned} \tag{17}$$

and for the hexdecagonal cylinders they are

$$\begin{aligned} C_f &= 0.83 - 1.08r \qquad 0.0 \leq r \leq 0.26 \\ C_f &= 0.55 \qquad\qquad\quad 0.26 \leq r \leq 1.00 \end{aligned} \tag{18}$$

These equations are in general within ± 5 percent of the data points. They are sufficiently accurate to provide a good estimate of the maximum force

coefficient that can be expected at any model-relative wind orientation for a given corner radius.

6. The coefficient of lift is approximately zero for the model rotations of flat side perpendicular to the relative wind and corner pointing directly into the relative wind. As the model is rotated, starting at the flat side perpendicular to the relative wind, before the rotation reaches one-half way to the orientation with the corner pointing forward a lift coefficient is produced that may be as large as 50 percent of the drag coefficient. This force acts toward the surface rotated in the downwind direction. The magnitude of the lift coefficient at Reynolds numbers greater than the critical Reynolds number are roughly 0.4 for the 8-sided and 0.2 for the 12-sided cylinders.
7. The magnitude of the lift force approaches zero as the rotation reaches one-half way between the extremes mentioned in 6. For rotations larger than this, the magnitude in general remains small but the direction of the force reverses. In these orientations the force acts toward the surface rotated upwind.
8. In general the maximum force coefficient occurs when the model is rotated so a corner is pointed

directly into the relative wind. In the octagonal cylinders this coefficient decreases for rotations 15°, 0° and 7.5°. In the dodecagonal cylinders the forces become decreasing smaller for rotations of 0°, 10° and 5° while for the hexdecagonal cylinders the 5.6° rotation produces the smallest force.

REFERENCES

1. E. Achenbach. "Influence of surface roughness on the cross-flow around a circular cylinder." Journal of Fluid Mechanics 46, part 2 (1971):321-335.

2. H. J. Allen and W. G. Vincenti. "Wall interference in a two-dimensional-flow wind tunnel, with consideration of the effect of compressibility." National Aeronautics and Space Administration, Washington, D.C., Tech. Report NACA TR 782, 1944.

3. C. F. Cowdrey and J. A. Lawes. "Force measurements on square and dodecagonal sectional cylinders at high Reynolds numbers." Aerodynamics Division, National Physical Laboratory, Department of Scientific and Industrial Research, Teddington, Middlesex, England, NPL/Aero/351, Aug. 1959.

4. N. K. Delany and N. E. Sorenson. "Low-speed drag of cylinders of various shapes." National Aeronautics and Space Administration, Washington, D.C., Tech. Note NACA TN 3038, 1953.

5. J. E. Fackrell. "Blockage effects on two-dimensional bluff body flow." The Aeronautical Quarterly 26, part 4 (1975):243-253.

6. H. Glauert. "Wind tunnel interference on wings, bodies and airscrews." Aeronautical Research Committee, London, England, Report and Memo. ARC R&M 1566, 1933.

7. S. Goldstein, ed. Modern Developments in Fluid Dynamics, Vol. II. New York, New York: Dover Publications, 1965.

8. E. L. Houghton. "A limited wind tunnel test on a symmetrical octagonal sectional cylinder." Geoffrey DeHavilland Aeronautical Lab., Hatfield Polytechnic, Hatfield, Herts, England, Feb., 1967.

9. W. D. James. "Wind tunnel tests of a two-dimensional round-cornered dodecagonal cylinder." Red Wing, Minn.: Meyer Industries, Inc., 1971.

10. G. W. Jones, Jr., J. J. Cincotta and R. W. Walker. "Aerodynamic forces on a stationary and oscillating circular cylinder at high Reynolds numbers." National Aeronautics and Space Administration, Washington, D.C., Tech. Report NASA TR R-300, Feb. 1969.

11. L. H. Jorgensen. "Prediction of static aerodynamic characteristics for space shuttle-like and other bodies at angles of attack from 0° to 180°." National Aeronautics and Space Administration, Washington, D.C., Tech. Note NASA TN D-6996, Jan. 1973.

12. L. H. Jorgensen. "Prediction of static aerodynamic characteristics for slender bodies alone and with lifting surfaces to very high angles of attack." National Aeronautics and Space Administration, Washington, D.C., Tech. Memo. NASA TM X-73, 123, June 1976.

13. A. H. Lefebvre. "A method of predicting the aerodynamic blockage of bluff bodies in a ducted airstream." The College of Aerodynamics, Cranfield, England, Report CoA REPORT AERO NO. 188, Nov. 1965.

14. E. C. Maskell. "A theory of the blockage effects on bluff bodies and stalled wings in a closed wind tunnel." Aeronautical Research Council, Ministry of Aviation, London, England, Report and Memo. ARC R&M 3400, 1963.

15. E. C. Maskell. "Bluff bodies and high-lift systems." In Subsonic Wind Tunnel Wall Corrections. Edited by H. C. Garner. North Atlantic Treaty Organization, Advisory Groups for Aerospace Research and Development, ASARDograph 109, 1966.

16. E. C. Polhamus. "Effect of flow incidence and Reynolds number on low-speed aerodynamic characteristics of several noncircular cylinders with applications to directional stability and spinning." National Aeronautics and Space Administration, Washington, D.C., Tech. Report NASA TR R-29, 1959.

17. A. Pope and J. J. Harper. Low-Speed Wind Tunnel Testing. New York, New York: John Wiley and Sons, Inc., 1966.

18. A. S. Ramamurthy and P. M. Lee. "Wall effects on flow past bluff bodies." Journal of Sound and Vibration 31, part 4 (1973):443-451.

19. A. Roshko. "Experiments on the flow past a circular cylinder at very high Reynolds number." Journal of Fluid Mechanics 10, part 3 (1961):354-356.

20. H. Schlichting. Boundary Layer Theory. New York, New York: McGraw-Hill Book Co., Inc., 1960.

21. Standard Specifications for Structural Supports for Highway Signs, Luminaires and Traffic Signals. Washington, D.C.: American Association of State Highways and Transportation Officials, 1975.

22. E. Szechenyi. "Supercritical Reynolds number simulation for two-dimensional flow over circular cylinders." Journal of Fluid Mechanics 70, part 3 (1975):529-542.

23. A. Thom. "Blockage corrections in a closed high speed wind tunnel." Aeronautical Research Committee, London, England, Report and Memo. ARC RcM 2033, 1943.

ACKNOWLEDGMENTS

The author wishes to thank A. B. Chance Co. of Houston, Texas, Meyer Industries, Inc. of Red Wing, Minnesota and Valmont Industries Inc., of Valley, Nebraska for their support in funding assistance for this research project and to Dr. Paul Peterson, director of the Engineering Research Institute, Iowa State University, for furnishing the remainder of the needed funds. Thanks are also due to Dr. E. W. Anderson who supplied guidance until his retirement, and to Dr. Len Wilson who had the difficult task of slipping into a project well underway. No experimental project of the magnitude of this one can succeed without the assistance of research assistants and machine shop personnel and Mike McClure, Edwin Mooney and Charles Burg are among the best.